Fundamental Studies of Electrochemical Oxide Formation on Platinum Single Crystal Electrodes
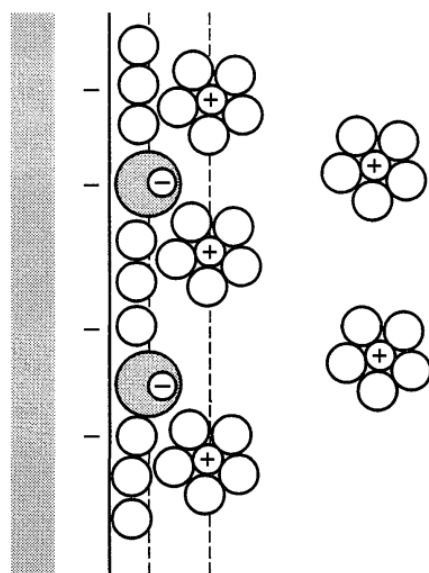
Katherine Hunter M.Chem

Department of Chemistry

Cardiff University

Acknowledgements

As no thesis is ever conquered alone, I would like to extend my thanks and gratitude to all those who have helped me along the way.

In particular, I would like to say a special thanks to my Supervisor Professor Gary Attard, for his support and guidance throughout my PhD. His continuous enthusiasm for research and tirelessly answering my many question is something that I will always be grateful for.

Secondly I would like to thank my friends in Cardiff University and specifically, the now-disbanded Electrochemistry Research Group for providing support, training, assistance and knowledge throughout my research time. I am especially grateful to Dr Ashley Brew for his specific training and support with my project. Other group members I would like to thank are Dr Peter Jenkins, Dr Charlie Davis, Dr Shaoliang Guan and Jinyu Ye for their support. I would also like to thank the undergraduate students I have worked with and other members of the Cardiff University Chemistry department who have greatly supported me in this venture. At Johnson Matthey, I would like to thank Dr Jonathan Sharman and Dr Ed Wright for extensive knowledge, guidance and funding throughout the project. Further thanks must be extended to other national and international friends and colleagues of whom helped with experiments and analysis along the way, specifically the electrochemistry group in the University of Alicante.

Finally, I would like to thank my friends and family for putting up with me through this and tirelessly listening to my woes and successes. Thank you for your encouragement over the last four years.

Publications

Gary A. Attard, Ashley Brew, Katherine Hunter, Jonathan Sharman, Edward Wright, **Specific adsorption of perchlorate anions on Pt{hkl} single crystal electrodes**, Phys. Chem. Chem. Phys., 16 (2014) 13689-98

[In Press]

Gary A. Attard, Katherine Hunter, Edward Wright, Jonathan Sharman, Ricardo Martínez-Hincapié and Juan M. Feliu, **The Voltammetry of Surfaces Vicinal to Pt{110}: Structural Complexity Simplified by CO Cooling**, Journal of Electroanalytical Chemistry (2016).

Summary

Platinum single crystal electrodes were used to investigate electrochemical oxides and related surface species and their impact upon important catalytic reactions such as the oxygen reduction reaction (ORR). Notions of perchlorate anions being "non-specifically adsorbed" were re-evaluated and challenged. For example, the voltammetry of Pt single crystal electrodes as a function of perchloric acid concentration (0.05–2.00 M) was studied in order to test the assertion by Watanabe *et al*. that perchlorate anions specifically adsorb on polycrystalline platinum. Specific adsorption of perchlorate anions was found in varying degrees for Pt(hkl) surfaces.

By flame-annealing and cooling a series of Pt n(110)x(111) and Pt n(110)x(100) single crystal electrodes in a CO ambient, new insights into the nature of the electrosorption processes associated with Pt{110} voltammetry in aqueous acidic media were elucidated. For Pt n(110)x(111) electrodes, a systematic change in the intensities of voltammetric peaks indicated a lack of surface reconstruction (in contrast to hydrogen cooled analogues). Pt n(110)x(100) stepped electrodes displayed a marked tendency towards surface reconstruction irrespective of cooling environment.

Pt(110) terrace sites were found to afford a specific affinity for sulphonate groups contained within a Nafion adlayer. Pt n(100)x(110) surfaces showed rapid quenching of the Nafion 'spike' as a function of increasing step density. Reactivity measurements involving oxygen reduction and hydrogen peroxide oxidation/reduction largely revealed the importance of adsorbed oxide/OH in regulating activity.

Kinetic studies suggested that for Pt(100) terraces, oxide formation was also accompanied by rapid surface reconstruction. Fast potential cycling of all electrode surfaces confirmed the likelihood of structural changes occurring in real fuel cells. It is deduced that roughened catalyst particles should actually exhibit an enhanced ORR activity, even in the presence of Nafion.

Contents

Investigations into the nature of a traditionally considered "non-adsorbing" anions

The Voltammetry of Surfaces Vicinal to Pt{110}: Structural Complexity Simplified by CO Cooling

Characterisation of stepped Pt single crystals in the [001] zone

Probing the nature of electrochemical oxides on Pt(hkl) single crystal surfaces

Conclusions

Important Symbols

Symbols Symbol	Description	Units
A	Electrode Area	cm^{-2}
	Symmetry factor	-
C	Capacitance	F
	Double layer capacitance	F
δ	Diffusion layer thickness	nm
D	Diffusion coefficient	$cm^2\ s^{-1}$
E	Applied potential	V
E_B	Electron binding energy	eV
E_{eq}	Equilibrium potential	V
E_o	Standard half-cell potential	V
$E_{1/2}$	Half wave potential	V
E	Cell potential	V
F	Faraday's constant	$9.649 \times 10^4\ C\ mol^{-1}$
η	Overpotential	V
η	Maximum energy efficiency	-
η	Carnot efficiency	-
/	Adsorbate coverage	-
	Tunnelling current	A
	Double layer charging current	A
	Net (observed) current	A
	Oxidative current (anodic)	A
	Reductive current (cathodic)	A
	Diffusional flux/current density	$mol^{-2}\ s^{-1}/A\ cm^{-2}$
	Limiting current density	$A\ cm^{-2}$
	Net current density	$A\ cm^{-2}$
	Kinetic current density	$A\ cm^{-2}$
0	Exchange current density	$A\ cm^{-2}$
	Rate constant at E_{eq}	-
m_T	Mass transport coefficient	$cm\ s^{-1}$
n	Number of electrons	-
	Partial pressure	atm
R	Gas constant	$8.314\ J\ K^{-1}\ mol^{-1}$
R_e	Reynold's number	-
T	Temperature	K
v	Sweep rate	$^{-1}$
V	Potential	V
	Work function	eV
	Rotation speed	Hz/rpm

Important Abbreviations

CV	Cyclic voltammetry/cyclic voltammogram
DMFC	Direct methanol fuel cell
DFT	Density functional theory
EV	Electric vehicle
FAFC	Formic acid fuel cell
fcc	Face centred cubic
FCEV	Fuel cell electric vehicle
GHG	Greenhouse gas
HEV	Hybrid electric vehicle
hcp	Hexagonal close packed
HHV	Higher heating value
HOR	Hydrogen oxidation reaction
HPORR	Hydrogen peroxide oxidation-reduction reaction
H UPD or H_{upd}	Hydrogen underpotential deposition
ICE	Internal combustion engine
IHP	Inner Helmholtz plane
LHV	Lower heating value
LEED	Low energy electron diffraction
NP	Nanoparticle
OHP	Outer Helmholtz plane
ORR	Oxygen reduction reaction
PEM	Proton exchange membrane
PEMFC	Proton exchange membrane fuel cell
PZC	Point of zero charge
PZTC	Point of zero total charge
RDE	Rotating disk electrode
RHE	Reversible hydrogen electrode
RRDE	Rotating ring disk electrode
SCE	Single Crystal Electrodes
STM	Scanning Tunnelling Microscopy
TST	Transition State Theory
UHV	Ultra high vacuum
UPD	Underpotential deposition
XPS	X-ray photoelectron spectroscopy

Introduction
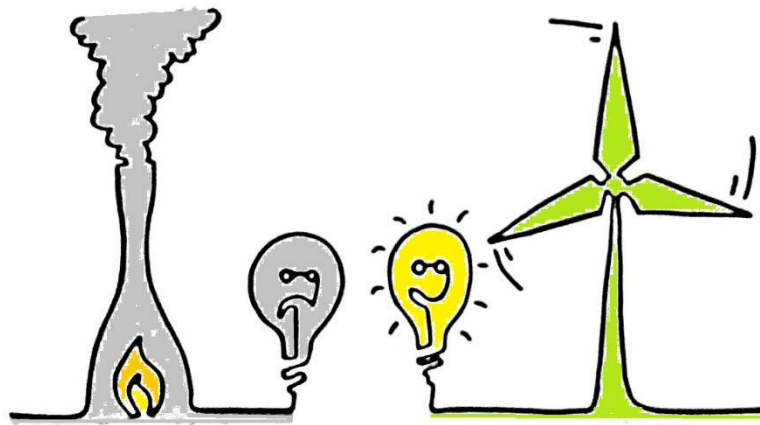
1.1. The challenge

As the world's population grows, so does the demand for energy. The increasing population puts many pressures on sustainability. Where fossil fuels once seemed inexhaustible, demand will soon outstrip supply. Modern society must be liberated from its dependence on these non-sustainable fuels, not only due to obvious availability issues, but to reduce environmental damage too.

The growing awareness about the dangers of fossils fuels has led to the development of greener energy alternatives. Alternative energy devices need to be sustainable but also produce minimal global emissions. The majority of the world's electricity production still relies heavily on the use of fossil fuels. In particular, Internal Combustion Engines (ICEs) in automotive applications are heavily dependent on oil resources, and are a huge contribution to generation of greenhouse emissions. The main technological options that are currently being considered are: improved internal combustion engine vehicles (ICEVs) powered by biofuels, battery electric vehicles (BEVs) and hydrogen fuel cell vehicles (FCVs). Hybrid solutions are also possible[1, 2]. Fuel Cells are one option that offer the capability to replace ICEs. They have the advantage of not being reliant on the use of fossil fuels as well as higher efficiency and clean by products released. Although fuel cell technology has been in existence for over 100 years, only in the last decade have significant advancements have been made to allow fuel cells to become economically viable for applications, especially in vehicles.

A thorough review of the fuel cell system is above the scope of this thesis and a short review to put the objectives of this research into perspective only, is provided.

1.2 Fuel Cells as an alternative energy device

Fuel cells are by no means "new" technologies. In fact, they are one of the oldest energy conversions known to man. First invented by Grove in the middle of the 19th century[3, 4] (Figure 1), fuel cells are the reverse of electrolysis; directly converting chemical energy into electrical energy. They work like a battery, but the fuel is stored externally[5, 6]. If the fuel is supplied continuously and not interrupted, a continuous electrical current is maintained. A battery relies on a fixed store of reactants (fuel), which can be recharged when depleted. Batteries are restricted by "memory effect" which results in degradation and lower efficiency over time. Fuel cells can weigh less overall (useful for vehicles) and are not restricted by "memory effect", resulting in better efficiency for longer periods of use[1].
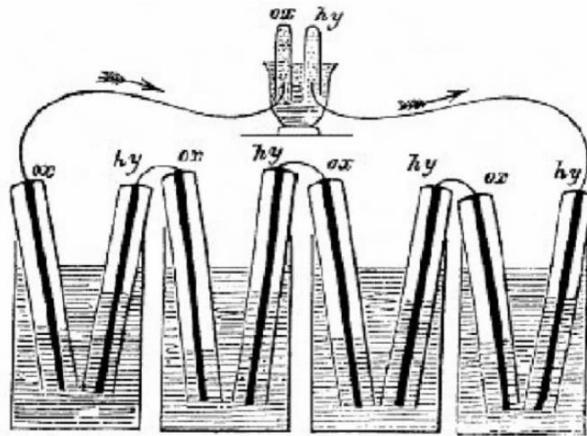
Figure 1: Diagram of the first fuel cell by Grove. Philosophical Magazine and Journal of Science 13,430

1.2.1 How Fuel Cells Work

Fuel cells are classified per their electrolyte material, which also dictates the operating temperature. Proton Exchange Membrane Fuel Cells (PEM fuel cells) (also sometime referred to as Polymer Electrolyte Membrane fuel cells) utilize a solid polymer electrolyte, and are currently present as an alternative energy device specifically for automotive applications. PEM fuel cells are particularly most suitable for automotive applications due to their fast start up, low working temperatures (around 80 °C) and longer distances they can perform to[1, 7, 8].

Fuels cells work by separating two electrodes (denoted as the anode and cathode) with an electrolyte. The anode facilitates oxidation of the fuel (such as hydrogen) whilst the cathode reduces the oxidant (usually oxygen). During oxidation or reduction, ions are generated and transported through the electronically insulating electrolyte. The electrolyte serves as a pathway to transport

ions from one electrode to another. In a PEM fuel cell, the ions are ideally protons (H^+). Electrons generated travel in an external circuit between electrodes which creates the electrical energy needed to power the device (Figure 2). For PEM fuel cells, hydrogen is the fuel at the anode resulting in a hydrogen oxidation reaction (HOR) and oxygen is reduced at the cathode (ORR). With pure hydrogen and oxygen supplied, only water is produced as waste. Unlike ICEs, a fuel cell is not limited by the Carnot efficiency (discussed later). Platinum is used as a catalyst at the electrode and will be discussed in further detail later.
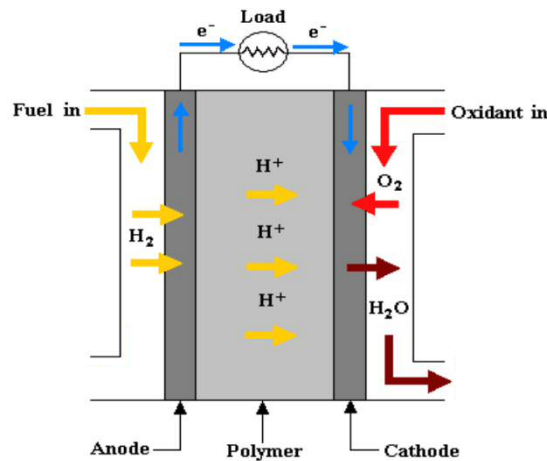
Figure 2: Schematic of how a PEM fuel cell works

1.2.1.1 Thermodynamic rationale behind fuel cells

In an ideal fuel cell, the simplest reaction encountered is the reaction of hydrogen and oxygen[9]. The fuel cell reaction can be divided into two half-cell reactions (corresponding to reactions at the anode and cathode respectively), with the standard reaction potentials (E^o)[10]:

$$H_2 \ (g, 1 \ atm) \rightarrow 2H^+ \ (aq, 1 \ M) + 2e^- \quad E^o = 0V$$

$$O_2 \ (g, 1 \ atm) + 4e^- + 4H^+(aq, 1 \ M) \rightarrow 2H_2O \quad E^o = 1.23 \ V$$

$$\text{Overall: } H_2 + \frac{1}{2}O_2 \rightarrow H_2O \quad E_{cell} = 1.23V$$
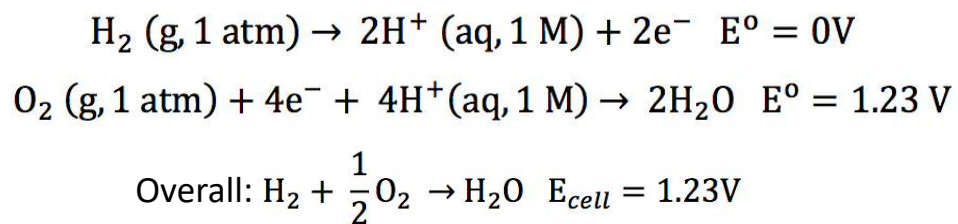
The maximum theoretical energy release is related to the free energy change [11] (Gibbs, standard T and P conditions). The standard free energy change of the overall reaction ($\Delta G^o = -nFE^o$) in the fuel cell indicates a spontaneous reaction (ΔG being the free energy change -237.1kJ mol^{-1}, n=2, F being Faradays constant and hence E^o=1.23 V).

The Nernst potential (E) (discussed later) or reversible cell electromotive force (emf), is a representation of the relationship between the ideal standard potential and equilibrium potential

for the fuel cell reaction[9]. It is often the value for which the performance of a fuel cell material is judged. It is represented as cell voltage and is the difference between the standard reduction potential of the anode and the cathode. For a hydrogen-oxygen PEM the cell emf is 1.23 V[5, 8].

1.2.1.2 Fuel Cell Efficiency

The first law of thermodynamics states that the total energy put into a system (Q_{in}) must equal the total energy output ($W_{out} + Q_{out}$)[9]. This equation can be used to define the maximum energy efficiency of a process. The efficiency of any energy conversion device such as a fuel cell is the ratio of useful energy output to energy input. For PEM fuel cells, the energy input is the enthalpy of formation for hydrogen (286 kJ mol^{-1}) and the energy output is E_{cell} (1.23 V), which equates to a Gibbs free energy change of 237.1 kJ mol^{-1}. Therefore, the efficiency (η) can be calculated as follows:

$$Q_{in} = W_{out} + Q_{out}$$

$$\eta_{max} = \frac{W_{out}}{Q_{in}}$$

$$\eta_{max} = \frac{\Delta G_f^0}{\Delta H_f^0} = \frac{237.1 \text{ kJ/mol}}{286 \text{ kJ/mol}} = 83\%$$

[9]

Where Q_{in} is the energy input into the system, W_{out} is the work output and Q_{out} is the waste heat output[9].

This efficiency of 83% is calculated at 298K, using hydrogens higher heating value (HHV) as the input energy. The HHV is the amount of energy released for 1 mol of hydrogen to combust at 298K and the product (water vapour) to return to 298K. Efficiency can be increased by using hydrogen's lower heating value(LHV), where the product is only returned to 423K (150°C). This increases the efficiency to ~95% but results in some unreturnable loss of water. This can cause problems in PEM fuel cells as optimum hydration in the electrolyte (explained later) is key to the cell working efficiently. These efficiencies correspond to the maximum thermodynamic limits[9].

In an ideal FC the cell voltage is independent of current, but practically this is not achieved[8-10]. The difference between theoretical cell voltage and reversible cell voltage (E- E°) is termed overvoltage or overpotential (η) when referring to a single electrode. Prominent sources of overpotential include: mixed potential at electrodes from fuel crossover, activation losses from sluggish electrode kinetics and mass transport losses. One of the largest losses for a PEMFC is the poor kinetics of the ORR half reaction in acidic media. Even with high loadings of expensive platinum,

the activation overpotential for the ORR is on the order of 400 mV at acceptable current densities (E^o=0.8 V)[10, 12].

1.2.1.3 Efficiency of ICE's

$$\text{Carnot Efficiency } (\eta_{Carnot}) = \frac{W_{out}}{Q_{in}} = \frac{T_1 - T_2}{T_1} \text{ or } 1 - \frac{T_2}{T_1}$$

[9]

The equivalent measure of efficiency of an internal combustion engine is known as the Carnot efficiency limit. It specifies the theoretical maximum efficiency that can be obtained from an ideal heat engine operating between two temperatures. The high temperature (T1) refers to the temperature of the combustion gases inside the engine and the cold temperature (T2) refers to the temperature at which the gases are exhausted from the engine. Temperatures in ICEs vary but can be several hundreds of degrees at specific points in the combustion[13]. Although it is theoretically possible to achieve 100% efficiency, T1 would need to be infinite or T2 at absolute zero. As well as the engine materials not being able to sustain incredibly high temperatures, implications of safety also arise with gaseous fuel at high temperatures in an automobile. Instead to increase the efficiency, the engine is kept cool by circulating coolant to protect the engine components. This also reduces the efficiency of the combustion process. Due to this issue, vehicles with ICEs have lower thermal efficiencies (typically 20-40%) than fuel cells[14], when operated in suitable temperatures.

1.2.2 .The role of platinum in PEM fuel cells

Although PEMFCs are a great alternative to ICEs they also have drawbacks. Two major factors inhibiting the commercial production of PEMFCs are durability and cost. The high price of FCs is mainly due to the large amount of expensive platinum utilised as the catalyst at the electrodes[12]. Pt loading in an 80kW PEMFC was reported to be ~17% of the total production cost[15]. Understandably, multiple alternatives are being investigated. The development of thin film catalysts[16], platinum alloys[6] and platinum nanoparticles (NPs)[17-19] have shown great promise in increasing the electrode activity, whilst also decreasing the % of Pt loading. Non platinum-group metals and non-metal catalysts are also being investigated[20, 21].

1.2.2.1 The durability challenge

Typical fuel cell lifetime targets are around 5,000-10,000 hrs for cyclic automotive applications. The electrocatalyst must retain activity over the fuel cell operation cycle. However, potential cycling

conditions greatly exacerbate problems such as metal dissolution, redeposition and precipitation of the metal, resulting in lowered performance[22].

1.2.2.2 Model PEMFC catalyst design

There are four key characteristics required for an effective PEMFC catalyst; activity, selectivity, stability and poisoning resistance. These properties are important when choosing and designing new catalyst systems in FCs and are discussed further below.

1.1.1.1.1 Activity
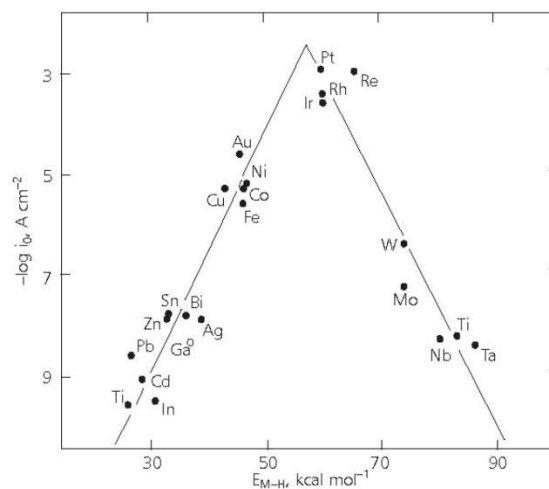
[23]

Figure 3: The logarithm of exchange current densities (log i0) for cathodic hydrogen evolution vs. the bonding adsorption strength of intermediate metal-hydrogen bond formed during the reaction itself.

The interactions between a catalyst and substrate must ideally obey the Sabatier principle[20], whereby, catalysts are active enough to adsorb reacting species strongly enough to facilitate the reaction, but also weakly enough to release the product once the reaction has occurred. Balandin's volcano plots are often used when choosing potential electrode materials[24]. For example, the volcano plot for Metal-H bonding in Figure 3 shows Pt has the highest activity of all bulk metals. Kinetics of the anodic HOR on Pt is facile. Voltage losses are extremely small even for low Pt loadings[25]. On the other hand, the sluggish kinetics of the cathodic ORR is the source of more than half voltage loss in PEMFCs[26]. The ORR is a complicated mechanism with various pathways [12, 27](discussed later). The ideal cathodic catalyst needs a high chemical activity to activate O_2. It then must also release the product quick enough to free up more surface for more ORR. Baladin's volcano plot (figure 4) for binding between single O atoms shows Pt is the best pure metal closest to optimum binding theory. It is important to note that Pt still binds O too strongly and this is one of the reasons for the overpotential in the PEM.

[14]
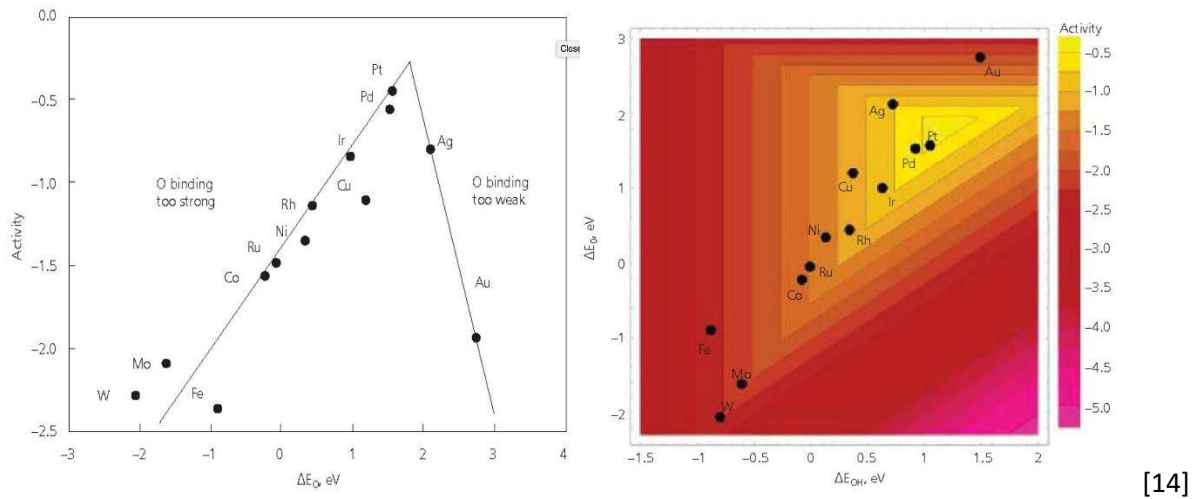
Figure 4: left) Trends in oxygen reduction activity plotted as a function of the oxygen binding energy and right) Trends in oxygen reduction activity plotted as a function of both the oxygen and the hydroxyl group binding energy, taken from [14]

1.1.1.1.2 Selectivity

Electrode catalysts must progress the reaction whilst minimizing production of undesirable by-products from side reactions. The ORR can proceed through a choice of pathways (discussed later). The pathway is determined by selectivity at the first step; the adsorption of O_2. The desired mechanism is the dissociative 4-electron reduction to produce water. It is desirable to minimize amounts of damaging H_2O_2 within the cell[28]. Various metal surfaces show that when the total number of electrons transferred in a reaction is 2, peroxide is produced but when 4 electrons are transferred, only water is produced. Previous work found Pt to be the most selective towards the desired 4-electron ORR pathway, at almost 100% selective for n=4 over a broad potential range. Figure 5 shows the selectivity of a variety of metals over a potential range towards the oxygen reduction reaction, including the number of electrons transferred [29].

[29]
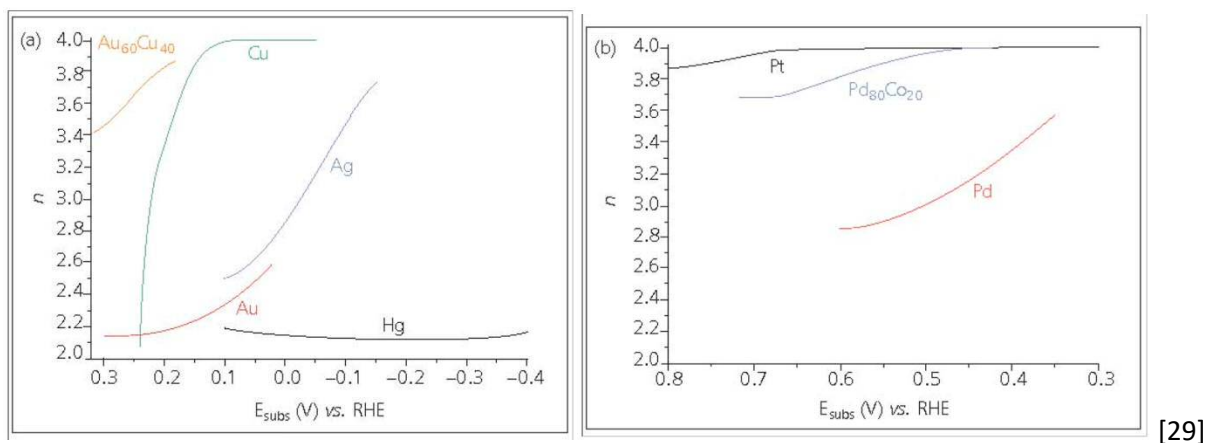
Figure 5: Number of electrons transferred (n) during oxygen reduction reaction at: (a) mercury, gold, silver, copper and Au60Cu40; and (b) platinum, palladium and Pd$_{80}$Co$_{20}$ as a function of applied potential in an oxygen saturated 0.5 M sulfuric acid solution, taken from [29]

17

1.1.1.1.3 Stability

The chemical environment within a fuel cell is harsh; strong oxidants, reactive radicals, acidic environment, high temperatures and rapid potential fluctuations[6]. Very few metals are active enough to facilitate ORR but resistant enough to avoid dramatic dissolution under fuel cell conditions. Materials that are stable have a tendency to be protected by an oxide layer that forms over the surface, which inhibits the ORR. Pourbaix diagrams have been used to map out the most thermodynamically stable domains for elements[30]. These work similar to phase diagrams by showing possible phases of an aqueous electrochemical system. Voltage is plotted against pH. Figure 6 shows the Pourbaix diagrams for a variety of elements listed in order of reactivity, (with 1 being least and 28 being most)[31]. Although there is a handful of more acid-stable metals than Pt, these have lower selectivity and activity towards the ORR, rendering Pt as the more superior metal for use in the PEMFC [30, 32].
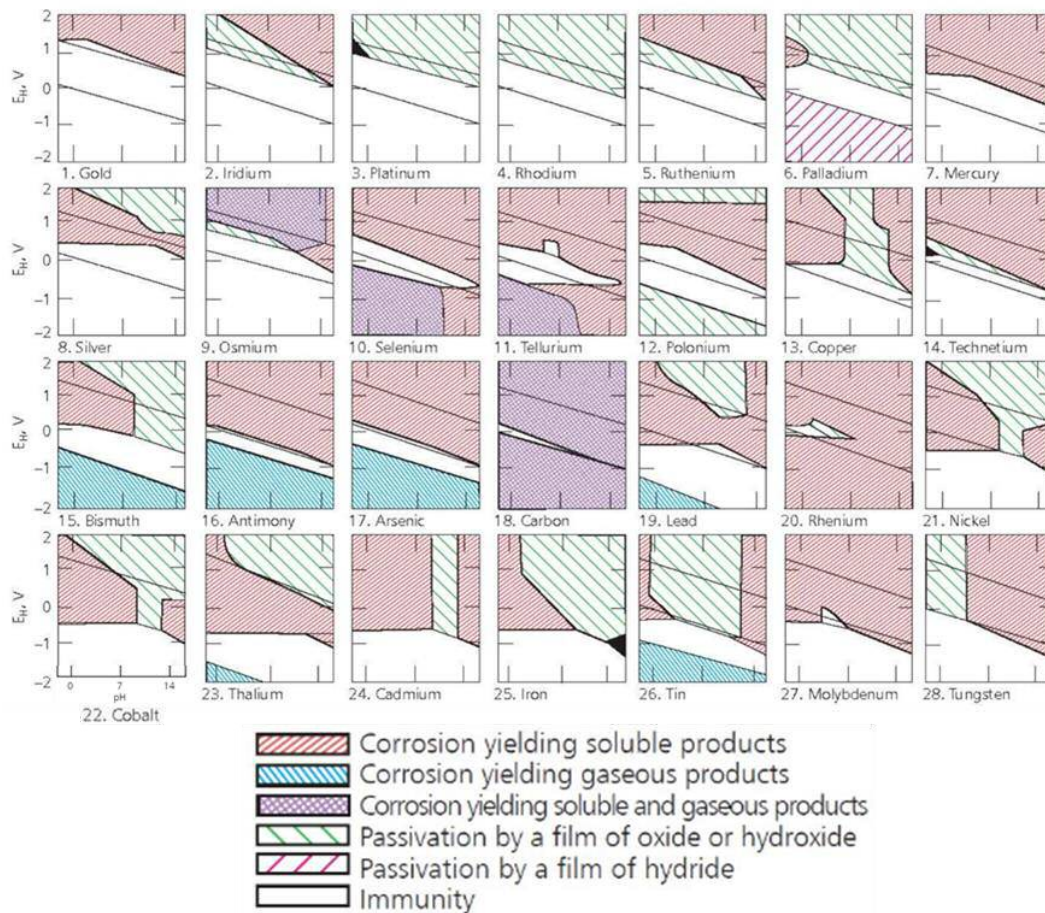
Figure 6: The Pourbaix diagrams for different elements listed in order of nobility. Taken from[30]

1.1.1.1.4 Poisoning resistance

In the fuel cell there are several opportunities of collecting impurities. All catalysts are susceptible to poisoning and the possibility of many different poisoning mechanisms makes it very difficult to create a meaningful ranking[33]. Due to Pt being successful in the previous three requirements, its poison shall be discussed. For platinum, sulphur[34] and CO[16] cause the largest poisoning problems. The source of sulphur and CO usually comes from contaminated fuels. The use of pure fuels is preferred to limit this contamination. Alloying the platinum with other metals less susceptible to these poisons also improves the tolerance of the catalyst, but can lead to lower activity towards the ORR. Increasing temperature particularly increases Pt's tolerance towards CO poisoning but this has consequences on other components in the fuel cell, namely the electrolyte. This is discussed in the next section.

To design a perfect catalyst that can be highly active towards the ORR, selective to only follow the 4-electron mechanism and be noble enough to resist against undesirable poisons, requires a deeper understanding of surface interactions. One way is to change the surface structure of the electrode. Fundamental studies on different surface structures of platinum and other metals have been undertaken[35-39], but there is still much more information to be learnt to enable significant improvements towards the ORR. This thesis explores one family of different surface structures of Pt that has not been fully investigated previously.

In a fuel cell the electrode materials (support and catalyst) are in contact with the PEM to enable transport of ions. Whilst it is important to isolate and understand the ORR on different surface structures of platinum, it is also important to understand how the presence of the PEM will impact upon this reaction. Nafion® is the material most commonly used for this[40-42].

1.2.3 The role of Nafion® in PEM Fuel Cells

The electrolytes purpose in a fuel cell is to allow only ions to transport through, whilst maintaining stability under the harsh conditions inside the cell. It must also keep the fuel and oxidant separated to avoid undesirable back reactions. The main features for a membrane in PEMFCs include; excellent proton conductivity, low cost to manufacture and excellent stability[42]. In PEM fuel cells, a solid polymer membrane is used as the electrolyte. The ionomer Nafion® has been at the forefront of the membrane electrode assembly (MEA) for a number of years[42].

1.2.3.1 The structure of Nafion
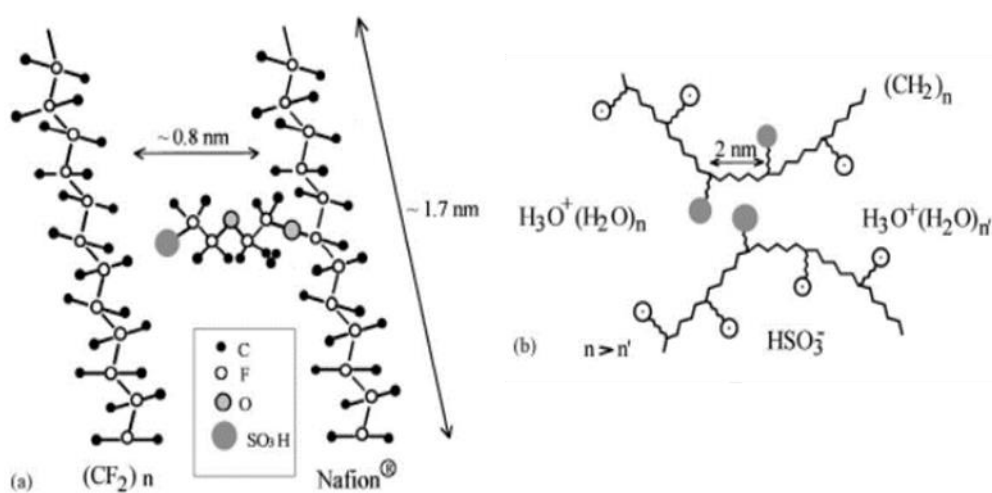
Figure 7: The structure of Nafion as shown in Ref [43]

Nafion® is a tetrafluoropolymer capable of conducting ions through its solid matrix when hydrated (Figure 7). Its structure consists of a Teflon backbone in which perfluorovinyl ether moieties ending in sulphonate groups branch off. Nafion® ionomers are produced by copolymerisation with perfluorinated vinyl ether and tetra flouroethylene[42]. Different varieties are produced depending on how many CF units separate the side chains. Equivalent weight (EW) is used to distinguish the different varieties of Nafion® and the calculation is shown below. The EW is defined as the weight of Nafion® (in molecular mass) per mole of sulphonic acid group[42]. Nafion® used in this study was 1100EW equivalent to ~14 CF_2 units separating side chains.

The structure of the Teflon backbone gives the Nafion® polymer a high operating temperature. However, Nafion® membranes only exhibit good thermal and mechanical stability in the fuel cell within lower operating temperatures (i.e. below 80 °C)[44, 45]. The membrane must also be hydrated for proton transfer to take place and the Nafion® membrane can easily dry out at higher operating temperatures (water evaporation at 100 °C). Proton transfer through the membrane of this type is very sensitive to water content, where too much water also reduces proton transfer [46, 47]. The Nafion® membrane is difficult to study due to the inconsistent solubility and crystalline structure among its various derivatives[48].

A great deal of research of the membrane and the interface has been conducted on macroscopic films[42, 49, 50]. This has provided useful insights into the behaviour of Nafion and platinum. In optimally hydrated membranes, sulphonic groups and water were found to develop an interconnected proton conducting network[40, 43, 51]. Protons transfer through the matrix by the Grotthuss mechanism[52] (Figure 8), passing along the length of the polymer chain, through the pores of the membrane. The fluorocarbon backbone forms a semi-crystalline hydrophobic phase and these regions are inactive[53]. Electrochemical processes take place at domains where hydrophilic ionic clusters are in contact with the electrode surface[50].
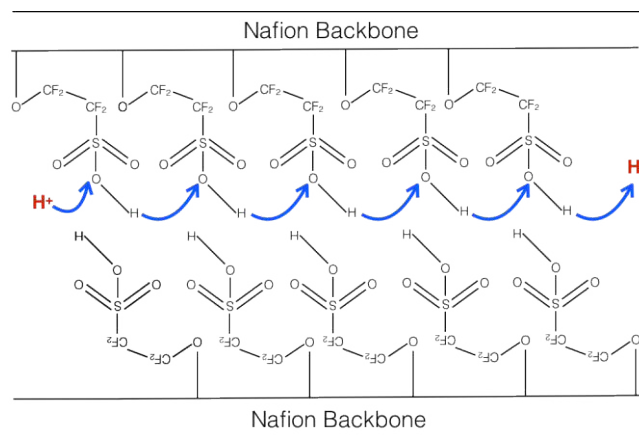
Figure 8: The Grotthuss mechanism theory applied to Nafion

Properties of interest relate to the Nafion® water content and the self-assembly of Nafion® into mesoporous structures, making its study difficult[40, 43]. Due to the actual interface being microscopic, models proposed are not always entirely fitting toward experimental data[40]. As a result, any surface model has had to rely on speculative assumptions. Owing to this fact, very little is known about the surface interactions of the membrane with catalysts[42]. It is important to fully

understand this interaction to improve the overall performance of the PEMFC (stability, selectivity etc.).

Tuning catalysts and electrolyte materials for optimum performance requires a detailed knowledge of chemical microstructure and nanoscale morphology[54]. For Nafion® membranes, proton conductivity, temperature stability and water management are some of the important properties that must be controlled in the design of near perfect membranes. This is a challenge to achieve whilst retaining a low cost. Although a number of alternate non-fluorinated polymer membranes have been developed, Nafion® is still considered the bench mark material to which most results are compared [8, 44, 48].

1.2.3.2 Bulk Studies

For the last thirty years, general concepts and morphology of ionomers have been actively debated in the literature[42]. The cluster network model (Figure 9) by Gierke *et al.* is a historical staring point of this expanding topic[49]. This model has been repeatedly used as a conceptual basis for rationalising the properties of Nafion® membranes, including such properties as ion permselectivity and transport.
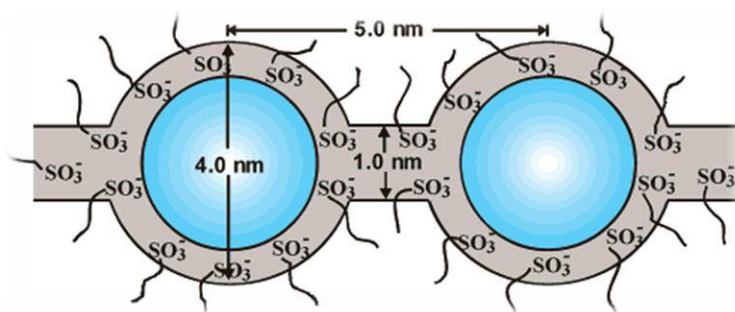
Figure 9: The cluster-network model proposed by Gierke[49]

Small angle X-ray scattering studies (SAXS) along with several postulations describe a water swollen morphology of Nafion®. It presumed that there are clusters of sulphonate ended perflouroalkyl ether groups approximately spherical in shape, organised with an inverted micellar structure. Channels were proposed to connect these spherical ionic clusters and account for the intercluster ion percolation of positively charge species through the membrane[48, 49]. As the channels would be sulphonate rich, repulsion of negative ions was also explained. Gierke's model accounted for

growth of clusters with increasing water content that later models did not. The small-angle scattering techniques used, only probed a small region of reciprocal space. Wide angle X-ray diffraction studies determined restricted polytetrafluoroethylene (PTFE) like crystallinity associated with the perfluorocarbon backbone that had not been previously considered[49]. Although it has received significant acceptance and is a foundation for many morphology studies, it has also been vigorously debated. Studies focused on variations in solvent swelling have raised critical questions related to the shape and spatial distribution of the ionic clusters within the matrix of Nafion®[42, 45, 48, 55]. The enlargement of clusters with rising water content was proposed to occur by an amalgamation of growth in cluster size and a redistribution of the sulphonate sites to yield fewer clusters in the fully hydrated material[56].
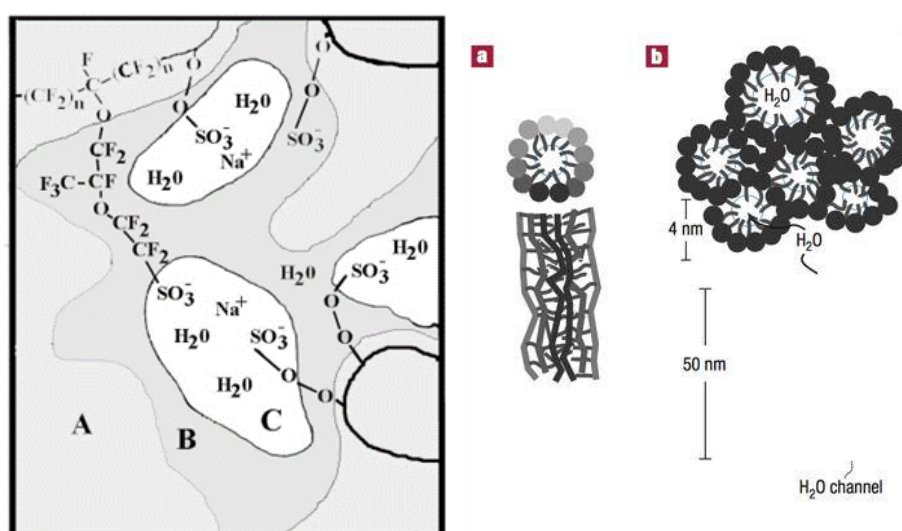
Figure 10: Left) The three-phase model proposed by Yeager and Steck[56]. Diagram corresponds to A) hydrophobic regions, B) transitional interphase between hydrophobic and hydrophilic regions and C) hydrophilic region. Right) Nafion models by Schmidt-Rohr [57] Parallel water-channel model of Nafion where a) Two views of an inverted-micelle cylinder, with the polymer backbones on the outside and the ionic side groups lining the water channel. Shading is used to distinguish chains in front and in the back. Schematic diagram of the approximately hexagonal packing of several inverted-micelle cylinders

More extensive structure investigations have been carried out following Gierke's beginning, which ultimately led to the suggestion of alternate morphologies. Yeager and Steck proposed a three phase model[56] significantly different to Gierke (Figure 10). The clusters were still found to be spherical inverted micelles connected by cylindrical pores with a low degree of order. Most importantly, it was found that there were transitional interphases between hydrophilic and hydrophobic regions. Schmidt-Rohr and Chen (Figure 10) also used neutron scattering to establish that self-assembly of Nafion® leads to the formation of hydrophilic and hydrophobic regions[57]. This concept is becoming increasingly accepted.

Roche *et al.* used SAXS and SANS (small-angle neutron scattering) techniques to investigate the morphology of Nafion® membranes in different states[58]. This included varying water contents and with the Nafion® being in acid/neutral forms. They found Nafion® to have three contrast regions and concluded that a non-random distribution of side chains existed in a portion of the membrane or the crystalline structure[58]. An inhomogeneous distribution of cluster within the matrix was also proposed to account for the zeroth order scattering results that were found. These results demonstrated that this order is not attributed to impurities as had been previously proposed for other ionomer systems[48, 56]. In agreement with the work of Gierke *et al.*, Roche and co-workers also found that the intensity of the ionomer peak (seen in X-ray diffraction studies) increased with increasing water content[56]. However, Roche *et al*. disagreed with some concepts associated with Gierke's cluster-network model. As an alternative, the origin of the ionomer peak found in XRD studies was attributed to an intra-particle scattering model for which the scattering maximum corresponded to characteristic distances between structural elements inside the ionic particles. While this intra-particle scattering model was consistent with the morphology proposed for other ionomers, a detailed quantitative analysis in support of this model was not provided by Roche.
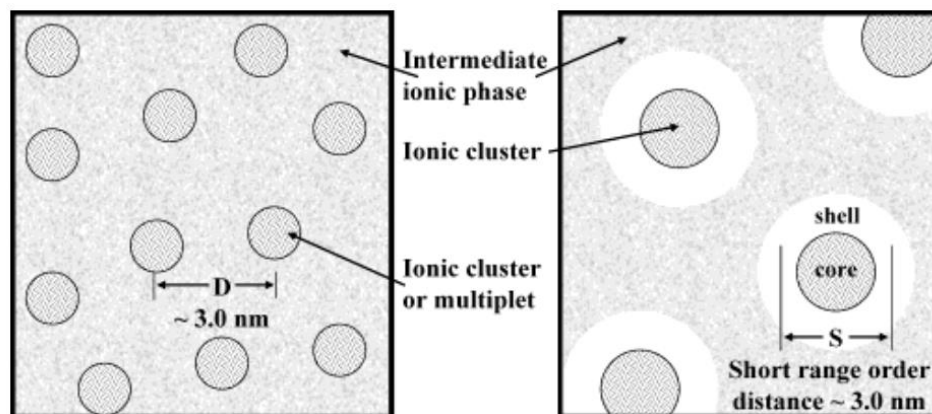
Figure 11: Two morphological models of Nafion used to describe SAXS results in [59]

Fujimura *et al.* focused on defining the morphological origins of the two scattering maxima and evaluating various scattering models for the origin of the ionomer peak (Figure 11). Again, with increasing water content, the cluster dimensions deduced from the scattering maxima were shown to increase. Over a range of water contents, the microscopic degree of swelling, as determined by SAXS, was found to be much greater than the macroscopic degree of swelling. It was concluded that the scattering behaviour of Nafion® is best described by an intra-particle core-shell model similar to that proposed by MacKnight and co-workers[58]. In this particular core-shell model an ion-rich core is enclosed by an ion-poor shell composed largely of perfluorocarbon chains. These core-shell

24

particles are dispersed in a matrix of fluorocarbon chains containing non-clustered ions and multiplets, such that the short-range order distance within the core-shell particle gives rise to the ionic scattering maximum[58].

It is important to note that the argument against the interparticle hard sphere model relies on the key assumptions that the clusters are uniformly distributed in space and that no redistribution of the ionic groups occurs during swelling. However, the cluster-network model proposed by Gierke clearly allows for cluster reorganization during swelling, and the low angle upturn in scattering intensity observed by Roche *et al*. strongly suggests an inhomogeneous distribution of clusters[49, 58].

As has been demonstrated, many models have been proposed about the bulk nature of Nafion®. Work has identified a semi-crystalline structure in which the hydrolysed form contains ionic clusters. The size of these clusters has been debated as well as the interconnectivity of them which allows swelling and permittivity to cations. Amendments to this original discovery had led to variation where the backbone can adopt a helical or laminar structure[42, 60]. Long range order has also been questioned. Although a more comprehensive review of the bulk structure of Nafion® is beyond the capacity of this investigation, this discussion was necessary to highlight factors of interest. We will take these ideas forward when discussing the Nafion®- Platinum-electrolyte interface in detail.

1.2.3.3 Interfacial Studies

The many interpretations for the bulk Nafion® structure all agree that the sulphonate groups are arranged into some form of clusters[42]. For the interface, only a few studies have been carried out using in-situ analysis. Malevich and co-workers found that the presence Nafion films on platinum NPs slowed the CO oxidation reaction[61]. SNIFTIRS (Subtractively Normalised Interfacial Fourier Transform Infrared Spectra), in IRRAS mode (infrared reflection absorption spectroscopy), also demonstrated that sulphonate groups orientate themselves towards the surface with potential[61]. When the potential is reversed the groups were then displaced. This study however was carried out on 5μm thick films, which are unlike the one or two atom layers used in this thesis.
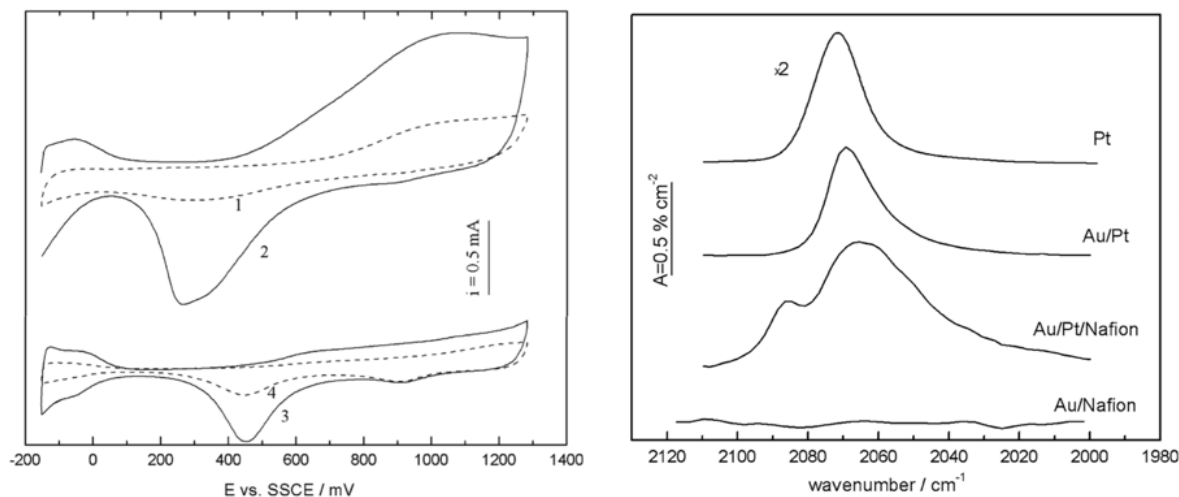
Figure 12: Results for Nafion on polycrystalline Pt [62]. Left) CVs in 0.1 M HClO4 and right) IR data of absorbed CO

Surface enhanced IR spectroscopy (SEIRAS) was employed by Ayato *et al.*, to analyse the Nafion®-platinum interaction in situ[62]. A Platinum-plated prism was coated in Nafion® and the spectrum compared with Nafion® on a silicon prism. Similarities with platinum adsorbed bisulphate and sulphate bands allowed an observed absorbance to be identified as the asymmetric stretch of the sulphonate anions. The sulphonate bands were found to be red-shifted by changing potential, suggesting that sulphonates interact with the platinum surface in a potential dependent manner. The long pendant structure and nature of the side chains were proposed to allow the sulphonate groups to behave as free anions[62].

1.2.3.4 Electrochemistry

Recently, electrochemical studies have been performed on Nafion® coated polycrystalline platinum electrodes. Jiang & Kucernak originally reported on the hydrogen oxidation and methanol electro-oxidation reactions when Nafion® was deposited on Pt and Au[63, 64]. The voltammograms produced of the Nafion® coated platinum films showed reduced charge under the H_{upd} and oxide regions. Both electro-oxidation reactions were found to be dependent on temperature and water content of Nafion®. Tu *et al.* reported on voltammograms of Pt/black powder electrocatalyst pressed against a Nafion® membrane[65]. The Pt features in the voltammograms were reported to be inhibited in the presence of Nafion, similar to that observed by sulphate®[66].
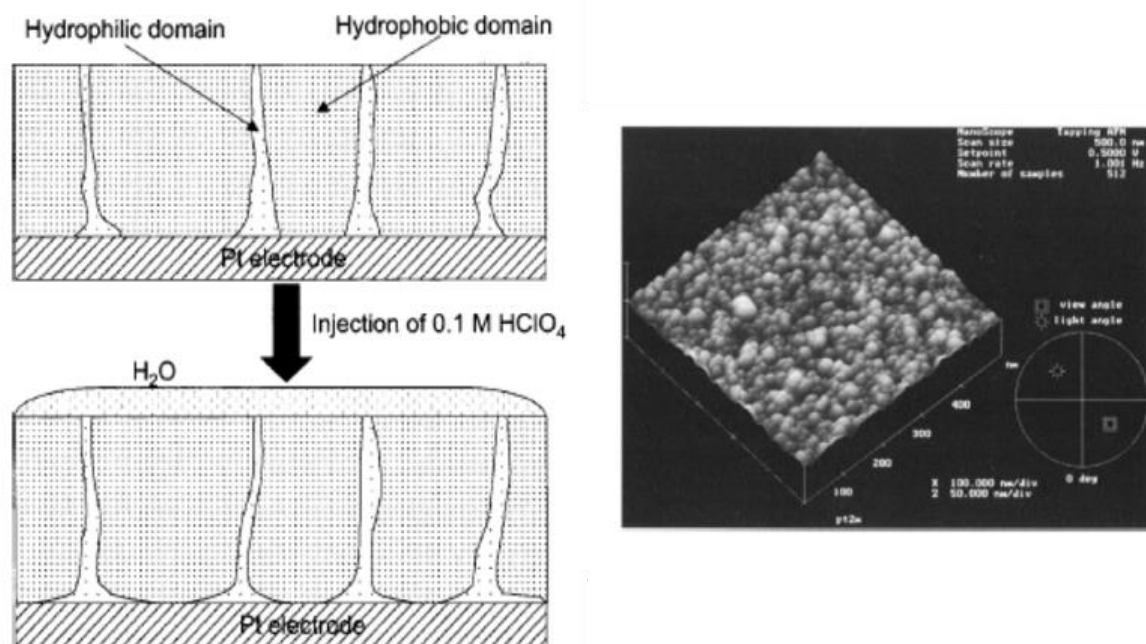
Figure 13: Findings from Gruger concerning Nafion adsorbed on polycrystalline platinum. Left shows a schematic illustration for the interfacial behaviour of the Nafion membrane on Pt electrode. Right shows an AFM image of the prepared Pt thin-film electrode[43].

Chu *et al.* studied the effect of Nafion® on the activity of PtRu electrocatalysts for methanol electro-oxidation[9]. No voltammograms were provided in order to characterise the Nafion® free and coated PtRu electrocatalyst in this study. However, Chu reported an enhancement in the electro-oxidation of methanol for the PtRu:Nafion® electrocatalyst. Maruyama *et al.* explored the influence of a Nafion® films in fuel cell reactions, more specifically on the hydrogen oxidation reaction[67]. This study on the HOR kinetics were found to be enhanced on the Nafion® coated electrode. Miyatake *et al.* explored ORR on a Pt-black electrocatalyst coated with a sulphonated polyimide sulphonated ionomer[68]. ORR was found to be kinetically controlled for a thin ionomer coating but for thicker ionomer films, oxygen diffusion through the film was found to be negligible. Lawson *et al.*, Gottesfeld *et al.* and Floriano *et al.* have shown in the cases of HOR and ORR, an increase in electrocatalytic activity in the presence of Nafion[69-71]. This was attributed to higher O_2 and H_2 solubilities in recast Nafion® than those in aqueous solutions, which is mainly due to the presence of the hydrophobic fluorocarbon phase. However, the detailed mechanism of these modifications is still under discussion.
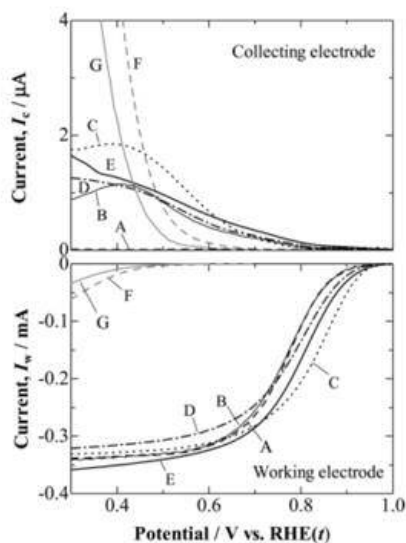
Figure 3. Hydrodynamic voltammograms for the ORR in O_2 saturated 0.1 M $HClO_4$ solution at Pt(bulk) (A), Nafion-coated Pt(bulk) (B), Nafion-Pt(46.7 wt %)/CB with $m_{Pt} = 4.78\ \mu g/cm^2$ (C), Nafion-Pt(19.3 wt %)/CB with $m_{Pt} = 1.30\ \mu g/cm^2$ (D), Nafion-Pt(19.3 wt %)/CB with $m_{Pt} = 2.60\ \mu g/cm^2$ (E), Nafion-CB (F), and Au (G) electrodes at 30 °C and simultaneously acquired currents (I_c) at Pt collecting electrodes for the oxidation of H_2O_2 (by-produced at the working electrodes). Potential scan rate = 0.5 mV s^{-1}. Potential of the collecting electrode = 1.2 V. Mean flow rate of electrolyte $U_m = 50$ cm s^{-1}.

Figure 14: Findings by Yano [72] concerning Nafion® coated Pt systems exhibiting lower ORR activity and more H_2O_2 production than the bare Pt electrode system

Work by Yano *et al.* and Ohma *et al.* have both shown that Nafion® coated Pt systems exhibited lower ORR activity and more H_2O_2 production than the bare Pt electrode system[72, 73]. This work suggested that sulphonate groups in Nafion® strongly adsorb on Pt sites and modify the surface properties. The behaviour of ORR on a Nafion® coated Pt microelectrodes was also reported to be inhibited compared to a bare Pt microelectrode[74]. Electrochemical Impedance Spectroscopic (EIS) analysis also found the ionic conductivity of Nafion® was potential dependent due to the production of water from ORR[75]. Chu *et al.* reported the behaviour of the redox couple Fe^{2+}/Fe^{3+} at a Pt/Nafion® interface and Au/Nafion® interface[76]. It was found that there is an enhancement in the electrosorption peaks of the redox couple at the Pt interface, however the redox couple is inhibited at the Au/Nafion® interface.

The studies performed in the previous references have been on platinum electrocatalysts and none were on single crystal electrodes. Using single crystal electrodes (SCE) and employing the use of surface sensitive electrochemical techniques such as cyclic voltammetry it is possible to characterise electrochemical processes and electrocatalytic reactions at a fundamental level.

1.2.3.5 Single Crystal Electrodes

Most recently, two separate research groups reached similar conclusions about the behaviour of Nafion on single crystal electrodes (SCE) [77-79]. Thin films of Nafion® were deposited onto clean, low Miller index platinum single crystal surfaces and CV were recorded in two acidic electrolytes ($HClO_4$ and H_2SO_4). The use of a sulphate electrolyte and a supposed 'special', non-adsorbing electrolyte made the true implications of the Nafion® clear. Voltammetry results observed by Markovic *et al.* (Figure 15), indicated some adsorbing species comparable to sulphate anions intrinsic to the Nafion® structure[79]. CVs exhibited quenching of OH_{ads} and a new peak at 0.54 V for Nafion® coated Pt(111). Given the positions of the Nafion® peaks in perchloric acid relative to the sulphate groups recorded in sulphuric acid, it was proposed that the adsorbing species is the sulphonate group[79]. Due to similarities in geometry, sulphonate groups were expected to coordinate with the Pt(*111*) surface in a similar manner to the bisulphate. The nature of the adsorbate was further investigated in a CO displacement experiment, which confirmed the adsorbed Nafion® species to be anionic.
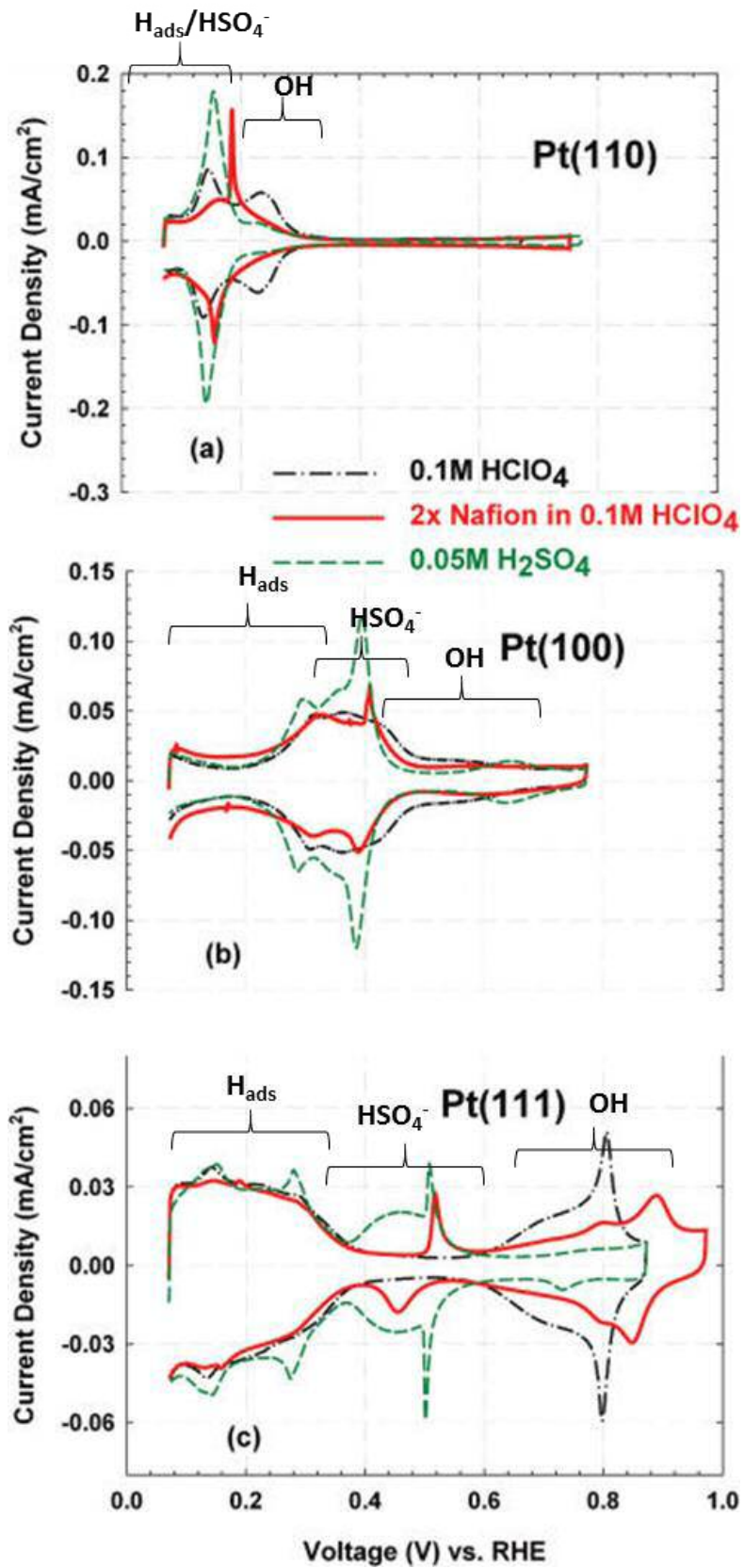
Figure 15: results of Nafion thin films on Pt(hkl) electrodes. Reprinted from Markovic paper[79].
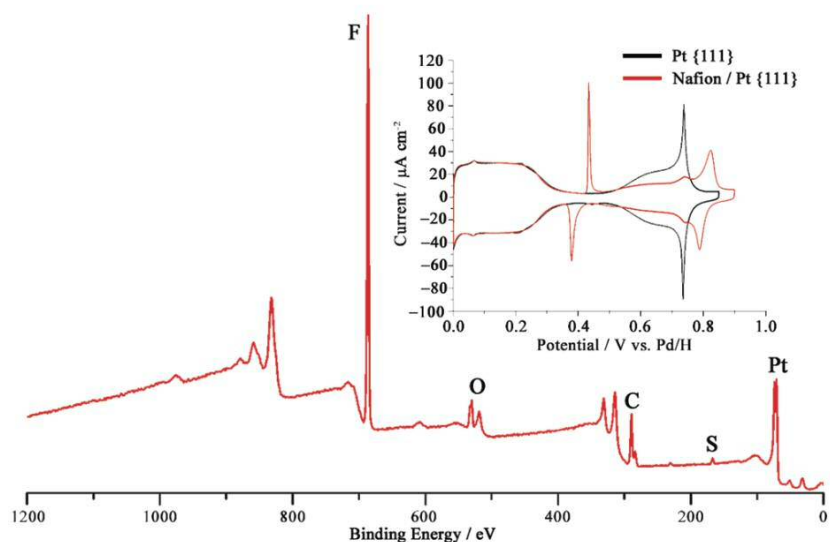
Figure 16: Comparable CV response to Markovic work[79] by the Attard group, showing XPS data of Nafion film on Pt(111) with corresponding CV data with and without Nafion adsorbed [78].

The intensity of the Nafion® sulphonate peak was much less than that of the bisulphate peak observed in the voltammograms[79]. When the bulkier structure of Nafion® is considered, a full monolayer of sulphonate anions would be geometrically unachievable. Nafion® sulphonate groups are not entirely free like sulphate ions, but are held in place at a certain distance by the flouropolymer backbone[42]. This inhibits desorption and explained the irreversibility of the new peaks seen in the voltammograms. Further investigation of Nafion® films with differing composition showed that larger cations affect the adsorption/desorption potentials and the amount of current exchanged[79-82]. It was also found that those with the highest degree of proton exchange transferred the biggest charge at the most negative potential. A 'spring-model' (Figure 17) was proposed, deducing the dependence of potential on sulphonate adsorption[79, 83]. The model works by two actions competing; counter-cation sulphonate and side chain interactions pull sulphonate groups away from the surface, whilst electrostatic forces pull them towards the metal surface when electrons bear a positive charge. This model explained the properties uncovered in studies with larger cations, (where a higher charged species decreases the influence of the electrostatic interactions and potential controlled adsorption is observed). Later, ORR studies on Nafion® coated low index platinum single crystals, found that the ORR was inhibited in the presence on Nafion® films, compared to bare platinum surfaces[79].
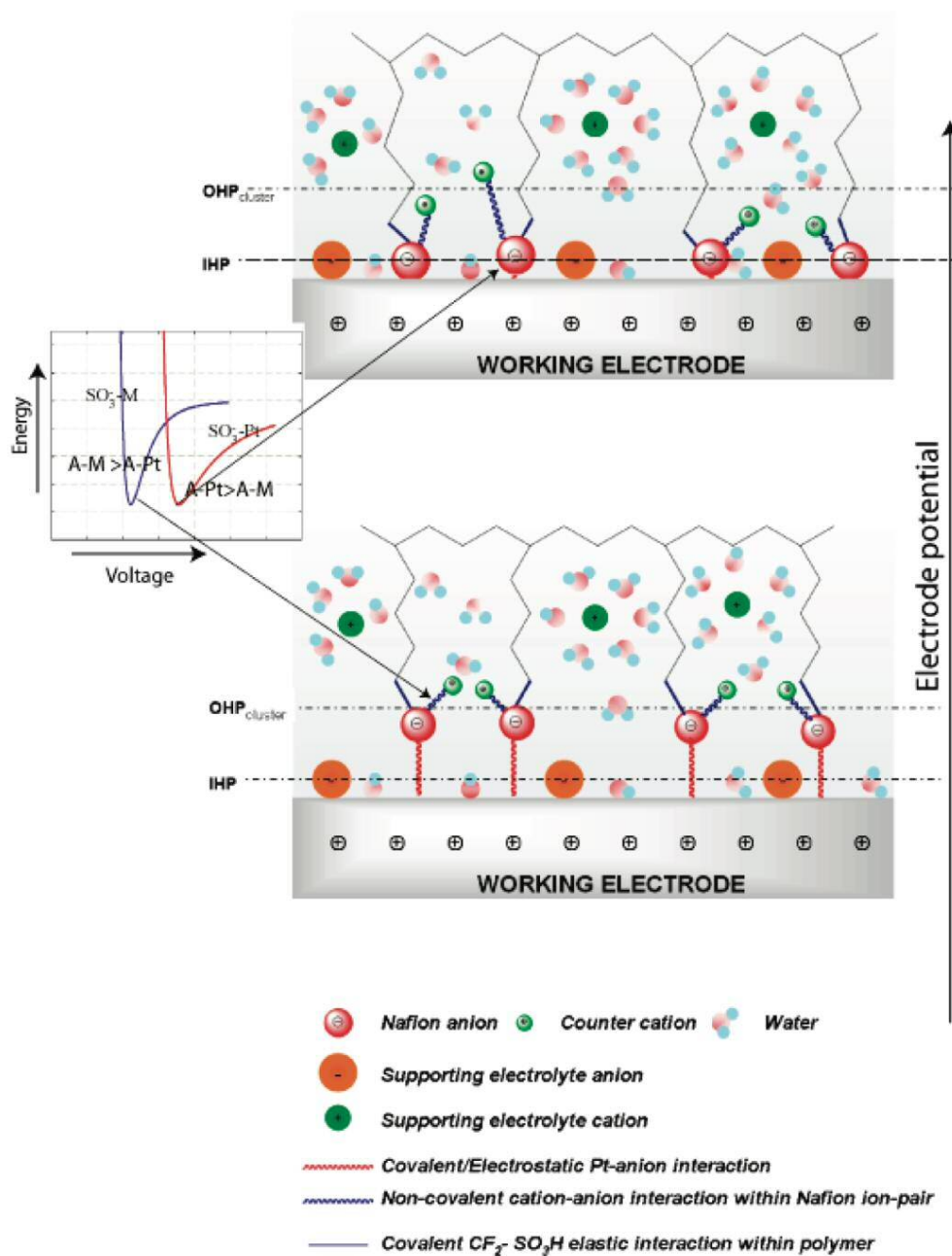
Figure 17: Schematic of the proposed "Spring Model" by Markovic. The anions' interaction with the polymer matrix are represented by noncovalent interaction with the counteraction, the interaction with the working electrode is represented as covalent/electrostatic interaction depending on whether the anion is specifically adsorbed on the surface (top) o away from the surface (bottom). The energy diagram shows the existence of two "energy wells" corresponding to anion-ionomer (A-M) equilibrium and anion-Pt (A-P) equilibriums. Electrode potential establishes the relative position of the anion compared to its energy minima. Not drawn to scale[79].

Attard and co-workers confirmed the findings for ultra-thin Nafion® films on platinum(*hkl*)(Figure 16), but also highlighted new data pertaining to the behaviour of Nafion® at stepped platinum electrodes (Figure 18) [78]. The main conclusion drawn from these studies was that Nafion® is an electrochemical probe of adsorbed OH as it acts as a specifically adsorbed anion.
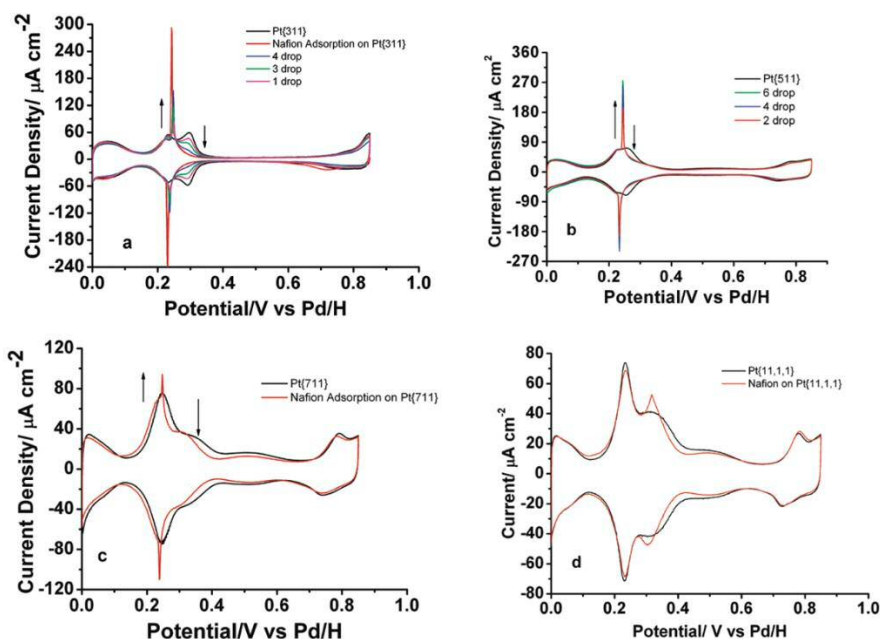
Figure 18: CVs response of Nafion covered Pt(hkl) with variety of coatings by Attard group [78].

Modern methods for obtaining clean electrochemistry have been shown to help understanding of complex hidden interfaces such as Nafion®-Pt. This is only a starting point however, as more understanding of this phenomenon, such as with other atomic surface structures of platinum, will allow for great steps to be taken in the development of fuel cells. The scope of this thesis will attempt to study Nafion films on Pt single crystals of high miller index planes.

1.3 Electrocatalysis

1.3.1 Introduction

Berzelius first identified a catalyst as[84, 85]:

"Reactions that are accelerated by substances that remain unchanged after the reaction"[86].

Lemoine later discovered catalysts do not change the position of the equilibrium as first thought, they only alter the rate at which it is reached[87]. Electrocatalysts are catalysts that participate in electrochemical reactions. They reduce the potential above or below the equilibrium potential (overpotential) required to create the same amount of chemical product as an uncatalysed reaction[87].
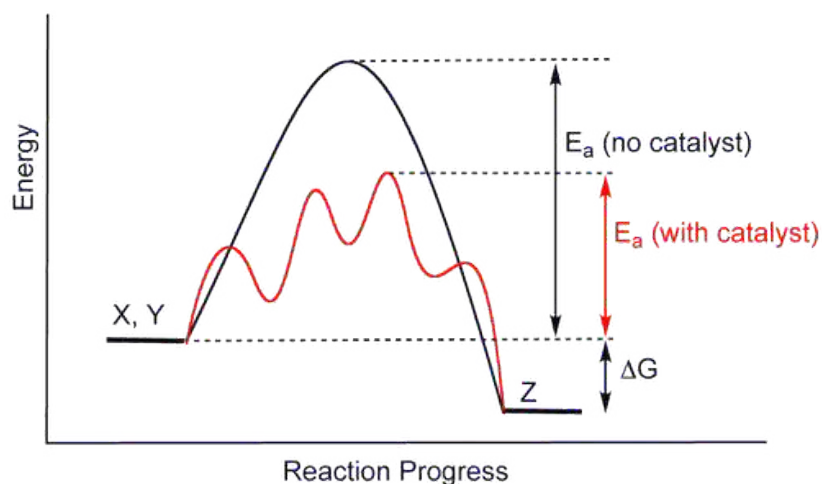
Figure 19: Energetics of a catalysed and non-catalysed reaction

Before the 19th century, electrochemical processes had not been identified and the field of electrochemistry did not exist. In trying to understand electricity and making the first battery in 1800, Volta planted the seeds for electrochemistry as a new field[88]. He proved that electricity flows between two different metals by creating a stack of alternating silver and zinc disks, separating each layer by moistened cardboard. In the early 1800's electricity was being used to cause chemical reactions without much understanding of the connection between electricity and chemistry[88]. It was Davy who first commented on this interaction by asserting that "electricity produced in electrolytic cells was caused by chemical reactions"[87]. Faraday quantified this interaction by discovering the two laws of electrochemistry[87];

1. The amount of a substance deposited on each electrode of an electrolytic cell is directly proportional to the amount of electricity passing through the cell.
2. The quantities of different elements deposited by a given amount of electricity are in the ratio of their chemical equivalent weights.

Kobozev had already coined the term electrocatalysis in 1936[86], but intentional use of electrocatalysts didn't occur until decades later. Grove's experiments the late 1830's proved that Faraday's laws (electrolysis) were also applicable in reverse[3]. Reactions between chemicals produced an amount of electricity proportional to the amount of chemicals consumed. Electrolysis was (and still is) one of the first processes utilised heavily in industry for extraction of pure elements (such as aluminum and chlorine)[54, 87]. As this field became a more academic as it was appreciated that electricity consumption in such processes such as electrolysis could be reduced by the right choice of electrode catalyst. This increasing awareness led to the understanding of electrocatalysis also being structure sensitive. This generated a surge of academic studies towards a greater understanding of electrochemical processes involved. In these studies, many techniques were devised that enabled investigating the electrode-electrolyte interface adsorption processes[88], including the use of single crystal electrodes[85, 89, 90].
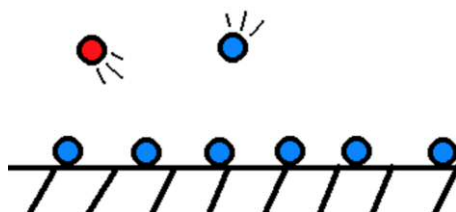
1.3.2 Adsorption

In catalysis, some form of intermediate adsorption process occurs between catalysts and reactants during the reaction and therefore it is imperative to understand the basic concepts of adsorption[91].

Surface atoms compared to the bulk are under coordinated. Therefore, there is excess energy at the surface compared to the bulk. To relieve this energy, the surface may relax, reconstruct or adsorb external species[85].

Adsorption is defined as [11]:

"an increase in the concentration of a substance at the interface owing to the operation of surface forces"

Adsorption is a thermodynamically favourable process by which molecules adhere to a surface[91-93]. Preferential concentration of species at the interface is the direct result of surface energy requirements. Surfaces can reduce their free energy by interacting strongly with ions in solution or molecule in the gas phase, to satisfy the valency of surface atoms exposed[11, 91]. There are two classifications of adsorption: Chemisorption and Physisorption[93, 94].

1.3.2.1 Chemisorption

Chemisorption is characterised by the exchange of electrons between adsorbate and surface. It is where 'real' covalent chemical bonds are formed[91]. A larger adsorption enthalpy results in greater extent of surface interaction and hence, coverage of the surface. If the interaction is too great, the adsorbate becomes difficult to remove from the surface and the surface is effectively 'poisoned'. The Sabatier principle postulates that the best interactions between catalyst and the substrate should be neither too strong nor too weak[54]. For effective catalysis, the formation of the chemical bond is often directional with respect to a particular molecular orbital and specific surface site. Typical chemisorption bonds are ~40-300 kJ mol^{-1}[91].

1.3.2.2 Physisorption

Physisorption is where surface bonds much lower in energy than those of chemisorption due to weak Van der Waals or dipole interactions. Electrons are redistributed within the molecule and surface forming a polarised state. No electrons are exchanged between the surface and adsorbed molecule. Typically, the energy of the physisorbed bond is ~2-30 kJ mol^{-1}[91].

Typically, traditional ideas of adsorption relate to gaseous molecules on a solid surface. In PEM fuel cells, adsorption occurs at the electrode-electrolyte interface. At the metal-solution interface all the molecules are already condensed. This is important to consider because when adsorption occurs, the adsorbate is always replacing some other species[11]. Interactions between solid electrode and electrolyte give rise to disruption of the components of the electrolyte solution. For electrodes under potentiostatic control, the charge held at the electrode influences adsorption. The electrochemical double layer is a model used to describe charge distribution and potential at the surface of a charged electrode in solution[91, 93].

1.3.3 Electrochemical Double Layer

When a metal is placed in contact with an electrolyte an interface is created. There is a potential difference between the two and therefore the electrode may be positively or negatively charged with respect to the electrolyte. Electrostatic interactions occur between the electrode and electrolyte. Ions of opposite charge are concentrated at the interface and dipole moments of the solvent molecules tend to orientate towards the electrode. As the strength of charge changes over distance, a structure distinct to the bulk electrolyte exists at the electrode-electrolyte interface. This interfacial structure is known as the electrical double layer[91, 95].

A number of models have been defined over a number of years to come to a distinguished understanding of the double layer. It is important to briefly discuss the evolution of its beginnings to gain a perspective of today's understanding.

1.3.3.1 Helmholtz double layer

Helmholtz considered the double layer to be analogous to a parallel plate capacitor, where two layers of charge are separated by a fixed distance. Whichever charge the electrode has, is cancelled out by the electrolyte, which contains a layer of opposite charge. The potential drop at the interface is abrupt and linear. Ions are assumed to approach the electrode from the bulk up to a specific distance, known as the outer Helmholtz plane (OHP). This is the closest distance that the ions can approach. The distance is limited by the ions solvation shell[96]. As the double layer capacitance is considered the same as a parallel plate capacitor, it assumes the differential capacitance (change in charge with potential) is constant. This was later found to be incorrect as the differential capacitance varies with potential, a factor accounted for in the Gouy-Chapmann double layer model[85, 96].
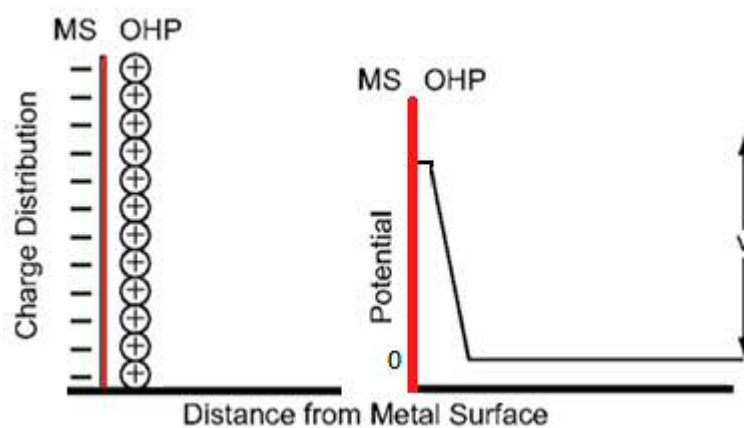
Figure 20: Helmholtz model of the double layer at the electrode/electrolyte interface. Charge distribution vs. distance, left, and potential variation vs. distance, right. MS = metal surface, OHP = outer Helmholtz plane. Reprinted from [97]

The Helmholtz double layer model was adapted to include a diffuse layer to model how the differential capacitance varied with potential[96]. In this model, ions at the electrode surface are not a single layer but are dispersed by Brownian motion. Layers of ions are in high concentration close to the electrode and decrease as distance from the electrode in increased. This model accurately simulated the capacitance observed at potentials close to the point of zero charge(PZC) but became more inaccurate at potentials further away from the PZC[97].
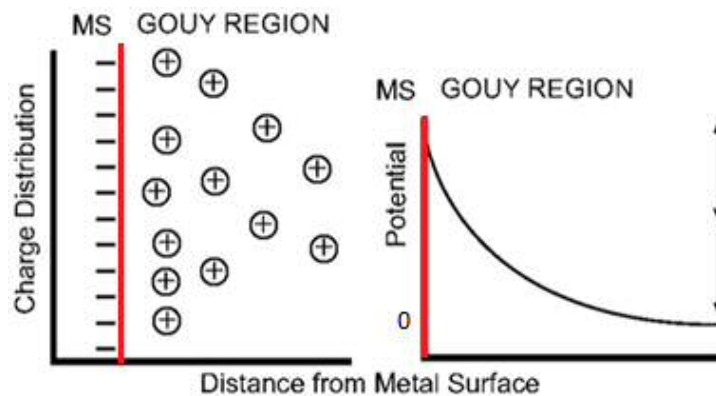
Figure 21: Gouy-Chapman model of the double layer at the electrode/electrolyte interface. MS = metal surface. Reprinted from [97]

1.3.3.2 Stern double layer model

Stern combined the Helmholtz and Guoy-Chapman models. Combining the ideas of the OHP and diffuse layer accurately described the observed potential differences from the electrode-electrolyte interface to the bulk electrolyte[97]. In this model, a linear potential drop is observed between the electrode and OHP, followed by a non-linear potential drop through the diffuse layer due to Brownian motion. The Stern model accounts for high and low concentrations of ions in the solutions but not the possibility of certain ions which may "specifically" adsorb[96].
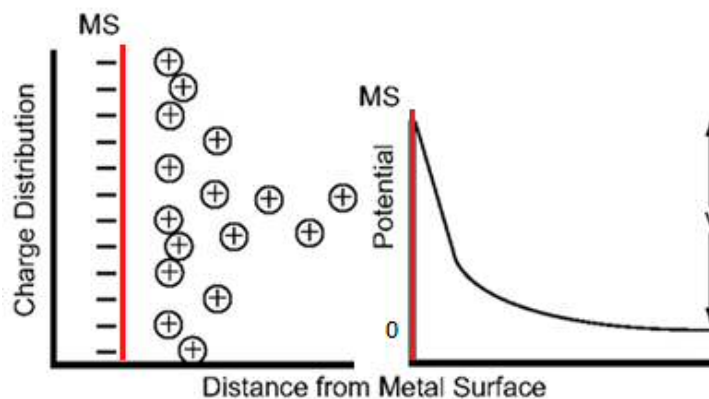
Figure 22: Stern model of the double layer at the electrode/electrolyte interface. Reprinted from [97]

1.3.3.3 Grahame

The Grahame model considered that some ions were able to approach closer to the electrode surface than the OHP[97, 98]. It was proposed that an ion could lose part, or all of its solvation shell to enable direct contact with the electrode surface. The closer distance was name as the inner Helmholtz plane (IHP) and ions able to achieve this were known as being "specifically adsorbed". Through specific adsorption, negatively charged species in the solution lose their weakly bound hydration shell in favour for a stronger connection with the surface. Small positive ions often exhibit strongly bound hydration shells and rarely specifically adsorb. The occurrence of these ions in solution could mean an electrolyte containing negatively charged ions in contact with a negatively charged electrode (depending upon the potential) could cause a small drop in potential before the increase from the IHP to the OHP[96].
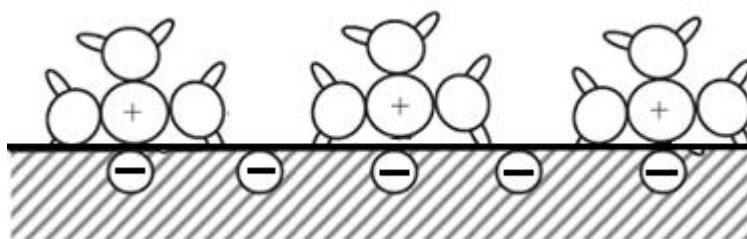
Figure 23: Schematic of molecules adsorbing closer than the OHP, known as specific adsorption

1.3.3.4 Bockris-Devanathan-Muller (BDM)

Final contributions to the understand of the double layer came in considerations of solvent molecules being orientated by the field of the electrode. The BDM model proposes that layers of solvent molecules are orientated to a progressively larger degree the closer to the surface they are. This explained how the dielectric constant varied through the solution[97]. In recent years, advances in technology and theoretical modelling have allowed even further understanding of the double layer through statistical mechanics[99-101], of which, is above the scope of this thesis.
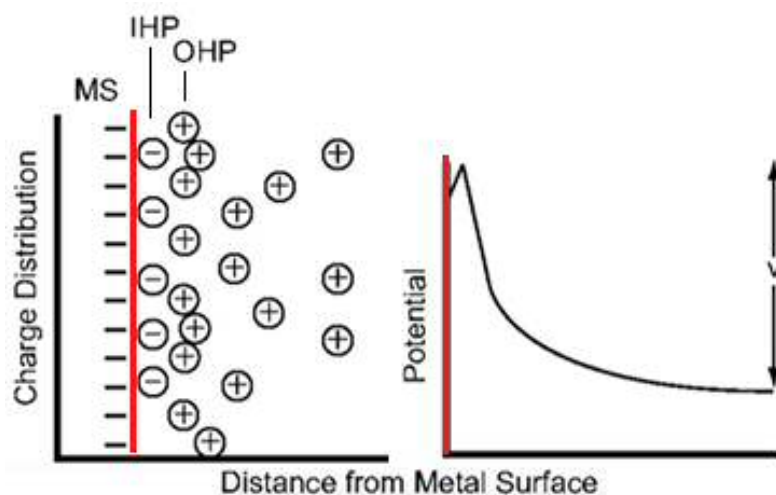
Figure 24: BDM model of the double layer at the electrode/electrolyte interface. IHP= Inner Helmholtz plane. [97]

As well as pure scientific interest, the use of electrocatalysis is paramount in tacking global challenges such as climate change. Improvements on current devices, and design of future electrocatalysts will only arise from a greater understanding of catalyst surface interactions. One of the most important features of electrocatalysis arises from the different electrode kinetics using different crystallographic orientations for the electrode surface[91, 93].

1.3.4 Surface Structure of Metal Electrodes

Surface structure plays an important role in the adsorption kinetics at the electrode-electrolyte interface. Real catalytic surfaces are not well-defined and can consist of a mixture of facets, steps, kinks, terraces and defect sites[102]. These different sites contain different energies due to different local atomic arrangements and therefore have different electronic properties[102-104]. Some sites may promote a specific reaction, whilst some may inhibit the same reaction. This is an important fact to consider when tuning the catalysts properties. Due to the expense of some catalysts (such as Pt in PEMFCs) it is vital not to waste any of the material by having the wrong atomic arrangement for a specific reaction. It is important to understand the relationships of specific surface atomic arrangements and reaction activity. Fundamental understanding will inform which atomic arrangements are most favourable towards said reaction. Catalysts can be designed which contain only the best sites for a specific reaction, such as shape nanoparticles[17, 105].

Real surfaces are not suitable to directly study as their electrochemical behaviour observed is a sum of the contributions from the individual sites. Instead, it is more desirable to use atomically well-defined surfaces that contain controlled specific sites. Well-defined surfaces can be obtained by cutting a single crystal along a given crystallographic plane to create a single crystal electrode[106].

1.3.4.1 Miller indices

The surface structure of a metal reflects its underlying bulk structure. Platinum forms a face centred cubic (fcc) bulk structure. Different surfaces can be formed using this arrangement and how they are identified is discussed below.

F (Face)
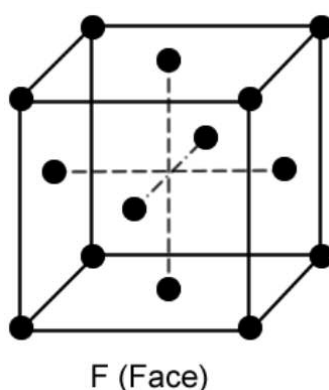
Figure 25: The unit cell for a face-centred cubic (fcc) crystal structure

A single crystal surface consists of one repeating pattern throughout the whole material. By cutting through a single crystal at various angles, a unique surface arrangement of atoms is exposed[106, 107]. The generated surface may be defined by its Miller Indices (hkl), which corresponds to the smallest three integers in the same ratio as the inverse of the coordinates of the plane with the crystallographic unit vectors (Figure 25)[106]. If h, k or l are either 1 or 0, then cutting through the crystal plane will form an atomically flat surface. For a FCC, the three low Miller index surfaces define the vertices of the stereographic triangle and are: (111), (100) and (110). These are known as the basal planes and are shown in Figure 26.
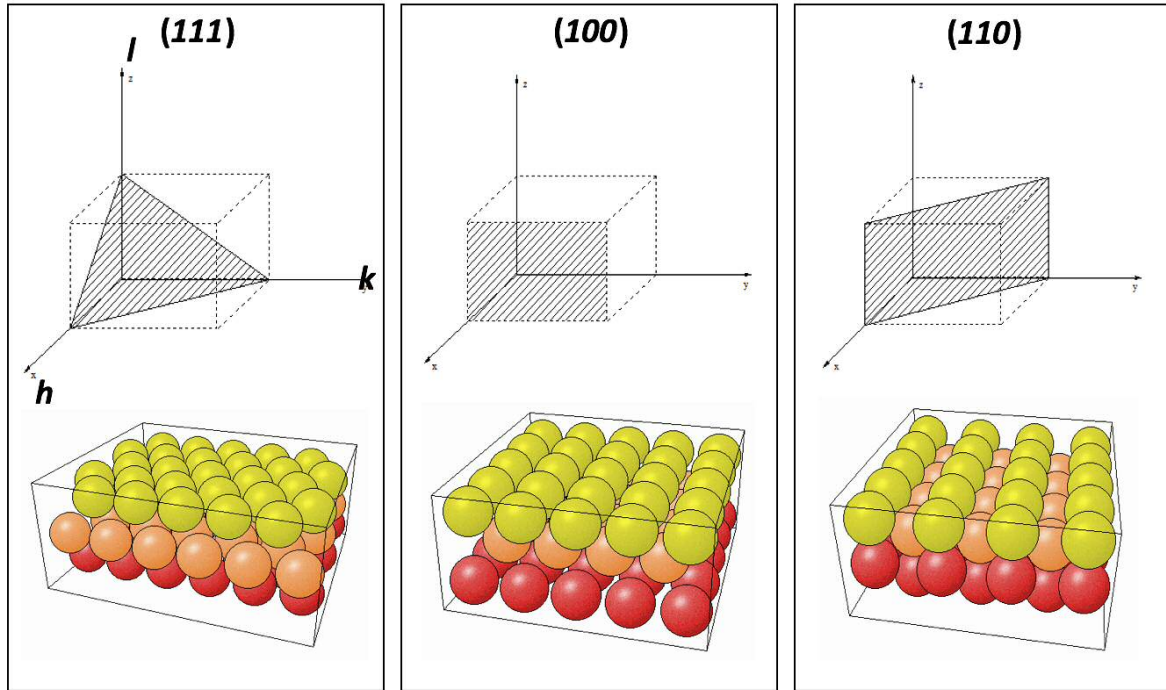
Figure 26: Base plane atomic arrangements of the fcc system. From left to right, (111), (100) and (110).

Introducing steps at regular intervals, gives rise to surfaces having miller indices greater than one. planes are referred to as high Miller index surfaces and may be defined by microfacet notation[85, 106]. These planes intercept at fractional values of the unit cell axis. These planes contain flat areas (terraces) which have an atomic arrangement of one of the three basal planes combined with monoatomic steps. The stereographic triangle (Figure 27) shows how the three basal planes as the poles of the stereographic triangle and the stepped surfaces associated with each pole represented at each zone (side). The current work is focused the surfaces between the (100) and (110). By investigating the individual basal planes with systematic changes, a clearer fundamental understanding of adsorption can be gained that can be taken forward to examine real surfaces in more detail.
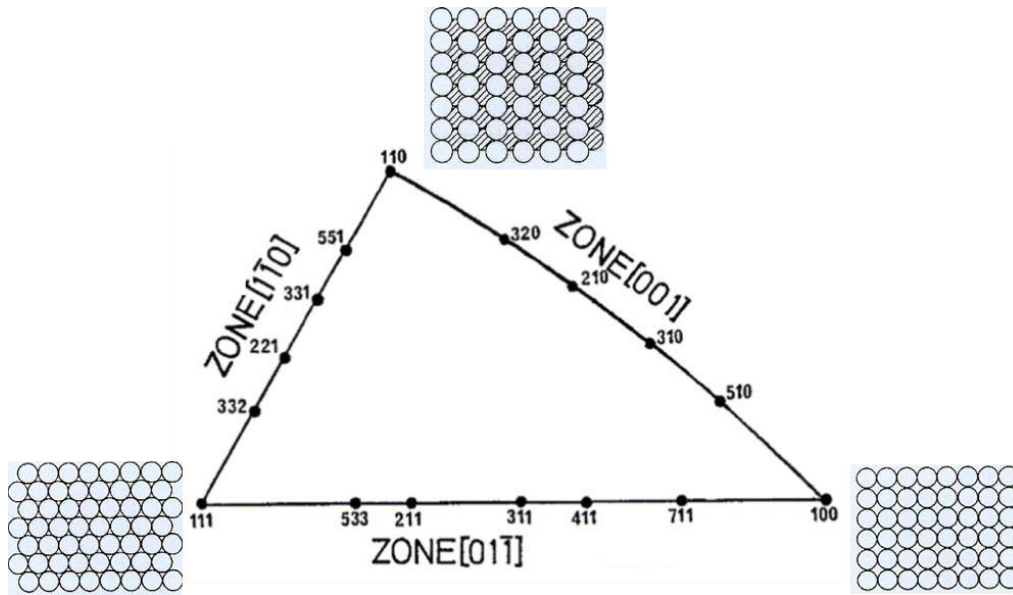
Figure 27: Stereographic triangle representing the relationship of different surface planes of the fcc system

1.3.4.2 Microfacet notation

This method is useful for visualizing a high miller index surfaces. For example, a surface denoted in miller index as (540) is a surface arrangement that contains (110) terraces that are 5 atoms wide separated by (100) steps. In microfacet notation this is written as 5(110)x(100)[108]. There are standard rules when converting between microfacet and Miller notations for each stepped surface family, (shown below) to avoid confusion between the different zones of the stereographic triangle. The rules are shown below. It shows different naming rules for all Pt fcc surfaces[106, 108].

Zone	Miller index (n≥2)	Microfacet notation
$[01\bar{1}]$	$(n+1, n-1, n-1)$	$n(111) \times (100)$
	$(2n-1, 1, 1)$	$n(100) \times (111)$
$[1\bar{1}0]$	$(n+1, n+1, n-1)$	$n(111) \times (110)$
	$(2n-1, 2n-1, 1)$	$n(110) \times (111)$
$[001]$	$(n, n-1, 0)$	$n(110) \times (100)$
	$(n, 1, 0)$	$n(100) \times (110)$

Figure 28: Relationship between the Miller index notation and microfacet notation [108]

1.3.5 Electrode processes

Electrode processes take place within the double layer and produce a slight unbalance of charges at the interface. These process are located across a very thin double layer between the electrode and electrolyte which can be related to electrode kinetics[96].

A typical electrode reaction involves the transfer of charge between an electrode and a species in solution (termed electrolysis). This can be affected by; applied voltage, reactivity of the species and electrode surface, and structure of the interfacial region[95, 96].

For a metal in solution, the relationship of the metals Fermi-level with the solutions HOMO and LUMO orbital energies determine if an electron transfer is thermodynamically favourable. Whether the process occurs depends upon the rate (kinetics).

Consider a simple one electron transfer. The electron needed for the for the reduction is supplied by the electrode. For every molecule reduced a single electron must flow. By keeping track of the number of electrons and hence the current it is possible to know how many molecules have been reduced[92].

The expression for current (i) can be controlled by two factors:

1. The rate of electron transfer between metal and species in solution (electrode kinetics)
2. The transport of material to and from the electrode surface (mass transport)

1.3.5.1 Electrode kinetics

Electrode kinetics describes how the rate of reaction at the electrode surface is affected by the applied voltage. A simple reversible redox reaction can be written as:

$$O + e^- \leftrightarrow R$$
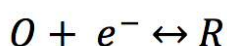
Where O represents the oxidized form and R represents the reduced form[9]. The rate of reaction for the forward (reduction) reaction is given by:

$$R_{Red} = k_{red}[O]$$

Where R is the rate of the reduction reaction, k is the rate constant for the reduction and (O) is the concentration of "O" species.

The reaction can be monitored by current (i) at the electrode surface. As this corresponds to rate of electron transfer, current or current density can be expressed as:

$$i_{Red} = nFAk_{red}[O]_s$$

where n is the number of electrons transferred, F is Faradays constant, A is the electrode area. The observed current is a net current, which is the combination of the reductive and oxidative currents[9, 86].

Electrode kinetics are considered analogous to chemical kinetics and therefore the relationships of rate constants and applied voltage are established using transition state theory (TST)[92, 95].
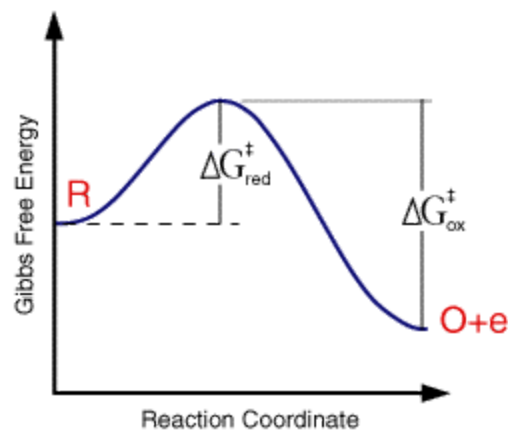
Figure 29: Graphical interpretation of energy vs reaction coordinate for a simple redox reaction

In TST the reaction is considered to proceed via an energy barrier where the summit of this barrier is referred to as the transition state (Figure 29). Rate constants vary with temperature and are described by Arrhenius. From this, the activation free energy (thermodynamics) for the reduction can be described[92, 95].

$$k_{red} = Z \exp\left(\frac{-\Delta G_{red}^{\ddagger}}{RT}\right)$$

Figure 30: Arrhenius equation applied to redox equation from figure above. Where Z relates to the pre-exponential factor, and ΔG_{red} relates to the activation energy for the reaction.

For a single applied voltage, the free energy profiles appear qualitatively to be the same as corresponding chemical processes. Activation energy alters as a function of applied potential and therefore the rate constants for both forward and reverse reactions will be affected[95].
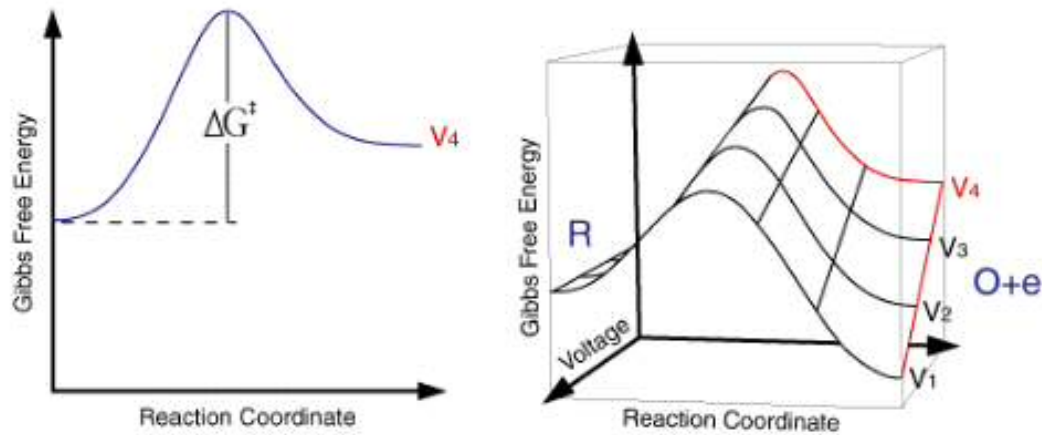
Figure 31: The change in Gibbs Free Energy plots as a function applied potential

Rate constants for the electron transfer steps are proportional to the exponential of the applied potential. The Butler-Volmer (BV) equation describes the effect of potential(E) upon the reaction rate. For a one electron transfer[92, 95]:

$$i_{net} = i_0 \left(e^{\frac{\alpha F(E-E_{eq})}{RT}} - e^{-\frac{(1-\alpha)F(E-E_{eq})}{RT}} \right)$$

Utilising the use of current density instead of current, the most common form of the BV equation is:

$$j_{net} = j_0 \left(e^{\frac{\alpha F\eta}{RT}} - e^{-\frac{(1-\alpha)F\eta}{RT}} \right)$$

Where E_{eq} is the equilibrium potential for the reaction and *E is* the potential applied to the electrode surface, j_0 is the exchange current density and j_{net} the net current density. α represents the symmetry factor and correspond to the position of the activation energy peak for the reaction along the reaction coordinate of the anodic reaction. A value of 0.5 signifies a symmetric current transfer. This implies half of the energy from the potential drop at the interface is used to push the reaction. It is common to assume symmetric electron transfer in the Butler-Volmer equation. Values of α that deviate from 0.5 imply asymmetry in forward and backwards reactions. η is the overpotential, which is the difference between equilibrium and applied potential (E-E_{eq})[92] Current density is

proportional to rate of an electrochemical reaction and it makes rate independent of the area of electrode[96].

Exchange current density, j_0 is vitally important in electrocatalysis as it describes the ability of an electrocatalyst to catalyse a reaction. The better the catalyst the higher its j_0 and larger currents can be observed close to the E_{eq} for the reaction. The influence of exchange current density on the current-potential response is shown in Figure 32[96].
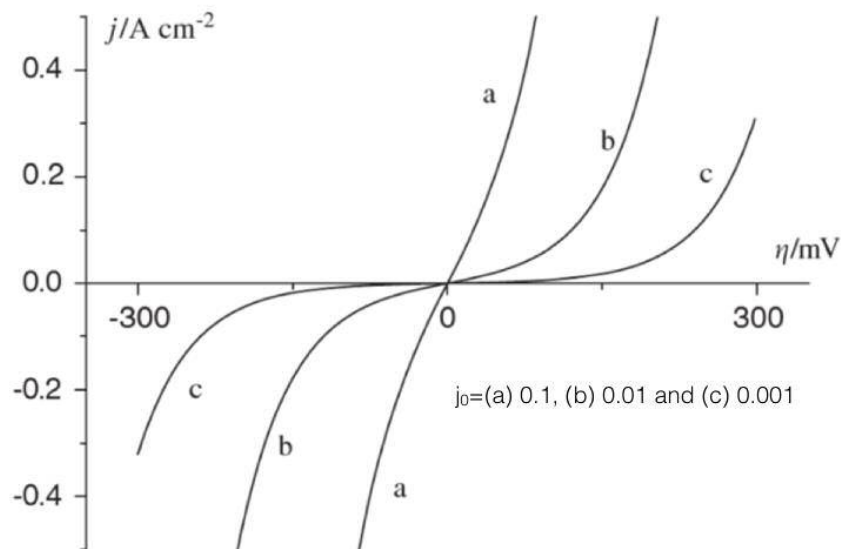
Figure 32: Influence of exchange current density(j_0) on the j- η response when n=1 and a=0.5

In PEM fuel cells the HOR has a large current density and hence is a facile reaction. A low overpotential is required to maintain a large current. However, the sluggish ORR has a very small exchange current density. To overcome this low j_0, a very large overpotential, η is needed to maintain the same current as the HOR. This results in a power (energy) loss (Figure 33)[86].
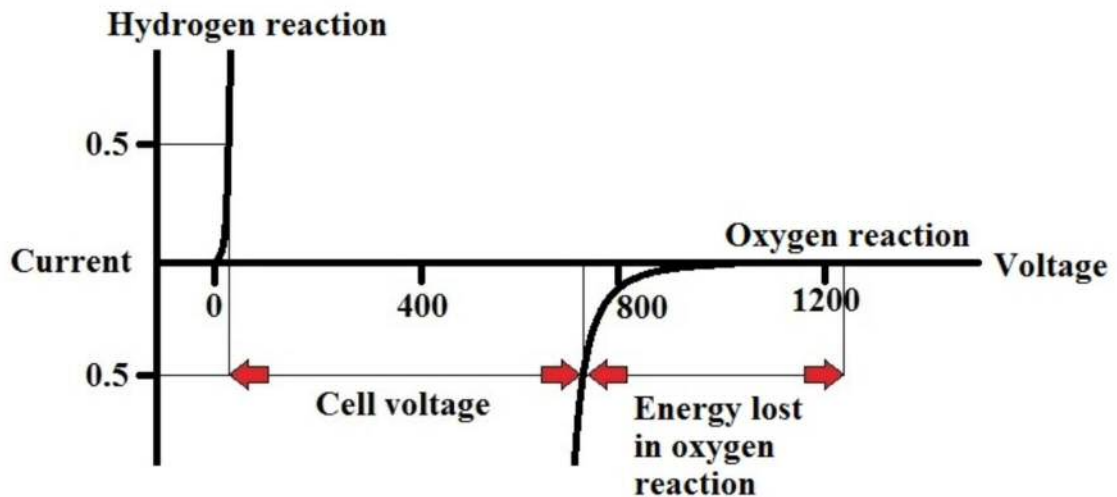
Figure 33: Illustration of the efficiencies of the reactions in a hydrogen PEMFC signifying the large overpotencial needed for the ORR. On this scale ORR E^o=1230 mV and HOR E^0= 0 mV. Taken from [86]

The electrode voltage and rate of electron transfer is an exponential relationship. Therefore, as the voltage is increased the reaction rate and therefore current will increase exponentially, meaning it would be possible to pass unlimited quantities of current. In reality this does not arise because the rate at which the solution species arrives at the surface is limited by mass transport effects[96].

1.3.6 Mass Transport
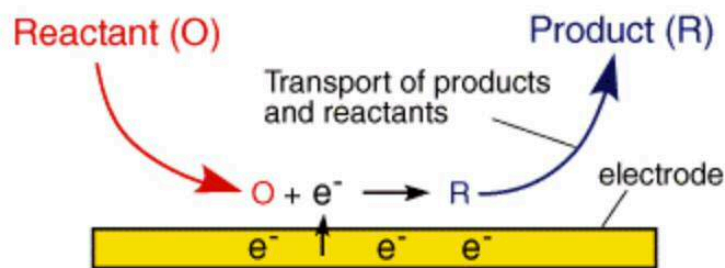
Figure 34: Schematic of the movement steps involved in an electrolysis reaction

The typical electrolysis reaction involves a series of steps shown in the figure above. If the rate constant is large then the current measured at the electrode will be controlled by the amount of fresh reactant reaching the interface from the bulk[95, 96].

A typical electrolysis reaction involves the charge transfer between electrode and species in solution. The current (and therefore current density) is dependent upon the surface concentration of the redox species at any potential difference to the equilibrium value. To enable an accurate

48

description of current density, the delivery of reactant species to the electrode surface and removal of the product formed, must be accounted for. This requires an understanding of how concentration gradients of reactants and products at electrode surface vary over time.

Mass transport is the means by which electroactive species reach the electrode surface from the bulk solution. It has three major components: diffusion (ions move in response to concentration gradient), migration (ions move in response to electric field) and convection (stirring, temperature and density gradients)[95].

1.3.6.1 Diffusion

Diffusion is particularly significant in an electrolysis experiment since the conversion reaction only occurs at the electrode surface. There will be a lower reactant concentration at the electrode than in the bulk solution. Therefore, a higher concentration of product will exist near the electrode than in the bulk. Diffusion is the movement of species from a high to low concentration, as predicted by Ficks first law[96]. Concentration gradients are created during electrochemical reactions at the electrode surface and therefore diffusion is the main mode of mass transport to consider during voltammetry. It is also important to know how the concentration of material varies as a function of time. Ficks second law[96] signifies a large concentration drop at the electrode results in a high diffusional mass transport. The steeper the change in concentration, the greater the rate of diffusion. Fick's second law is an important relationship since it predicts the variation of concentration of different species as a function of time within the electrochemical cell[92].
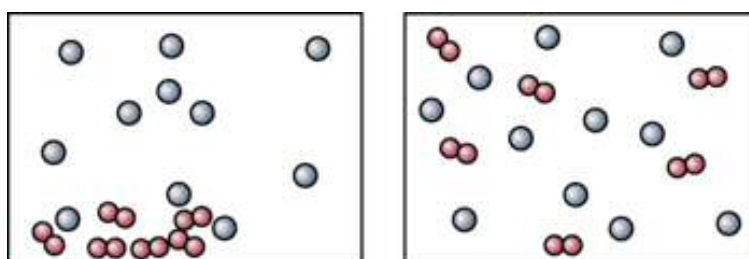
Figure 35: Basic diagram of diffusion

1.3.6.2 Migration

In migration, charged solution particles are attracted or repelled by a charged surface. Reactants and products are often charged species and may therefore be affected by migration. To minimise this

effect, a large excess of electrolyte is used in electrochemical experiments and it is the electrolyte ions that carry the majority of charge through solution[96].

1.3.6.3 Convection

Convection is the movement of a species due to external mechanical forces[96]. Controlled convection is often used in order to elucidate reaction parameters as it can be described mathematically[92]. It is typically several orders of magnitude greater than any natural convection effects and therefore effectively removes the random aspect of diffusion from the experimental measurements. The convection applied must be well controlled. If the rate if correct, the profile will become stable and laminar flow is created. If the solution is pumped at too high a rate, then the transport can become turbulent. This cause the movement to be random and unpredictable. Using convection can help remove complexity involved in electrochemical measurement. In a later section, the use of convection to create a laminar flow in the rotating disk electrode (RDE) is discussed.
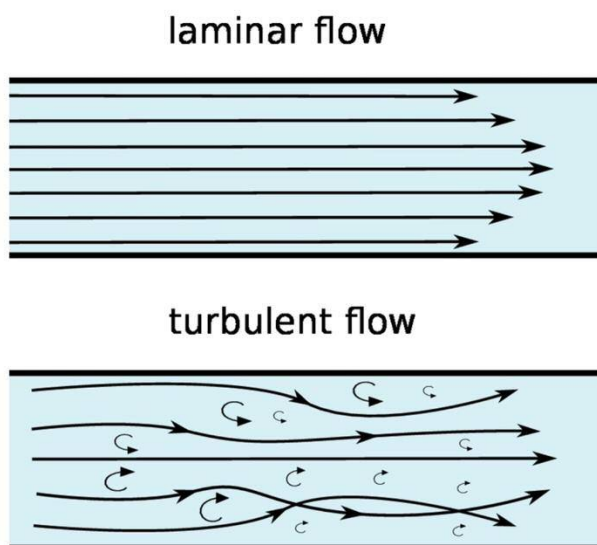
Figure 36: Schematic of laminar flow vs turbulent flow from forced convection

1.4 Electrochemical Methods

Electrochemistry is intrinsically surface sensitive and can detect minute changes in composition of electrode materials[109]. There is a wide range of coulometric experimental setups that utilise electrochemistry to study the electrode-electrolyte interface. Most cases require a three electrode setup for correct quantitative analysis. This includes the electrode of interest, known as the working electrode (WE), a reference electrode (RE) and counter electrode (CE). The reference electrode maintains a fixed potential and is used as a potential control between itself and the working electrode. The counter electrode completes the electrical circuit by allowing current between itself and the working electrode. The three electrode system allows the RE to be separated from the flow of current which helps it maintain its fixed potential[92, 110].

Three experimental setups were utilised in this work:

1. Chronoamperometry (CA)
2. Cyclic Voltammetry (CV)
3. Rotating Disk Electrode (RDE)

1.4.1 Chronoamperometry

In this technique, the potential is at first held at a particular value, then, after a set time, is stepped to another value. The potentials may be chosen so that the first does not cause electrolysis of the analyte and the second does. At the beginning of the reaction the concentration of the reactants at the surface is equal to the bulk. When the potential is stepped, the reaction proceeds and after a short period of time the concentration of the reactant at the surface is zero. Chronoamperometry is a very powerful tool for the quantitative analysis of a nucleation process[96].

1.4.2 Cyclic Voltammetry

CV is a potentiodynamic electrochemical measurement. It is the most widely used procedure for acquiring qualitative information on electrochemical reactions[111], hence why it is being used in this investigation.
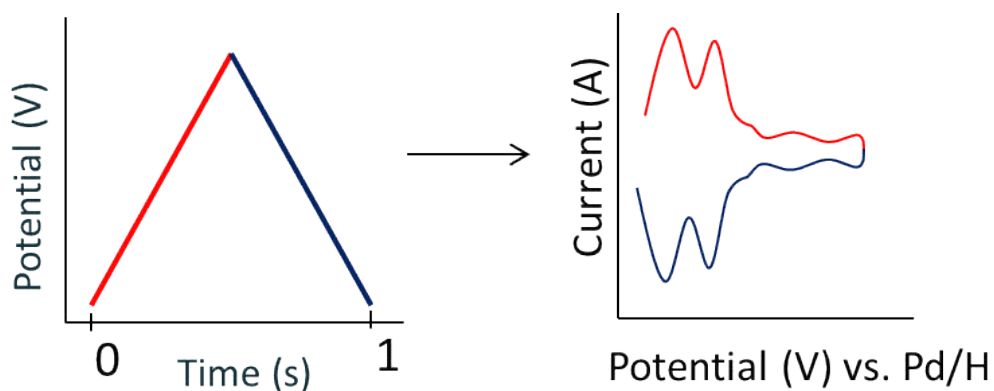
Figure 37: Potential waveform of CV (left) with a corresponding typical response(right)

CV is an extension of linear sweep voltammetry (LSV). Potential is swept in a linear fashion whilst the current is monitored. Potential is swept over a defined range, from a start value to final value, at which point the potential is reversed back to the start potential. It creates what is known as a sawtooth waveform. This can be repeated a number of times (cycles). The resulting current is collected in a fingerprint curve and plotted as a function of potential, known as a voltammogram[111, 112]. The CV can be modified by dividing the current by the electrode area to give the current density and this is plotted against potential. The use of current density allows direct comparison between electrodes of different areas and is widely used in the literature.

The voltammogram provides information about the different electrochemical processes occurring at the electrode surface. Each peak is characteristic of a different electrode interaction taking place. It is dependent on a number of factors[92, 112]:

- The rate of the electron transfer reaction
- The chemical reactivity of the electroactive species
- The voltage scan rate

Positive currents are described as anodic (oxidation) where negative currents are termed cathodic (reduction). The sweep rate is predetermined and kept constant throughout the scan. It can range from a few millivolts to a hundred volts per second.

1.4.2.1 CV Theory

In CV, two processes are occurring at the electrode surface; Faradaic and non-Faradaic processes. Hence, the total current that flows is the sum of both of these contributions [107, 111].

Faradaic processes comprise of charge transfer across the metal-solution interface and are governed by Faraday's laws of electrolysis. Electron transfer gives rise to redox reactions occurring at the interface. The amount of charge passing through the electrode is governed by the extent of the reactions occurring or charge transfer and termed faradaic current due to it obeying Faraday's Law[92]:

Where Q is charge, N is the amount of reactant, n_e is the number of electron exchanged, v is reaction rate, A is surface area and F is faradays constant. The result from this equation is that current resulting from the faradaic processes (I_F) is directly related to reaction rate for a given surface area.

For a Faradaic process, the reversible redox reaction can be described[91]:

In CV, faradaic current resulting from redox processes at the surface is measured as a function of the potential. The current detected is a response to the potential applied. Provided the rate of electron transfer at the surface of the electrode is fast and the peak potential is independent of sweep rate and concentration, the reaction is deemed reversible. For a reversible redox reaction, no new reactions occur upon reversing the cell current and a CV shows reversible peaks [93]. The Nernst equation can be used to describe this process[11].

Where E^o is the standard electrochemical cell potential, R is the universal gas constant, T is the temperature, n is the number of electrons, F is the Faraday constant and Ox/Red is the concentration of the oxidised and reduced species at the electrode surface.
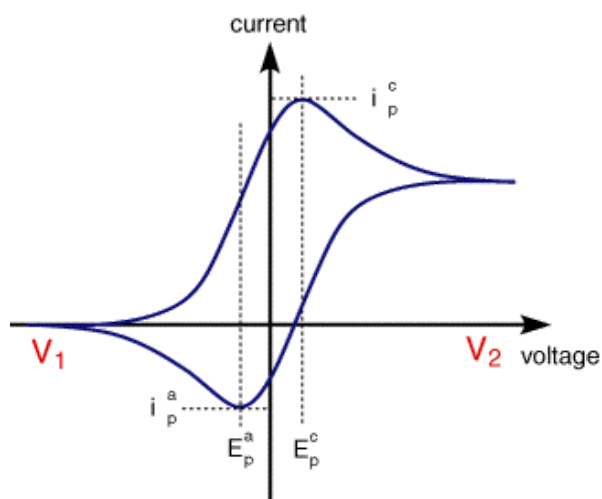
Figure 38: A typical cyclic voltammogram recorded for a reversible single electrode transfer reaction

The Nernst equation relates the cell potential to the standard potential and to the activities of the electroactive species [11]. The exact form of the voltammogram shown in the figure above can be rationalised by considering what is happening when the potential is swept from low to high and current begins to flow from the electrode to the solution species. As the potential is swept from its initial value, the equilibrium position is shifted to the right and converting the reactant. The further the potential is swept; the more reactant is converted and hence more current is observed in the voltammogram. The peak occurs due to the fact at some point the diffusion layer on the electrode has grown so large that the flux of the reactant to the electrode is not fast enough to satisfy that required by the Nernstian equation. This results in a drop of current and is also described by the Cottrell equation*. When the scan is reversed, the electrolysis product is converted back to reactant. The current flow is now from the solution species to the electrode. The amount of current measured in the voltammogram is proportional to the scan rate. The faster the scan rate the smaller the diffusional layer and the quicker the flux towards the electrode is.

The position of the peak in the voltammogram is characteristic of electrode reactions which have rapid electron transfer and do not change upon scan rate. The peak separation of a reversible redox reaction in a CV can be defined as [11]:

Where cathodic and anodic peaks are separated by a potential of 56.5/n. Here   and   are the electrode potentials of the oxidation and reduction processes.

In a cyclic voltammogram, the peak current is the same for both forward and reverse reactions and can be calculated from the Randles-Sevcik equation[11, 92]:

where i_p is peak current, A is the electrode area, D_o is the diffusion coefficient, v is the scan rate and C_o is concentration of the electroactive species in bulk solution. The peak current is proportional to the concentration and square root of scan rate. The faster the scan rate, the smaller the diffusional layer and the quicker the flux towards the electrode and the larger current measured. The positions of the observed peaks do not alter as a function of voltage [11, 92].
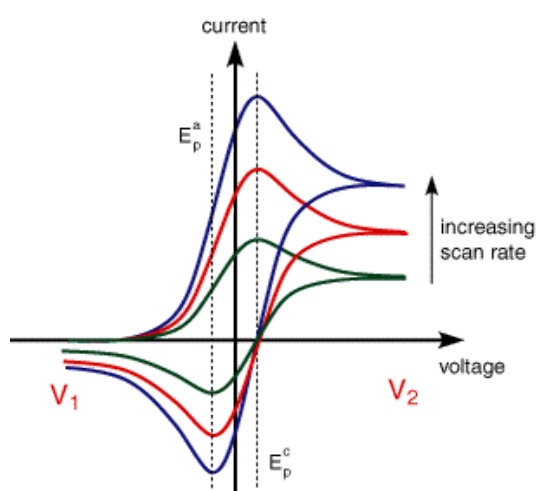
Figure 39: (left) relationship between scan rate and peak height, (right)

There can also be irreversible reactions associated with Faradaic processes. Quasi-reversible or irreversible electron transfer reaction cannot be predicted by the Nernst equation. This is because an equilibrium cannot be established fast enough in comparison to the scan rate. This results in asymmetric voltammetric peaks. For an irreversible process, the electrode potential (E_p) is not independent of scan rate since the system is not at equilibrium whilst the peak current (i_p) remains proportional to the square root of the scan rate.
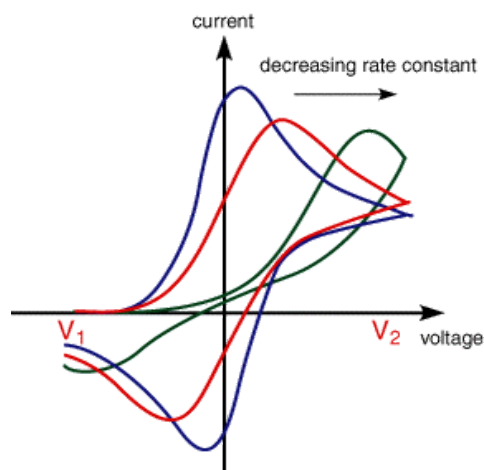
Figure 40: CV for cases where the electron transfer is not reversible

Non-Faradaic Processes

Non-Faradaic processes are a result of thermodynamic and kinetic conditions that don't allow charge transfer reactions to occur to, or from the bulk. This results in adsorption and desorption of ions occurring which cause changes to surface structure when the potential or the electrolyte is changed. Charge does not cross the metal-solution interface under these conditions, but external currents can flow. When a potential is changed across the metal, the metal-solution interface behaves analogous to a capacitor. A whole array of charges build up across the surface of the metal and orientate in the solution creating an electrical double layer [92, 93, 107]:

Where double layer current (I_{DL} measured in amps, A) is proportional to the surface electrode area (A measured in cm^{-2}), the capacitance of the double layer (C_{DL} measured in farads, F) and the scan rate (V measured in V s^{-1})[91]. The nature of the double layer can change depending on the potential applied, the material of the working electrode and the chemical species in solution. For example, if the potential is changed such that the metal electrode acquires a negative charge. positive ions will more likely orientate themselves in the double layer and vice versa if the metal is positively charged.

Anions near the electrode's surface respond to this negative charge by migrating away from the electrode; Cations on the other hand, migrate toward the electrode. This migration of ions occurs until the electrode's positive surface charge and the negative charge of the solution near the electrode are equal. Because the movement of ions and the movement of electrons are indistinguishable, the result is a small, short-lived non-faradaic current. Every time the potential of the metal electrode is changed a transient charging current flows [98].

56

1.4.2.2 CV of Well-defined Platinum Single Crystals

There are many different metals that have been used for heterogeneous catalyst but the most common in electrochemistry is platinum[35]. It has also been the main metal employed for electrodes in cyclic voltammetry. The normal potential window for platinum is between the range of 0-1.7 V. At more negative potential hydrogen evolution occurs, whereas at more positive potentials oxygen is evolved. Hence the 1.7 V potential window between these two extremes constitutes the bulk stability of the electrolyte[107].

Due to different surface sites exhibiting different activities, it is vital that reproducible electrode surfaces are used for electrochemical studies. The electrode must be prepared so that the same surface is obtained every time. Although Will did pioneering work in this area[113, 114], the greatest advances stem from the efforts of Clavilier *et al.*[35, 115, 116]

1.4.2.3 CV of polycrystalline platinum

Before studies on single crystal electrodes began, a method for the production of reproducible polycrystalline platinum electrode surfaces was created. This involved applying multiple voltammetric scans to the surface, with potentials between hydrogen evolution and oxygen evolution[117]. As a result, the reproducible CV of polycrystalline platinum was obtained in various acid electrolytes.
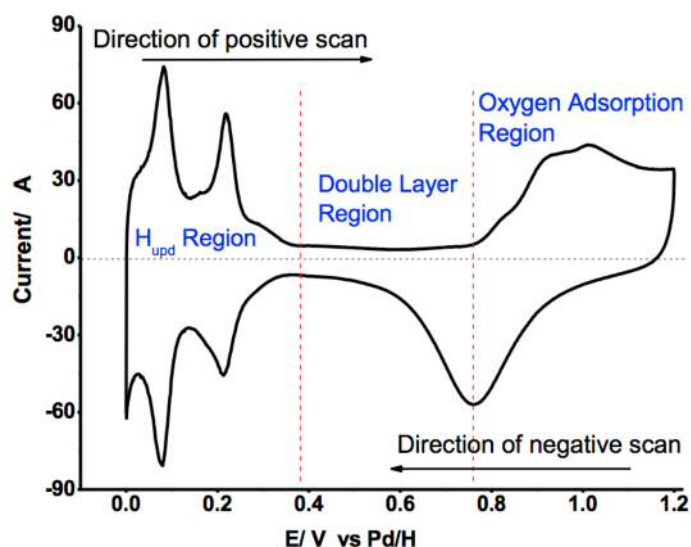
Figure 41: CV of a polycrystalline platinum electrode showing typical adsorption regions

Figure 41 shows the CV of polycrystalline platinum electrode in 0.1 M sulphuric acid electrolyte. Several distinct regions are labelled where different electronic processes are taking place:

1.1.1.1.5 H_{upd} Region

This is the hydrogen underpotential deposition region where adsorption/desorption of cations (usually H+) usually occurs in the lower potential region, 0-0.4 V (vs Pd/H)[113-115, 118-120]. Due to the sample being polycrystalline more than one peak is observed corresponding to adsorption on different atomic sites. On the positive scan the platinum surface is negatively charged and covered in hydrogen atoms. As the potential is increased (getting closer to the surfaces' PZC) the surface becomes more positive and hydrogens desorb/replaced with other ions. The general reaction here is:

For the negative scan the platinum surface is negatively charge in this potential region. As the potential is decreased the metal surface becomes more negatively charged and adsorbs more hydrogen atoms until saturation. The general reaction here is:

Around 0 V, the surface region has one complete monolayer of hydrogen. If the potential is taken more negative it induces the evolution of hydrogen. Once a monolayer of hydrogen is achieved no more hydrogen will adsorb[121, 122].

Accurate integration of the H_{UPD} region can be used to estimate the real surface area of the working electrode. It is assumed that one electron is transferred per surface platinum atom. The integrated charge is divided by the specific charge density of one of the three basal planes to find the area. The relative size of the hydrogen adsorption peaks of principle index planes can be used to measure electrolyte cleanliness and single crystal quality[114, 120, 121].

1.1.1.1.6 Double Layer Region

The only current flowing in this region is capacitive charge resulting from the charging of the IHP/OHP. No redox processes occur here. Non-faradaic processes are occurring, where ions of opposite charge migrate towards the electrode surface as the potential is changed. The thickness of

this region in the CV, is significant as its size is proportional to the capacitance of the electrode, which not only depends on the material but also the surface area[123].

1.1.1.1.7 Oxygen Adsorption Region

At potentials above ~0.8 V, is associated with platinum oxidation where hydroxides and oxides are formed[124-126]. Depending on the species in the solution, this region can also include specific adsorption of other anions. The positive scan exhibits a fairly broad oxidation process, where some peaks can be discerned. This is evident of the likelihood of multiple adsorption processes. The negative scan shows the reduction of the platinum surface, where a single sharp reduction peak is observed. The position of this peak differs from the one seen in the positive scan. The asymmetry of this peak was found to be reduced if the higher potential limit is lowered[26, 70, 127-130]. Much work has been undertaken on Pt surface oxidation and, although still not completely understood, can be expressed as the following[35]:

$$Pt + H_2O \rightarrow PtOH + H^+ + e^- \qquad\qquad 0.85\text{-}1.10V \quad (2)$$

$$PtOH \xrightarrow{\text{Place Exchange}} PtO + H^+ + e^- \qquad\qquad 1.10\text{-}1.40V \quad (3)$$

$$PtO + H_2O \rightarrow PtO_2 + 2H^+ + 2e^- \qquad\qquad >1.4V \qquad (4)$$
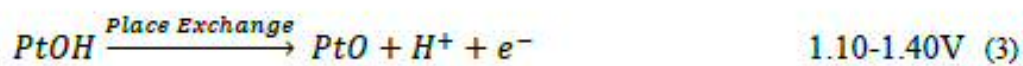
1.4.2.4 Platinum Single Crystals

The development of methods to create platinum surfaces that only exhibited a single plane began over 50 years ago. Will was the first to study electrochemistry of platinum single crystal electrodes by CV[113]. An electrochemical activation procedure was used to produce a clean electrode surface[118]. Subsequently, many researchers have examined single crystal electrodes in order to characterise their voltammetric behaviour and kinetic response[35, 114]. Electrochemical kinetic measurements on single crystal electrodes were conducted during the 1960s and 1970s by Piontelli, Bockris and Razumney, Damjanovic *et al.* and Budevski[35]. More recently, Clavilier *et al.* and Hamelin examined the degree to which reaction rate varied depending on the exposed crystal surface. Hamelin has extended such studies to metals other than platinum, particularly gold[35, 86]. Clavilier accelerated studies of single crystal electrode surfaces by showing how they can be prepared by a novel, simple and ingenious flame-annealing method[115]. Clavilier's pioneering

method for producing clean, well defined single crystal electrodes opened the field of surface characterisation to many scientists not equipped with ultra-high vacuum instrumentation.

Since then, multiple studies on single crystal electrodes have been undertaken, including characterising voltammetric behaviour and kinetic response[35, 38, 116, 131-134]. The electrosorption of hydrogen and oxygen is found to be highly sensitive to the surface atom arrangement of an electrode.[35] Each basal plane being studied gives rise to a voltammogram that acts as a fingerprint for that surface (Figure 42) [111].
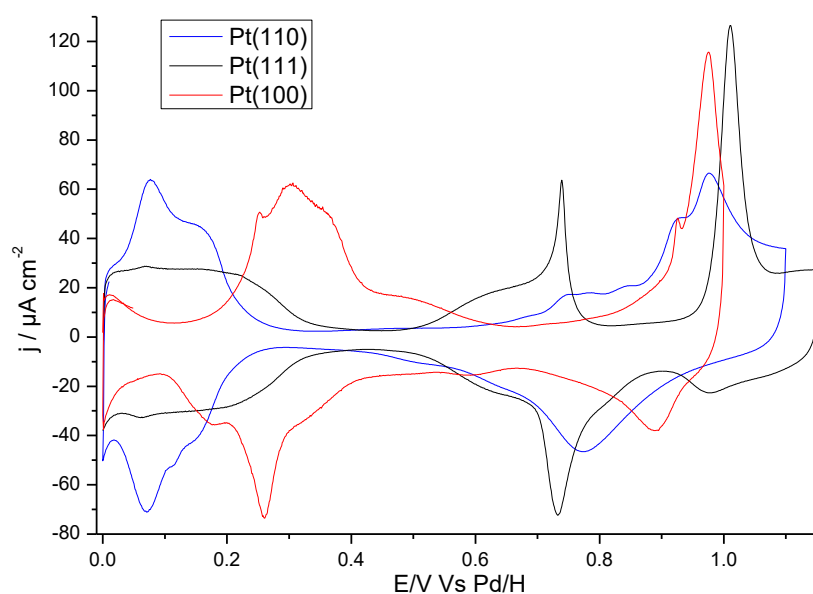
Figure 42: CV responses of Pt base planes in 0.1 M HClO₄

1.4.2.5 CV of Well-defined NPs

Platinum nanoparticles are made to exhibit specific surface structure on their faces. The shape of the nanoparticle is dependent on the surface atomic structure desired. Nanocubes have (100) faces exposed and exhibit voltammetry in common with (100) and (100)x(111) sites, the latter being due to interactions at the edges and vertices of the nanocube (Figure 43) [134]. Nano-tetrahedrons and nano-octahedrons have (111) faces and exhibit voltammetry related to the (111) and (111)x(111). Again the latter is due to interaction at edges and vertices[29]. Other shapes of nanoparticles exhibit varying proportions of (111), (100) or (110) sites and therefore exhibit cyclic voltammetry that is just as characteristic as those observed for single crystals[134]. Voltammetry may be used to identify the relative proportions of the crystallographic faces exposed to the electrolyte. Care must be taken however, as the same voltammetric responses will be seen for nanoparticles different in shape, but contain similar features. For example, cubes and cuboids would both exhibit (100) faces with (100)x(111) edge sites. Their resulting voltammograms would be identical. Therefore, it is common

that other techniques such as transmission electron microscopy (TEM) are used in combination with CV.
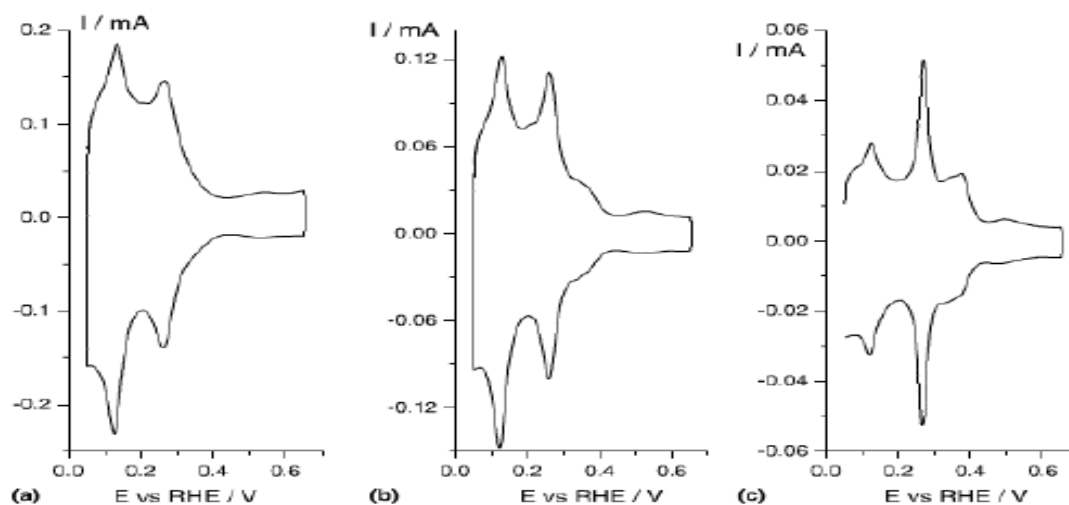
Figure 43: Voltammograms of Pt nanoparticles with increasing (100) features[86]

In fuel cells the platinum catalyst is usually in nanoparticle form. The surface atomic structure of the catalyst is very sensitive to specific reactions such as the ORR, where different activities have been seen for different surface arrangements. This has been exhibited in both SCE and NP studies. In the field of NPs, there has been great development in trying to incorporate the highest amount of active sites into catalysts in the last 20 years. Synthesis methods have become more sophisticated, with greater control over the arrangement of atoms. Far more structures such as nano-frames[135], cages and rings[136] are now obtainable through directed nanoparticle synthesis. The partnership of work on platinum single crystals with NPs is crucial, as it helps with the goal of creating highly active catalysts at low catalyst loading.

1.4.3 Hydrodynamic Effects

Hydrodynamic devices use controlled convection to enhance the rate of mass transport to the electrode surface. They offer advantages over stationary solutions such as increased current and sensitivity. The use of controlled convection (at the correct rate) helps remove the random mass transport contributions to the measurements. The transition between laminar and turbulent flow can be predicted using the concept of the Reynolds number. Reynold's number is defined as the ratio of inertial to viscous forces[96] . Laminar flow has been found to occur at Reynold values of 2 x 10^3[11].

1.4.3.1 Rotating Disk Electrode

The rotating disk electrode is a common experimental setup that is utilized to create laminar flow. In this arrangement, the working electrode is rotated to bring the solution towards its surface. The electrode is usually embedded an inert substance (such as Teflon) in order to only allow the solution to be in contact with the surface (Figure 44) [86]. Alternatively, a hanging meniscus configuration may also be employed [137, 138]. This can be tricky to ensure the meniscus contact is high enough so that the solution does not touch the side but able to stand up to the rotating procedure.
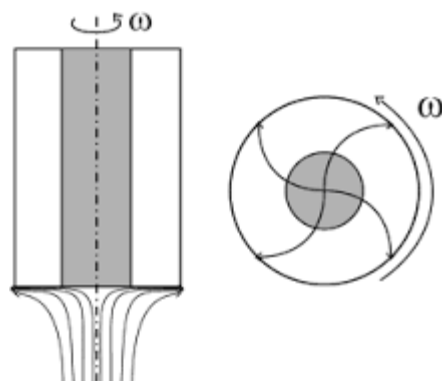
Figure 44: Schematic of laminar flow projection introduced in the RDE

Introducing a laminar flow at the rotating disk electrode conveys a steady stream of material to the electrode surface from the bulk. Movement of material to the electrode surface can be described by fluid dynamics[95, 96, 111]. During rotation, a portion of solution close to the electrode surface rotates with the electrode and can appear relatively stagnant. This creates a layer known as the hydrodynamic boundary layer (δ_H). Transport of the solution to the hydrodynamic boundary layer is dominated by convection. After the material reaches the hydrodynamic layer and moves closer to the electrode surface, a diffusion layer and hence diffusional transport dominates. The diffusion layer thickness (δ_F) can be approximated:

$$\delta_F = 1.61 \ (D_F)^{1/3} \ v^{1/6} \ \omega^{-1/2}$$

Where D_F is the diffusion coefficient of the molecule, v is the kinematic viscosity of the solution, and ω is the angular rotation (where $\omega = 2 \pi f / 60$, and f being the rotation speed in rpm)[96]. The diffusion layer is around twenty times thinner than the hydrodynamic layer. Levich found a mathematical method to treat convection and diffusion at the RDE[96, 139, 140].

1.4.4 Oxygen Reduction Reaction

$$O_2(b) \xrightarrow{\text{diff.}} O_2^* \underset{k_{-2}(-2e^-)}{\overset{k_2(+2e^-)}{\rightleftharpoons}} H_2O_2(a) \xrightarrow{k_3(+2e^-)} H_2O$$

with $k_1(+4e^-)$ connecting O_2^* to H_2O, and k_4, k_6, k_5 pathways to $H_2O_2^*$ which diffuses to $H_2O_2(b)$.
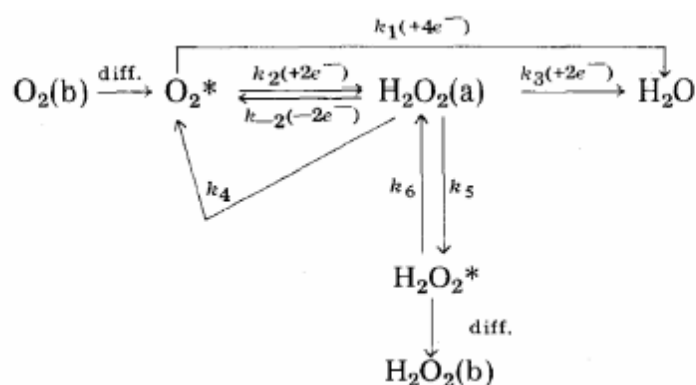
Oxygen reduction to water can occur by a choice of pathways[14, 32]. The mechanism where hydrogen peroxide is not considered to be formed is known as the "direct" mechanism. The stepwise mechanism of oxygen reduction, which proceeds by the reduction to hydrogen peroxide and then water, is known as the "series" pathway. The general scheme of oxygen reduction does not consider every elementary, single electron transfer, step. ORR mechanisms that take these into account have different nomenclature [141].

$$2O^{ads} \xrightarrow{+2e^-} \quad \text{dissociative mechanism}$$
$$O^{ads} + OH^{ads} \xrightarrow{+e^-} \quad \text{associative mechanism}$$
$$O_2^{bulk} \longrightarrow O_2^{ads} \underset{}{\overset{+e^-}{\rightleftharpoons}} HOO^{ads} \overset{+e^-}{\rightleftharpoons} HOOH^{ads} \rightleftharpoons 2OH^{ads} \overset{+2e^-}{\rightleftharpoons} 2H_2O \quad \text{"peroxo"-mechanism}$$
$$HOOH^{bulk}$$

[142]
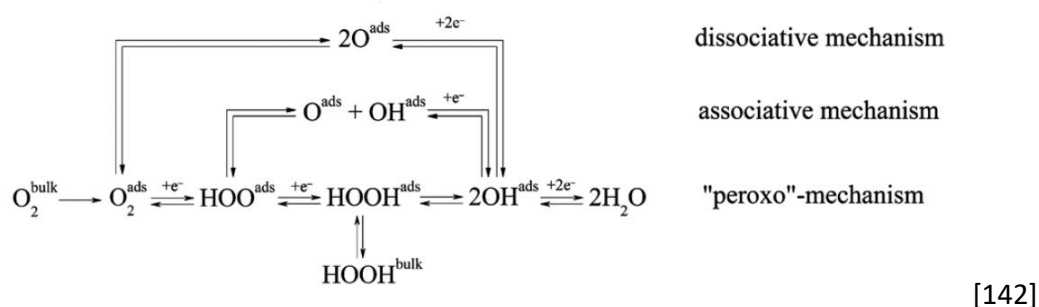
The "dissociative" mechanism, is when bond breaking precedes the reduction. The "associative" mechanism involves a one electron reduction step preceding the bond breaking. Finally, the "peroxo"-mechanism, (which is also an associative mechanism), two reduction steps precede the bond breaking, which can proceed with or without desorption of the H_2O_2 intermediate[96].

1.4.4.1 Analysis of the ORR

A typical voltammetric measurement used with the RDE is CV[96]. The current (or current density) is monitored as a function of potential as the electrode is rotated. A typical voltammetric curve for the ORR is shown below.
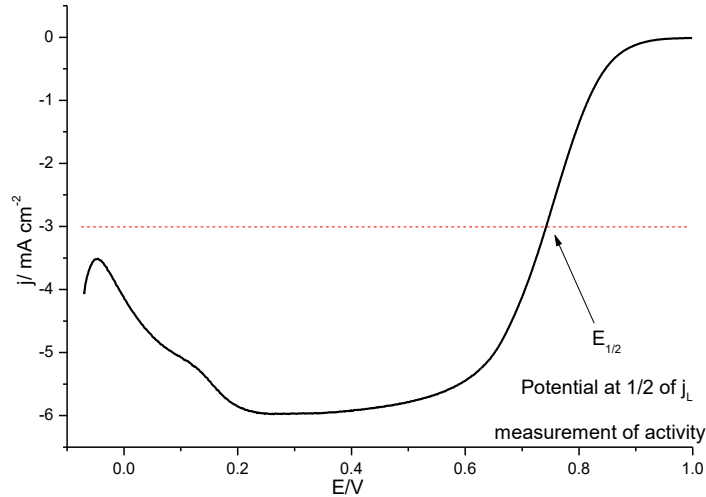
Figure 45: Typical voltammetric curve of the ORR on Pt single crystals using the RDE

For ORR experiments utilising the RDE setup, the limiting current density (j_L, A cm^{-2}) can be found from the Levich equation[143]:

Where n is the number of electrons, F is Faradays constant, A is electrode area, C_b is the bulk concentration of oxygen in solution, D_o is the diffusion coefficient of oxygen, v is the kinematic viscosity of the solution and ω is the angular rotation rate. A series of voltammograms can be acquired over a range of different rotation rates. The limiting current density increases linearly with the square root of the rotation rate. A plot of 1/j vs 1/ω^{½} shows a linear dependence where the gradient is proportional to the number of electrons. For ORR, this should be equal to four as the complete reduction of O_2 to H_2O is a four electron process. When the reaction is limited and hydrogen peroxide is produced, the line is equal to two electrons[138, 143, 144].

The complete transition from the reduction occurring under kinetic control (at low overpotentials) to the reaction occurring under diffusion control (at high overpotentials) can be observed, as well as a mixed kinetic-diffusion controlled regime at intermediate potentials. The kinetic current density (j_k) can be found from the Koutecky-Levich equation[143]:

$$ - \quad - \quad - $$

Where j_K is the kinetic current density, j_L is the mass transport limited current density and j is the recorded current density. The kinetic current density contains the rate constant for the reaction as[143]:

At low overpotentials, the j_K term dominates the reaction and therefore j_L can be ignored. At high overpotentials, the rate becomes large and j_K becomes insignificant compared to j_L. At intermediate potentials both terms are important and the kinetic current density can be obtained using[143]:

$$\overline{}$$

This equation can be applied to current density (*j*) measured at every potential to find j_K. In an alternative method, the j_K can be found by measuring a series of voltammograms in varying rotation rates. Further analysis includes using Tafel plots to interpret the mechanism involved[143].

Tafel analysis allows one to determine the reaction mechanism that is occurring. For a reaction requiring a large overpotential the Tafel equation is:

$$\overline{}$$

This can be rearranged to give:

$$\overline{} \qquad\qquad \overline{}$$

By plotting log j_K against overpotential (η, potential -1.23 V), the exchange current density, j_0, can be found from the intercept. This is related to the electrochemical rate constant for the reaction. The number of electrons before and up to the rate determining step of the reaction can be calculated from the gradient. Changes in Tafel slope are traditionally interpreted as changes in reaction mechanism or rate determining step[143].

For the ORR over Pt{*hkl*}, changes in Tafel slope are not always explained by mechanistic effects, but by the interference of OH/O_{ads}. Tafel analysis is usually performed in the potential region where the

65

surface is changing and therefore OH/O_{ads} may affect platinum sites electronically. The effects of adsorbed species on Tafel slopes have been described by Markovic *et al.[9]*. Tafel analysis is not perfect but gives some insight into the ORR reaction.

1.4.5 Hydrogen Peroxide Reaction

Hydrogen peroxide is an intermediate in the oxygen reduction reaction if it follows a series pathway. There is evidence of this pathway potentially occurring on platinum[142]. Rotating ring disc electrode (RRDE) and single crystal studies have shown that hydrogen peroxide is detectable in the H_{upd} region where hydrogen peroxide is produced when oxygen is reduced on a Pt-H surface[29, 145-147]. Other studies on NPs have also shown that H_2O_2 is produced during the ORR and may desorb from its reaction site before further reduction to water[141]. Recent studies of hydrogen peroxide with platinum have been investigated over a polycrystalline platinum surface[147]. It was found that 2 electron reduction current was observed below 0.9 V vs. RHE, quickly switching to a 2 electron oxidation current above 1.0 V[142].

These results have important consequences for ORR studies. If hydrogen peroxide is created as an intermediate at potentials 0.6-1.0 V, it is likely that it cannot be detected due to the fast kinetics of it being consumed in either potential sweep direction. The potential at which the peroxide oxidation/reduction occurs was found to be an extent of PtOH and PtO coverage[86]. As adsorption processes are highly sensitive to atomic surface arrangement, then investigating the hydrogen peroxide oxidation/reduction reaction (HPORR) as a function of crystal arrangement may give further insights into the effect of these surface species on the HPORR[142]. This could also result in significant consequences for the ORR.

1.4.5.1 Analysis of the HPORR

CV is a typical voltammetric measurement used to analyse the HPORR reaction. Current is monitored during a potential sweep and results a voltammogram similar to the ORR[86]. The figure below shows a typical voltammogram.

At potentials below 0.8 V the 2-electron reduction of hydrogen peroxide occurs. In the low potential region (0-0.3 V), the reduction of hydrogen peroxide occurs. Between 0.8 and 1.0 V the activity quickly changes from reduction to oxidation of hydrogen peroxide over all the platinum surface. It is

this crossover between reduction and oxidation that has been seen to change with changing structure. Quantitative analysis can be undertaken similar to ORR Tafel analysis (discussed later)[142, 147].
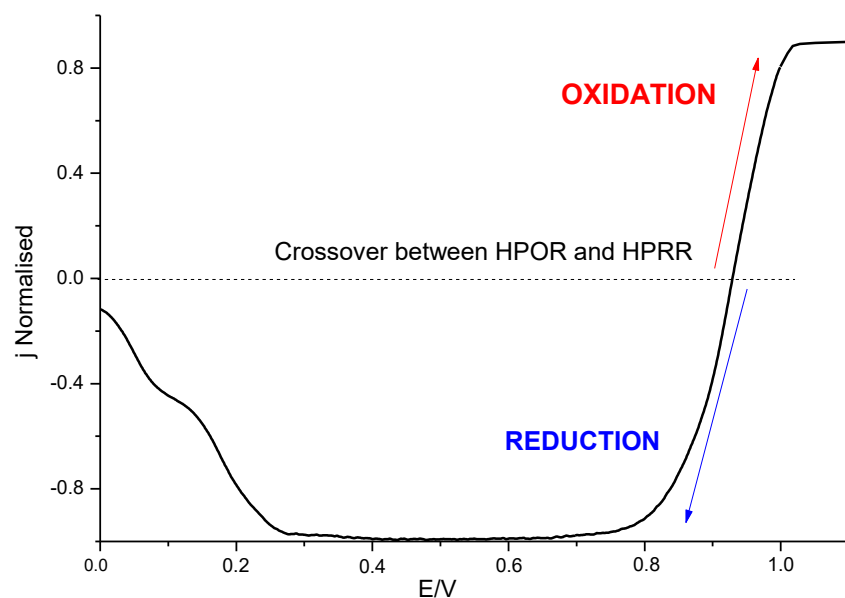
Figure 46: Typical voltammogram for a Pt SCE HPORR experiment using the RDE, 1mM H_2O_2 in 0.1M $HClO_4$ solution, N_2 atmosphere.

1.4.6 CO Displacement Experiment

The CO displacement experiment enables one to obtain the potential of zero total charge (PZTC) of the surface. This is the potential at which the surface changes from being negatively charged, to being positively charged. This is very important when analysing the species adsorbed on single crystal surfaces of different orientations in different electrolytes[148, 149].

A typical method. Firstly, a clean CV of the electrode of interest is recorded. The potential is then held at a value whilst the CO is introduced into the electrochemical cell, dosing CO under potentiostatic conditions. Current flows through the circuit and is recorded until it reaches zero. CO has typically been found to be a neutral probe on platinum surfaces and displaces any other species previously adsorbed onto the surface. It does not undergo any faradaic reaction, which is significant, as it therefore does not contribute to any charge flowing during the transient measured. The charge flowing during this process is equal to the difference between the charge on the electrode before and after the experiment. The potential is still maintained whilst the electrochemical cell is purged of any excess CO in the solution. The CO adsorbed on the platinum surface remains. At this point a

voltammogram at a low potential will give information on the charging of the double layer. Following this, a high potential scan results in stripping of the CO and recovery of the initial voltammogram. The initial and final states should coincide, guaranteeing significance of the experiment[91, 109, 148-150].
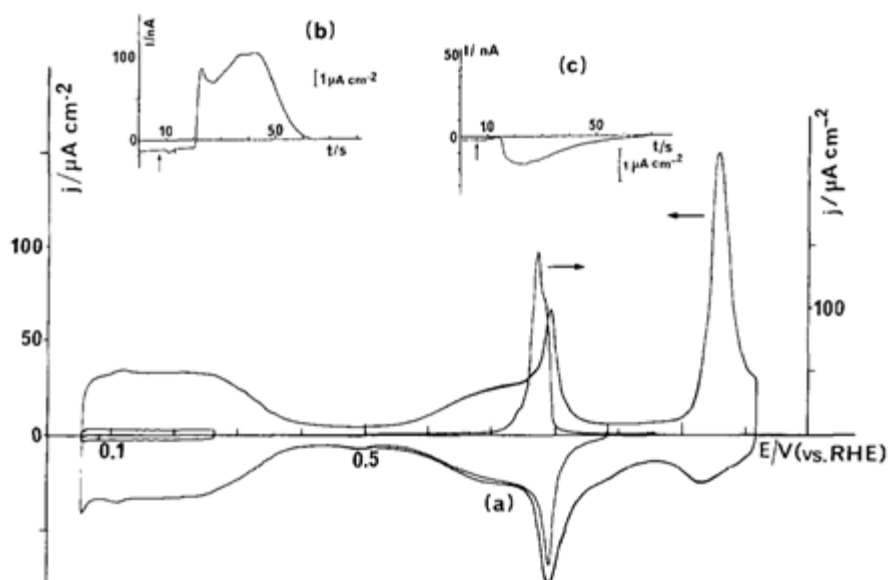
Figure 47: Example of typical CO displacement data, where a) shows a clean CV of Pt{111} along with CO stripping peaks at 0.8 V, b) oxidation transient and c) reductive transient.

At low potentials, oxidation transient current reflects oxidative displacement of adsorbed hydrogen or cationic species. At high potentials, reduction transient currents are reflective of reductive displacement of anionic species. This behaviour is observed for all platinum surfaces, even those which do not show a clear separation between H_{upd} and OH_{ad} regions. The charge displacement is not sensitive to species, only it's charge. It must also be noted that the displaced current can be the net result of several opposing contributions. The negative charges displaced at high potentials mean that anion desorption is the dominant process. This result does not exclude, however, the existence of other processes that can take place in smaller extension[149, 150].

1.5 Objectives of current research

The general objectives of this research is to investigate the effect of electrochemical oxides and such related surface species have upon important catalytic reactions such as the oxygen reduction reaction. This shall be undertaken employing the use of single crystals electrodes and these investigations shall be carried out:

- [Pt n(100)x(110)] and [Pt n(110)x(100)] single crystals shall be created and characterised using CV. These surfaces have not been thoroughly discussed in literature and it is important to understand the behaviour of surface species on all Pt surface arrangements.

- ORR and hydrogen peroxide oxidation/reduction reaction activities of Pt n(100)x(110)] and [Pt n(110)x(100)] single crystal surfaces. The ORR is an important reaction in fuel cell catalysis and requires a deeper understanding of its mechanism on platinum. Hydrogen peroxide is an ORR intermediate which exhibits a switch-over in the potential range relative to oxygen reduction and OH_{ads}/O_{ads} processes.

- The role of platinum and electrochemical oxides relationship will be probed. This will include further elucidating possible mechanisms and testing the nature of the electrochemical oxide as a function of coverage, pH and structure.

- The influence of the proton conducting ionomer Nafion upon the reaction kinetics in the oxide region will be scrutinised.

1.6 References

[1] C.E. Thomas, Fuel cell and battery electric vehicles compared, International Journal of Hydrogen Energy 34(15) (2009) 6005-6020.

[2] C.E.S. Thomas, Transportation options in a carbon-constrained world: Hybrids, plug-in hybrids, biofuels, fuel cell electric vehicles, and battery electric vehicles, International Journal of Hydrogen Energy 34(23) (2009) 9279-9296.

[3] W.R. Grove, XXIV. *On voltaic series and the combination of gases by platinum*On voltaic series and the combination of gases by platinum, Philosophical Magazine Series 3 14(86) (1839).

[4] W.R. Grove, LVI. *On a new voltaic combination*On a new voltaic combination, Philosophical Magazine Series 3 13(84) (1938).

[5] Y. Wang, K.S. Chen, J. Mishler, S.C. Cho, X.C. Adroher, A review of polymer electrolyte membrane fuel cells: Technology, applications, and needs on fundamental research, Applied Energy 88(4) (2011) 981-1007.

[6] O.T. Holton, J.W. Stevenson, The Role of Platinum in Proton Exchange Membrane Fuel Cells Evaluation of platinum's unique properties for use in both the anode and cathode of a proton exchange membrane fuel cell, Platinum Metals Review 57(4) (2013) 259-271.

[7] K.E. Martin, J.P. Kopasz, K.W. McMurphy, Status of Fuel Cells and the Challenges Facing Fuel Cell Technology Today, Fuel Cell Chemistry and Operation 1040 (2010) 1-13.

[8] S.J. Peighambardoust, S. Rowshanzamir, M. Amjadi, Review of the proton exchange membranes for fuel cell applications, International Journal of Hydrogen Energy 35(17) (2010) 9349-9384.

[9] J. Zhang, PEM Fuel Cell Electrocatalysts and Catalyst Layers: Fundamentals and Applications, Springer London2008.

[10] J. Zhang, Electrocatalysts for PEM fuel cell oxygen reduction reaction: Challenges and perspectives, Abstracts of Papers of the American Chemical Society 239 (2010).

[11] P.W. Atkins, J. De Paula, Physical Chemistry, W.H. Freeman2006.

[12] F.T. Wagner, B. Lakshmanan, M.F. Mathias, Electrochemistry and the Future of the Automobile, Journal of Physical Chemistry Letters 1(14) (2010) 2204-2219.

[13] J. Heywood, Internal Combustion Engine Fundamentals, McGraw-Hill Education1988.

[14] J.K. Nørskov, J. Rossmeisl, A. Logadottir, L. Lindqvist, J.R. Kitchin, T. Bligaard, J. H., Origin of the Overpotential for Oxygen Reduction at a Fuel-Cell Cathode, *The Journal of Physical Chemistry B*The Journal of Physical Chemistry B 108(46) (2004) 17886-17892.

[15] J. Spendelow, J. Marcinkoski, Fuel Cell System Cost - 2012, 2012. www.hydrogen.energy.gov/pdfs/12020_fuel_cell_system_cost_2012.pdf.

[16] X. Cheng, Z. Shi, N. Glass, L. Zhang, J. Zhang, D. Song, Z.-S. Liu, H. Wang, J. Shen, A review of PEM hydrogen fuel cell contamination: Impacts, mechanisms, and mitigation, Journal of Power Sources 165(2) (2007) 739-756.

[17] F. Maillard, P. Sergey, E. Savinova, Size Effects in Electrocatalysis of Fuel Cell Reactions on Supported Metal Nanoparticles, (2008) 507--566.

[18] J. Ledesma-Garcia, R. Barbosa, T.W. Chapman, L.G. Arriaga, L.A. Godinez, Evaluation of assemblies based on carbon materials modified with dendrimers containing platinum nanoparticles for PEM-fuel cells, International Journal of Hydrogen Energy 34(4) (2009) 2008-2014.

[19] E. Qayyum, V.A. Castillo, K. Warrington, M.A. Barakat, J.N. Kuhn, Methanol oxidation over silica-supported Pt and Ag nanoparticles: Toward selective production of hydrogen and carbon dioxide, Catalysis Communications 28 (2012) 128-133.

[20] D.A. King, D.P. Woodruff, The Chemical Physics of Solid Surfaces and Heterogeneous Catalysis: Chemisorption systems (2 v.), Elsevier Scientific Pub. Co.1990.

[21] M. Kuhn, J.A. Rodriguez, Interaction of sulfur with bimetallic surfaces - coadsorption of sulfur and noble-metals on Ru(001), Journal of Physical Chemistry 98(46) (1994) 12059-12066.

[22] H.A. Gasteiger, S.S. Kocha, B. Sompalli, F.T. Wagner, Activity benchmarks and requirements for Pt, Pt-alloy, and non-Pt oxygen reduction catalysts for PEMFCs, Applied Catalysis B-Environmental 56(1-2) (2005) 9-35.

[23] J.M. Jaksic, N.M. Ristic, N.V. Krstajic, M.M. Jaksic, Electrocatalysis for hydrogen electrode reactions in the light of Fermi dynamics and structural bonding factors - I. Individual electrocatalytic properties of transition metals, International Journal of Hydrogen Energy 23(12) (1998) 1121-1156.

[24] A.A. Baladin, Modern State of the Multiplet Theor of Heterogeneous Catalysis, Advances in Catalysis 19 (1969) 1-210.

[25] K.C. Neyerlin, W.B. Gu, J. Jorne, H.A. Gasteiger, Study of the exchange current density for the hydrogen oxidation and evolution reactions, Journal of the Electrochemical Society 154(7) (2007) B631-B635.

[26] W.C. Sheng, H.A. Gasteiger, Y. Shao-Horn, Hydrogen Oxidation and Evolution Reaction Kinetics on Platinum: Acid vs Alkaline Electrolytes, Journal of the Electrochemical Society 157(11) (2010) B1529-B1536.

[27] H.A. Gasteiger, N.M. Markovic, Just a Dream-or Future Reality?, Science 324(5923) (2009) 48-49.

[28] R. Borup, J. Meyers, B. Pivovar, Y.S. Kim, R. Mukundan, N. Garland, D. Myers, M. Wilson, F. Garzon, D. Wood, P. Zelenay, K. More, K. Stroh, T. Zawodzinski, J. Boncella, J.E. McGrath, M. Inaba, K. Miyatake, M. Hori, K. Ota, Z. Ogumi, S. Miyata, A. Nishikata, Z. Siroma, Y. Uchimoto, K. Yasuda, K.I. Kimijima, N. Iwashita, Scientific aspects of polymer electrolyte fuel cell durability and degradation, Chemical Reviews 107(10) (2007) 3904-3951.

[29] C.M. Sanchez-Sanchez, A.J. Bard, Hydrogen Peroxide Production in the Oxygen Reduction Reaction at Different Electrocatalysts as Quantified by Scanning Electrochemical Microscopy, Analytical Chemistry 81(19) (2009) 8094-8100.

[30] M. Pourbaix, Lectures on Electrochemical Corrosion, Springer US2012.

[31] E. Bardal, Corrosion and Protection, Springer London2007.

[32] I.E.L. Stephens, A.S. Bondarenko, U. Gronbjerg, J. Rossmeisl, I. Chorkendorff, Understanding the electrocatalysis of oxygen reduction on platinum and its alloys, Energy & Environmental Science 5(5) (2012) 6744-6762.

[33] C.H. Bartholomew, Mechanisms of catalyst deactivation, Applied Catalysis a-General 212(1-2) (2001) 17-60.

[34] V.A. Sethuraman, J.W. Weidner, Analysis of sulfur poisoning on a PEM fuel cell electrode, Electrochimica Acta 55(20) (2010) 5683-5694.

[35] V. Climent, J.M. Feliu, Thirty years of platinum single crystal electrochemistry, Journal of Solid State Electrochemistry 15(7-8) (2011) 1297-1315.

[36] S. Motoo, N. Furuya, Electrochemistry of platinum single crystal surfaces. 2.Structural effect on formic-acid oxidation and poison formation on Pt(111), (100) and (110), Journal of Electroanalytical Chemistry 184(2) (1985) 303-316.

[37] J. Inukai, M. Ito, Electrodeposition processes of palladium and rhodium monolayers on Pt(111) and Pt(100) electrodes studied by IR reflection-absorption spectroscopy, Journal of Electroanalytical Chemistry 358(1-2) (1993) 307-315.

[38] J. Clavilier, M. Wasberg, M. Petit, L.H. Klein, Detailed analysis of the voltammetry of Rh(111) in perchloric-acid solution, Journal of Electroanalytical Chemistry 374(1-2) (1994) 123-131.

[39] N.M. Markovic, T.J. Schmidt, V. Stamenkovic, P.N. Ross, Oxygen Reduction Reaction on Pt and Pt Bimetallic Surfaces: A Selective Review, Fuel Cells 1(2) (2001) 105-116.

[40] K. Broka, P. Ekdunge, Oxygen and hydrogen permeation properties and water uptake of Nafion(R) 117 membrane and recast film for PEM fuel cell, Journal of Applied Electrochemistry 27(2) (1997) 117-123.

[41] S. Slade, S.A. Campbell, T.R. Ralph, F.C. Walsh, Ionic conductivity of an extruded Nafion 1100 EW series of membranes, Journal of the Electrochemical Society 149(12) (2002) A1556-A1564.

[42] K.A. Mauritz, R.B. Moore, State of understanding of Nafion, Chemical Reviews 104(10) (2004) 4535-4585.

[43] A. Gruger, A. Regis, T. Schmatko, P. Colomban, Nanostructure of Nafion (R) membranes at different states of hydration - An IR and Raman study, Vibrational Spectroscopy 26(2) (2001) 215-225.

[44] R. Mallant, PEMFC systems: the need for high temperature polymers as a consequence of PEMFC water and heat management, Journal of Power Sources 118(1-2) (2003) 424-429.

[45] J.T. Wescott, Y. Qi, L. Subramanian, T.W. Capehart, Mesoscale simulation of morphology in hydrated perfluorosulfonic acid membranes, Journal of Chemical Physics 124(13) (2006) 14.

[46] D.J. Gargas, D.A. Bussian, S.K. Buratto, Investigation of the connectivity of hydrophilic domains in nafion using electrochemical pore-directed nanolithography, Nano Letters 5(11) (2005) 2184-2187.

[47] E. Iyer, S. Subramaniam, A. Datta, Importance of Electrostatic Interactions in The Mobility of Cations in Nafion, Journal of Physical Chemistry B 115(27) (2011) 8707-8712.

[48] C. HeitnerWirguin, Recent advances in perfluorinated ionomer membranes: Structure, properties and applications, Journal of Membrane Science 120(1) (1996) 1-33.

[49] T.D. Gierke, G.E. Munn, F.C. Wilson, The morphology in nafion perfluorinated membrane products, as determined by wide-angle and small-angle x-ray studies, Journal of Polymer Science Part B-Polymer Physics 19(11) (1981) 1687-1704.

[50] T.L. Yu, H.L. Lin, K.S. Shen, L.N. Huang, Y.C. Chang, G.B. Jung, J.C. Huang, Nafion/PTFE composite membranes for fuel cell applications, Journal of Polymer Research-Taiwan 11(3) (2004) 217-224.

[51] P. Choi, N.H. Jalani, R. Datta, Thermodynamics and proton transport in Nafion - I. Membrane swelling, sorption, and ion-exchange equilibrium, Journal of the Electrochemical Society 152(3) (2005) E84-E89.

[52] N. Agmon, The Grotthus Mechanism, Chemical Physics Letters 244(5-6) (1995) 456-462.

[53] P. Choi, N.H. Jalani, R. Datta, Thermodynamics and proton transport in Nafion - II. Proton diffusion mechanisms and conductivity, Journal of the Electrochemical Society 152(3) (2005) E123-E130.

[54] M. Bowker, The basis and applications of Hetergenous catalysis, Oxford University Press, Oxford, 1998.

[55] D.A. Bussian, J.R. O'Dea, H. Metiu, S.K. Buratto, Nanoscale current imaging of the conducting channels in proton exchange membrane fuel cells, Nano Letters 7(2) (2007) 227-232.

[56] H.L. Yeager, A. Eisenberg, Perfluorinted Ionomer Membranes - Introduction, Acs Symposium Series 180 (1982) 1-6.

[57] K. Schmidt-Rohr, Q. Chen, Parallel cylindrical water nanochannels in Nafion fuel-cell membranes, Nature Materials 7(1) (2008) 75-83.

[58] E.J. Roche, M. Pineri, R. Duplessix, A.M. Levelut, Small-angle scattering studies of Nafion membranes, Journal of Polymer Science Part B-Polymer Physics 19(1) (1981) 1-11.

[59] M. Fujimura, T. Hashimoto, H. Kawai, Small-angle-xray-scattering studyof perfluorinated ionomer membranes. 1.origin of 2 scattering maxima, Macromolecules 14(5) (1981) 1309-1315.

[60] K. Kodama, R. Jinnouchi, T. Suzuki, H. Murata, T. Hatanaka, Y. Morimoto, Increase in adsorptivity of sulfonate anions on Pt (111) surface with drying of ionomer, Electrochemistry Communications 36 (2013) 26-28.

[61] D. Malevich, V. Zamlynny, S.G. Sun, J. Lipkowski, In situ infrared reflection absorption spectroscopy studies of the interaction of Nafion (R) with the Pt electrode surface, Zeitschrift Fur Physikalische Chemie-International Journal of Research in Physical Chemistry & Chemical Physics 217(5) (2003) 513-525.

[62] Y. Ayato, K. Kunimatsu, M. Osawa, T. Okada, Study of Pt electrode/Nafion ionomer interface in HClO4 by in situ surface-enhanced FTIR spectroscopy, Journal of the Electrochemical Society 153(2) (2006) A203-A209.

[63] J.H. Jiang, A. Kucernak, Investigations of fuel cell reactions at the composite microelectrode vertical bar solid polymer electrolyte interface. I. Hydrogen oxidation at the nanostructured Pt

vertical bar Nafion(R) membrane interface, Journal of Electroanalytical Chemistry 567(1) (2004) 123-137.

[64] J.H. Jiang, A. Kucernak, Mass transport and kinetics of electrochemical oxygen reduction at nanostructured platinum electrode and solid polymer electrolyte membrane interface, Journal of Solid State Electrochemistry 16(8) (2012) 2571-2579.

[65] W.Y. Tu, W.J. Liu, C.S. Cha, B.L. Wu, Study of the powder/membrane interface by using the powder microelectrode technique I. The Pt-black/Nafion (R) interfaces, Electrochimica Acta 43(24) (1998) 3731-3739.

[66] A. Kolics, A. Wieckowski, Adsorption of bisulfate and sulfate anions on a Pt(111) electrode, Journal of Physical Chemistry B 105(13) (2001) 2588-2595.

[67] J. Maruyama, I. Abe, Cathodic oxygen reduction at the interface between Nafion (R) and electrochemically oxidized glassy carbon surfaces, Journal of Electroanalytical Chemistry 527(1-2) (2002) 65-70.

[68] K. Kunimatsu, B. Bae, K. Miyatake, H. Uchida, M. Watanabe, ATR-FTIR Study of Water in Nafion Membrane Combined with Proton Conductivity Measurements during Hydration/Dehydration Cycle, Journal of Physical Chemistry B 115(15) (2011) 4315-4321.

[69] M. Koper, A. Wieckowski, Fuel Cell Catalysis: A Surface Science Approach, Wiley2009.

[70] S. Gottesfeld, I.D. Raistrick, S. Srinivasan, Oxygen reduction kinetic on a platinum RDE coated with recast nafion film, Journal of the Electrochemical Society 134(6) (1987) 1455-1462.

[71] J.B. Floriano, E.A. Ticianelli, E.R. Gonzalez, Influence of the supporting electrolyte on the oxygen reduction reaction at the platinum proton-exchange membrane interface, Journal of Electroanalytical Chemistry 367(1-2) (1994) 157-164.

[72] H. Yano, T. Akiyama, H. Uchida, M. Watanabe, Temperature dependence of oxygen reduction activity at Nafion-coated Pt/graphitized carbon black catalysts prepared by the nanocapsule method, Energy & Environmental Science 3(10) (2010) 1511-1514.

[73] A. Ohma, K. Fushinobu, K. Okazaki, Influence of Nafion (R) film on oxygen reduction reaction and hydrogen peroxide formation on Pt electrode for proton exchange membrane fuel cell, Electrochimica Acta 55(28) (2010) 8829-8838.

[74] J.H. Jiang, A. Kucernak, Solid polymer electrolyte membrane composite microelectrode investigations of fuel cell reactions. II: voltammetric study of methanol oxidation at the nanostructured platinum microelectrode vertical bar Nafion(R) membrane interface, Journal of Electroanalytical Chemistry 576(2) (2005) 223-236.

[75] R. Yadav, P.S. Fedkiw, Analysis of EIS Technique and Nafion 117 Conductivity as a Function of Temperature and Relative Humidity, Journal of the Electrochemical Society 159(3) (2012) B340-B346.

[76] D. Chu, D. Tryk, D. Gervasio, E.B. Yeager, Examination of the ionomer electrode interface using the ferric ferrous redox couple, Journal of Electroanalytical Chemistry 272(1-2) (1989) 277-284.

[77] A. Ma Gomez-Marin, A. Berna, J.M. Feliu, Spectroelectrochemical Studies of the Pt(111)/Nafion Interface Cast Electrode, Journal of Physical Chemistry C 114(47) (2010) 20130-20140.

[78] M. Ahmed, D. Morgan, G.A. Attard, E. Wright, D. Thompsett, J. Sharman, Unprecedented Structural Sensitivity toward Average Terrace Width: Nafion Adsorption at Pt{hkl} Electrodes, Journal of Physical Chemistry C 115(34) (2011) 17020-17027.

[79] R. Subbaraman, D. Strmcnik, V. Stamenkovic, N.M. Markovic, Three Phase Interfaces at Electrified Metal-Solid Electrolyte Systems 1. Study of the Pt(hkl)-Nafion Interface, Journal of Physical Chemistry C 114(18) (2010) 8414-8422.

[80] D. Strmcnik, K. Kodama, D. van der Vliet, J. Greeley, V.R. Stamenkovic, N.M. Markovic, The role of non-covalent interactions in electrocatalytic fuel-cell reactions on platinum, Nature Chemistry 1(6) (2009) 466-472.

[81] D. Strmcnik, D.F. van der Vliet, K.C. Chang, V. Komanicky, K. Kodama, H. You, V.R. Stamenkovic, N.M. Markovic, Effects of Li+, K+, and Ba2+ Cations on the ORR at Model and High Surface Area Pt and Au Surfaces in Alkaline Solutions, Journal of Physical Chemistry Letters 2(21) (2011) 2733-2736.

[82] K. Kodama, Y. Morimoto, D.S. Strmcnik, N.M. Markovic, The role of non-covalent interactions on CO bulk oxidation on Pt single crystal electrodes in alkaline electrolytes, Electrochimica Acta 152 (2015) 38-43.

[83] M. Escudero-Escribano, M.E.Z. Michoff, E.P.M. Leiva, N.M. Markovic, C. Gutierrez, A. Cuesta, Quantitative Study of Non-Covalent Interactions at the Electrode-Electrolyte Interface Using Cyanide-Modified Pt(111) Electrodes, Chemphyschem 12(12) (2011) 2230-2234.

[84] E. Yeager, D. Scherson, Electrocatalysis - Fundamental aspects and recent, Journal of the Electrochemical Society 128(3) (1981) C127-C127.

[85] E. Santos, W. Schmickler, Fundamental aspects of electrocatalysis, Chemical Physics 332(1) (2007) 39-47.

[86] A. Brew, *Electrochemical studies of the oxygen reduction reaction: platinum and platinum bimetallic single crystal electrodes.*Electrochemical studies of the oxygen reduction reaction: platinum and platinum bimetallic single crystal electrodes., Chemistry, Cardiff University, 2015.

[87] B. Lindstrom, L.J. Pettersson, A brief history of catalysis, Cattech 7(4) (2003) 130-138.

[88] J.T. Stock, M.V. Orna, A.C.S.D.o.t.H.o. Chemistry, A.C.S.D.o.A. Chemistry, A.C.S. Meeting, Electrochemistry, past and present, American Chemical Society1989.

[89] N.M. Markovic, R.R. Adzic, B.D. Cahan, E.B. Yeager, Structural effects in electrocatalysis - oxygen redution on platinum low-index single crystal surfaces in perchloric acid solutions, Journal of Electroanalytical Chemistry 377(1-2) (1994) 249-259.

[90] V.R. Stamenkovic, B.S. Mun, M. Arenz, K.J.J. Mayrhofer, C.A. Lucas, G. Wang, P.N. Ross, N.M. Markovic, Trends in electrocatalysis on extended and nanoscale Pt-bimetallic alloy surfaces, Nature Materials 6(3) (2007) 241-247.

[91] L.R.F. Allen J. Bard, Electrochemical Methods: Fundamentals and Applications, Wiley India Limited2001.

[92] A.J. Bard, L.R. Faulkner, Electrochemical methods: fundamentals and applications, Wiley1980.

[93] V.S. Bagotskiĭ, Fundamentals Of Electrochemistry, Wiley-Interscience2006.

[94] M.E.M. Carlos F. Zinola , Elena Pastor Tejera ,   Newton Pimenta Neves Jr., Electrocatalysis: Fundamentals and Applications, International Journal of Electrochemistry 2012(874687) (2012).

[95] A.C. Fisher, Electrode Dynamics, Oxford University Press1996.

[96] D. Pletcher, R.S.o. Chemistry, A First Course in Electrode Processes, Royal Society of Chemistry2009.

[97] S. Srinivasan, Fuel Cells: From Fundamentals to Applications, Springer US2006.

[98] D.C. Grahame, The electrical double layer and the theory of electrocapillarity, Chemical Reviews 41(3) (1947) 441-501.

[99] J. Sanabria-Chinchilla, M.P. Soriaga, R. Bussar, H. Baltruschat, A DEMS study of the electrocatalytic hydrogenation and oxidation of p-dihydroxybenzene at polycrystalline and monocrystalline platinum electrodes, Journal of Applied Electrochemistry 36(11) (2006) 1253-1260.

[100] V. Climent, G.-A. N., F.J. M., Clues for the Molecular-Level Understanding of Electrocatalysis on Single-Crystal Platinum Surfaces Modified by p-Block Adatoms, (2008) 209--244.

[101] G. Feng, J. Huang, B.G. Sumpter, V. Meunier, R. Qiao, Structure and dynamics of electrical double layers in organic electrolytes, Physical Chemistry Chemical Physics 12(20) (2010) 5468-5479.

[102] G. Attard, C. Barnes, Surfaces, Oxford Science Publications New York, 1998.

[103] K. Wandelt, Properties and influence of surface-defects, Surface Science 251 (1991) 387-395.

[104] J.O.M. Bockris, S.U.M. Khan, *Surface electrochemistry, "A Molecular Level Approach"*Surface electrochemistry, "A Molecular Level Approach", Plenum Press, new york and london, 1993.

[105] M.T.M. Koper, Structure sensitivity and nanoscale effects in electrocatalysis, Nanoscale 3(5) (2011) 2054-2073.

[106] M.J. Buerger, Elementary Crystallography An introduction to the fundamental geometrical features of crystals, Wiley, New York,N.Y., 1956.

[107] O.A. Hazzazi, **ELECTROCHEMICAL STUDIESOFMETAL DEPOSITION AND SURFACE CHIRALITYAT**

 WEL**L-DEFINED PLATINUM SINGLE CRYSTAL ELECTRODES**Electrochemical studies of metal deposition and surface chirality at well-defined platinum single crystal electrodes, University of Wales, Cardiff, 2002.

[108] N. Tian, Z.Y. Zhou, S.G. Sun, Platinum Metal Catalysts of High-Index Surfaces: From Single-Crystal Planes to Electrochemically Shape-Controlled Nanoparticles, Journal of Physical Chemistry C 112(50) (2008) 19801-19817.

[109] R. Gomez, A. Rodes, J.M. Perez, J.M. Feliu, A. Aldaz, Electrochemical and in-situ FTIR tudies of the CO adsorption at palladium and rhodium multilayers deposited on platinum single-crystal surfaces. 1.Pt(110) substrate, Surface Science 327(3) (1995) 202-215.

[110] D.M. Kolb, Electrochemical surface science, Angewandte Chemie-International Edition 40(7) (2001) 1162-1181.

[111] G.A. Mabbott, An Introduction to Cyclic Voltammetry, Journal of Chemical Education 60(9) (1983) 697-702.

[112] P.T. Kissinger, W.R. Heineman, Cyclic Voltammetry, Journal of Chemical Education 60(9) (1983) 702-706.

[113] F.G. Will, Hydrogen adsorption on plaitnum singe crystal electrodes I. Isotherms and heats of adsorption, Journal of the Electrochemical Society 112(4) (1965) 451-&.

[114] F.G. Will, Bendanie.Dj, Hydrogen adsorbed by clean platinum electrodes, Journal of the Electrochemical Society 114(12) (1967) 1271-&.

[115] J. Clavilier, R. Faure, G. Guinet, R. Durand, Preparation of mono-crystalline Pt microelectrodes and electrochemical study of the plane surfaces cut in the direction of the (111) and (110) planes, Journal of Electroanalytical Chemistry 107(1) (1980) 205-209.

[116] J.M. Feliu, A. Rodes, J.M. Orts, J. Clavilier, The problem of surface order of Pt single crystals in electrochemistry, Polish Journal of Chemistry 68(8) (1994) 1575-1595.

[117] M.W. Breiter, Voltammetric study of halide ion adsorption on platinum in perchloric acid solutions, Electrochimica Acta 8(12) (1963) 925-935.

[118] J.C. Canullo, W.E. Triaca, A.J. Arvia, Changes in the electrochemical rsponse of polycrystalline platinum-electrodes promoted by the fast repetitive square-wave potential signals, Journal of Electroanalytical Chemistry 175(1-2) (1984) 337-340.

[119] W.E. Ogrady, M.Y.C. Woo, P.L. Hagans, E. Yeager, Electrochemical hydrogen adsorption on Pt(111) and (100) surfaces, Journal of the Electrochemical Society 124(3) (1977) C131-C131.

[120] K. Yamamoto, D.M. Kolb, R. Kotz, G. Lehmpfuhl, Hydrogen adsorption and oxide formation on platinum single crystal electrodes, Journal of Electroanalytical Chemistry 96(2) (1979) 233-239.

[121] J. Clavilier, D. Armand, Electrochemical induction of changes in the distribution of the hydrogen adsorption states on Pt(100) and Pt(111) surfaces in contact with sulfuric acid solution, Journal of Electroanalytical Chemistry 199(1) (1986) 187-200.

[122] N. Markovic, M. Hanson, G. McDougall, E. Yeager, The effects of anions on hydrogen electrosorption on platinum sinlge crystal electrodes, Journal of Electroanalytical Chemistry 214(1-2) (1986) 555-566.

[123] J. O'M. Bockris, Brian E. Conway, E. Yeager, Comprehensive Treatise of Electrochemistry

The Double Layer, 1980.

[124] Angerste.H, B.E. Conway, W.B.A. Sharp, Real Condition of Electrochemically Oxidized Platinum Surfaces. 1.Resolution of Components Processes, Journal of Electroanalytical Chemistry 43(1) (1973) 9-36.

[125] B.V. Tilak, B.E. Conway, Angerste.H, Real condition of oxidised Pt electrodes. 3. Kinetic-theory of formation and reduction of surface oxides, Journal of Electroanalytical Chemistry 48(1) (1973) 1-23.

[126] B.E. Conway, G. Jerkiewicz, Surface orientation dependence of oxide film growth at platinum single-crystals, Journal of Electroanalytical Chemistry 339(1-2) (1992) 123-146.

[127] A.J. Appleby, Theory of Successive Electron-Transfer Steps in Cyclic Voltammetry - Application to Oxygen Pseudocapacitance on Platinum, Journal of the Electrochemical Society 120(9) (1973) 1205-1214.

[128] D. Gilroy, B.E. Conway, Surface oxidation and reduction of platinum electrodes - coverage kinetic and hysteresis studies, Canadian Journal of Chemistry 46(6) (1968) 875-&.

[129] B.E. Conway, Electrochemical oxide film formation at noble-metals as a surface-chemical process, Progress in Surface Science 49(4) (1995) 331-452.

[130] V. Stamenkovic, N.M. Markovic, P.N. Ross, Structure-relationships in electrocatalysis: oxygen reduction and hydrogen oxidation reactions on Pt(111) and Pt(100) in solutions containing chloride ions, Journal of Electroanalytical Chemistry 500(1-2) (2001) 44-51.

[131] J. Clavilier, D. Armand, S.G. Sun, M. Petit, Electrochemical adsorption behaviour of platinum stepped surfaces in sulfuric-acid solutions, Journal of Electroanalytical Chemistry 205(1-2) (1986) 267-277.

[132] D. Armand, J. Clavilier, Influenceof specific adsorption of anions on the electrochemical-behaviour of the Pt(100) surface in acid-medium - comparisons with Pt(111), Journal of Electroanalytical Chemistry 270(1-2) (1989) 331-347.

[133] A. Rodes, J. Clavilier, Electrochemical study of step reconstruction on platinum surfaces belonging to the 011 zone between Pt(3111) and Pt(111), Journal of Electroanalytical Chemistry 344(1-2) (1993) 269-288.

[134] J. Solla-Gullon, F.J. Vidal-Iglesias, P. Rodriguez, E. Herrero, J.M. Feliu, J. Clavilier, A. Aldaz, In situ surface characterization of preferentially oriented platinum nanoparticles by using electrochemical structure sensitive adsorption reactions, Journal of Physical Chemistry B 108(36) (2004) 13573-13575.

[135] J. Xu, A.A. Abd-El-Latif, Y.X. Chen, H. Baltruschat, Electrodeposition of silver on stepped platinum electrode surfaces with (100)-oriented terraces: Generation of confined reaction sites, Journal of Electroanalytical Chemistry 716 (2014) 93-100.

[136] F. ChunJie, F. YbuJun, Z. ChunHua, Z. QingWei, S. ShiGang, Studies of surface processes of electrocatalytic reduction of CO2 on Pt(210), Pt(310) and Pt(510), Science in China Series B-Chemistry 50(5) (2007) 593-598.

[137] B.D. Cahan, H.M. Villullas, The hanging meniscus rotating-disk (HMRD), Journal of Electroanalytical Chemistry 307(1-2) (1991) 263-268.

[138] H.M. Villullas, M.L. Teijelo, The hanging meniscus rotating-disk (HMRD) 1. Dependence of hydrodynamic behaviour on experimental-variables, Journal of Electroanalytical Chemistry 384(1-2) (1995) 25-30.

[139] M.D. Macia, J.M. Campina, E. Herrero, J.M. Feliu, On the kinetics of oxygen reduction on platinum stepped surfaces in acidic media, Journal of Electroanalytical Chemistry 564(1-2) (2004) 141-150.

[140] J.X. Wang, N.M. Markovic, R.R. Adzic, Kinetic analysis of oxygen reduction on Pt(111) in acid solutions: Intrinsic kinetic parameters and anion adsorption effects, Journal of Physical Chemistry B 108(13) (2004) 4127-4133.

[141] J.K. Norskov, J. Rossmeisl, A. Logadottir, L. Lindqvist, J.R. Kitchin, T. Bligaard, H. Jonsson, Origin of the overpotential for oxygen reduction at a fuel-cell cathode, Journal of Physical Chemistry B 108(46) (2004) 17886-17892.

[142] I. Katsounaros, W.B. Schneider, J.C. Meier, U. Benedikt, P.U. Biedermann, A.A. Auer, K.J.J. Mayrhofer, Hydrogen peroxide electrochemistry on platinum: towards understanding the oxygen reduction reaction mechanism, Physical Chemistry Chemical Physics 14(20) (2012) 7384-7391.

[143] S. Treimer, A. Tang, D.C. Johnson, A consideration of the application of Koutecky-Levich plots in the diagnoses of charge-transfer mechanisms at rotated disk electrodes, Electroanalysis 14(3) (2002) 165-171.

[144] H.M. Villullas, V. Brunetti, M.L. Teijelo, The hanging meniscus rotating disk - Part 4. Application to catalytic processes, Journal of Electroanalytical Chemistry 437(1-2) (1997) 255-258.

[145] T.J. Schmidt, V. Stamenkovic, P.N. Ross, N.M. Markovic, Temperature dependent surface electrochemistry on Pt single crystals in alkaline electrolyte - Part 3. The oxygen reduction reaction, Physical Chemistry Chemical Physics 5(2) (2003) 400-406.

[146] A.M. Gomez-Marin, K.J.P. Schouten, M.T.M. Koper, J.M. Feliu, Interaction of hydrogen peroxide with a Pt(111) electrode, Electrochemistry Communications 22 (2012) 153-156.

[147] A.M. Gomez-Marin, R. Rizo, J.M. Feliu, Oxygen reduction reaction at Pt single crystals: a critical overview, Catalysis Science & Technology 4(6) (2014) 1685-1698.

[148] A. Wieckowski, Interfacial Electrochemistry: Theory: Experiment, and Applications, Taylor & Francis1999.

[149] V. Climent, G.A. Attard, J.M. Feliu, Potential of zero charge of platinum stepped surfaces: a combined approach of CO charge displacement and N2O reduction, Journal of Electroanalytical Chemistry 532(1-2) (2002) 67-74.

[150] V. Climent, N. Garcia-Araez, E. Herrero, J. Feliu, Potential of zero total charge of platinum single crystals: A local approach to stepped surfaces vicinal to Pt(111), Russian Journal of Electrochemistry 42(11) (2006) 1145-1160.

Experimental Procedures

2.1 Introduction

Cyclic voltammetry was the main experimental technique used in this study.

2.1.1 Reagents and solutions

Reagent	Formula/Code	Grade	Supplier
Platinum wire	Pt	99.999%	Goodfellows
Palladium wire	Pd	99.99%	Advent research materials
Grit paper	Si/C	4000, 2400, 1200 μm	Struer
Diamond polish	DP Spray P	6, 1, 0.25 μm	Struer
Nylon pads	NMH S/ADH	250mm	Kemet
DP Lubricant blue	N/A	Lubricant	Struer
Dichloromethane	DCM	Reagent	Fisher Scientific
Sulphuric Acid	H_2SO_4	Reagent	Fisher Scientific
Potassium Permanganate	$KMnO_4$	Reagent	BDH
Perchloric Acid	$HClO_4$	70% Suprapur	Merck
Sulphuric Acid	H_2SO_4	95%	Aristar
Nafion	$C_7HF_{13}O_5SC_2F_4$	5% 1100 EW	Johnson Matthey
Potassium Bromide	KBr	99.999%	Sigma Aldrich
Sodium Hydroxide	NaOH	≥99.9995%	Sigma-Aldrich
Potassium Chloride	KCl	99%	Sigma-Aldrich
Potassium perchlorate	$KClO_4$	99%	Sigma-Aldrich
Sodium Fluoride	NaF	99%	Sigma-Aldrich
Lithium Hydroxide	LiOH	99.99%	Sigma-Aldrich
Nitrogen Gas	N_2	Pureshield	BOC
Hydrogen Gas	H_2	99.995%	BOC
Oxygen Gas	O_2	100% N6.0	BOC
Carbon monoxide Gas	CO	99.99%	BOC

Figure 48: Table of chemical reagents used in experiments

2.1.1.1 Water Purification

Millipore Milli Q-plus water system (resistivity >18.2 MΩ cm) was used to provide research grade ultra-pure water (UPW).

2.2 Procedures

2.2.1 Fabrication and preparation of platinum single crystal electrodes

Platinum single crystals were manufactured in house in accordance to methods first reported by Clavilier *et al.* [1]. Briefly, the extremity of a high purity platinum wire (99.999%) was melted in an oxygen/gas flame until a spherical bead of approximately 2-3mm was obtained on the end of the wire. Impurities were removed by gently heating and cooling the bead continuously, allowing the crystallisation of the single crystal structure. Single crystal facets for (111) and (100) planes are visible by eye on the bead. The quality of the bead was further checked by He-Ne 4mW laser alignment in a three-circle goniometer at the end of an optical bench. When a true single crystal has been formed, the laser diffraction spots from 100 and 111 facets are seen at the correct angles (Figure 49).
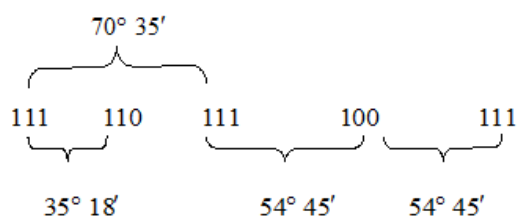

Figure 49: Angles between facets of an f.c.c. crystal

Once this was achieved, the bead is orientated to a specific angle depending on surface structure desired. By simple geometry, the angles for cutting the crystal is started using a (111) or (100) facet as a starting point. The angle was calculated as follows:

hkl based on *efg* facet, where *hkl* is desired surface –

To ensure no movement of the single crystal for the next stage, it is carefully set in epoxy resin. Use of a mechanical polishing machine, a combination of grit paper of decreasing particle size, lubricant and diamond sprays were used to cut the bead half way and polish to a mirror finish. This exposed the surface of specific atomic arrangement required for investigations. The epoxy was removed by soaking in dichloromethane overnight to enable extraction of the crystal with no damage to the surface.

Figure 50: Fabrication and preparation of single crystal electrodes

2.2.1.1 Preparation of Pt single crystals for analysis

After polishing, the single crystal surface is disordered and slightly contaminated. Flame annealing using a Bunsen burner (crystal glows bright yellow/white), followed by cooling in a reducing atmosphere such as hydrogen results in a well-ordered Pt single crystal surface. Care was taken to avoid any ignition of the hydrogen gas. When transferring from the H_2 bubbler to the electrochemical cell, a protecting droplet of ultra-pure water (UPW) was attached to the surface by dipping. This was the standard preparation method of well-defined single crystal surfaces.

Experiments using CO as the cooling environment were also undertaken. The Pt single crystal was flame annealed until white hot in a blue Bunsen burner flame then allowed to cool in a CO atmosphere for 2-5 minutes. This allowed a protective layer of CO to cover the surface and allowed transferring to the electrochemical cell without the need for a protective droplet of UPW. The CO layer was removed from the surface electrochemically, ensuring the potential remained below the potential of the Pt-oxide region, using a potential window 0-0.8 V (Pd/H) for a perchloric acid electrolytic solution.
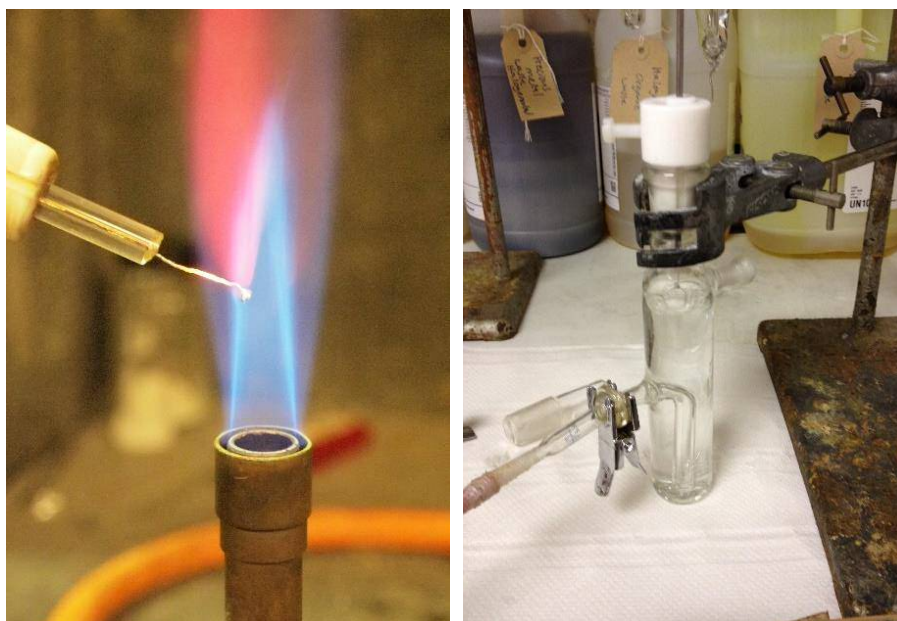
Figure 51: Flame annealing technique and cooling bubbler

2.2.2 Single Crystal measurements

2.2.2.1 Cyclic Voltammetry

Cyclic voltammetry was performed using a CHI800/600 potentiostat. Electrochemical measurements were performed in a three electrode, two compartment Pyrex glass cell. A three-electrode configuration was used consisting of: a palladium/hydride reference, platinum mesh counter and Pt single crystal working electrode (Figure 52).

The palladium reference electrode was a 1 mm rough Pd wire spot-welded onto a 1 mm Pt wire encased in a glass jacket. The reference electrode was prepared by gentle heating in Bunsen flame to remove surface contaminants and charged by immersing in a UPW filled, hydrogen bubbler for 30 minutes. This allows the β-Pd-H phase to form[2], which exhibits a stable potential of -50 mV vs a Standard Hydrogen Electrode (SHE) for several hours in solution.

All glassware was kept free of contamination by following a strict cleaning regime. All glassware was immersed in a solution of dilute permanganic acid for at least one hour. The solution was then safely decanted and all glassware rinsed thoroughly with UPW to remove most the acid. Glassware was steam cleaned for a couple of hours with several periods of rinsing every 20 minutes to ensure any traces of acid were removed.

Once the cell was filled with the desired electrolyte up to the second bridge (Figure 48). The solutions were degassed by bubbling nitrogen through an inlet for 30 minutes to remove any dissolved oxygen. During experiments, a positive overpressure of nitrogen was maintained by flowing the gas over the top of the solution to inhibit any oxygen from entering the cell. The single

crystal was placed in a glass-stemmed Teflon holder and post flame annealing, was then connected to the solution via a good meniscus contact.

A potential window of 0-0.85 V (vs Pd/H) and sweep rate of 0.05 V/s was used for all electrochemical measurements, unless otherwise stated.
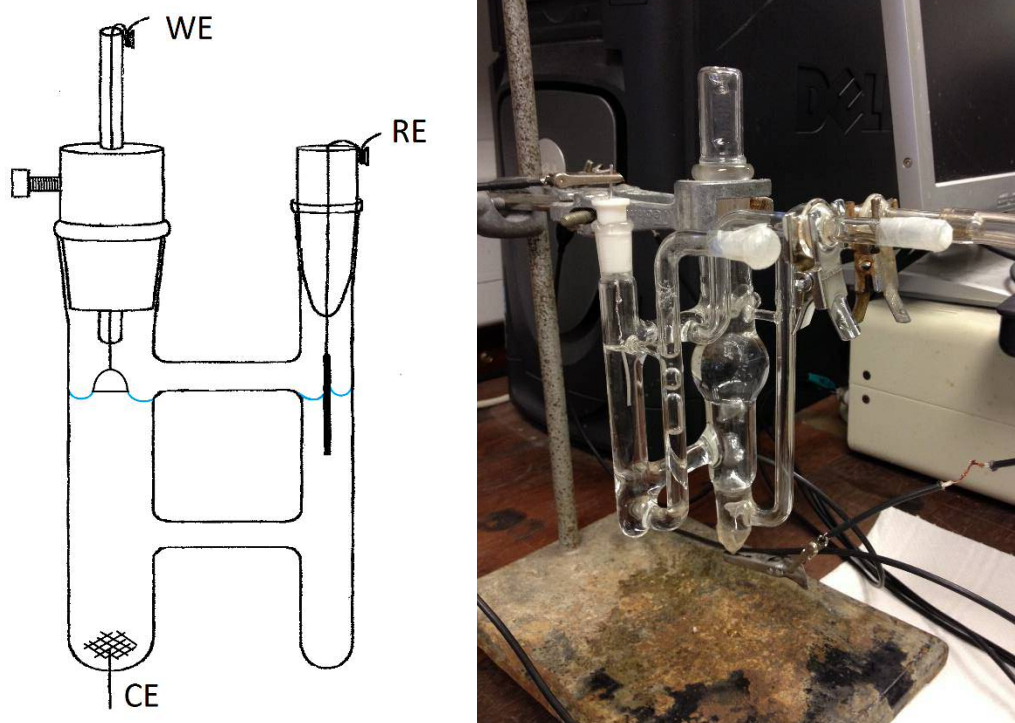

Figure 52: Schematic and photographic CV setup

2.2.2.2 Nafion film Preparation

Nafion solutions were prepared by diluting the as received Nafion solution (from Johnson Matthey) by a factor of 1000. Film deposition was established once a clean cell and well-defined single crystal electrode surface had been achieved (checked by doing a CV). The single crystal surface was first dipped in a dilute solution of ultrapure KBr (10^{-3} M), then washed with UPW ensure a monolayer of bromide ions covered the surface. This allowed better control of Nafion particles to adsorb onto the crystal surface. A droplet of Nafion solution was attached to the surface of the crystal by dipping into a dilute Nafion solution, then dried, using a controlled heating treatment, allowing a polymer film to form. The single crystal was reintroduced to the electrochemical cell *via* a meniscus contact. Rapid potential cycling, using a potential window of -0.1 V to 0.85 V (vs Pd/H) and sweep rate of 0.5 V/s, desorbed the bromide and left behind an ordered the Nafion layer. This is evidenced by observation of "blocked" Pt CV changing into a well-defined voltammogram. Following this, bromide free voltammograms were collected.

2.2.2.3 Chronoamperometry

Once a clean CV had been established, chronoamperometric measurements were undertaken by stepping the potential and measuring the resulting current response.

2.2.2.4 Rotating disk electrode (RDE)

The RDE was used for oxygen reduction reactions and hydrogen peroxide studies. All experiments were performed using a RDE-2, purchased from Basi Analytical, and a CHI 800/600 potentiostat. A three electrode, one compartment Pyrex glass cell was manufactured in house (Figure 53). The Pd/H reference was prepared as described previously then inserted into a Luggin capillary containing the experimental electrolytic solution. All RDE glassware was cleaned as described previously.

The RDE CHI programme used a potential window of -0.04 to 1.0 V (vs Pd/H) and sweep rate 0.03 V/s. All experiments were conducted using a rotation rate of 1600rpm unless otherwise stated.

2.2.2.5 Oxygen reduction reactions

The cell was half filled with a pure solution of 0.1 M $HClO_4$. Oxygen gas was bubbled through the solution *via* the gas inlet for 20 minutes before maintaining a positive overpressure of oxygen by flowing oxygen over the top of the solution gently so the solution surface was not disturbed. Post-flame annealing the Pt single crystal was protected with UPW, connected to the RDE rotating shaft and aligned to be perfectly centred by adjusting the stem (figure 53). It was then introduced to the cell *via* a correct hanging meniscus configuration[3, 4].

2.2.2.6 Hydrogen Peroxide Studies

The cell was half filled with a pure solution of 0.1 M $HClO_4$ and 10^{-3} M H_2O_2. Nitrogen gas was bubbled through the solution via the gas inlet for 20 minutes before maintaining a positive overpressure as described previously, allowing for no oxygen to enter the cell. The Pt single crystal was connected as described above.
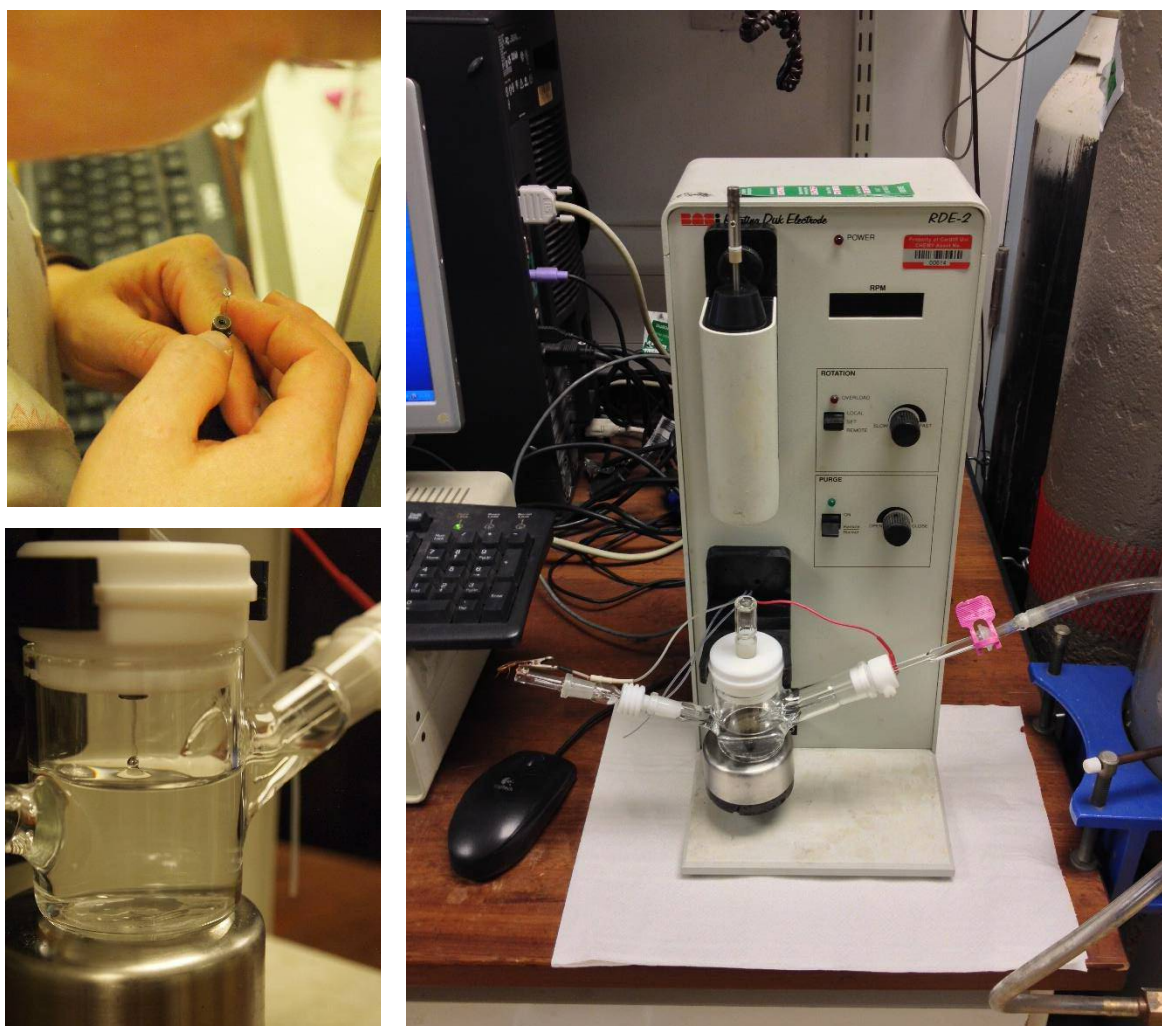
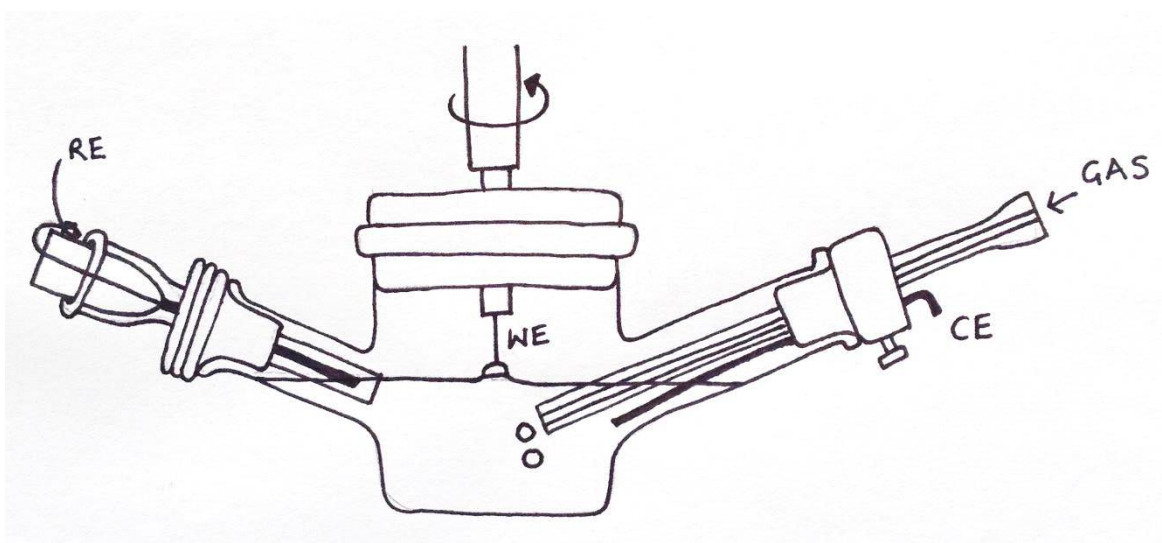*Figure 53: Photographic setup of the RDE*

Figure 54: Schematic of the RDE setup

2.2.2.7 CO displacement and PZTC calculations

CO displacements were undertaken to investigate the PZTC of Pt single crystals [5, 6].

Electrochemical measurements were performed in a three-electrode cell (Figure 55) and setup as CV

experiments. A SHE reference electrode was used connected to the cell via a Luggin capillary and all

potentials are quoted versus this reference unless stated. Once a clean cell and a well-ordered Pt

single crystal electrode was established, the potential was held at 0.1 V. CO(g) was introduced into

the cell, allowing diffusion through the solution towards the interface. During CO adsorption, current

flows as a consequence of the displacement at the interface. This is monitored until it reaches zero.

Still holding the potential at 0.1 V, the cell was then purged of CO by degassing with nitrogen. This

takes around 5 minutes. CO remains adsorbed at the surface during this process. A high potential

voltammogram (above 0.8 V) to ensure the complete oxidation of the adsorbed CO molecules is

undertaken. Following this, a standard voltammogram was taken to ensure the original clean and

well-defined Pt single crystal remained.

Figure 55: Setup for CO oxidation experiments

*PZTC calculations (*Figure 56*)*
1. The positive sweep of a clean CV is integrated to produce a plot of charge versus potential (q vs. E).

2. The CO displacement measurement is integrated to produce a value.

3. A new charge vs potential plot is produced using equation in schematic below (taken from ref [7]), using the CV charge values plus the CO displacement charge.

4. The potential at which the line crosses the zero on the charge axis is the calculated PZTC.
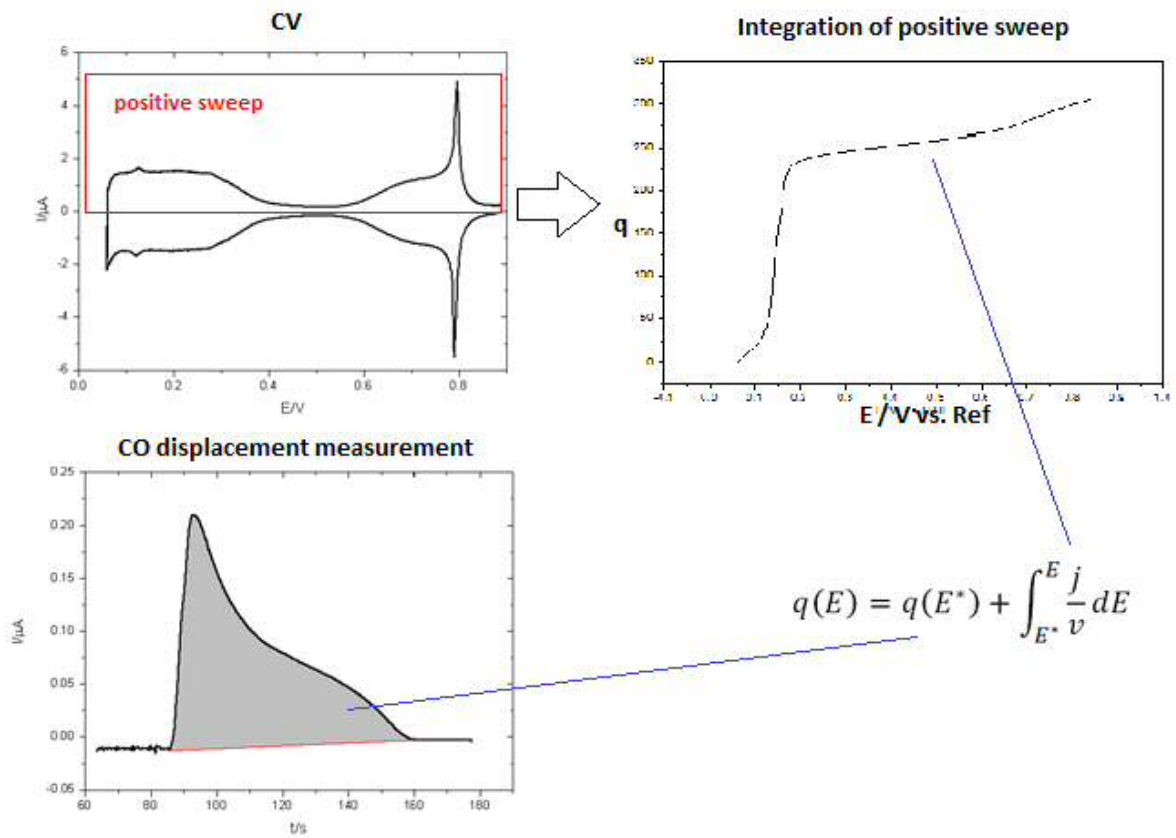
Figure 56: Schematic of PZTC calculations, showing corresponding graphs and equation.
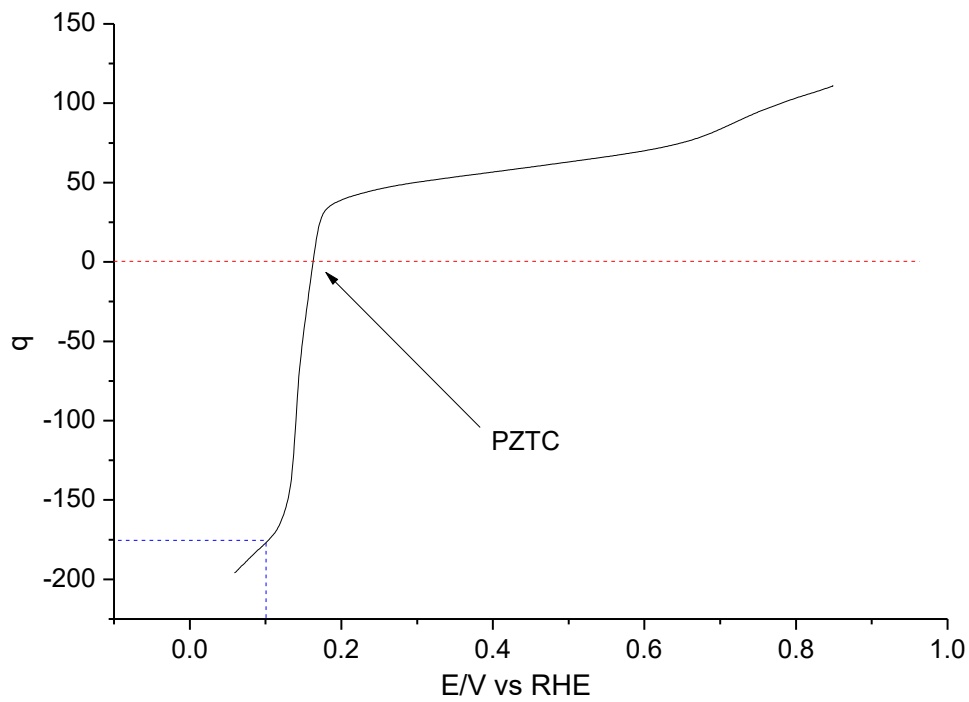
$$q(E) = q(E^*) + \int_{E^*}^{E} \frac{j}{v} dE$$

Figure 57: Charge vs potential curve example post CO displacement processing to reveal the PZTC

2.2.3 References

[1] D. Armand, J. Clavilier, Influenceof specific adsorption of anions on the electrochemical-behaviour of the Pt(100) surface in acid-medium - comparisons with Pt(111), Journal of Electroanalytical Chemistry 270(1-2) (1989) 331-347.

[2] F.A. Lewis, The palladium hydrogen system, Academic Press1967.

[3] H.M. Villullas, M.L. Teijelo, The hanging meniscus rotating-disk (HMRD) 1. Dependence of hydrodynamic behaviour on experimental-variables, Journal of Electroanalytical Chemistry 384(1-2) (1995) 25-30.

[4] H.M. Villullas, M. Lopez Teijelo, Meniscus shape and lateral wetting at the hanging meniscus rotating disc (HMRD) electrode, Journal of Applied Electrochemistry, 1996.

[5] A. Cuesta, Measurement of the surface charge density of CO-saturated Pt(111) electrodes as a function of potential: the potential of zero charge of Pt(111), Surface Science 572(1) (2004) 11-22.

[6] C.R. Gomez, J.M. Orts, A. Aldaz, J.M. Feliu, The potential of zero total charge of single crystal electrodes of platinum group metals, Proceedings of the Symposium on the Electrochemical Double Layer 97(17) (1997) 222-237.

[7] V. Climent, N. Garcia-Araez, E. Herrero, J. Feliu, Potential of zero total charge of platinum single crystals: A local approach to stepped surfaces vicinal to Pt(111), Russian Journal of Electrochemistry 42(11) (2006) 1145-1160.

Investigations into the nature of a traditionally considered "non-adsorbing" anions

$$O_2 + 4H^+ + 4e^- \quad 2H_2$$

$$O_2 \qquad O_2$$
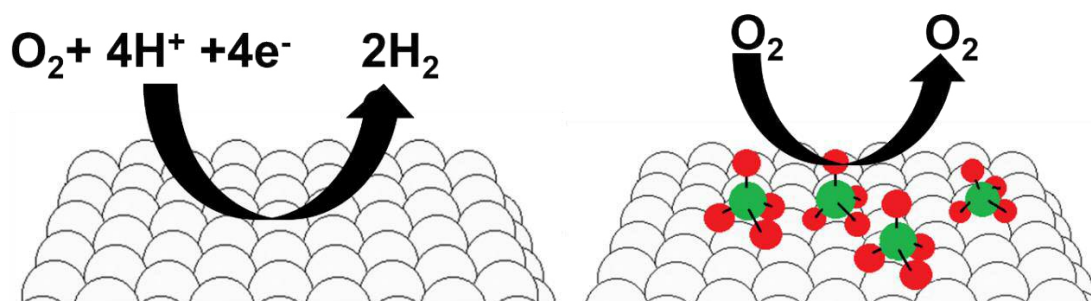
3.1 Introduction

The oxygen reduction reaction (ORR) requires a large overpotential and consequently a large amount of platinum catalyst to run at an appreciable rate. Therefore, understanding the origin of the overpotential for this reaction on real platinum nanoparticle surfaces would represent a crucial [1-7] advance in our fundamental knowledge and this problem lies at heart of much scientific endeavour[3-16].

Since the composition and structure of the electrocatalyst surface are paramount in relation to many electrocatalytic reactions, much work has been carried out using single crystal electrode surfaces to simplify the problem[4-6, 8-10]. Exposing only a specific electrode surface with the desired atomic arrangement to an electrolyte enables structure–activity relationships to be obtained between the adsorbate and surface of electrochemical reactions under investigation and thus may direct synthesis of ''shape-controlled'' nanoparticles for optimal electrocatalytic performance[16, 17]. Early work used single crystals to study the ORR over the basal planes of platinum[8-10]. In these studies, it was shown that in sulphuric acid electrolyte, the activity was relatively low due to the strong specific adsorption of bisulphate anions which block O_2 adsorption and its subsequent reduction at more negative potentials[8-16, 18-20]. In fact, strongly adsorbed ions and impurities often facilitated the two-electron reduction of oxygen to hydrogen peroxide on platinum electrodes[21, 22]. A higher activity for ORR of stepped Pt{111} surfaces in sulphuric acid electrolyte relative to the Pt{111} plane itself has been attributed to the breaking up of an ordered sulphate/bisulphate adlayer formed on Pt{111} at potentials commensurate with the on-set of ORR, thus facilitating greater O_2 adsorption and dissociation due to decreased competition for metallic platinum adsorption sites[4, 5]. To understand the ORR mechanism in the absence of such anion adsorption effects, investigations have

also been carried out using perchloric acid, an electrolyte widely considered to exhibit zero or negligible specific adsorption of ClO_4^- upon Pt(hkl) surfaces[4, 5, 23-27].

However, recent papers by Watanabe and co-workers using CV, in situ infra-red and quartz crystal microbalance measurements have demonstrated on polycrystalline platinum electrodes that perchlorate anions may specifically adsorb, and, as a consequence inhibit ORR, due to introducing a potentially site-blocking specifically adsorbing anion which competes successfully for adsorption sites with O_2[28, 29]. Since it is already well-known that single crystal platinum electrode voltammetry is highly sensitive to specific adsorption, it was thought prudent to test the notion of perchlorate specific adsorption using Pt(hkl) since the effect should be much more prominent compared to polycrystalline substrates[29]. When electrosorption peaks do not overlap with specific adsorption processes (as is found for hydrogen underpotential deposition (H_{upd}) states on Pt{111} electrodes in acidic media for example), no perturbation of these states is observed when switching from non-specific to specific anion containing aqueous media. However, for states corresponding to OH_{ad} formation on Pt(hkl), such electrosorption peaks are strongly modified by specific adsorption, shown by the comparison between cyclic voltammograms of particular Pt(hkl) electrodes obtained in aqueous perchloric or sulphuric acid[14, 19, 20, 30-34]. Specific adsorption of anions may also increase the onset potential for electrochemical oxide formation, again presumably due to competition for adsorption sites between the anion and water dissociation pathways.

Hence, the extent of specific adsorption should also be reflected in the shift in potential for the formation of electrosorbed oxide. The activity towards ORR of basal plane and stepped platinum surfaces is strongly attenuated as electrosorbed oxide is formed since O_2 adsorption and dissociation is facilitated at metallic sites[4, 5, 8]. Hence, both oxide formation and specific adsorption of anions are found to inhibit ORR activity. Recent work has demonstrated that optimisation of adsorbate–substrate interactions (using the Sabatier principle) is also crucial in optimising ORR activity[1, 3, 7, 35], with a number of bimetallic platinum alloy electrodes affording superior activity to platinum in this regard[7, 13, 15], although electrocatalyst stability still remains a challenging problem[36, 37].

Considering the fact that ClO_4^- is known to adsorb (and decompose) at a number of other metal electrode surfaces (including Rh, Ir, Ru and Pd)[38-42], it is important to consider the possibility that ClO_4^- in acidic aqueous media may have more of a role to play in the electro-oxidation of platinum surfaces and also in electrocatalytic reactions such as oxygen reduction. This view contrasts with the role of spectator that this anion currently is thought to hold in most interpretations of platinum electrocatalytic research.

In the present study, the case for specific adsorption of ClO_4^- in perchloric acid electrolyte (as reported by Watanabe *et al*.[28, 29, 43]), is explored by employing cyclic voltammetry studies of Pt(*hkl*) electrodes. The impact that this anion may have on the ORR in relation to Nafions adsorption and other specifically adsorbing species on Pt{111} electrodes will also be discussed.

3.2 Results of specific adsorption investigations

3.2.1 Pt{111} Results

Figure 58 (below) shows CV data collected using a Pt{111} electrode as a function of increasing the concentration of aqueous perchloric acid. The CV responses are typical of a well-ordered Pt{111} in this electrolyte, showing a clear separation between the H_{upd} (0-0.3 V), OH (0.5-0.8 V) and electrochemical oxide (0.95-1.1 V) states[25, 44]. For the H_{upd} electrosorption peaks, there is no impact either upon the magnitude or distribution of electrosorption charge as acid concentration is increased. This suggests that the strength of perchlorate anion adsorption (if occurring) is insufficient to perturb these adsorption states. In contrast, both the OH_{ad} and electrochemical oxide peaks show modifications in their shape and magnitude. The electrochemical oxide peak in particular is observed to shift from 0.98 V (0.05 M) to 1.03 V (2.0 M) with a corresponding increase in intensity and narrowing in half-width. This behaviour would be consistent with the presence of a specifically adsorbing anion competing successfully for adsorption sites with water splitting pathways. In fact, this point is also reflected in the marked attenuation in the broader component of the so-called ''butterfly'' peak (0.5-0.7 V) and the narrower spike (0.74 V), which also shifts to more positive potentials as acid concentration is increased. Both of these components of the butterfly peak have been ascribed to reaction of two types of water with the Pt{111} plane to form OH_{ad}[45].

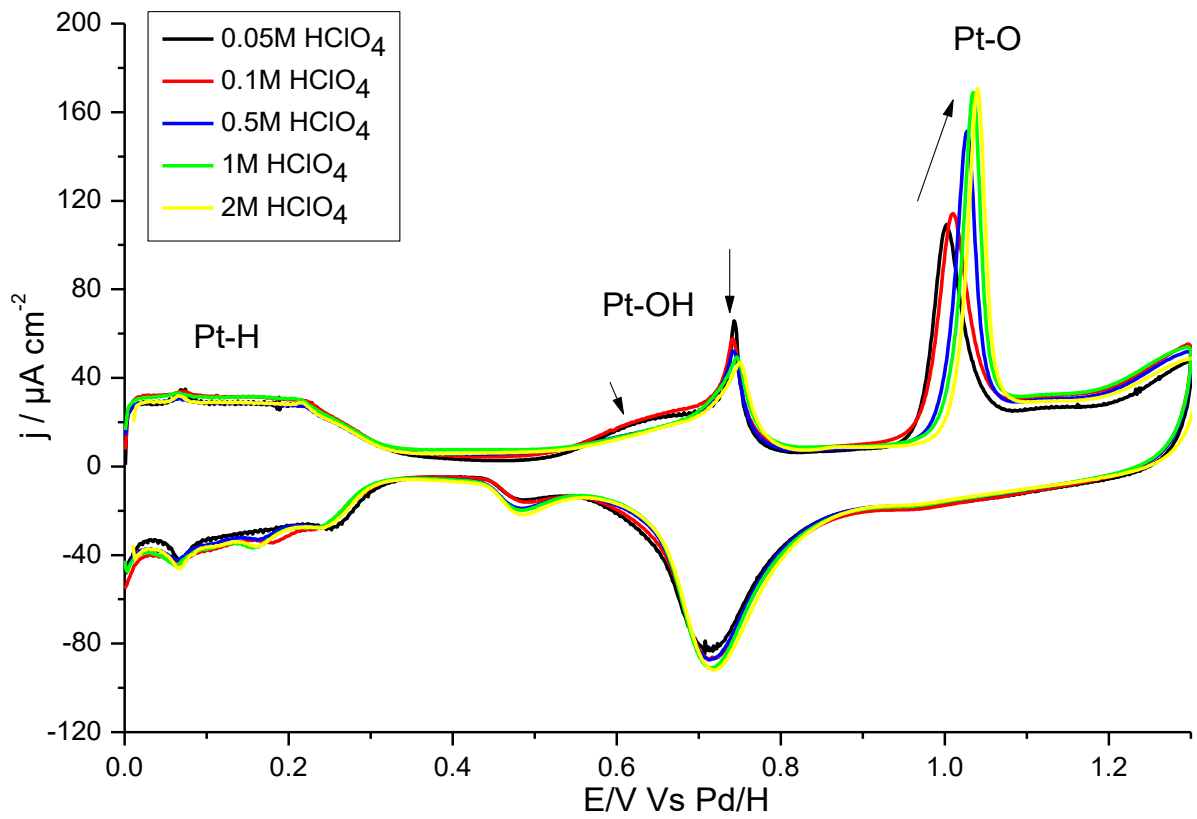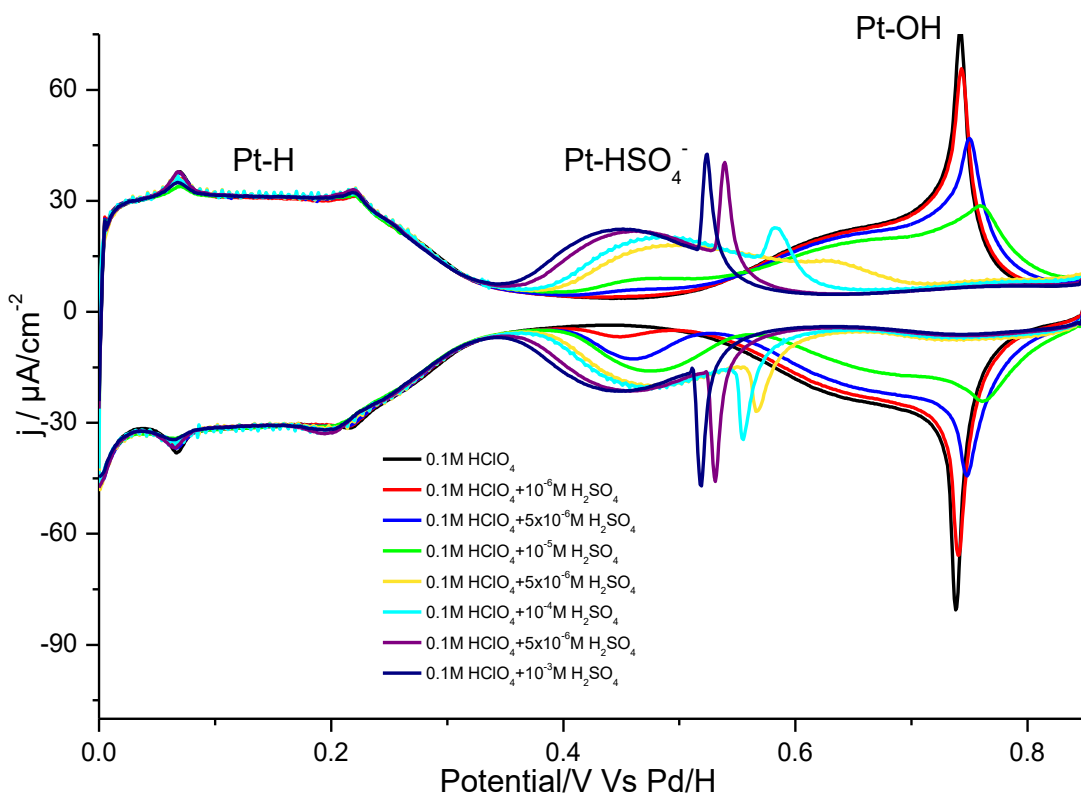*Figure 58: CVs of Pt{111} in varying concentrations of HClO$_4$*

Figure 59: CV of Pt{111} in 0.1 M HClO$_4$ and varying amounts of H$_2$SO$_4$

In Figure 59 we try to mimic this effect by adding small amounts of sulphuric acid to the perchloric acid electrolyte, since sulphate is known to specifically adsorb on Pt{111}. The changes outlined in Figure 58: CVs of Pt{111} in varying concentrations of $HClO_4$ in relation to OH_{ad} are also observed in Figure 59: CV of Pt{111} in 0.1 M $HClO_4$ and varying amounts of H_2SO_4, exemplified by the shift to more positive potentials of the spike and quenching of the broad peak situated at more negative potentials. Of course a new state begins to appear between 0.4 and 0.6 V corresponding to the specific adsorption of sulphate anions[25]. The asymmetry in this feature at concentrations of sulphuric acid less than approximately 10^{-4} M are associated with mass transport effects[45]. Nonetheless, it is clear that when both OH_{ad} and electrochemical oxide formation states are taken together, it suggests strongly that there is a specifically adsorbing anion present. Since perchlorate anions are known to be electrochemically reduced to chloride on some transition metal surfaces[42], measurements of perchloric acid deliberately spiked with chloride were also taken, in order to eliminate the possibility of the strongly adsorbing chloride anion being responsible for the behaviour reported above.

Figure 60 shows data for 0.1 M perchloric acid with 10^{-6} M chloride added as a function of potential sweep rate. Since adsorption of chloride was being determined by mass transport limitations under these conditions, it was possible, by slowing down the sweep rate of the CV, to afford larger and larger degrees of chloride coverage.
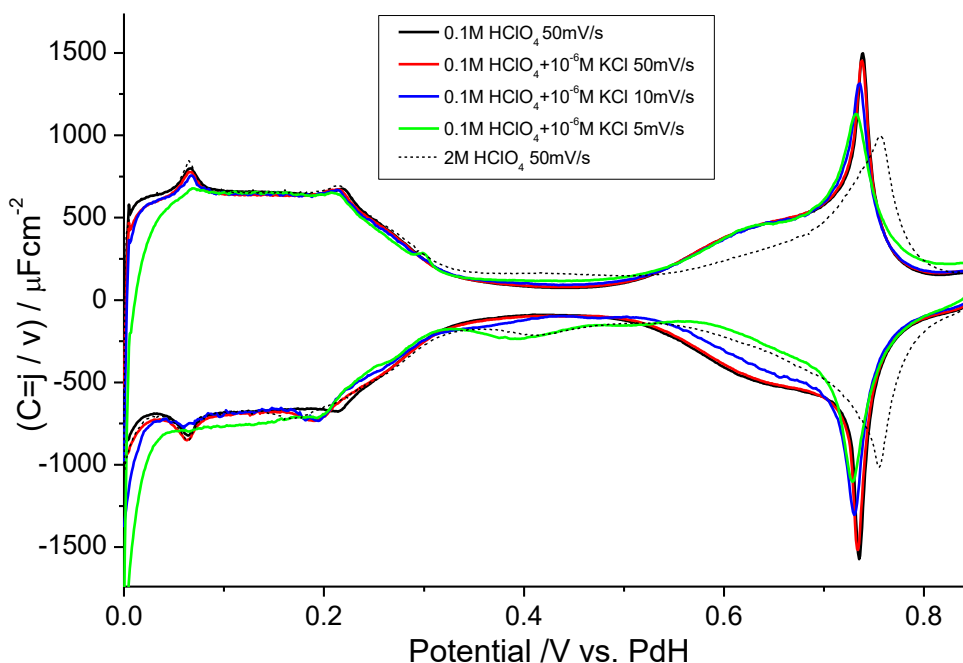

Figure 60: Capacitance versus potential for Pt{111} in 0.1 M $HClO_4$ as a function of uptake of chloride anions

On the positive sweep, the effect of chloride is hardly observed for the broad butterfly peak component but in contrast, the spike systematically shifts to more negative potentials as the sweep rate decreases (in contrast to sulphate). This behaviour has already been reported by Berna *et al.*[45].   On the negative sweep, because the time spent at the more positive potential is greatest, it allows more time for chloride to adsorb (this is also true of the sulphate peaks in Figure 59, where a higher intensity was seen on the negative sweep). As a consequence, the broad butterfly peak feature begins to be attenuated since adsorbed chloride has blocked OH_{ad} sites and a new peak is observed in the 5 mV s^{-1} scan, ascribable to specific adsorption of chloride at 0.4 V. The Pt-H region (0-0.3 V) is unaffected by chloride ions.

The dotted curve in this figure is the superposition of the Pt{111} CV collected in 2 M aqueous perchloric acid. It is evident that an extra peak in this CV upon sweeping negative from 0.85 V is observed at precisely the potential associated with specifically adsorbed chloride. However, when chloride is present as an impurity in the electrolyte, it manifests itself as both a blocking of the OH_{ad} states in the broad butterfly peak feature and a shift to negative potentials in the spike. Yet in 2 M perchloric acid, the spike shifts positively from its position in 0.1 M perchloric acid (like sulphate). Therefore, it is unlikely that the changes seen to peaks in solutions of varying perchloric acid concentrations is due to chloride contamination. Later findings also suggest chloride cannot be present in the electrolyte based on the CV response of Pt{100} in particular (Figure 64). It could be suggested that Pt{111} slowly catalyses the reduction of perchlorate anions at potentials at the beginning of the H_{upd} region and the double layer as found on Rh, Ir and Pd[39, 40, 42] and indeed polycrystalline Pt[38]. On Pt{111} the degree of perchlorate adsorption is extremely small in 0.1 M perchloric acid and hence, only after a x20 increase in perchlorate concentration is this weak effect observed. Evidently, specific adsorption of perchlorate (unlike for bisulphate and dihydrogen phosphate which are isoelectronic with perchlorate), leads to an unstable adsorbed species that decomposes to give chloride anions. The mechanism and kinetics of perchlorate electroreduction have been thoroughly reviewed by Horanyi *et al.*[28, 39, 42] and in particular, the reduction may even be observed by CV at platinised Pt electrodes at slow sweep rates (1 mV s^{-1}) for temperatures greater than 298 K[38]. It should be mentioned also, that spectroscopic evidence for the specific adsorption of perchlorate on Pt{111} was also first reported by Ito *et al.*[46, 47].

3.2.2 Pt{100} Results

Figure 61 shows changes in the voltammetric behaviour (positive sweep) of Pt{100} as a function of increasing perchloric acid concentration. The sweep corresponding to 0.1 M electrolyte is typical of

a well-ordered Pt{100} electrode and, as for Pt{111}, may be delineated into various regions according to the nature of the electrosorption processes occurring.

From 0 to 0.1 V, the oxidation of hydrogen gas formed in the previous negative sweep is recorded[48, 49]. The feature between 0.1 and 0.4 V broadly corresponds to H_{upd} processes, although these are overlapped by a broad feature extending to about 0.6 V that is associated with OH_{ad} on Pt{100}[50]. Finally, at potentials greater than 0.8 V, electrochemical oxidation of the Pt{100} surface takes place, leading to the formation of platinum oxide species[48, 49]. The H_{upd} region of Pt{100} in 0.1 M perchloric acid is noteworthy because it actually consists of two states at approximately 0.3 and 0.4 V. Hence, the potential region 0.1–0.6 V on Pt{100} contrasts quite markedly with Pt{111}, since it comprises of a series of overlapping electrosorption states.
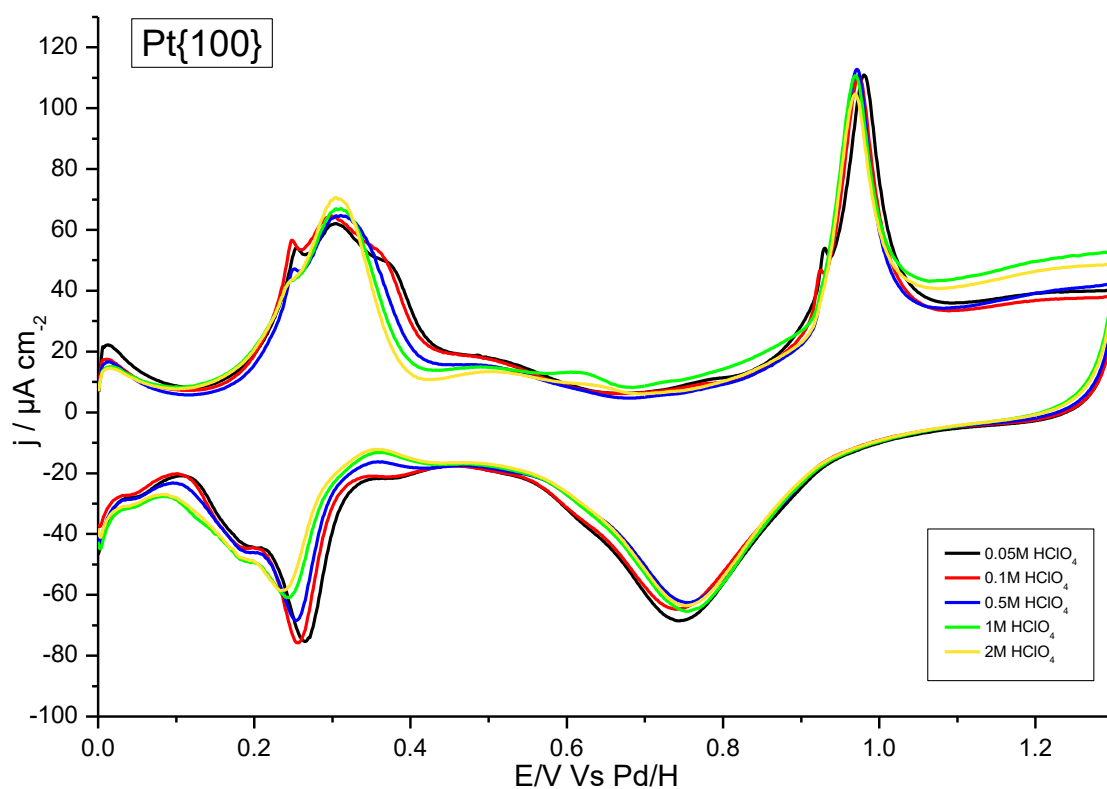
Figure 61: CVs of Pt{100} in varying concentrations of HClO$_4$ including high potential scans

The first noteworthy feature of Figure 61 compared to Figure 58 is that there is hardly any variation in either the onset of platinum oxide formation nor in the potential of the platinum oxide peak itself, irrespective of perchloric acid concentration. Furthermore, although there are clearly redistributions of charge from the H_{upd} state at 0.4 V to that at 0.3 V as acid concentration increases, there is no effect on the OH_{ad} state at 0.5 V. Hence, there appears to be somewhat contradictory behaviour so

far as the possibility of specific adsorption is concerned. The electrochemical oxide and OH_{ad} states of Pt{100} do not appear to be affected by the increase in perchlorate concentration, consistent with non-specifically adsorbing anion behaviour. In contrast, a shift of H_{upd} charge from more positive to more negative potentials as a function of increasing anion concentration is usually a sign of strong specific adsorption with the extent of this shift dependent on the strength of interaction of the anion with the electrode surface[48].

In order to clarify the influence of specific adsorption on Pt{100} electrosorption peaks, solutions of 0.1 M perchloric acid deliberately spiked with small amounts of sulphate were investigated as electrolytes for Pt{100} (Figure 62). The effect of specific adsorption of sulphate anions results in both a shift to more positive potentials of the OH_{ad} peak at 0.5 V, and a displacement of H_{upd} charge from positive to more negative potentials resulting in a new, sharper peak at 0.36 V associated with H_{upd} and sulphate adsorption on Pt{100} extended terraces[49, 51]. However, it should be noted that the strength of specific adsorption of sulphate is insufficient to displace this new sulphate-induced under- potential deposition peak to 0.3 V (the original value of the H_{upd} state at most negative potentials on Pt{100}). In fact, the intensity of the original, lower potential H_{upd} state remains essentially unchanged with the addition of small amounts of sulphuric acid to the 0.1 M perchloric acid electrolyte.
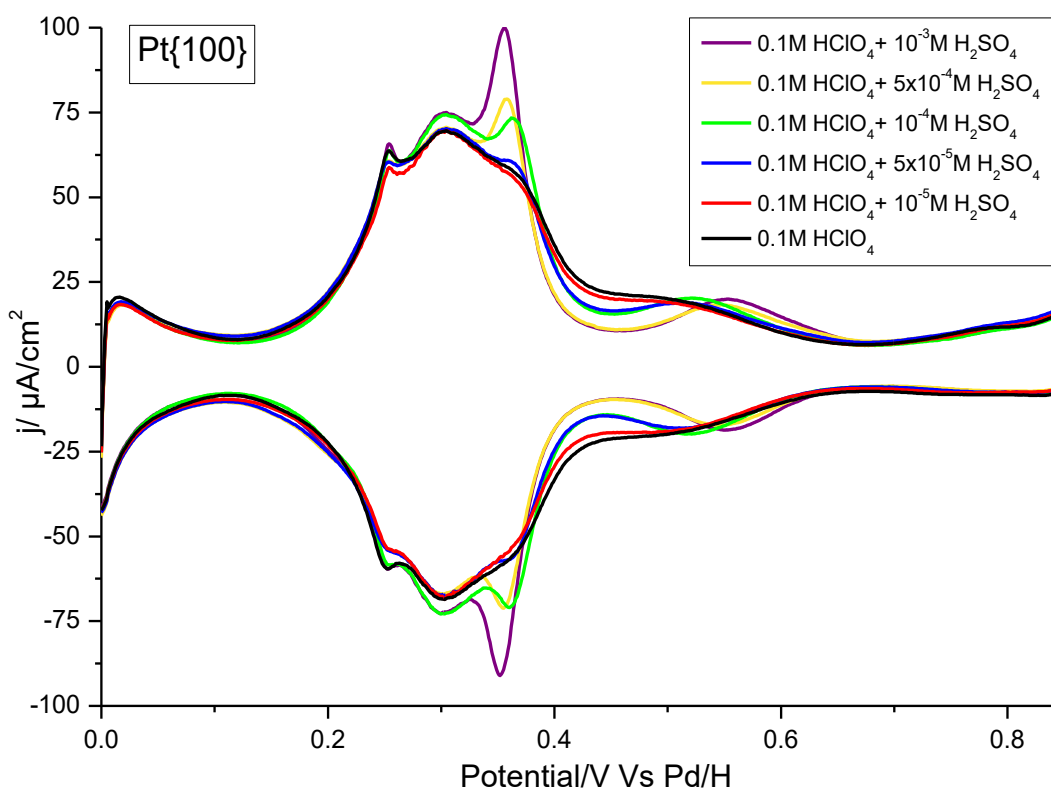

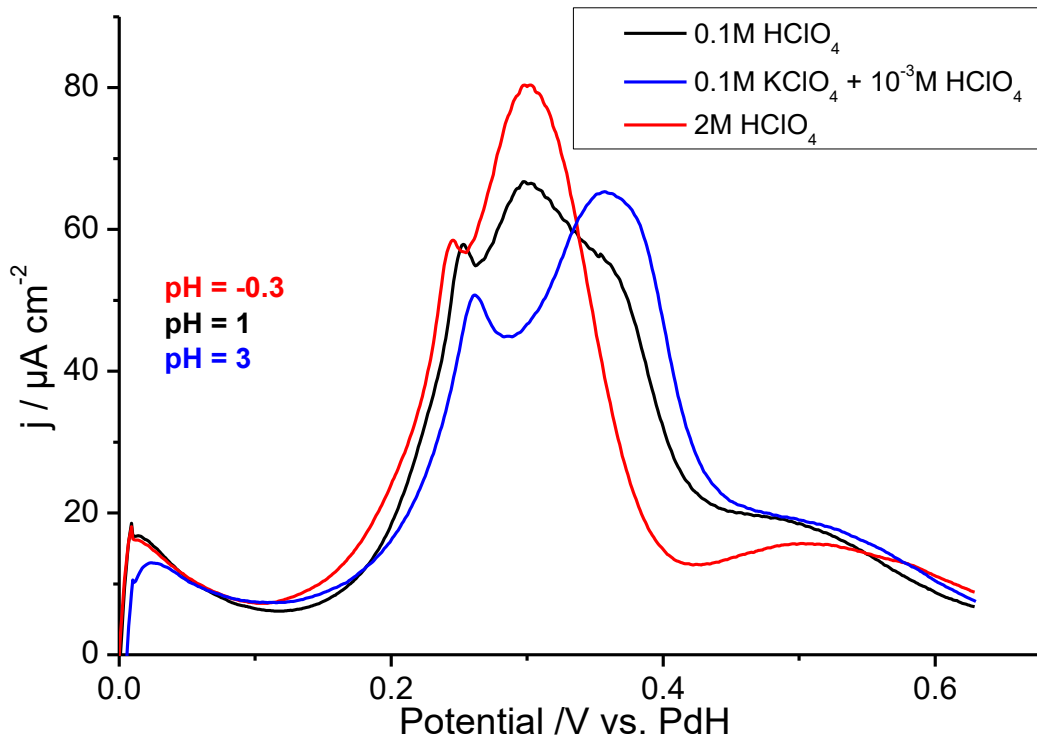Figure 62: CV of Pt{100} in 0.1 M HClO$_4$ and varying amounts of H$_2$SO$_4$

Figure 63: CV data for Pt{100} as a function of perchloric acid concentration and pH
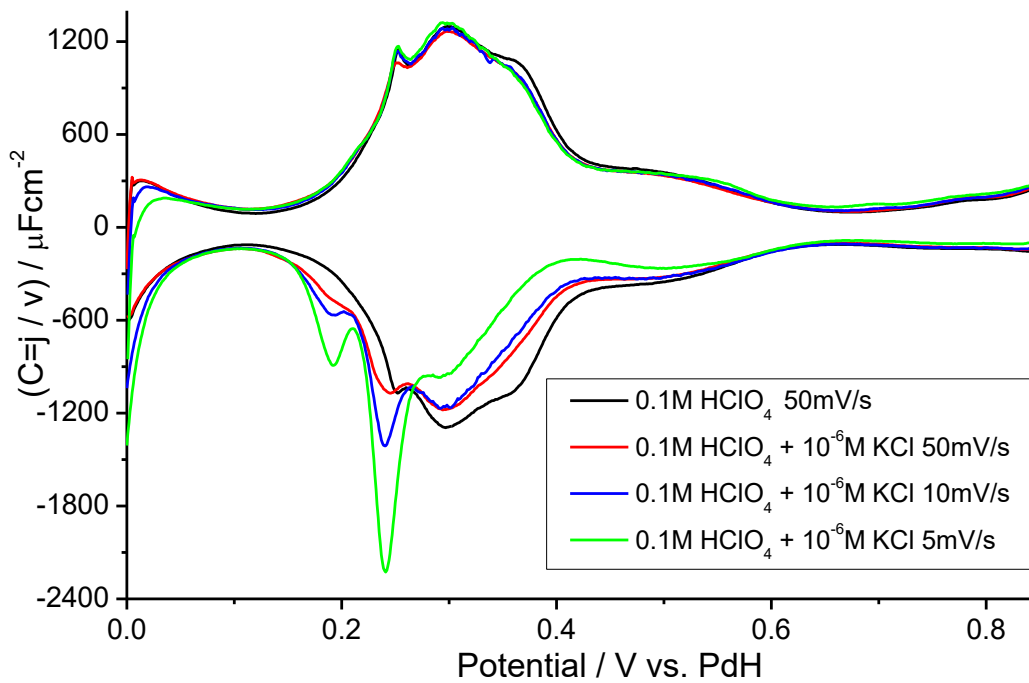

Figure 64: Capacitance versus potential for Pt{100} in 0.1 M HClO$_4$ as a function of uptake of chloride anions

Since even sulphate cannot displace the H_{upd} electrosorption charge into the 0.3 V peak, it is clear that the influence of pH rather than perchlorate anion concentration is the key factor in controlling the relative populations of the two H_{upd} states on Pt{100} with the state at most negative potential being favoured at low pH and the state at higher potential being preferred at higher pH. To test this hypothesis, an electrolyte containing 10^{-3} M perchloric acid in 0.1 M KClO$_4$ was examined. Inspection of Figure 63 confirms that the occupation of sites corresponding to the 0.4 V state are favoured at higher pHs and in fact an isopotential point is observed at 0.33 V between the two peaks. The result at pH = 3 was also obtained in ref.[52]. It may well be that such behaviour may reflect changes in both adsorption energy and the stability of different adsorbate configurations as noted in ref.[53].

Finally, Figure 64 shows the effect of chloride on the voltammetry of Pt{100} in perchloric acid. On the positive sweep, there is hardly any perturbation of the CV obtained in 0.1 M perchloric acid irrespective of potential sweep rate. It should be noted that at 10^{-6} M chloride, the CV profile on the positive sweep bears no relationship to that of Pt{100} in 2 M perchloric acid, attesting to the fact that the possibility of contamination by chloride anions is negligible. Upon engaging the reverse sweep however, significant changes in the H_{upd} states (though not OH_{ad}) are engendered with features negative of 0.3 V consistent with specific adsorption of chloride anions starting to appear as sweep rate is reduced. The large negative shift in H_{upd} charge relative to sulphate behaviour is due to chloride's stronger interaction with the platinum surface.

Taking all of the results of Pt{100} together, it is evident that specific adsorption of perchlorate anions cannot explain all of the changes described. Rather, pH dependent occupation of H_{upd} states appears to interpret the data most satisfactorily, especially the lack of perturbation of OH_{ad} and electrochemical oxide peaks as perchloric acid concentration is increased.

3.2.3 Pt{110} Results

Figure 65 shows how both changes in pH and perchlorate anion concentration influence the CV profile obtained using Pt{110} electrodes. In 0.1 M perchloric acid, the H_{upd} region consists of two states at 0.09 V and 0.22 V. As found for Pt{100}, strong changes in the relative intensities of both states as a function of pH are observed. However, in contrast to Pt{100}, there are also marked changes in the potential of these H_{upd} states as a function of pH. For the peak at 0.09 V, a very small shift of potential is seen from pH = 0.3 to pH = 1, but a shift of 21 mV per pH is observed from pH = 1 to pH = 3. This non-linear variation with pH is somewhat unusual, especially when one realises that a Pd/H reference electrode is being used (if the peak corresponds solely to $H^+_{(aq)} + e^- = H_{ads}$, then no

shift should occur whatsoever relative to a Pd/H reference electrode contained within the electrolyte).

At low pH, this adsorption state does seem to conform to expectations corresponding to electron transfer consistent with the reduction of protons. However, at higher pH, other processes may be occurring. Detailed discussion of such behaviour for step sites on Pt has recently been published by Koper *et al.*[54], whereby rationalisation of step peak shifts as a function of pH is found by having various amounts of hydrogen and water at steps being replaced by OH_{ad} and O_{ad} species. For the H_{upd} peak at 0.22 V, the shift in peak potential is constant over the pH range 0.3 to 1 at 37 mV per pH but shifts by only 15 mV per pH in the range 1–3.
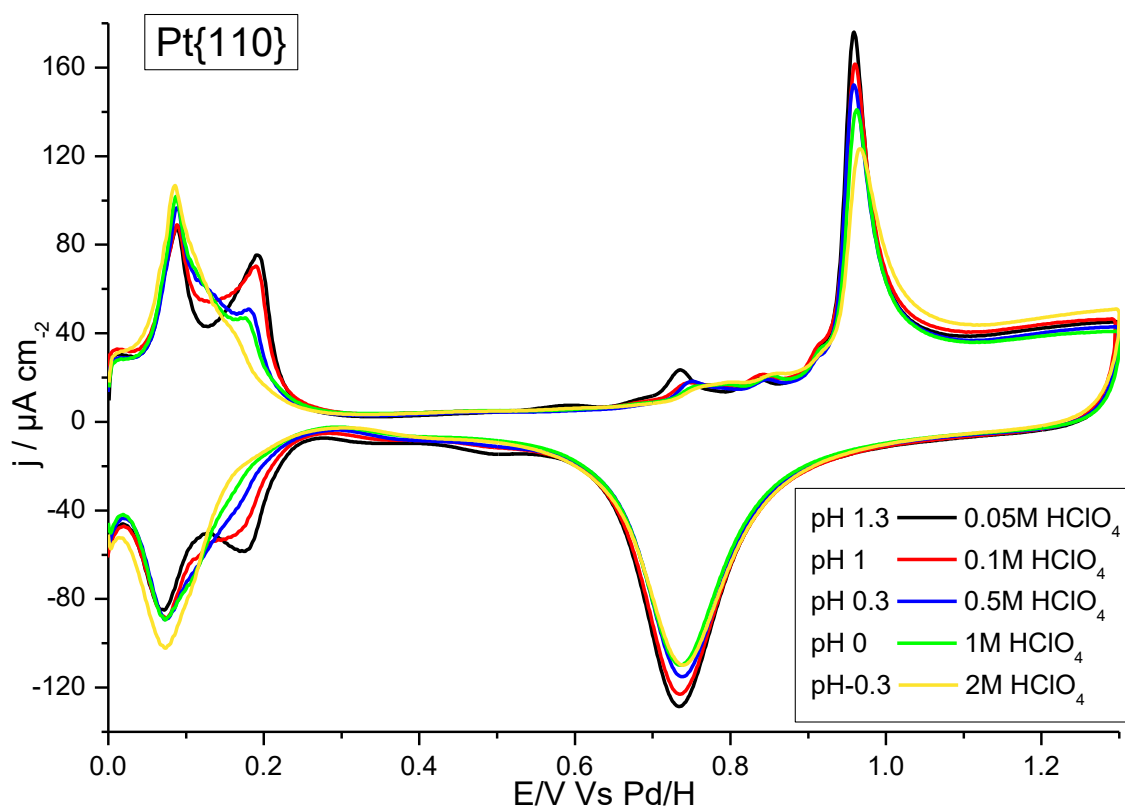
Figure 65: CVs of Pt{110} in varying concentrations of HClO₄

Hence, the hypothesis that OH-type species may be involved also in the H_{upd} process associated with the CV peak at 0.22 V is consistent with its pH dependence (versus a Pd/H reference electrode). It is also evident from Figure 65 that there is a 1:1 correlation between the attenuation in the intensity of the 0.22 V H_{upd} peak and growth in the intensity of the 0.09 V peak, similar to what was observed with Pt{100}, as perchloric acid concentration was increased.

In contrast to Pt{100}, Figure 65 seems to show some inhibition of electrochemical oxide formation between 0.7 and 0.9 V as perchloric acid concentration is increased. This weak inhibition of the onset of oxide formation may be mimicked by spiking the perchloric acid electrolyte with sulphuric acid (Figure 67) whereby a shift of the small oxide peak at 0.74 V can be induced even at 10^{-5} M sulphate concentration. As expected, addition of specifically adsorbing sulphate anions also causes a marked shift to more negative potentials of the H_{upd} state at 0.22 V to 0.11 V. In this context, the shift to more negative potentials of the 0.22 V peak with increasing perchloric acid concentration, seems to imitate the action of adding sulphate anions. However, in one respect it differs markedly. It is found that instead of merely transferring electrosorption charge from the 0.22 V feature into the 0.09 V peak, specifically adsorbed sulphate acts exclusively on the charge associated with the 0.22 V peak and does not in any way increase the intensity of the 0.09 V peak. Again, since sulphate clearly specifically adsorbs more strongly than perchlorate, why should sulphate not cause a more negative shift in H_{upd} charge from the state at 0.22 V? i.e. why does the sulphate induced H_{upd} peak not appear at potentials negative of 0.09 V? As for Pt{100}, the changes induced in the H_{upd} region must be largely the result of changes in pH. Clearly, (as for Pt{100} H_{upd} states), the nature of the H_{upd} peak at more negative potentials is quite different to the peak at more positive potentials, based on pH changes and behaviour exhibited towards specific adsorption. Hence, for Pt{110} the majority of changes in the H_{upd} region as perchloric acid concentration is increased may be ascribed to pH effects, although some perturbation of initial electrochemical oxide phase formation suggests specific adsorption of perchlorate may be causing this effect.
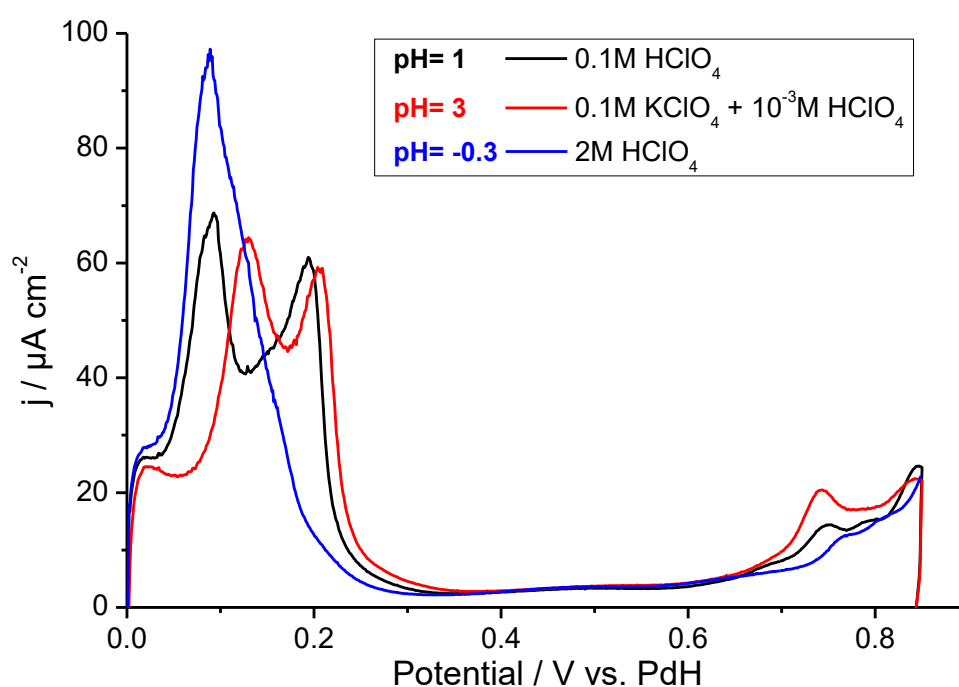
Figure 66: CV data for Pt{110} as a function of perchloric acid concentration and pH
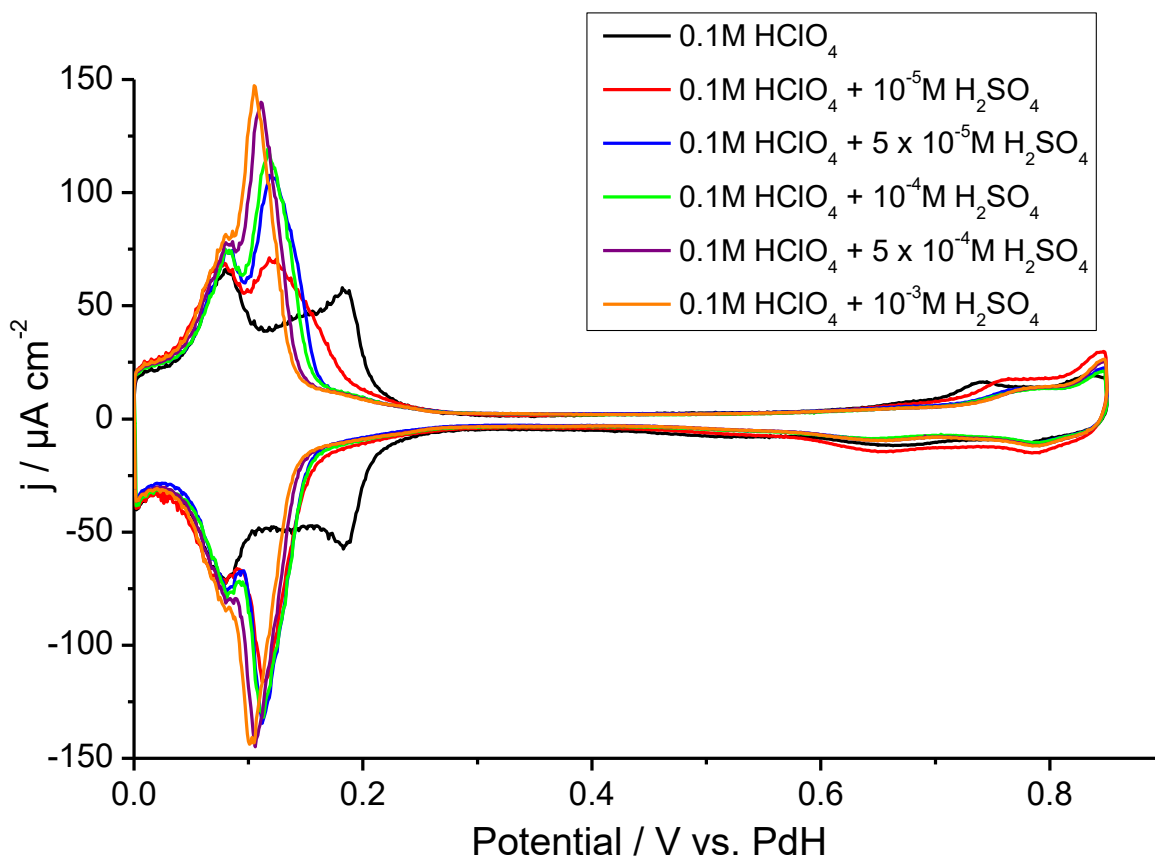
Figure 67: CV of Pt{110} in 0.1 M HClO₄ and varying amounts of H₂SO₄

3.2.4 Results of other platinum surfaces

In order to examine the influence of steps on the possibility of specific adsorption by perchlorate anions, a Pt(311); (a Pt electrode containing 2 atom wide {111} terraces broken up by {100} steps) electrode was examined. Figure 68 shows CV data collected using a Pt(311) electrode as a function of increasing the concentration of aqueous perchloric acid. In 0.05 M perchloric acid, three distinct H_{upd} states at 0.07, 0.24 and 0.32 V are identified. Of these, the peak at 0.07 V remains unchanged in potential and magnitude upon increasing perchloric acid concentration to 2 M. The 0.24 V peak shifts to more negative potentials by 11 mV, whereas the 0.32 V peak shifts by 44 mV when acid concentration is increased, causing appreciable overlap of these two peaks. The magnitudes of changes in peak potentials are similar with those reported for Pt{110} and which suggests a similar underlying mechanism. Namely, that for zero or small changes in H_{upd} peak potential as pH decreases, the important surface process occurring is proton electrosorption.

However, for the 0.32 V peak, a process of H replacement by OH-type species would rationalise the shift[54]. Interestingly, it is the same H_{upd} peaks that are also strongly perturbed by Nafion adsorbed on Pt{hkl}, compared to the states lying more negative of the PZTC of the surface[55]. The possible nature of the OH-type species being perturbed by the Nafion layer was also discussed in ref.[55] and the link with PZTC would in the present study also rationalise why the peaks at most negative potentials are hardly changed by anions (either OH, perchlorate or sulphate) because such peaks lie negative of the PZTC, thus inhibiting anion adsorption.
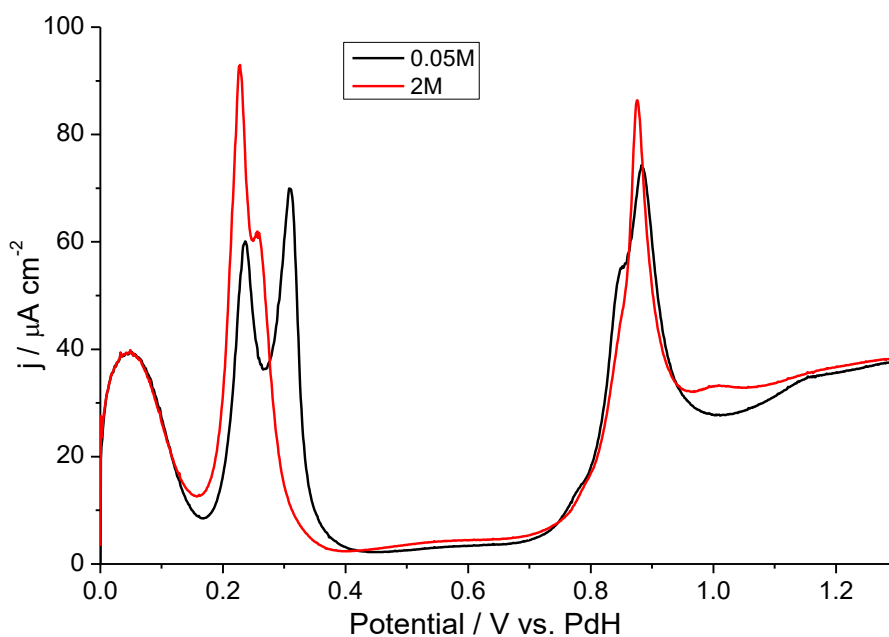
Figure 68: CV data for Pt(311) in various concentrations of HClO₄

Modest changes in the CV of Pt(311) in the range of electrochemical oxide formation are observed upon increasing perchloric acid concentration from 0.05 M to 2 M. The large peak at 0.9 V is seen to narrow, with loss of intensity from the small shoulder at 0.86 V seen in 0.05 M acid and a new state appearing at 1 V. Again, such changes have been attributed to weak specific adsorption of perchlorate.

It is interesting now to compare all of the perchloric acid results reported (especially the electrochemical oxide regions) with a recent paper by Feliu *et al.* (Figure 69) in which the CVs of Pt{111}, Pt{100} and Pt{110}, using 0.1 M perchloric acid aqueous electrolyte are compared with 0.1 M trifluoromethanesulphonic acid (TFMSA) aqueous electrolyte[56]. In ref. [56], the Pt–O peak (at 1 V) on Pt{111} is situated at more positive potentials in perchloric acid compared with TFMSA. We suggest that TFMSA is truly non-specifically adsorbed, but perchlorate is, and it is weak specific adsorption of perchlorate causing this difference in potential of the Pt–O peak.

Similarly, the small oxide peak at 0.74 V on Pt{110} referred to earlier, is found to occur at a more negative potential in TFMSA compared to perchloric acid. We suggest that this is further evidence that TFMSA is non-specifically adsorbed, whereas Perchlorate exhibits a weak specific adsorption on platinum. Finally, for Pt{100}, hardly any change in the Pt–O oxide peak is reported in ref.[56] for the two electrolytes, in agreement with our findings that Pt{100} exhibits the weakest interaction with perchlorate anions. Therefore, it is recommended that any electrocatalytic studies that wish to eliminate the possibility of specific adsorption on platinum should use TFMSA instead of perchloric acid. It is also interesting to note that according to work reported previously from the Frumkin School[57], that specific adsorption of anions is favoured as pH decreases. Hence, there is almost certainly a pH effect also being afforded in the present study in that as pH decreases, the actually interaction of perchlorate anion with the metal surface (if specifically adsorbed) should increase as seen for example in the case of Pt{111}.
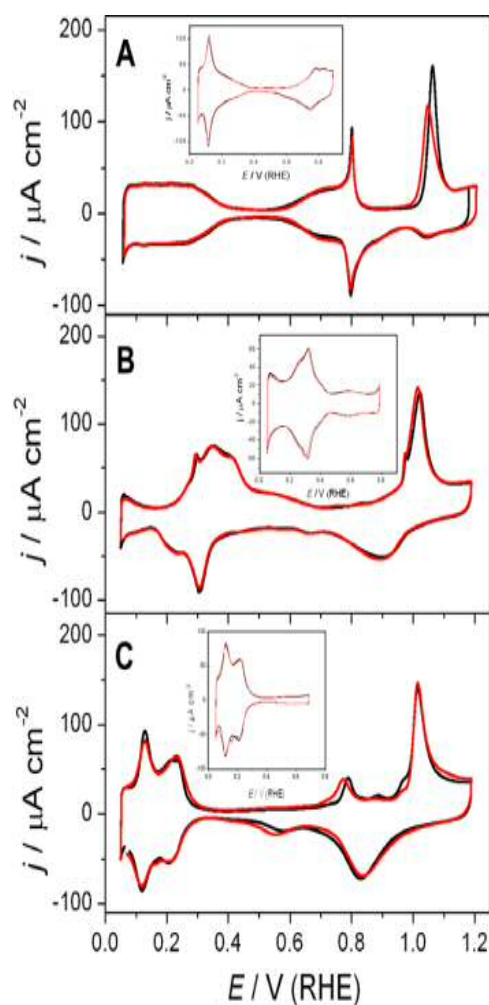
A. Berná et al. / Electrochemistry Communications 10 (2008) 1695–1698

Figure 69: Pt{hkl} in 0.1 M HClO$_4$ (red) and 0.1 M TFMSA (black) from ref [56]

3.2.5 Oxygen reduction

The oxygen reduction reaction (ORR) has been shown in many studies to be sensitive to the presence of any anions in solution that may specifically adsorb on the surface of platinum[4, 5, 9, 21, 22, 58]. On Pt{111}, (bi)sulphate adsorption from sulphuric acid solutions inhibits the ORR so that the half-wave potential ($E_{1/2}$) is 200 mV more negative in potential than that observed in perchloric acid[8, 9]. A similar effect has also been observed in phosphoric acid solutions due to the specifically adsorbing phosphate anion[33]. Bromide and chloride anions also cause an inhibition in the ORR due to their strong specific adsorption on Pt surfaces[21, 22]. In order to emphasise correlations between ORR activity and specific adsorption, Pt{111} in a series of electrolytes is shown (Figure 70 and Figure 71).

As has been shown previously, specific adsorption of (bi)sulphate at potentials around 0.4 V in sulphuric acid protects this surface from oxidation such that the Pt–O peak appears at a rather positive potential (1.3 V), compared to observations in perchloric acid (1 V)[44]. Using the Pt–O peak as a test for specific anion adsorption, then comparing results of 0.1 M HClO$_4$ with 0.1 M NaOH reveals that ClO$_4^-$ also specifically adsorbs (since the Pt–O peak is located at more positive potentials than in 0.1 M NaOH). Presumably, ClO$_4^-$ adsorption "protects" the surface against oxidation, not forming Pt–O until higher potentials are reached (1.00 V) compared with NaOH (0.95 V). The specific adsorption of the sulphonate groups of Nafion[55, 59] also shows to affect the oxide peak of Pt{111} in perchloric acid by shifting Pt–O formation to 1.05 V. The ''butterfly'' peak seen in perchloric acid also follows the exact same trend as for Pt–O as a function of electrolyte specific adsorption strength. The sulphuric acid electrolyte containing the bisulphate adsorption peak at 0.5 V is not included in this analysis because it does not involve OH$_{ad}$.

Figure 71 compares the ORR activity of Pt{111} in electrolytes with varying strengths of anion adsorption (based on the analysis above). ORR activity (as measured using a rotating disc electrode in a hanging meniscus configuration) in 0.1 M NaOH, 0.1 M HClO$_4$, 2 M HClO$_4$, 0.1 M HClO$_4$ with Nafion adsorbed, and 0.1 M H$_2$SO$_4$ are shown.
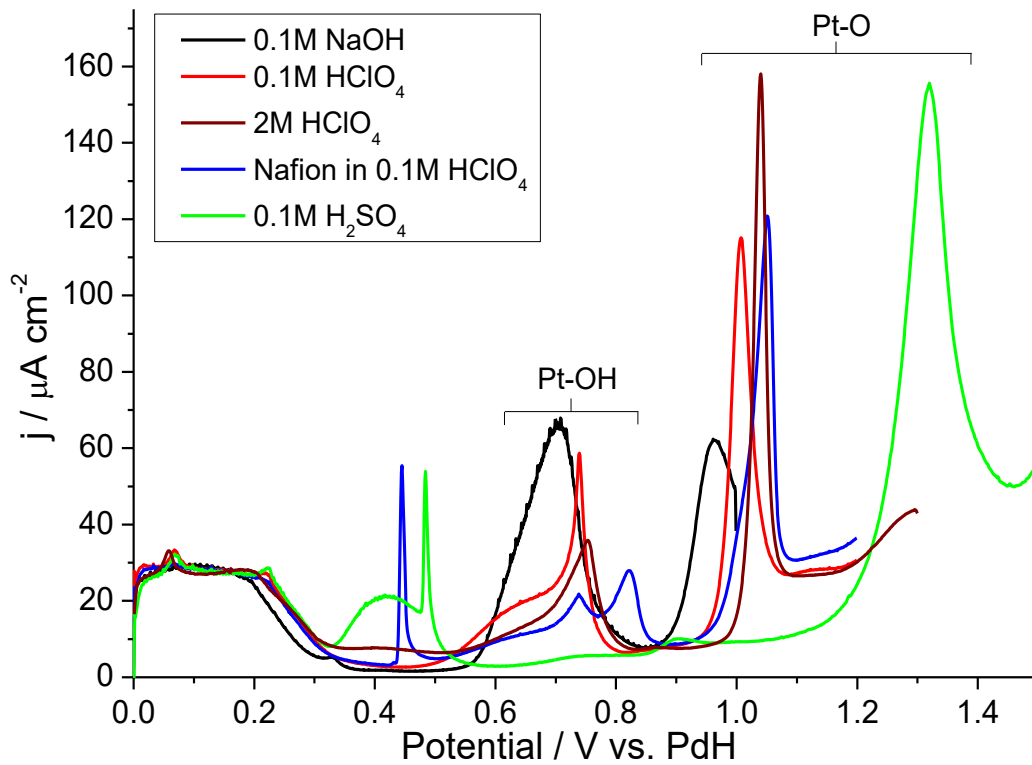
Figure 70: CV data for Pt{111} as a function of specific anion adsorption in various aqueous electrolytes
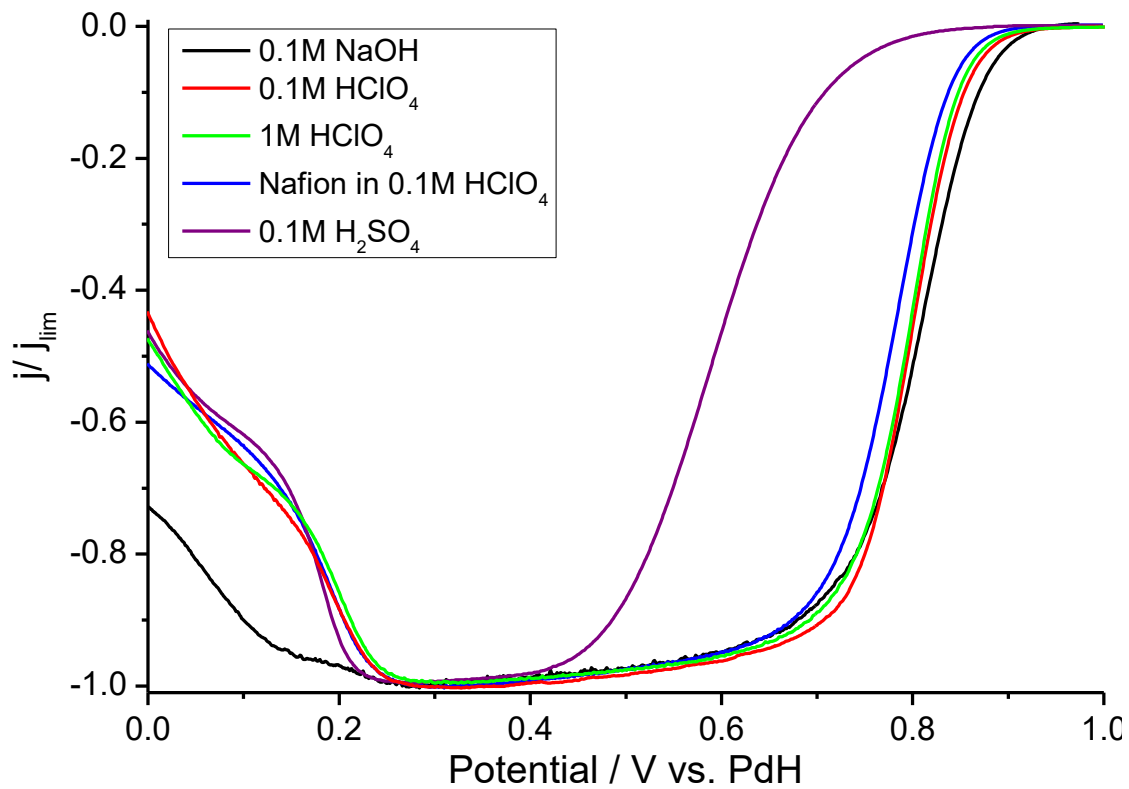

Figure 71: ORR data for Pt{111} in a hanging meniscus rotating disc electrode configuration in various aqueous electrolytes

In 0.1 M H_2SO_4, the activity of Pt{111} is very low, with an $E_{1/2}$ at ~0.6 V, in agreement with previous reports[28, 38, 42]. The other solutions investigated in this study show ORR half-wave potentials clustered around 0.8 V, with their exact order correlating well with the strength of anion adsorption discussed earlier. The ORR of Pt{111} in 0.1 M $HClO_4$ with adsorbed Nafion exhibits the second most negative $E_{1/2}$ value at ~0.775 V, followed by ~0.790 V for 2 M $HClO_4$. The difference in activity for ORR between 2 M and 0.1 M perchloric acid electrolytes is very small, with the lower concentration resulting in a higher activity at ~0.795 V, presumably due to there being less specifically adsorbed perchlorate blocking the reduction of oxygen at lower concentrations of $HClO_4$. The highest activity is seen in 0.1 M NaOH, which presents an $E_{1/2}$ value of ~0.805 V, putting it slightly more positive than 0.1 M $HClO_4$ (Figure 71). This suggests that the hydroxide anion specifically adsorbs weaker than any other anions tested here. Therefore, its inhibitory effect on the ORR is the lowest. It is predicted that TFMSA electrolytes would also exhibit slightly greater ORR activity than 0.1 M perchloric acid due to the non-specifically adsorbing nature of the TFMSA anion.

3.3 Further investigations into the true nature of the perchlorate anion and the effect of pH

Supplementary experiments were carried out to gain further insights regarding the nature of the perchlorate anion adsorption. Potassium perchlorate containing electrolytes were prepared to study both the pH and specific adsorption effects separately.

3.3.1 Pt{111}

Voltammograms of Pt{111} obtained in electrolytes of pH 1, 2, and 3 at constant perchlorate anion concentration (0.1 M) are shown in Figure 72. For the H_{upd} electrosorption peaks, there is no significant impact either upon the magnitude or distribution of electrosorption charge as pH is increased. Since this electrosorption state solely involves hydrogen underpotential deposition (no anions), this is exactly as expected using a Pd/H reference scale. The OH_{ad} (0.5 -0.8 V) and electrochemical oxide peaks (around 1 V) show changes in their shape and magnitude as a function of pH indicating co-adsorption of at least two different species (non-Nernstian shift). The electrochemical oxide peak is observed to shift negatively with a corresponding decrease in intensity as pH is increased. This is consistent with the trend seen in the initial perchloric acid studies and would reflect the weakening of perchlorate-Pt{111} surface interactions as pH increases (figure 13). Additionally, the distribution of charge in the broader component of the so-called ''butterfly'' peak

changes, shifting positive and growing in magnitude as pH increases. The butterfly spike shifts positive and decreases in magnitude, corresponding to different types of water interacting with the surface[45]. This is the opposite trend to what was seen in the initial perchloric acid studies (Figure 58), where a decrease of pH and increase of perchlorate concentration was also shown to shift the butterfly peak to more positive potentials. It has previously been found that potassium cations can also influence how the water interacts[60-62] in this state and so changes seen here could be due to both pH and cation influences. As pH increases, cations should tend to interact more strongly with the Pt electrode surface according to Frumkin[63].
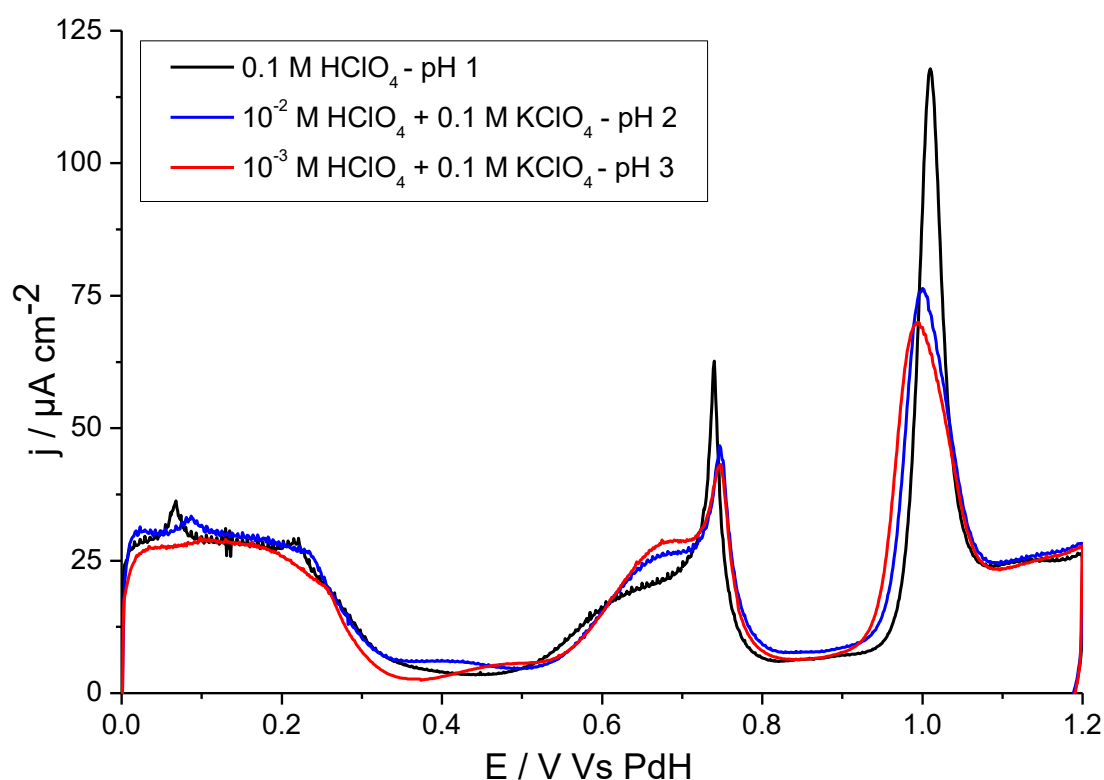
Figure 72: CVs of Pt{111} at constant perchlorate anion concentration and varying pH

Figure 73 shows CV data collected using a Pt{111} electrode as a function of increasing perchlorate concentration in electrolytes at constant pH (pH 3). Inspection of the CVs shows that increasing the perchlorate concentration at constant pH results in the butterfly spike and oxide adsorption state becoming more defined, although there is no shift in potential for any of the adsorption states. This contrasts to the initial perchloric acid results, where an increase of perchloric acid concentration was shown to inhibit the OH butterfly spike and shift it positive. Hence, the slight changes observed probably relate purely to cation effects (so-called non-covalent interactions, Markovic *et al.*[60, 61, 64, 65]).
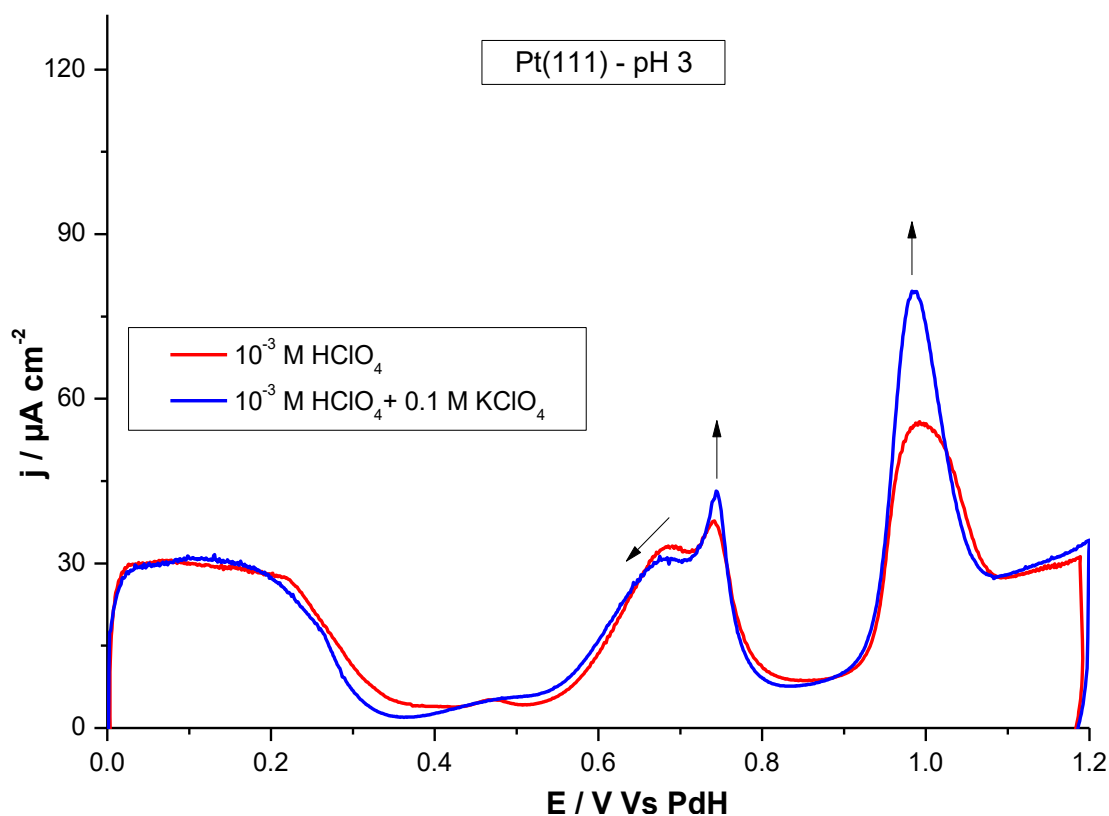
Figure 73: CVs of Pt{111} at constant pH (pH = 3) but varying potassium perchlorate concentration

3.3.2 Pt{100}

Cyclic voltammograms were obtained for Pt{100} in three different pH solutions; 1,2,3. Potassium perchlorate was used to ensure all solutions were near the same concentrations of perchlorate (0.1 M) and the results are shown in Figure 74. The results show that as pH increases from 1 to 3, there are some significant changes in the voltammetric profile of Pt{100}. First, there is a transfer of charge from the adsorption state at 0.3 V to the adsorption state at 0.4 V. Both of these states relate to H_{upd} processes. Secondly, the state at 0.5 V, corresponding to OH_{ad}, shows no change. Finally, the oxide peak at 0.9 V shifts to more positive potentials upon increasing pH. This latter point contrasts strongly with data shown in Figure 73 for Pt{111}. Hence, specific adsorption of perchlorate cannot be used to interpret this effect. However, the shift to more positive potentials as pH increased would be wholly consistent with increasing interaction of potassium cations with the oxide surface. It would also possibly account for changes in the H_{upd} peaks. Recent work by McCrum *et al.*[66] has shown that alkali cations may have profound effects on the H_{upd} region of Pt single crystal electrodes and in fact may afford an explanation for the non-Nernstian shifts in certain H_{upd} peaks as a function of pH. The obvious question to be answered if this is indeed the case would be: why Pt{111} oxide

formation differs from Pt{100} at 1 V? The most obvious difference is the rate of place exchange of the oxide phase itself (see later for chapter six). For Pt{111}, even adsorbing up to 1.2 V in perchloric acid does not lead to reconstruction of the Pt{111} surface upon stripping of the oxide. That is, the Pt{111} voltammetric response remains unchanged after oxide adsorption. In contrast all other Pt{hkl} electrode surfaces are strongly perturbed when oxide formation at potentials > 0.9 V occurs such that massive restructuring of the surface is induced. This place-exchange of oxygen and platinum[67] is also reflected in a strong accumulation of negative charge in [57]. Given these previous findings, it is not too unusual that the potassium cations would interact more strongly with a more negatively charged oxide such that inhibition of oxide formation would take place especially at the higher pH. Thus, it is speculated that the very nature of the surface oxide (oxide overlayer versus place-exchanged bulk oxide phase) determines that cations control the onset of oxide formation in the case of Pt{100} rather than anions. For the H_{upd} region, co-adsorption of cations with H_{upd} states probably induces the variation of voltammetric response as a function of pH [66].
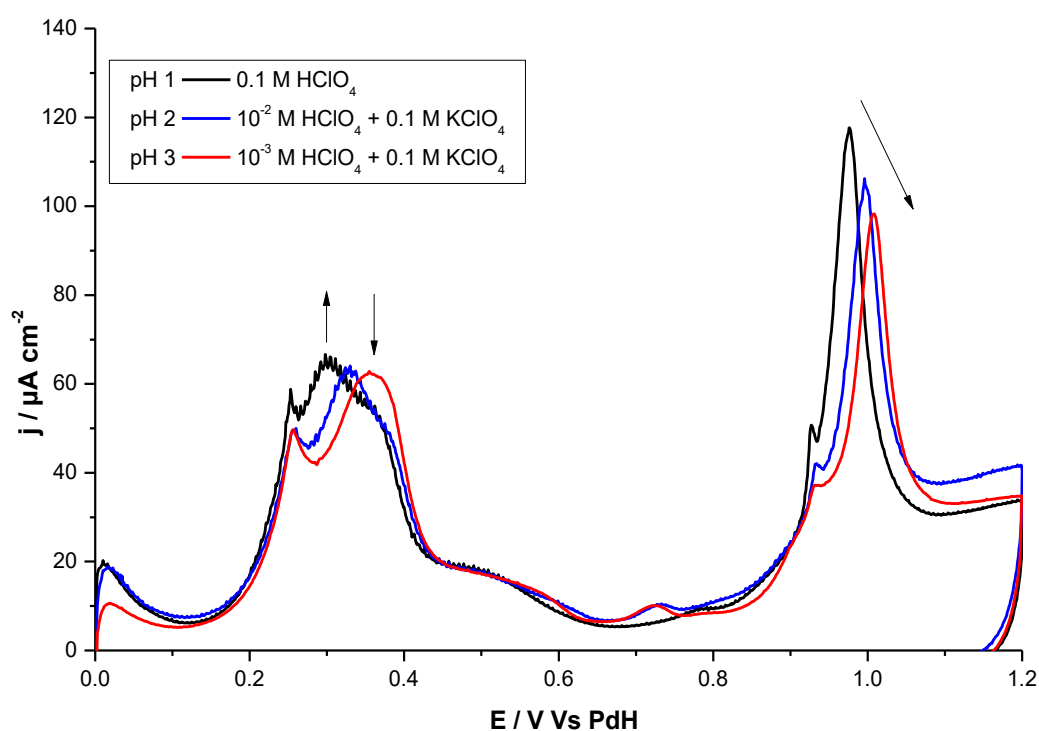

Figure 74: CVs of Pt{100} at constant perchlorate concentration but varying potassium concentration and pH

3.3.3 Pt{110}

The effect of concentration of perchlorate on Pt{110} at constant pH was investigated by obtaining voltammograms of Pt{110} in 10^{-3} M $HClO_4$ and 10^{-3} M + 0.1 M $KClO_4$ (Figure 75). Results show all

adsorption peaks to be sharper upon increasing the concentration of perchlorate whilst keeping the pH constant. For oxide adsorption at potentials > 0.9 V, the lack of a shift in potential of the oxide peaks suggests a lack of "anion control" on the formation of this state (more anions would presumably inhibit oxide formation to a greater extent). However, there is a definite narrowing in the state at 1 V indicating much stronger lateral interactions between the adsorbed species [68]. It is difficult to know if excess perchlorate or potassium cation is responsible for this effect. However, the H_{upd} region changes would certainly indicate a very subtle influence of cations and anions on the H_{upd} states. For the state at 0.21 V, a shift to more negative potentials with increasing anion concentration would certainly reflect specific adsorption of anions as being operational. Conversely, the shift to more positive potentials of the peak at 0.1 V would be a consequence of increased cation adsorption. We shall see in the next chapter, based on local and global values of PZTC data [69, 70], that this is precisely the expected behaviour since the former peak is found to be dominated by anion adsorption and the latter by cation adsorption. The influence of "Ohmic drop" in the cell is

discounted based on the coincident potentials of all oxide peaks at similar current densities and the opposite peak potential shifts exhibited by the H_{upd} region.
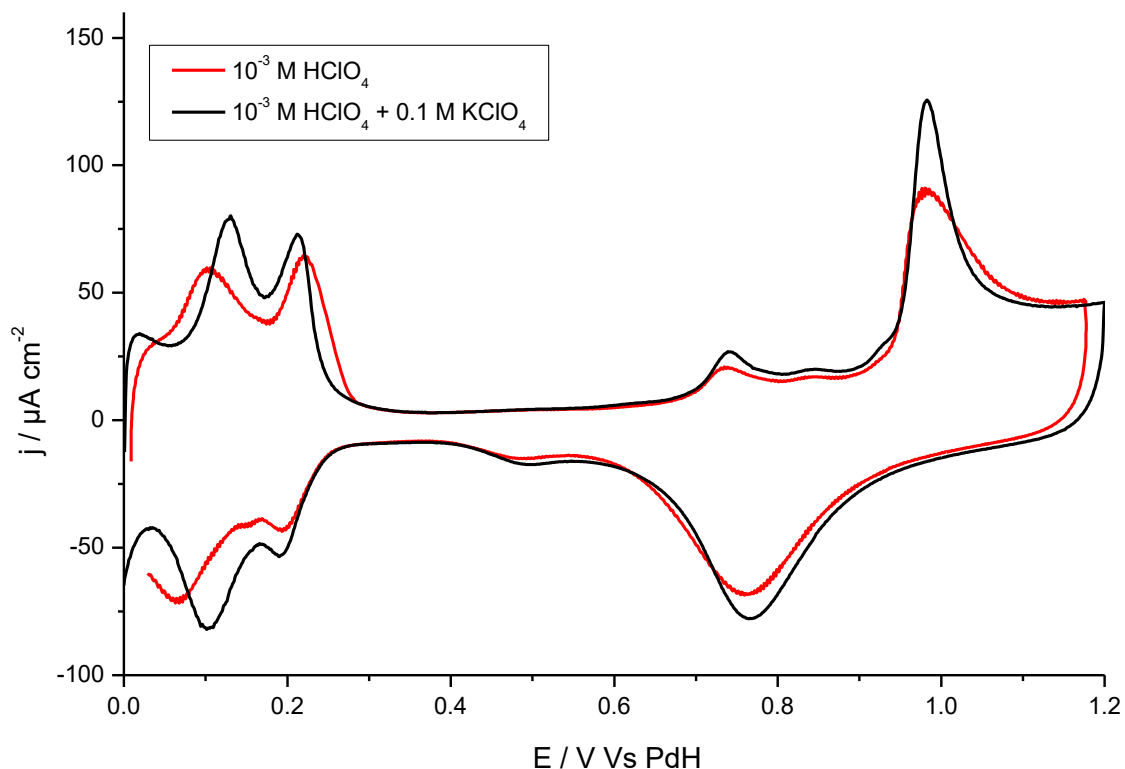

Figure 75: CVs of Pt{110} in pH 3 solutions

3.3.4 The influence of Nafion on Pt{111}

Due to the fact that Nafion can be used as a probe of OH_{ad} on platinum (due to its specifically adsorbing nature which inhibits some OH adsorption [55]), experiments were undertaken to delineate the effect of perchlorate adsorption on platinum in the presence of Nafion. Figure 76 shows CV data collected using a Nafion coated Pt{111} electrode as a function of increasing concentration of aqueous perchloric acid.

The CV responses for the 0.1 M $HClO_4$ solution are typical of Nafion-modified, well-ordered Pt{111} electrode in this electrolyte, showing a clear separation between the H_{upd} (0 - 0.3 V), Nafion spike (0.45 V), perturbed OH_{ad} (0.5 - 0.8 V) and electrochemical oxide states (0.95 - 1.1 V) [55, 71, 72]. For the H_{upd} electrosorption feature, there is negligible impact upon the magnitude or distribution of electrosorption charge as acid concentration is increased. This suggests that the strength of perchlorate anion adsorption (if occurring) is insufficient to perturb these adsorption states. The OH_{ad}, now perturbed by the presence of Nafion at 0.82 V, has not been affected by the change in perchloric acid concentration, again, contrasting with the Nafion-free Pt{111} studies (Figure 58). In Figure 76, the OH_{ad} feature showed a shift towards more positive potential with increasing perchloric acid concentration. Increasing the perchloric acid concentration does influence the adsorption states corresponding to Nafion (0.4-0.55 V) together with the electrochemical oxide adsorption peak at 1.1 V. The Nafion spike is seen to shift negatively upon increasing perchloric acid concentration/decreasing pH. The electrochemical oxide peak does not shift with changes in perchloric acid but the magnitude of the peak is affected for the lowest concentration perchloric acid solution. The Nafion spike is a manifestation of specific adsorption of sulphonate anions [59] and therefore, an increase in pH would be expected to decrease the strength of specific adsorption and result in a shift to more positive potentials as observed. It means that the Nafion layer in this case must be thin enough to equilibrate with the bulk electrolyte such that local pH (associated with the highly acidic Nafion) is not established, otherwise no shift in sulphonate adsorption potential should occur when changing bulk pH. The changes in oxide peak with acid concentration at 1.1 V probably indicate a mixture of Nafion-influenced and Nafion-free surface (the fact that the normal "butterfly" feature is observed means a heterogeneous distribution of Nafion is present on the surface of Pt{111}). The part of the peak shifting to more negative potentials as pH increases is what would be expected for Nafion-free regions (see Figure 76). The negligible change in oxide peak potential suggests that persulphonate anions specifically adsorb more strongly than perchlorate, (in accordance with earlier published work[55]), and so the peak potential remains unaffected by perchlorate. Although in Figure 58, it was seen that perchloric acid concentrations > 2M might afford some persulphate displacement by perchlorate, according to the oxide peak shifts at least.
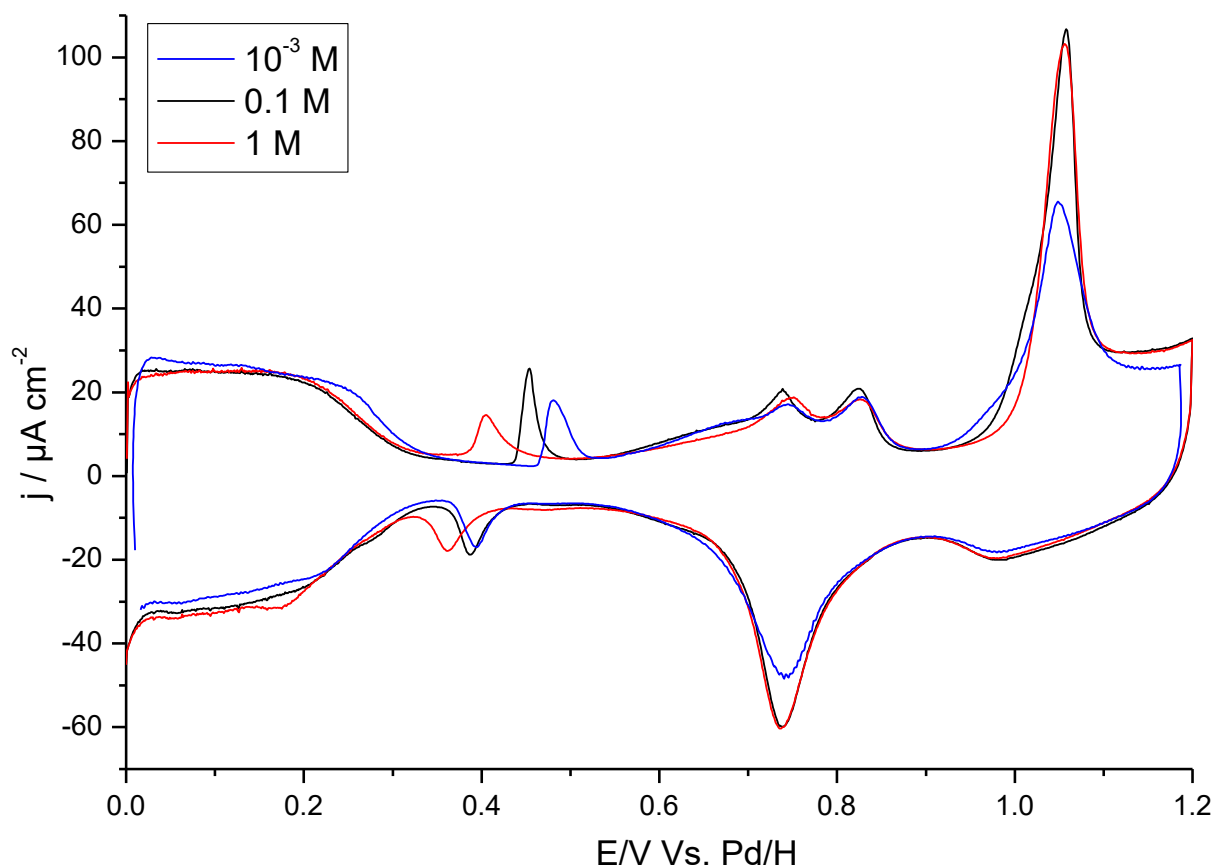
Figure 76: CVs of Nafion-modified Pt{111} as a function of HClO$_4$ concentration

Figure 77 shows how pH as a function of constant perchlorate anion concentration impacts upon a Nafion-modified Pt{111} electrode. It should be noted that the potassium cation concentration is also varying. Some common features discussed earlier are apparent. The first of these is in relation to the Nafion "spike" at 0.45 V which is seen to shift to more positive potentials as pH increases. This is interpreted as before in terms of a weakening of the Pt{111}-sulphonate surface interaction and a shift to more positive potentials of sulphonate adsorption as pH increases. The shift to more negative potentials of the oxide peak around 1 V reflects a weakening of both sulphonate and perchlorate specific adsorption as pH increases, thus decreasing the inhibition of oxide formation by these anions as pH increases. Similar to Figure 76, the sharp peak component of the so-called "butterfly" feature, ascribable to the Nafion-free surface (peak at 0.72 V), does not change potential and therefore does not relate to anion or cation interactions changing. As asserted by Feliu *et al.*, it more likely involves different forms of water[45, 50]. The only feature that is perturbed by increasing pH (and by extension potassium cation concentration) is the Nafion-induced OH$_{ad}$ peak at 0.82 V which shifts to more negative potentials. If this feature was associated with anions, it should shift in the opposite direction due to anions adsorbing more strongly at lower pH (hence seen at lower potentials). Furthermore, pH does not influence the position of this peak. Therefore, it is concluded

that the increase in potassium cation concentration (coupled with an increase in pH) causes potassium cations to interact with the water layer around the Nafion-covered surface via non-covalent interactions [60, 61]. Presumably, potassium cations at low pH do not influence water adsorbed at Nafion-free regions in a similar manner.
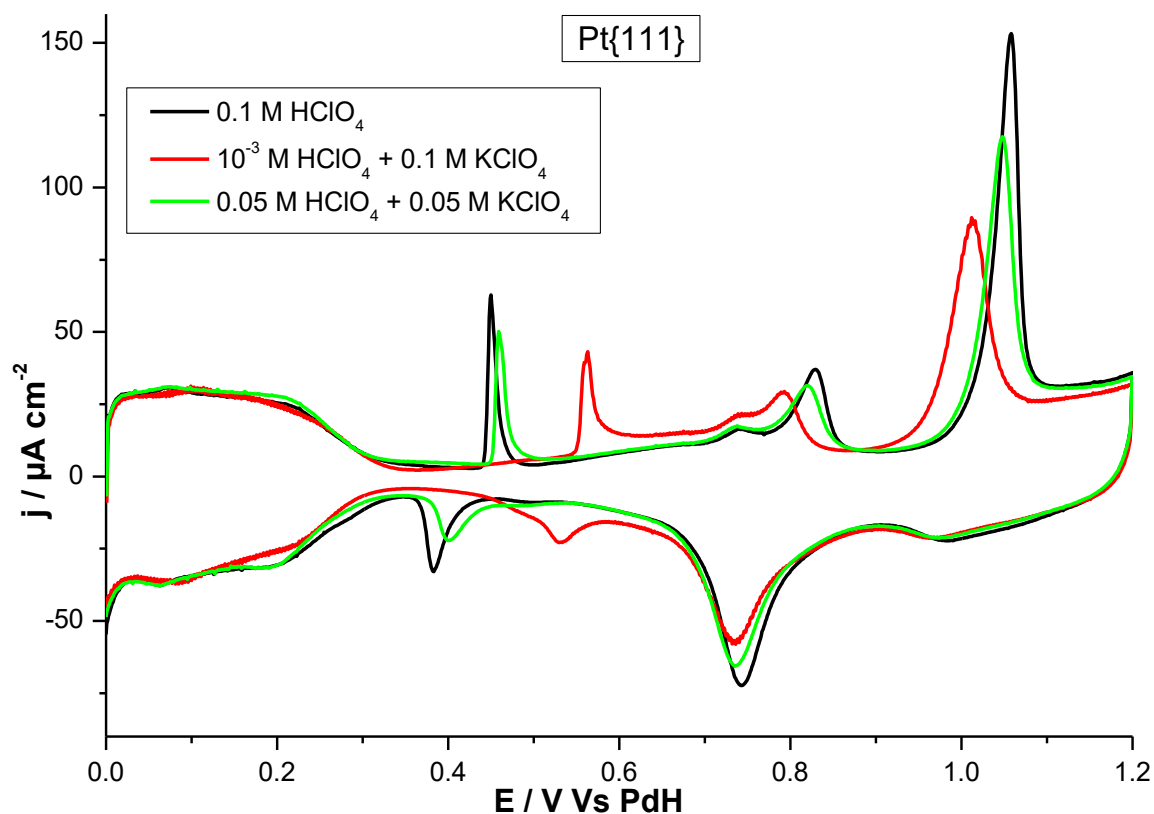
Figure 77: CVs of Nafion on Pt{111} in solutions containing ~ 0.1 M ClO$_4^-$

3.3.5 Conclusions

The voltammetry of Pt{111}, Pt{100}, Pt{110} and Pt(311) single crystal electrodes as a function of perchloric acid concentration (0.05 – 2.00 M) has been studied in order to test the assertion made in recent reports by Watanabe *et al.*[40, 41, 43, 73] that perchlorate anions specifically adsorb on polycrystalline platinum. Such an assertion would have significant ramifications for our understanding of electrocatalytic processes at platinum surfaces since perchlorate anions at low pH have classically been assumed not to specifically adsorb. For Pt{111}, it is found that OH$_{ad}$ and electrochemical oxide states are both perturbed significantly as perchloric acid concentration is increased. This is suggested to be due to specific adsorption of perchlorate anions competing with OH$_{ad}$ for adsorption sites. The hydrogen underpotential deposition (H$_{upd}$) region of Pt{111} however remains unchanged although evidence for perchlorate anion decomposition to chloride on Pt{111} is

found. In contrast, for Pt{100}, no variation in the onset of electrochemical oxide formation is detected nor any shift in the potential of the OH_{ad} state which normally results from the action of specifically adsorbing anions. This suggests that perchlorate anions are non-specifically adsorbed on this plane although strong changes in all H_{upd} states are observed as perchloric acid concentration is increased. This manifests itself as a redistribution of charge from the H_{upd} state situated at more positive potential to the one at more negative potential. For Pt{110} and Pt(311), marginal changes in the onset of electrochemical oxide formation are recorded, associated with specific adsorption of perchlorate. Specific adsorption of perchlorate anions on Pt{111} is deleterious to electrocatalytic activity in relation to the oxygen reduction reaction (ORR) as measured using a rotating disc electrode (RDE) in a hanging meniscus configuration. This study supports previous work suggesting that a large component of the ORR activity on platinum is governed by simple site blocking by specifically adsorbed anions and/or electrosorbed oxide.

When anion adsorption is probed as a function of pH and constant perchlorate anion concentration, it is found that, in agreement with findings from the Frumkin School[57], decreasing pH leads to an increase in perchlorate-surface interactions. However, at constant pH and varying perchlorate anion concentration, a more complicated set of interactions are observed whereby both cation and anion adsorption may be observed. This is exemplified for oxide formation on Pt{100} in which cations are found to inhibit oxide formation. Other examples are outlined and in the case of Nafion-modified P({111} surfaces, a specific cation interaction with the OH/water peak is noted leading to a shift to more negative potentials. The possibility of non-covalent interactions of cations with electrosorbed water[60, 61] and specific cation adsorption influencing non-Nernstian peak potential shifts[66] have recently been highlighted and the present study is in accordance with these experimental and theoretical investigations.

3.4 References

1.   Watanabe, M., et al., *Overview of recent developments in oxygen reduction electrocatalysis.* Electrochimica Acta, 2012. **84**: p. 187-201.
2.   van der Vliet, D., et al., *Platinum-alloy nanostructured thin film catalysts for the oxygen reduction reaction.* Electrochimica Acta, 2011. **56**(24): p. 8695-8699.
3.   Nørskov, J.K., et al., *Origin of the Overpotential for Oxygen Reduction at a Fuel-Cell Cathode. The Journal of Physical Chemistry B*The Journal of Physical Chemistry B, 2004. **108**(46): p. 17886-17892.
4.   Kuzume, A., E. Herrero, and J.M. Feliu, *Oxygen reduction on stepped platinum surfaces in acidic media.* Journal of Electroanalytical Chemistry, 2007. **599**(2): p. 333-343.
5.   Macia, M.D., et al., *On the kinetics of oxygen reduction on platinum stepped surfaces in acidic media.* Journal of Electroanalytical Chemistry, 2004. **564**(1-2): p. 141-150.
6.   Rizo, R., E. Herrero, and J.M. Feliu, *Oxygen reduction reaction on stepped platinum surfaces in alkaline media.* Physical Chemistry Chemical Physics, 2013. **15**(37): p. 15416-15425.
7.   Stamenkovic, V.R., et al., *Trends in electrocatalysis on extended and nanoscale Pt-bimetallic alloy surfaces.* Nature Materials, 2007. **6**(3): p. 241-247.
8.   Markovic, N.M., et al., *Structural effects in electrocatalysis - oxygen redution on platinum low-index single crystal surfaces in perchloric acid solutions.* Journal of Electroanalytical Chemistry, 1994. **377**(1-2): p. 249-259.
9.   Markovic, N.M., H.A. Gasteiger, and P.N. Ross, *Oxygen reduction on platinum low-index single crystal surfaces in sulfuric acid solution - rotating ring -Pt(hkl) disk studies.* Journal of Physical Chemistry, 1995. **99**(11): p. 3411-3415.
10.   Markovic, N.M., H.A. Gasteiger, and N. Philip, *Oxygen reduction on platinum low-index single-crystal surfaces in alkaline solution: Rotating ring disk(Pt(hkl)) studies.* Journal of Physical Chemistry, 1996. **100**(16): p. 6715-6721.
11.   Climent, V. and J.M. Feliu, *Thirty years of platinum single crystal electrochemistry.* Journal of Solid State Electrochemistry, 2011. **15**(7-8): p. 1297-1315.
12.   Liu, Y., et al., *Oxygen Reduction Reaction on Electrodeposited Pt100-xNix: Influence of Alloy Composition and Dealloying.* Journal of Physical Chemistry C, 2012. **116**(14): p. 7848-7862.
13.   Stephens, I.E.L., et al., *Tuning the Activity of Pt(111) for Oxygen Electroreduction by Subsurface Alloying.* Journal of the American Chemical Society, 2011. **133**(14): p. 5485-5491.
14.   Attard, G.A., et al., *Citrate adsorption on Pt{h kl} electrodes and its role in the formation of shaped Pt nanoparticles.* Journal of Electroanalytical Chemistry, 2013. **688**: p. 249-256.
15.   Stamenkovic, V.R., et al., *Improved oxygen reduction activity on Pt3Ni(111) via increased surface site availability.* Science, 2007. **315**(5811): p. 493-497.
16.   Markovic, N.M., et al., *Oxygen Reduction Reaction on Pt and Pt Bimetallic Surfaces: A Selective Review.* Fuel Cells, 2001. **1**(2): p. 105-116.
17.   Yu, T., et al., *Platinum Concave Nanocubes with High-Index Facets and Their Enhanced Activity for Oxygen Reduction Reaction.* Angewandte Chemie-International Edition, 2011. **50**(12): p. 2773-2777.
18.   Hwang, S.-M., et al., *Oxygen reduction reaction on electrodeposited Pt100-x-yNixPdy thin films.* Electrochimica Acta, 2010. **55**(28): p. 8938-8946.
19.   Markovic, N.M., N.S. Marinkovic, and R.R. Adzic, *Electrosorption of hydrogen and sulfuric acid anions on single crystal platinum stepped surfaces. 1.The 110 zone.* Journal of Electroanalytical Chemistry, 1988. **241**(1-2): p. 309-328.
20.   Markovic, N.M., N.S. Marinkovic, and R.R. Adzic, *Electrosorption of hydrogen and sulfuric acid anions on single crystal platinum stepped surfaces. 2.The 110 zone.* Journal of Electroanalytical Chemistry, 1991. **314**(1-2): p. 289-306.
21.   Markovic, N.M., et al., *Oxygen reduction reaction on Pt(111): effects of bromide.* Journal of Electroanalytical Chemistry, 1999. **467**(1-2): p. 157-163.

22. Stamenkovic, V., N.M. Markovic, and P.N. Ross, *Structure-relationships in electrocatalysis: oxygen reduction and hydrogen oxidation reactions on Pt(111) and Pt(100) in solutions containing chloride ions.* Journal of Electroanalytical Chemistry, 2001. **500**(1-2): p. 44-51.

23. Clavilier, J., et al., *Study of the charge displacement at the constant potential during CO adsorption on Pt(110) and Pt(111) electrodes in contact with a perchloric acid solution.* Journal of Electroanalytical Chemistry, 1992. **330**(1-2): p. 489-497.

24. Lazarescu, V. and J. Clavilier, *pH effects on the potentiodynamic behavior of the Pt(111) electrode in acidified NaClO4 solutions.* Electrochimica Acta, 1998. **44**(6-7): p. 931-941.

25. Aljaafgolze, K., D.M. Kolb, and D. Scherson, *On the Voltammetry Curves of Pt(111) in aqeous solutions.* Journal of Electroanalytical Chemistry, 1986. **200**(1-2): p. 353-362.

26. Wagner, F.T. and P.N. Ross, *Long range structural effects in the anomalous voltammetry on ultahigh vacuumLprepared Pt(111).* Journal of Electroanalytical Chemistry, 1988. **250**(2): p. 301-320.

27. Teliska, M., et al., *Site-specific vs specific adsorption of anions on Pt and Pt-based alloys.* Journal of Physical Chemistry C, 2007. **111**(26): p. 9267-9274.

28. Uchida, H., H. Ozuka, and M. Watanabe, *Electrochemical quartz crystal microbalance analysis of CO-tolerance at Pt-Fe alloy electrodes.* Electrochimica Acta, 2002. **47**(22-23): p. 3629-3636.

29. Kunimatsu, K., et al., *Role of adsorbed species in methanol oxidation on Pt studied by ATR-FTIRAS combined with linear potential sweep voltammetry.* Journal of Electroanalytical Chemistry, 2009. **632**(1-2): p. 109-119.

30. Mostany, J., et al., *Thermodynamic studies of anion adsorption at stepped platinum(hkl) electrode surfaces in sulfuric acid solutions.* Journal of Physical Chemistry B, 2002. **106**(49): p. 12787-12796.

31. Garcia-Araez, N., et al., *Thermodynamic studies of chloride adsorption at the Pt(111) electrode surface from 0.1 M HClO4 Solution.* Journal of Electroanalytical Chemistry, 2005. **576**(1): p. 33-41.

32. Mostany, J., et al., *Thermodynamic studies of phosphate adsorption on Pt(111) electrode surfaces in perchloric acid solutions.* Electrochimica Acta, 2009. **54**(24): p. 5836-5843.

33. He, Q., et al., *Influence of phosphate anion adsorption on the kinetics of oxygen electroreduction on low index Pt(hkl) single crystals.* Physical Chemistry Chemical Physics, 2010. **12**(39): p. 12544-12555.

34. Rodes, A., E. Pastor, and T. Iwasita, *An FTIR study on the adsorption of acetate at the basal planes of platinum single crystal electrodes.* Journal of Electroanalytical Chemistry, 1994. **376**(1-2): p. 109-118.

35. Zhang, J.L., et al., *Controlling the catalytic activity of platinum-monolayer electrocatalysts for oxygen reduction with different substrates.* Angewandte Chemie-International Edition, 2005. **44**(14): p. 2132-2135.

36. Cui, C., et al., *Compositional segregation in shaped Pt alloy nanoparticles and their structural behaviour during electrocatalysis.* Nature Materials, 2013. **12**(8): p. 765-771.

37. Colon-Mercado, H.R. and B.N. Popov, *Stability of platinum based alloy cathode catalysts in PEM fuel cells.* Journal of Power Sources, 2006. **155**(2): p. 253-263.

38. Horanyi, G. and I. Bakos, *Experimental evidence demonstrating the occurence of reduction processes of ClO4- ions in acid-medium at platinized platinum-electrodes.* Journal of Electroanalytical Chemistry, 1992. **331**(1-2): p. 727-737.

39. Lang, G.G., et al., *The kinetics of the electrochemical reduction of perchlorate ions on rhodium.* Electrochimica Acta, 2008. **53**(25): p. 7436-7444.

40. Ahmadi, A., R.W. Evans, and G. Attard, *Anion Surface Interactions 1. Perchlroate Decomposition and Sulfate Adsorption Hysteresis Studied by Voltammetry.* Journal of Electroanalytical Chemistry, 1993. **350**(1-2): p. 279-295.

41. Rusanova, M.Y., et al., *Electrochemical reduction of perchlorate ions on platinum-activated nickel.* Electrochimica Acta, 2006. **51**(15): p. 3097-3101.

42. Lang, G.G. and G. Horanyi, *Some interesting aspects of the catalytic and electrocatalytic reduction of perchlorate ions.* Journal of Electroanalytical Chemistry, 2003. **552**: p. 197-211.

43. Omura, J., et al., *Electrochemical Quartz Crystal Microbalance Analysis of the Oxygen Reduction Reaction on Pt-Based Electrodes. Part 1: Effect of Adsorbed Anions on the Oxygen Reduction Activities of Pt in HF, HClO4, and H2SO4 Solutions.* Langmuir, 2011. **27**(10): p. 6464-6470.

44. Bjoerling, A., E. Herrero, and J.M. Feliu, *Electrochemical Oxidation of Pt(111) Vicinal Surfaces: Effects of Surface Structure and Specific Anion Adsorption.* Journal of Physical Chemistry C, 2011. **115**(31): p. 15509-15515.

45. Berna, A., V. Climent, and J.M. Feliu, *New understanding of the nature of OH adsorption on Pt(111) electrodes.* Electrochemistry Communications, 2007. **9**(12): p. 2789-2794.

46. Sawatari, Y., J. Inukai, and M. Ito, *The structure of bisulfate and perchlorate on a Pt(111) electrode surface studied by infrared-spectroscopy and ab-initio molecular-orbital calculation.* Journal of Electron Spectroscopy and Related Phenomena, 1993. **64-5**: p. 515-522.

47. Hirota, K., M.B. Song, and M. Ito, *In-situ infrared spectroscopy of water and electrolytes adsorbed on a Pt(111) electrode surface in acid solution. Structural changes of adsorbed water molecules upon an electrode potential.* Chemical Physics Letters, 1996. **250**(3-4): p. 335-341.

48. Rodes, A., et al., *Electrochemical behaviour of Pt(100) in various acidic media. 1.On a new voltammetric profile of Pt(100) in perchloric-acid and effects of surface defects.* Journal of Electroanalytical Chemistry, 1991. **305**(1): p. 115-129.

49. Rodes, A., et al., *Electrochemical-behaviour of Pt(100) in various acidic media. 2.On the relation between the voltammetric profiles induced by anion specific adsorption studied with a transfer technnique preserving surface cleanliness and structure.* Journal of Electroanalytical Chemistry, 1992. **338**(1-2): p. 317-338.

50. Climent, V., et al., *Thermodynamic analysis of the temperature dependence of OH adsorption on Pt(111) and Pt(100) electrodes in acidic media in the absence of specific anion adsorption.* Journal of Physical Chemistry B, 2006. **110**(23): p. 11344-11351.

51. Gamboaaldeco, M.E., et al., *Adsorption of bisulfate anion on a Pt(100) electrode - a comparision with Pt(111) and Pt(poly).* Journal of Electroanalytical Chemistry, 1993. **348**(1-2): p. 451-457.

52. Garcia-Araez, N., V. Climent, and J. Feliu, *Potential-Dependent Water Orientation on Pt(111), Pt(100), and Pt(110), As Inferred from Laser-Pulsed Experiments. Electrostatic and Chemical Effects.* Journal of Physical Chemistry C, 2009. **113**(21): p. 9290-9304.

53. Schmidt, D.J., et al., *Performance of Cluster Expansions of Coverage-Dependent Adsorption of Atomic Oxygen on Pt(111).* Journal of Chemical Theory and Computation, 2012. **8**(1): p. 264-273.

54. van der Niet, M.J.T.C., et al., *Water dissociation on well-defined platinum surfaces: The electrochemical perspective.* Catalysis Today, 2013. **202**: p. 105-113.

55. Ahmed, M., et al., *Unprecedented Structural Sensitivity toward Average Terrace Width: Nafion Adsorption at Pt{hkl} Electrodes.* Journal of Physical Chemistry C, 2011. **115**(34): p. 17020-17027.

56. Berna, A., et al., *Voltammetric characterization of Pt single crystal electrodes with basal orientations in trifluoromethanesulphonic acid.* Electrochemistry Communications, 2008. **10**(11): p. 1695-1698.

57. Frumkin, A.N., O.A. Petrii, and B.B. Damaskin, *Comprehensive Treatise of Electrochemistry*. 1980.

58. Strmcnik, D., et al., *Enhanced electrocatalysis of the oxygen reduction reaction based on patterning of platinum surfaces with cyanide.* Nature Chemistry, 2010. **2**(10): p. 880-885.

59. Subbaraman, R., et al., *Three Phase Interfaces at Electrified Metal-Solid Electrolyte Systems 1. Study of the Pt(hkl)-Nafion Interface.* Journal of Physical Chemistry C, 2010. **114**(18): p. 8414-8422.

60. Strmcnik, D., et al., *The role of non-covalent interactions in electrocatalytic fuel-cell reactions on platinum.* Nature Chemistry, 2009. **1**(6): p. 466-472.

61. Escudero-Escribano, M., et al., *Quantitative Study of Non-Covalent Interactions at the Electrode-Electrolyte Interface Using Cyanide-Modified Pt(111) Electrodes.* Chemphyschem, 2011. **12**(12): p. 2230-2234.

62. Lopes, P.P., et al., *Relationships between Atomic Level Surface Structure and Stability/Activity of Platinum Surface Atoms in Aqueous Environments.* ACS Catalysis, 2016. **6**(4): p. 2536-2544.

63. Climent, V., et al., *Potential of zero total charge of platinum single crystals: A local approach to stepped surfaces vicinal to Pt(111).* Russian Journal of Electrochemistry, 2006. **42**(11): p. 1145-1160.

64. Stoffelsma, C., et al., *Promotion of the Oxidation of Carbon Monoxide at Stepped Platinum Single-Crystal Electrodes in Alkaline Media by Lithium and Beryllium Cations.* Journal of the American Chemical Society, 2010. **132**(45): p. 16127-16133.

65. Strmcnik, D., et al., *Effects of Li+, K+, and Ba2+ Cations on the ORR at Model and High Surface Area Pt and Au Surfaces in Alkaline Solutions.* Journal of Physical Chemistry Letters, 2011. **2**(21): p. 2733-2736.

66. McCrum, I.T. and M.J. Janik, *pH and Alkali Cation Effects on the Pt Cyclic Voltammogram Explained Using Density Functional Theory.* Journal of Physical Chemistry C, 2016. **120**(1): p. 457-471.

67. Conway, B.E. and G. Jerkiewicz, *Surface orientation dependence of oxide film growth at platinum single-crystals.* Journal of Electroanalytical Chemistry, 1992. **339**(1-2): p. 123-146.

68. Koper, M.T.M. and J.J. Lukkien, *Modeling the butterfly: influence of lateral interactions and adsorption geometry on the voltammetry at (111) and (100) electrodes.* Surface Science, 2002. **498**(1-2): p. 105-115.

69. Climent, V., G.A. Attard, and J.M. Feliu, *Potential of zero charge of platinum stepped surfaces: a combined approach of CO charge displacement and N2O reduction.* Journal of Electroanalytical Chemistry, 2002. **532**(1-2): p. 67-74.

70. Attard, G.A., et al., *On the global and local values of the potential of zero total charge at well-defined platinum surfaces: stepped and adatom modified surfaces.* Journal of Electroanalytical Chemistry, 2004. **568**(1-2): p. 329-342.

71. Malevich, D., et al., *In situ infrared reflection absorption spectroscopy studies of the interaction of Nafion (R) with the Pt electrode surface.* Zeitschrift Fur Physikalische Chemie-International Journal of Research in Physical Chemistry & Chemical Physics, 2003. **217**(5): p. 513-525.

72. Mauritz, K.A. and R.B. Moore, *State of understanding of Nafion.* Chemical Reviews, 2004. **104**(10): p. 4535-4585.

73. Omura, J., et al., *Electrochemical Quartz Crystal Microbalance Analysis of the Oxygen Reduction Reaction on Pt-Based Electrodes. Part 2: Adsorption of Oxygen Species and ClO4-Anions on Pt and Pt-Co Alloy in HClO4 Solutions.* Langmuir, 2014. **30**(1): p. 432-439.

The Voltammetry of Surfaces Vicinal to Pt{110}: Structural Complexity Simplified by CO Cooling
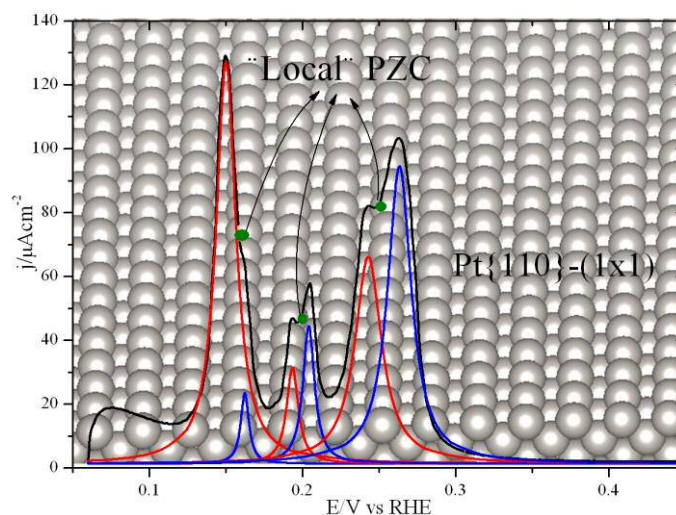
4.1 Introduction

In electrochemical surface studies, it is imperative to create a reproducible electrochemical interphasial region. If the electrode surface structure and composition are not reproducible, structure activity relationships and a true understanding of any surface electrode process will be impossible to deduce. It is well known that heating and cooling conditions put upon a single crystal electrode can affect the surface configuration[1-5]. In the case of Pt{111} surfaces, the reconstructed state is not normally accessed under ambient electrochemical conditions[6]. For Pt{100}, differences in the reconstructive state of the electrode surface may be obtained by simply changing the ambient in which the electrode is prepared[3, 6]. The Pt{110} surface can have (1x1) and (1x2) "missing row" configurations and has been extensively studied using various conditions into understanding each of these arrangements[1, 4, 5, 7-10].
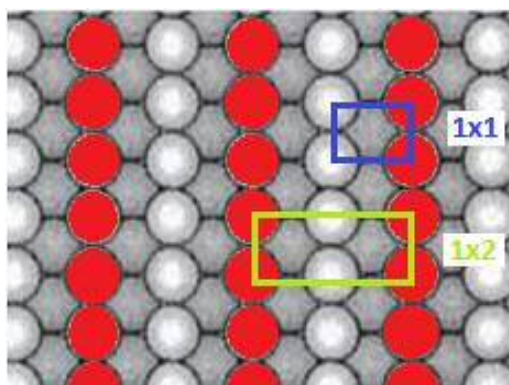

Figure 78: Hard sphere model of Pt{110} showing a (1x1) configuration in blue, and (1x2) configuration in green.

In a recent paper [11], the voltammetry of Pt{110} in aqueous perchloric acid and sodium hydroxide was reported. In agreement with previous studies[4, 12], depending on the cooling environment after flame annealing, the surface of the electrode could be prepared in a (1x2) (nitrogen-cooled), (1x1) (CO-cooled) or "rough" (1x1) (hydrogen-cooled) state. In 0.1 M perchloric acid especially, a new voltammetric profile was observed in which the presence of long range, two dimensionally ordered Pt{110} terraces (after CO cooling) gave rise to singular H_{upd}/OH and oxide electrosorption features (H_{upd} in this context refers to Pt electrosorption peaks in the range 0.05 - 0.4 V versus RHE irrespective of whether or not they arise from hydrogen, OH or anion adsorption). Moreover, the electrocatalytic activity towards the oxygen reduction reaction (ORR) was found to differ significantly from previous reports which asserted that Pt{110} electrodes exhibit ORR activity equivalent to or greater than that of Pt{111} in aqueous perchloric acid[13-17]. In reference[5], when all defects were eliminated from the electrode surface via CO cooling, ORR activity in aqueous perchloric acid was found unequivocally to be lower than that of Pt{111}.

Hence, it is important to undertake an extensive re-evaluation of previous electrocatalytic studies involving Pt{110} and related surfaces since nearly all of these earlier investigations involved a flame-anneal/hydrogen cooling surface preparation protocol leading to the generation of defective surfaces[18-24]. Since ORR was shown previously to be highly sensitive to surface disordering, it was thought prudent to explore in a more controlled fashion the introduction of surface defects to a Pt{110}-(1x1) surface and its impact on surface voltammetry.

A series of stepped Pt{110} surfaces have been prepared based on either {111} or {100} linear steps. By cooling these surfaces in CO following flame annealing, they can be compared and contrasted with earlier results pertaining to hydrogen-cooled stepped surfaces[25, 26]. It was hypothesised that the complexity associated with both terrace and step reconstruction might be reduced or even eliminated using adsorbed CO, allowing for more detailed insights relating to the distinctive voltammetry of Pt{110}. In particular, the very broad and asymmetric H_{upd} electrosorption peak centred around 0.2 – 0.25 V (Pd/H) observed in aqueous perchloric acid [27, 28](referred to this state throughout as the "classical Pt{110} terrace peak" or "Pct" for short) has posed an ongoing puzzle to surface electrochemists even since the earliest voltammetric measurements were performed [7]. More recently, Taguchi and Feliu asserted that Pct may be ascribed to "narrow" {111} terraces similar to those comprising the missing-row (1x2) reconstruction of Pt{110} [29]. This was because when Pt n{111}x{111} electrodes were studied using aqueous perchloric acid, a similar peak appeared for n < 4, i.e. the interaction of {111} steps at narrow terrace widths led to the generation

of the "Pt{110}" 0.2 – 0.25 V feature. In contrast, Souza-Garcia *et al.* suggested that because the intensity of Pct grew with increasing values of n (using Pt n{110}x{111} electrodes) that it was probably associated with the average terrace width of the {110} terraces themselves meaning that the Pt n{111}x{111} surfaces at small values of n are reconstructed, and therefore must contain narrow {110} terraces [26]. In situ XRD investigations by Hoshi and co-workers [30] also demonstrated that Pt{331} (Pt 3{111}x{111} or Pt 2{111}x{110} in microfacet notation) remains in its unreconstructed (1x1) state after flame annealing and cooling in a hydrogen/argon environment supporting the view that narrow {110} terraces are not formed and that "splitting" of the {110} H_{upd} step peak for n < 4 into two components (using perchloric acid electrolyte) seems more linked to step-step interactions. Interestingly, a similar "splitting" of the {111}x{100} step feature around the turning point of the stereographic triangle travelling from the {111} pole to the {100} pole (Pt{211}, Pt{311} and Pt{511} surfaces) is also observed in perchloric acid electrolytes [31], presumably again due to step-step interactions. However, the expectation of a splitting of the H_{upd} electrosorption peak associated with closely spaced steps is not fulfilled for small n either using Pt n{110}x{100} or Pt n{100}x{110} electrodes[25, 32] (i.e. travelling along the stereographic triangle from the {100} pole to the {110} pole). In this case, evidence in support of such step sites being rather unstable has been put forward such that reconstruction of steps probably occurs[32]. This aspect will be explored in detail and moreover, suggestions of a new model to interpret the complex voltammetry of surfaces vicinal to Pt{110}. The differing degrees of surface order resulting from particular annealing/cooling steps together with intrinsic structural instabilities associated with the presence of {110}x{100} step sites are discussed.

4.2 Results and Discussion

4.2.1 Voltammetry of Pt n{110}x{111} electrodes cooled in CO after flame anneal

Because some of this work was carried out in collaboration with the University of Alicante, a RHE, (Reversible Hydrogen Electrode), rather than a Pd/H reference electrode was employed. However, a simple subtraction of 55 mV will convert all potentials to a Pd/H reference scale. In Figure 79, a series of cyclic voltammograms for flame annealed and CO-cooled Pt n{110}x{111} surfaces in 0.1 M aqueous perchloric are shown. As reported previously [11], for Pt{110} in perchloric acid, the so-called H_{upd} region from 0.3 to 0.05 V is rather complex containing numerous reversible electrosorption peaks centred at 0.25, 0.20 and 0.145 V (Figure 79). In reference [5], all of these were associated with the presence of extended Pt{110}-(1x1) domains since electrosorption into the

oxide peak at 1.1 V (electrochemical surface roughening) caused the attenuation and broadening of all peaks such that the CV would subsequently resemble a hydrogen-cooled electrode.

As the surface density of {111} steps is steadily increased, it is apparent that a systematic decrease in H_{upd} and oxide peak intensity ascribable to Pt{110} terraces is observed, but no change in peak potential, general shape or width (except for Pt{331}). This is consistent with maintenance of Pt{110} terrace symmetry. A peak appearing at 0.90 V as step density increases is proposed to be ascribed to electrosorption of oxide at the {111}x{111} linear step site. Figure 80 shows linear relationships between terrace and step oxide peak electrosorption charges as a function of step surface density. This behaviour is in accordance with expectations based on a hard sphere model of an unreconstructed Pt surface. An isopotential point is observed at 0.12 V in which the peak at 0.145 V transforms into a peak centred at 0.12 V (see Pt{331} in particular). The Pt{331} CV is interesting because the peak at 0.20 V, previously ascribed to either narrow {111} terraces [29] or {110} reconstructed facets [26], is clearly well separated in potential from the Pt{110} terrace feature at 0.25 V. The Pt{331} represents a turning point whereby step and terrace sites become indistinguishable and can explain this. In addition, there is significant peak broadening for oxide electrosorption at the step (0.90 V). This is correlated with the appearance of the 0.20 V peak and is speculated to arise from step-step interactions for narrow average terrace widths close to the turning point of the zone. For Pt{331}, the oxide peak associated with Pt{110} terraces at 1.1 V has almost completely vanished. If Pt{110} terraces were present, both the 0.25 V and 1.1 V peaks would be expected to also be visible for Pt{331}.
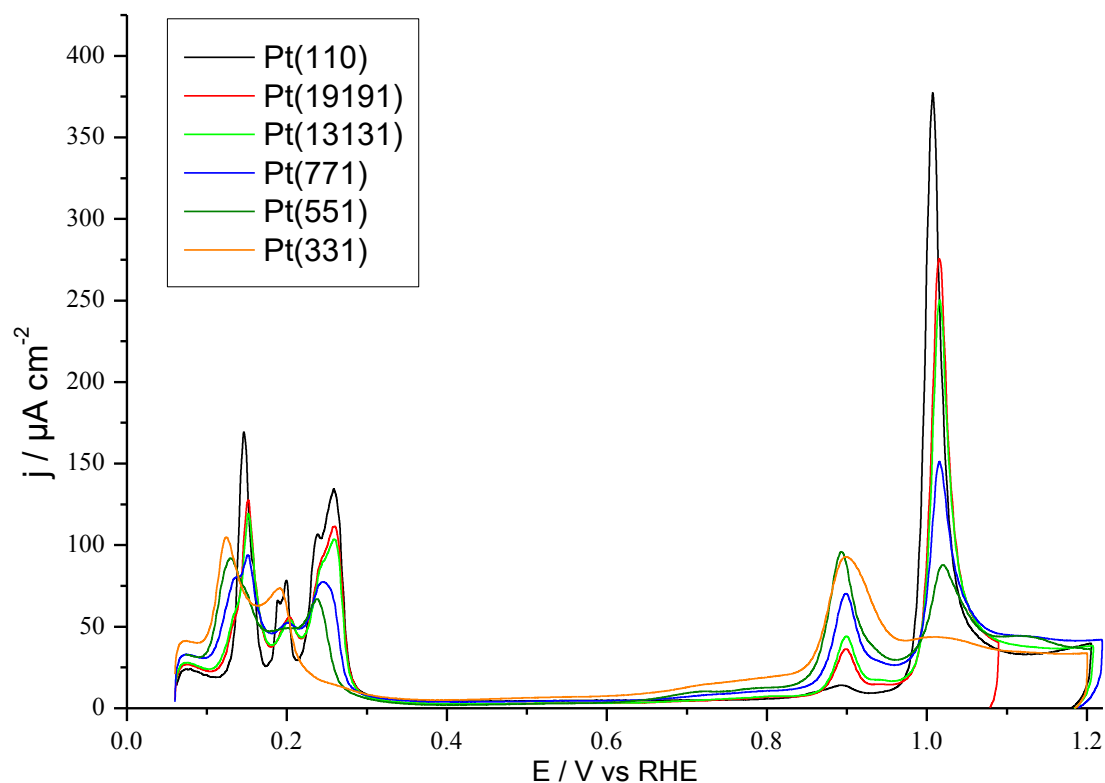
Figure 79: Cyclic voltammograms of Pt n{110}x{111} electrodes in 0.1 M aqueous perchloric acid. Sweep rate = 50 mV/s.

Weaker and more subtle changes observed in Figure 79 include charge growing between 0.60 and 0. 85 V, has been ascribable to "OH" (in fact, the beginning of O_{upd}, which is more complex than that H_{upd} for obvious reasons) adsorption on narrow Pt{111} terraces. As reported previously, when Pt n{111}x{110} surfaces are considered for n > 2, this charge component continues to grow as the average {111} terrace width increases [29]. The corresponding development in the (well-separated) H_{upd} Pt{111} charge is still visible for Pt{331}, as signified by a weak, rising current density from 0.30 to 0.20 V but obscured by the larger, 0.20 V peak at more negative potentials. In sulphuric acid electrolyte, this feature is much more marked (later). In summary, all surfaces vicinal to Pt{110} containing {111} linear steps remain unreconstructed when prepared via CO cooling. This suggestion is in accordance with previous in situ XRD measurements on Pt{331} [30].
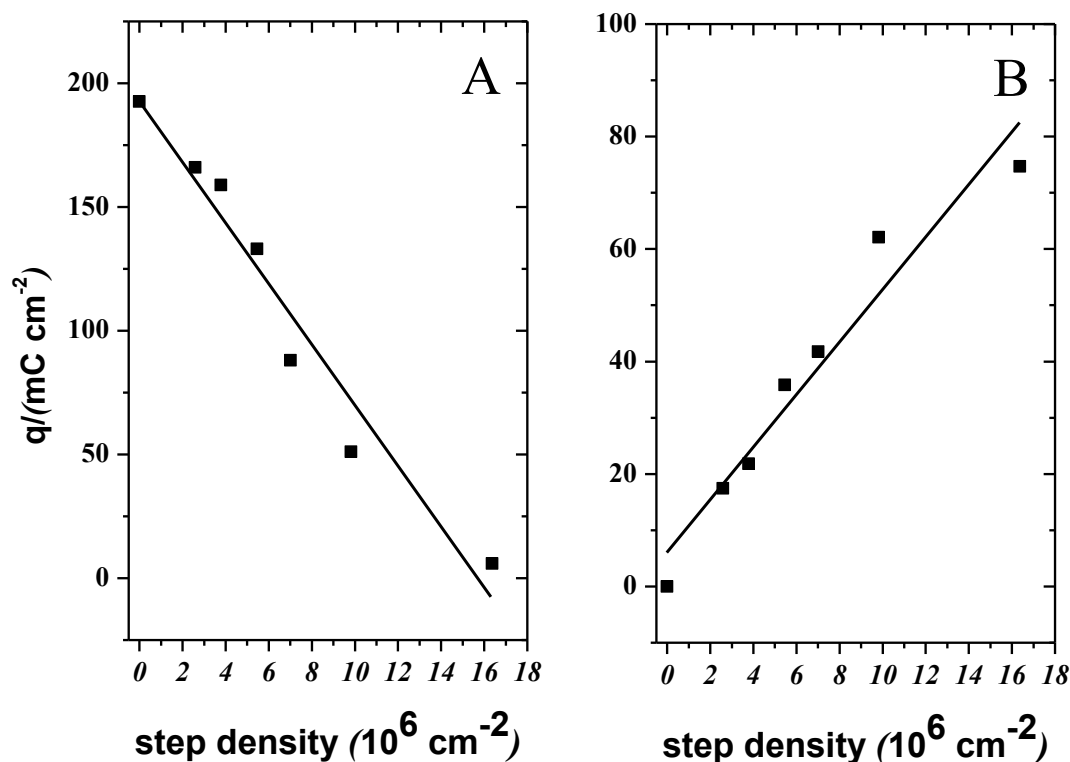
Figure 80: Plots of Pt{110} (A) terrace and (B) {111}x{111} step oxide electrosorption charge as a function of step density for Pt n{110}x{111} electrodes in 0.1 M perchloric acid.

In contrast to the results presented here, reference [26] presented hydrogen - cooled Pt n{110}x{111} voltammetry and only the broad and asymmetric Pct feature centred at 0.25 V was reported. This gradually diminished in magnitude with a slight shift to more negative potentials as surface step density increased. A gradual increase in the peak intensity associated with steps (at 0.12 V) was also observed. In terms of 2D Pt{110} terrace order, all hydrogen - cooled samples failed to sustain the presence of a 0.25 V 2D ordered terrace peak (although there is good overlap with Pct for Pt{110} in particular). Therefore, these samples must be intrinsically disordered relative to CO-cooled analogues.

The nature of the broadness of Pct is speculated to stem from the presence of narrow {111} terraces as residuals left over upon lifting of the (1x2) terrace reconstruction (electrosorption charge at the more negative potential of Pct). This explanation accounts for the influence of both step-step interactions and residual Pt{110} 2D order, leading to an increase in peak magnitude of Pct as step density diminishes. The nature of the actual, adsorbed species constituting this unusual electrosorption peak will be deliberated later.

In Figure 82, the voltammetry of Pt{332} and Pt{110} is compared. Pt{332} in microfacet notation corresponds to Pt 6{111}x{111}. The junction of the two {111} sites corresponds to a {110} linear step (hard sphere model shown in Figure 81 below). This "step" feature gives rise to a well-defined voltammetric peak at 0.12 V when incorporated into Pt{110} and Pt{111} terrace sites [26, 29] and is clearly associated with 1D {110} step order. Figure 82 shows that the 0.12 V and 0.145 V peaks have different origins. Even after varying the surface step density (including for hydrogen - cooled Pt{110}), the 0.12 V peak does not vary in potential. Therefore the 0.145 V peak reported here is unique and cannot be ascribed to {111}x{111} step sites. The 0.145 V peak is potentially caused by electrosorption on 2D Pt{110} terrace sites. The isopotential point at 0.12 V is the result of a one to one correspondence between the number of 1D Pt{110} and 2D Pt{110} sites as step density is varied, in accordance with a hard sphere interpretation of all surfaces being in their (1x1) unreconstructed state.
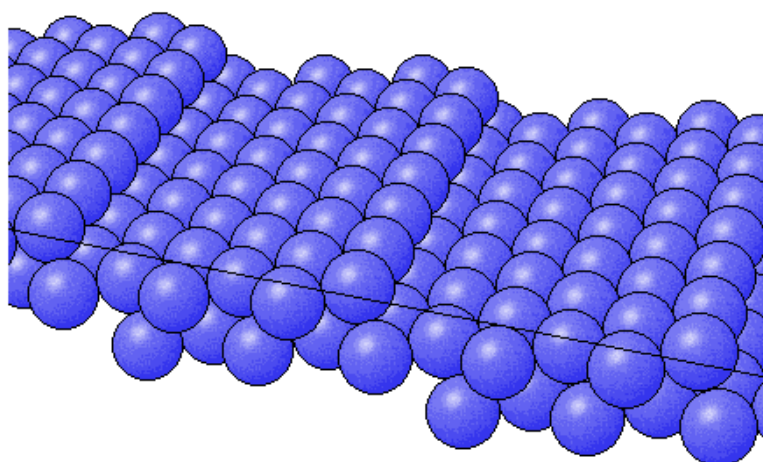

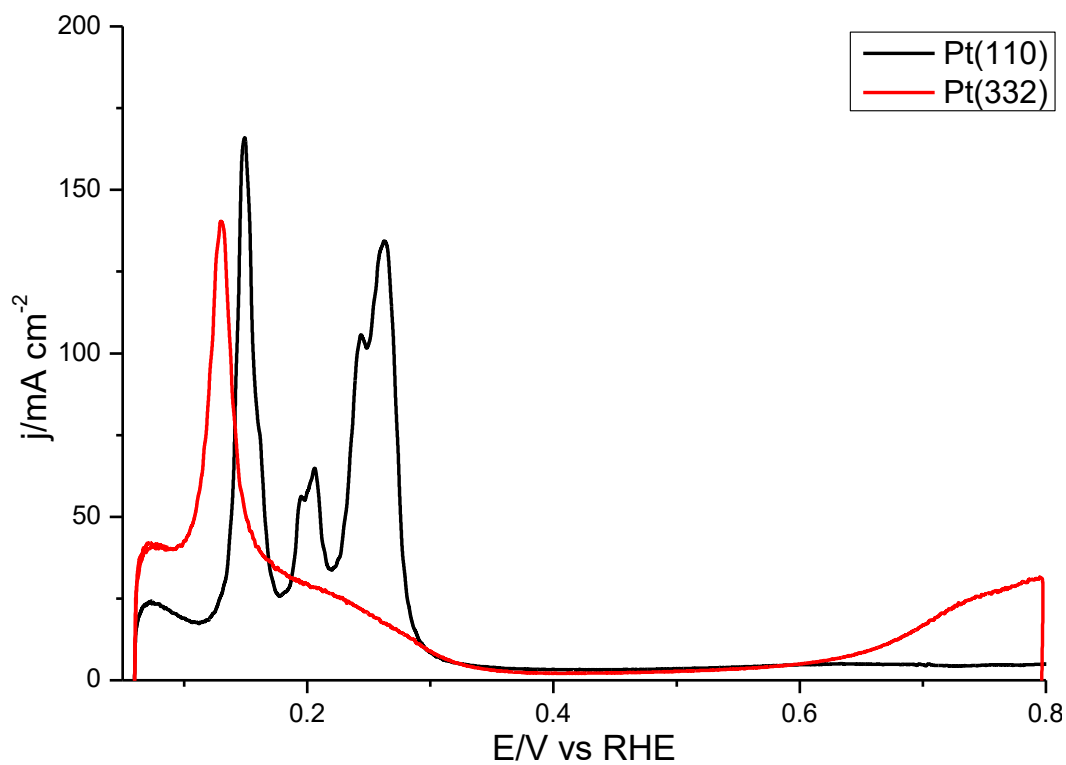*Figure 81: Hard sphere model of Pt{332}*

Figure 82: Cyclic voltammograms of Pt{110}-(1x1) (black) and Pt{332} (red) in 0.1 M aqueous perchloric acid. Sweep rate = 50 mV/s.
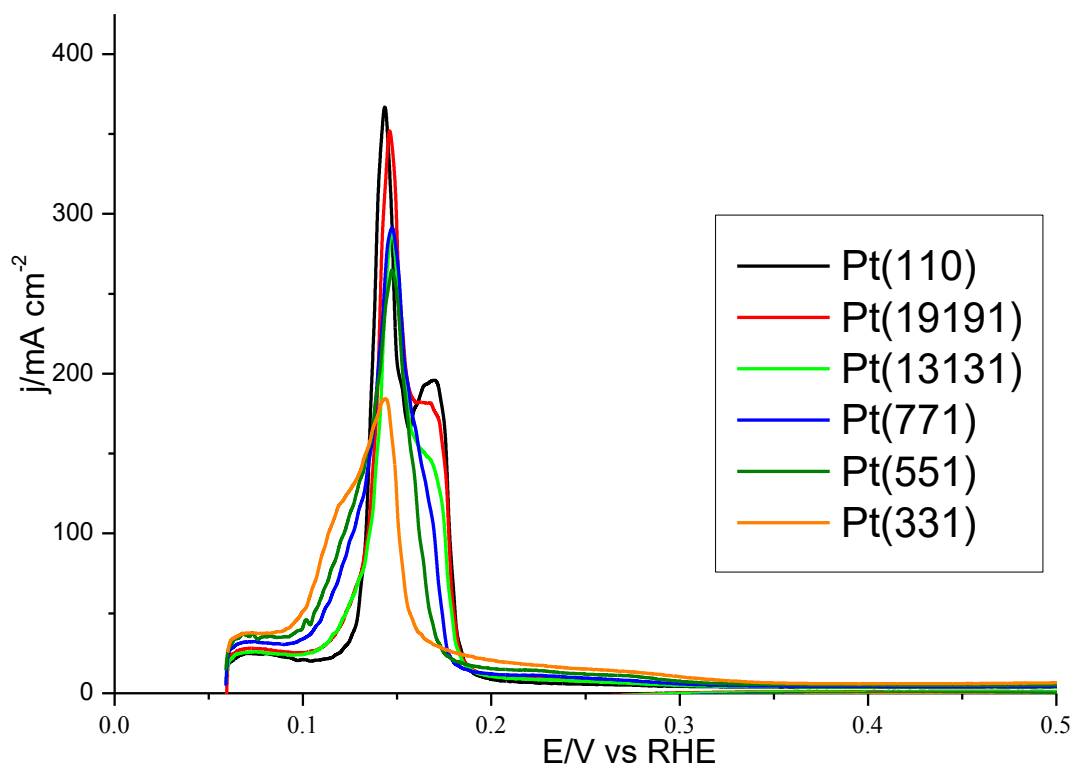

Figure 83: Cyclic voltammograms of Pt n{110}x{111} electrodes in 0.1 M sulphuric acid. Sweep rate = 50 mV/s.

Figure 83 shows a family of CVs for CO - cooled Pt n{110}x{111} stepped surfaces in aqueous 0.1 M sulphuric acid. The potential scale is expanded to show the H_{upd} peaks more clearly. Using a similar analysis to that described above, it is evident that the multiplicity of overlapping H_{upd} peaks is now confined to a much narrower range of potential than seen in perchloric acid electrolyte, as expected for more strongly specifically adsorbing anions such as sulphate. In fact for Pt{111} and after much discussion in the literature, sulphate rather than bisulphate has been demonstrated to be the specifically adsorbing species[33]. This has been assumed that this is indeed true for Pt{110}[34-36].
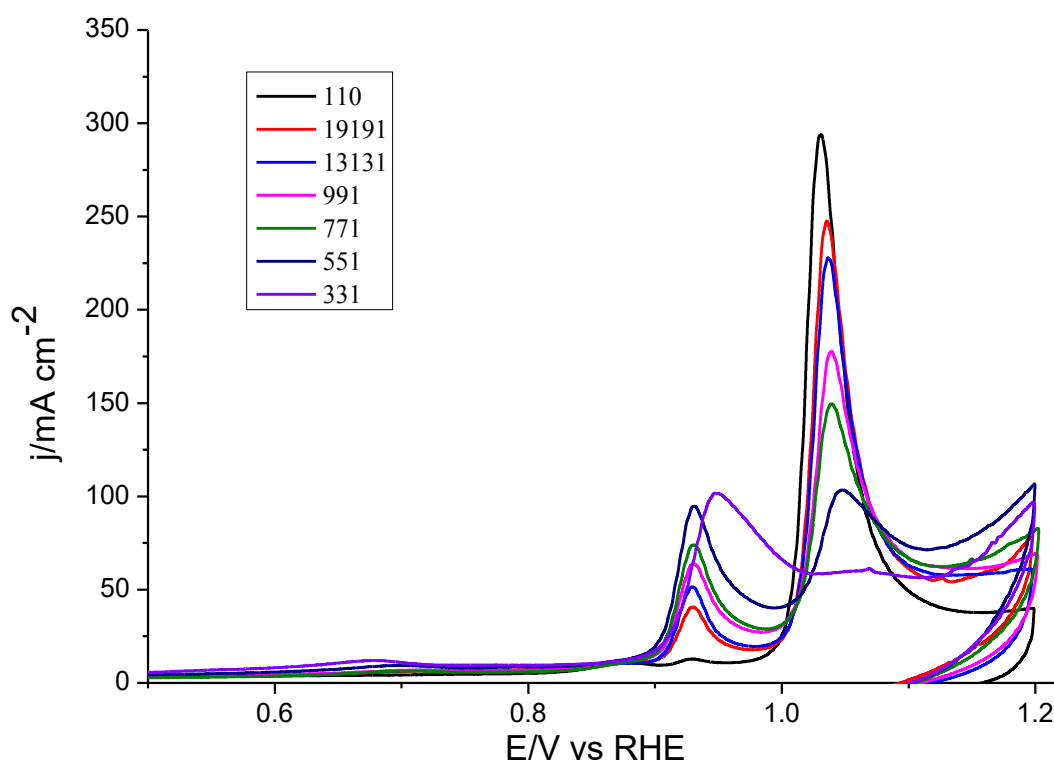

Figure 84: Expanded oxide potential range of cyclic voltammograms using Pt n{110}x{111} electrodes in 0.1 M aqueous sulphuric acid. Sweep rate = 50 mV/s.

The oxide electrosorption peaks shown in Figure 84 also reflect the presence of specifically adsorbing sulphate anions relative to perchloric acid, with peaks at 1.03 V and 0.92 V corresponding to electrosorption of oxide at terrace and step sites respectively. Figure 85 shows how the charge under each of the oxide peaks is linearly correlated as a function of step density in agreement with previous assertions that all electrode surfaces exhibit a (1x1) terminated structure.
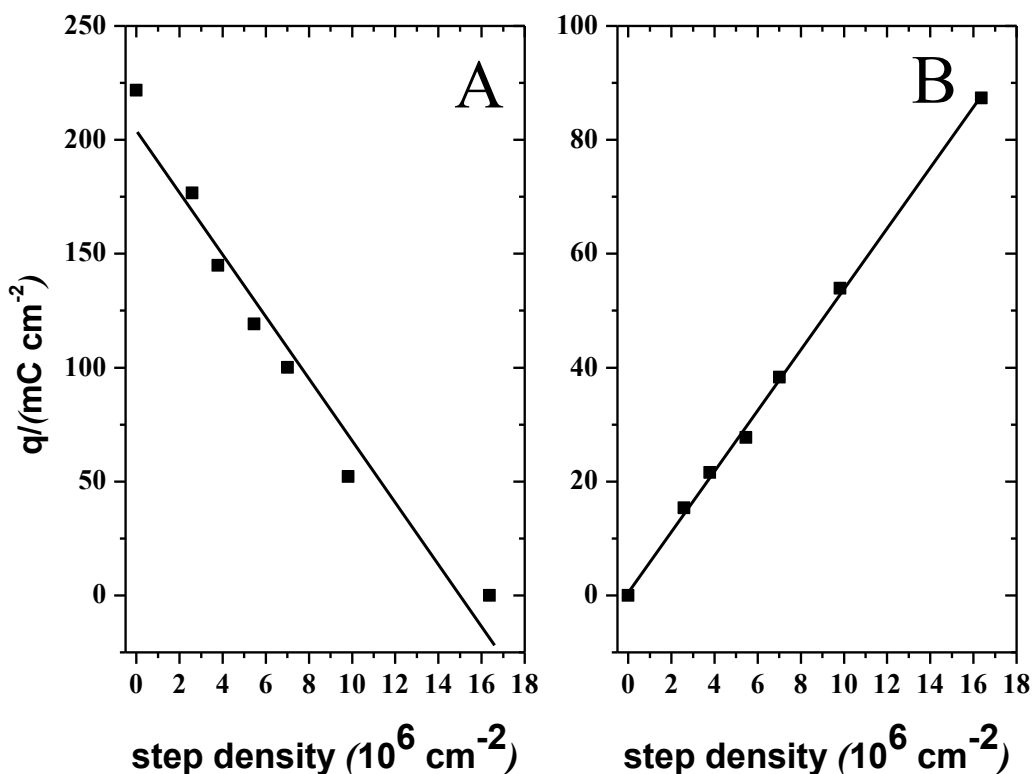
Figure 85: Plots of (A) terrace and (B) step oxide electrosorption charge as a function of step density for Pt n{110}x{111} electrodes in 0.1 M sulphuric acid.

Returning to the H_{upd} potential region, if one assumes that the same electrosorption processes are occurring as for perchloric acid but confined within a narrower potential range, it is possible to make logical assignments concerning most of the features and suggest good candidates for the remainder. For example, the peak component at 0.17 V, which is attenuated as step density is increased, is almost certainly ascribable to the same process as was occurring in the 0.25 V peak in perchloric acid and is proposed to be a manifestation of long range Pt{110}-(1x1) 2D surface order. The correlated growth in the shoulder at most negative potentials (0.11 V) as step density increases must then be characteristic of 1D Pt{110} order (linear steps). Further progress can be made if Pt{331} voltammetry is scrutinised, whereby the electrosorption charge between 0.15 and 0.32 V with a very broad feature between 0.5 and 0.8 V are considered together. Both of these may be positively identified as being due to H_{upd} and sulphate adsorption respectively on very narrow Pt{111} terraces[37]. In fact, because the Pt{111} H_{upd} peak is identical in both sulphuric and perchloric acid, it is no surprise that the same potential range is exhibited by the Pt{331} "{111} terrace" contributions in both perchloric and sulphuric acids. Also, the slight shift to more positive potentials of the Pt{111} anion electrosorption charge upon changing from sulphuric to perchloric acid aqueous media is also in accordance with these peak assignments[38].

128

The more complicated issue arises from consideration of the intense peak centred 0.145 V. It is found to decrease in intensity (as step density increases) to about 50% of its original value in the case of the Pt{331} surface. Since Pt{331} contains no 2D ordered Pt{110} terrace sites, this 50% "residual" charge is ascribed to purely 1D Pt{110} order. Hence, two components of 1D Pt{110} may be discerned – a contribution at more negative potential (0.11 V) and one at more positive potentials (0.145 V). As a tentative suggestion, both peaks are ascribed to adsorption at Pt{110} 1D steps, with (for positive potential sweep) cations desorbing in the peak at 0.11 V and anions adsorbing in the peak 0.145 V. This demarcation of cationic and anionic charge separation overlapping with what is referred to classically as "hydrogen adsorption" has already been mentioned in relation to Pt{111} terraces. In a similar fashion, an interpretation of why for Pt{110}, the peak at 0.145 V is almost twice the size of that for Pt{331} could be that this "extra" charge is wholly caused by adsorption into 2D Pt{110} surface ordered sites, which overlap with the step contribution. Two contributions towards electrosorption at 2D Pt{110} ordered sites may also be delineated; that due broadly to anions at 0.16 V and that due broadly to cations at 0.145 V. A test of this hypothesis may be attempted by evaluations of PZTC. More importantly, the consequence of the hypothesis here may be framed within the following:

Is it possible that all electrosorption at well-defined sites may ultimately be broken down into two contributions, anion adsorption at the more positive potential and cation adsorption at the more negative potential? The separation of these two processes would depend on the specific adsorption site, the relative strengths of anion and cation adsorption and the degree of lateral interaction occurring as each site is occupied. This happens with Pt(111) and Pt(100) in alkaline media [39]. Another thing to consider is that water interaction changes with potential [40, 41]. The notion of a local potential of zero charge has previously been discussed by [42, 43]. This concept fits well the model being proposed in the present work in which a "patchwork" of locally charged states switch from negative to positive as a function of increasing potential and thus causing the generation of the various peaks recorded during CV (via adsorption/desorption of ions) depending on the sign of the excess charge at a specific site.

Looking back at the multiplicity of CV peaks seen for Pt{110} in perchloric acid, the 0.145, 0.20 and 0.25 V are all doublets and each doublet could be seen as the cationic/anionic pair pertaining to 2D Pt{110} sites. However, the ratio of cations/anions in each state is predicted to change as the coverage of electrosorbed hydrogen changes (more sites for anion adsorption will become available as potential increases since more hydrogen leaves the surface and vice versa). This means that the

0.25 V peak would be largely dominated by the anionic component and the 0.145 V peak by the cationic component. The 0.20 V peak is therefore a more equal distribution of cationic/anionic charges. This has already been suggested in [11] and is in line with recent thinking concerning the pH dependence of H_{upd} peaks at platinum electrodes [44].

4.2.2 Voltammetry of Pt n{110}x{100} electrodes cooled in CO after flame anneal

In Figure 86 the first voltammetric sweep from 0.05 to 1.2 V of freshly flame annealed and CO – cooled Pt n{110}x{100} electrodes in 0.1 M aqueous perchloric acid is shown. In contrast to data depicted in Figure 79, inspection of Figure 86 reveals that the introduction of {100} linear steps into the Pt{110} surface plane. This leads to voltammetry much more closely akin to hydrogen – cooled samples [25]. For example, what were well-defined doublets at 0.25 V and 0.145 V ascribable to the presence of 2D Pt{110} surface order, even at relatively low step density (n = 10) evolve immediately towards peaks that are much broader whilst simultaneously diminishing in intensity and shifting to more negative potentials. A lack of a distinct isopotential point around 0.12 V is also noteworthy when comparing data in Figure 79. The 0.20 V doublet observed with CO-cooled Pt{110} is immediately quenched upon the introduction of step sites attesting to the surface structural sensitivity of this state.
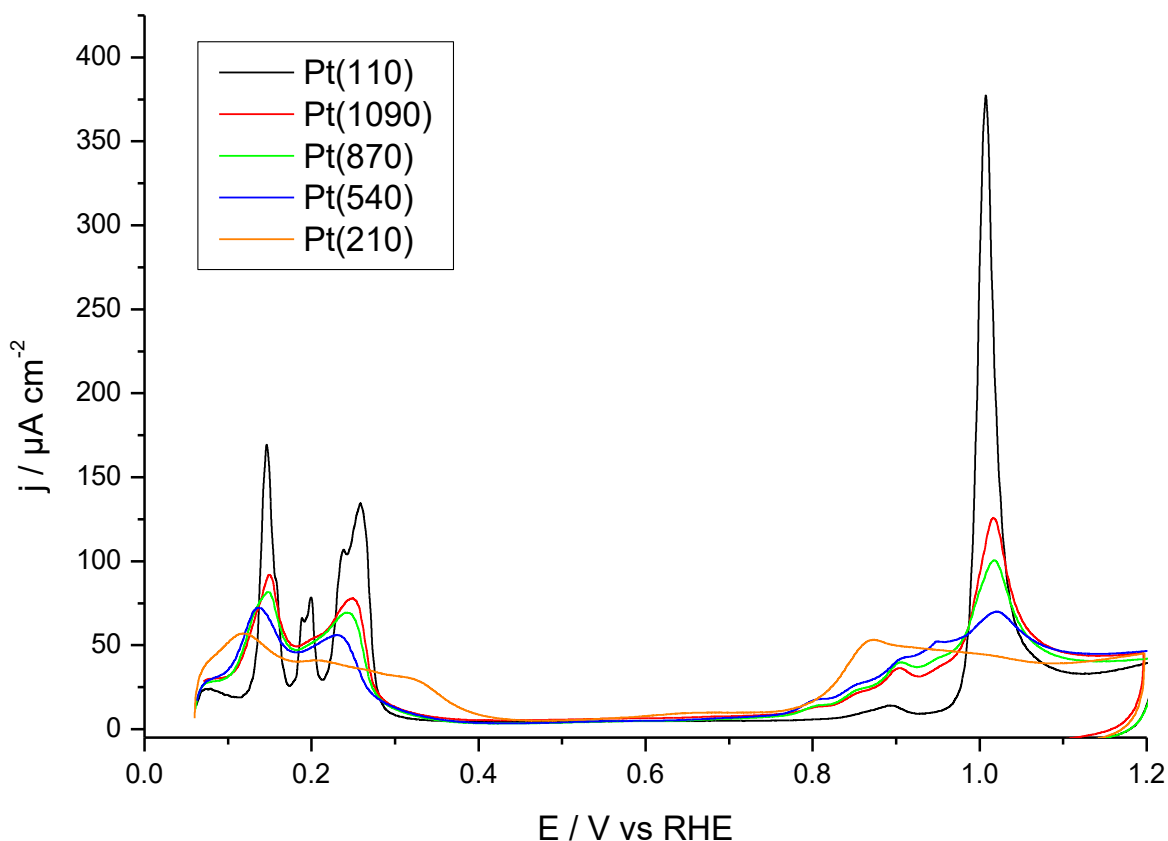
Figure 86: Cyclic voltammograms of Pt n{110}x{100} electrodes in 0.1 M aqueous perchloric acid prepared at Alicante University. Sweep rate = 50 mV/s.

The oxide electrosorption potential range between 0.8 and 1.2 V also changes in a less straightforward manner than for Pt n{110}x{111} stepped surfaces. Rather than observing two distinct and well-separated oxide adsorption peaks denoting step and terrace electrosorption, a multiplicity of adsorption peaks between 0.80 V and 0.90 V is evident. However, it is clear that the 0.89 V step adsorption peak (at Pt{111}x{111} sites) is prominent amongst this complexity. Taking into account the absence of an analogous Pt{110}x{100} oxide peak growing steadily with step density together with the presence of the 0.89 V peak, it is clear that the step sites are reconstructed. This symmetry is not expected to occur for this surface if it reflected a purely hard sphere (1x1) truncation of the platinum crystal. This would also be in accordance with the lack of surface 2D order in the H_{upd} potential region alluded to above. The Pt{110}-(1x1) terrace peak at 1.1 V is observed to decrease as step density decreases until it completely vanishes for Pt{210}, as expected since Pt{210} is the turning point of the zone. Interestingly, the reproducibility between Cardiff and Alicante Pt n{110}x{100} substrates was also found to be less marked here with Cardiff samples displaying a slightly larger 0.89 V oxide step peak than those depicted in Figure 86. This was probably due to minute differences in the alignment of the cutting plane which possibly tipped the

131

reconstruction direction towards the formation of {111}x{111} steps for the Cardiff electrodes (Figure 87). Irrespective of the number of {111}x{111} steps formed after step reconstruction, the model being proposed is completely consistent with previous work by Garcia-Araez *et al.*, demonstrating the reconstruction of {110}x{100} steps to form {111}x{111}structures for flame annealed and hydrogen- cooled stepped Pt{100} [32].

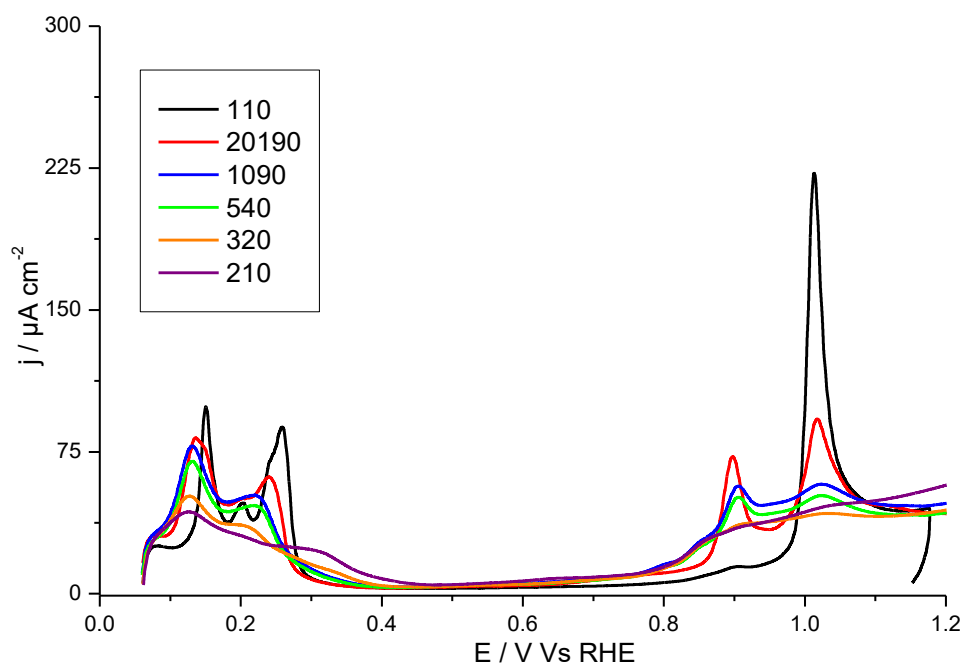*Figure 87: Cyclic voltammograms of Pt n{110}x{100} electrodes in 0.1 M aqueous perchloric acid prepared at Cardiff University. Sweep rate = 50 mV/s.*

In addition, the rate at which the terrace oxide peak is attenuated is quite different to that observed in Figure 79. This point is emphasised in Figure 88, where a plot of the electrosorption charge associated with the Pt{110}-(1x1) terrace sites is plotted as a function of step density for both Pt n{110}x{111} and Pt n{110}x{100} electrodes. For all step densities up to n = 2, it is found that the terrace charge for Pt n{110}x{100} electrodes is consistently smaller than that for the analogous Pt n{110}x{111} stepped surface. It is then concluded from this that for a specified step density, the long range order of the terraces is also influenced by the reconstruction of the steps and that overall 2D long range order is diminished relative to Pt n{110}x{111} planes.
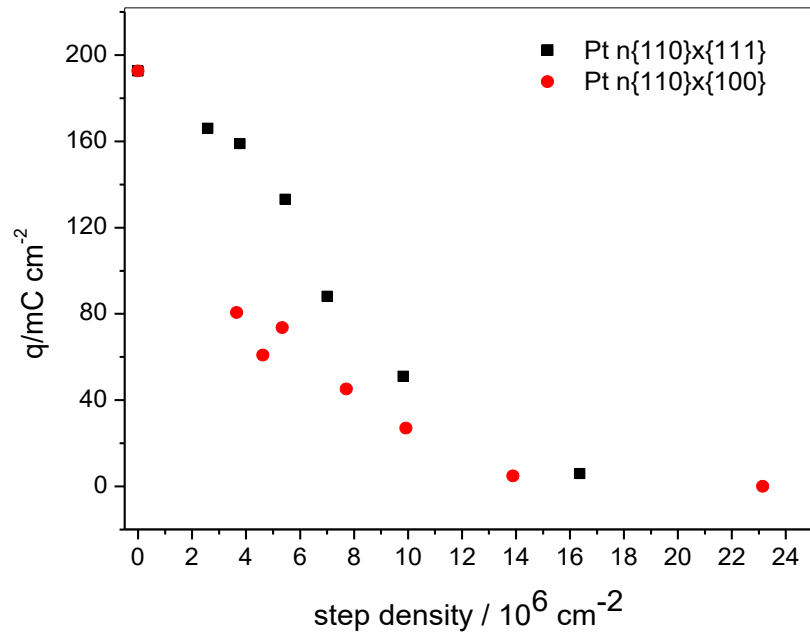
Figure 88: Graph showing how the Pt{110} terrace oxide electrosorption charge in 0.1 M perchloric acid electrolyte varies as a function of step density for Pt n{110}x{111} electrodes (black) and Pt n{110}x{100} (red) electrodes.
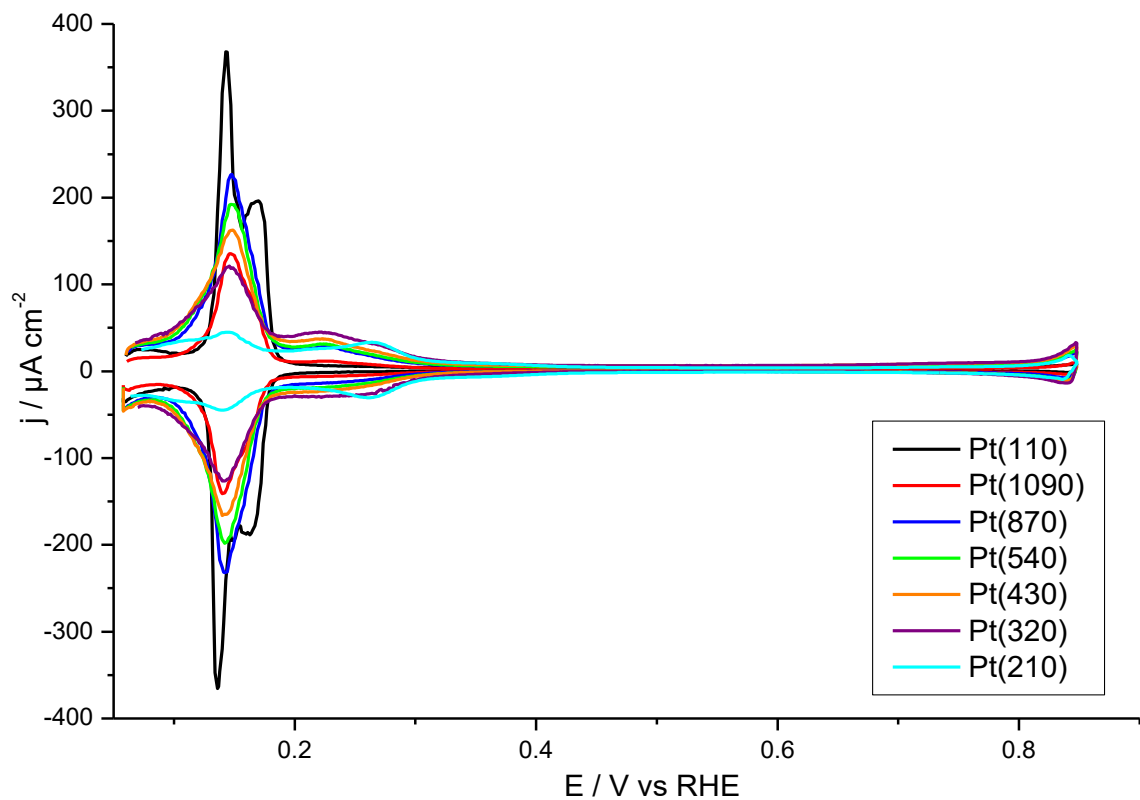
Figure 89: Cyclic voltammograms of Pt n{110}x{100} electrodes in 0.1 M aqueous sulphuric acid. Sweep rate = 50 mV/s.

Figure 89 also highlights changes in Pt n{110}x{100} voltammetry occurring when perchloric acid is replaced by sulphuric acid. As remarked earlier, the effect of the more strongly specifically adsorbing

anion is to narrow the potential range of H_{upd} response. In this case, the emergence of {111}x{100} H_{upd} step sites is evident at 0.28 V (Pt{110} is actually a compound step in microfacet notation denoted {111}x{111}). Again, the oxide electrosorption peaks are all shifted to slightly more positive potentials in sulphuric acid electrolyte with the Pt{110} terrace peak at 1.03 V and the {111}x{111} step peak situated at 0.93 V. This is especially prominent for Pt{10,9,0}) (see Figure 90). The increase in oxide peak intensity between 0.80 and 0.90 V is attributed to the presence of {110}x{100} steps, although a comparison with this potential region in perchloric acid suggests quite a number of distinct adsorption sites are subsumed within this broad feature.

Unlike for Pt n{110}x{111} surfaces, in Figure 89 the 0.17 V 2D Pt{110} terrace feature is immediately quenched for n=10, a distinct 1D Pt{110} peak is absent at 0.11 V and a complete absence of an isopotential point for the H_{upd} peaks confirms that a simple hard sphere, (1x1) truncation of the bulk crystal would not fit with the data. Charge observed at potentials negative of 0.14 V appears to be an off-shoot of the broadened 0.14 V peak discussed earlier. For Pt{210}, the emergence of H_{upd} charge in the potential range 0.30 to 0.45 V is consistent with the presence of narrow {100} terraces[45].
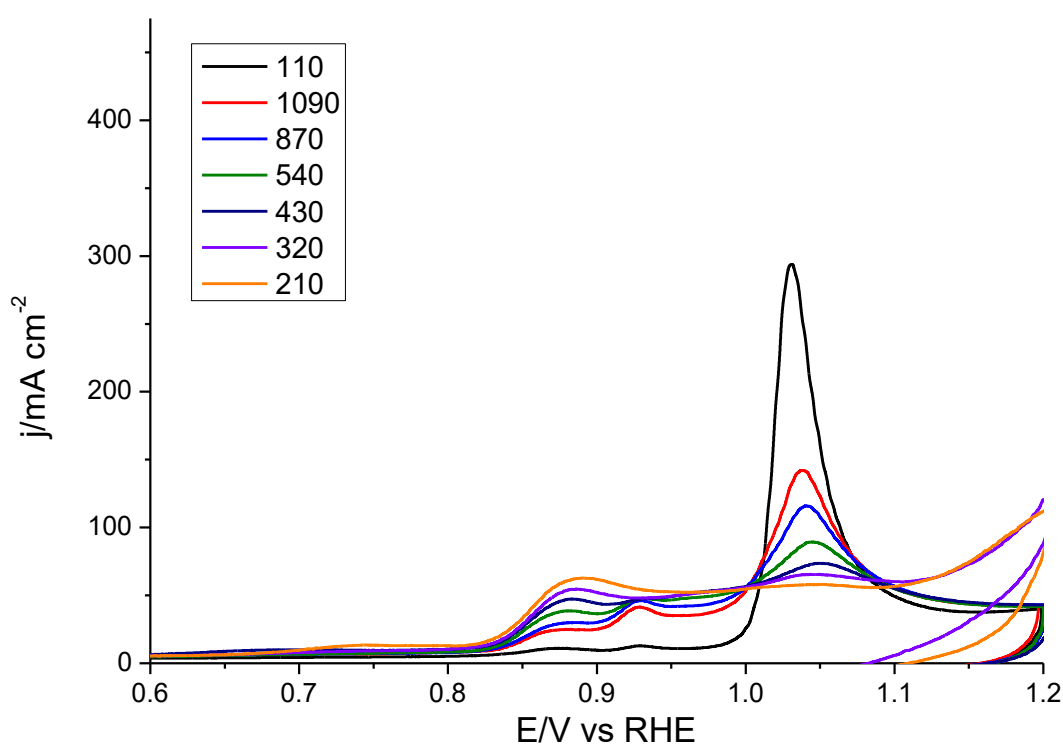

Figure 90: Expanded oxide potential range of cyclic voltammograms using Pt n{110}x{100} electrodes in 0.1 M aqueous sulphuric acid. Sweep rate = 50 mV/s.

4.2.3 Potential dependence of H_{upd} electrosorption peaks on specific adsorption strength and pH

In order to gain further insight into the electrosorbing species responsible for the principal 2D Pt{110} voltammetric peaks recorded for CO - cooled electrodes, CV data were collected in electrolytes containing anions of differing specific adsorption strength at almost constant pH. These included: (bi)sulphate, fluoride, methyl sulphonate and perchlorate (Figure 91). Studies with methanesulfonic or trifluoromethanesulfonic acids illustrate the effect of non-adsorbing anions on the structure of interfacial water [46, 47]. In addition, the pH dependence of the H_{upd} region of Pt{110} was investigated using a sodium fluoride buffer [48]. The data is shown in Figure 92.
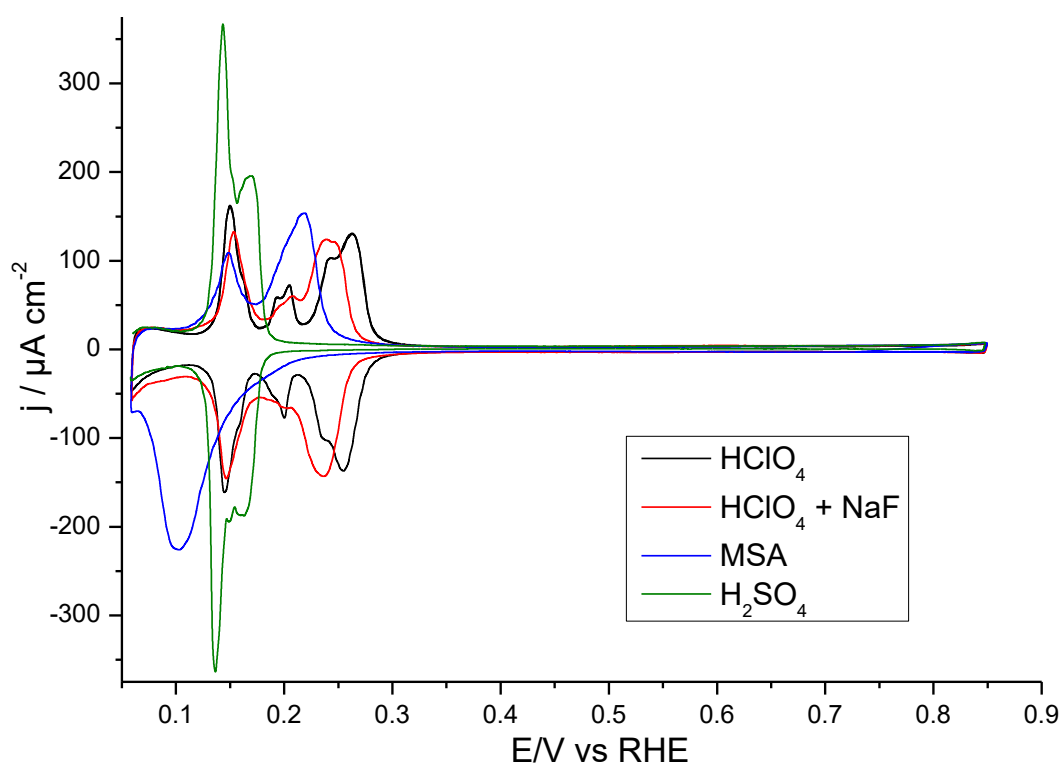
Figure 91: Cyclic voltammograms of CO – cooled Pt{110} electrodes as a function of increasing anion adsorption strength (sulfate > methyl sulphonate > fluoride > ¨OH¨).

In Figure 91, the influence of different anions at almost constant pH is shown. The main change observed is a shift to more negative potentials of the 0.25 V peak. In reference[49], the Pct peak was associated with very weakly specifically adsorbing perchlorate anions influencing the electrosorption of an "OH" containing species. The presence of an OH containing species during the formation of the Pct electrosorption state has also been supported using PZTC and thermodynamic analyses [31]. In the present study, as the nature of the anion is changed, the systematic potential shift observed may

be interpreted as more successful competition for adsorption sites by the more strongly specifically adsorbing anion. This interpretation has already been used in the case of Pt{111} and Pt{100}[49] to explain marked potential shifts in the potential of anion adsorption and ultimately, complete blockage of any Pt-OH bond formation when sulphate is present. (This could be due to the anion effect on H_2O structure [50]). The data in Figure 92 therefore suggests that in terms of the strength of anion specific adsorption, the order of interaction is:

sulphate > methanesulphonate > fluoride > perchlorate ≥ "OH"

It is also noteworthy that the peak at 0.145 V hardly changes potential at all, irrespective of the nature of the anion indicating that the extent of anion adsorption at such negative potentials is rather small if not zero. This would be consistent with the potential of zero charge occurring at a value positive of 0.145 V (to anions at 0.145 V, the surface ostensibly bears a negative charge at all sites and therefore precludes electrosorption).

Thus, support for the initial assignment of the origins of the major H_{upd} 2D Pt{110} voltammetric peaks (mainly anion electrosorption at 0.25 V, mainly cation electrosorption at 0.145 V) is evident from these anion studies.
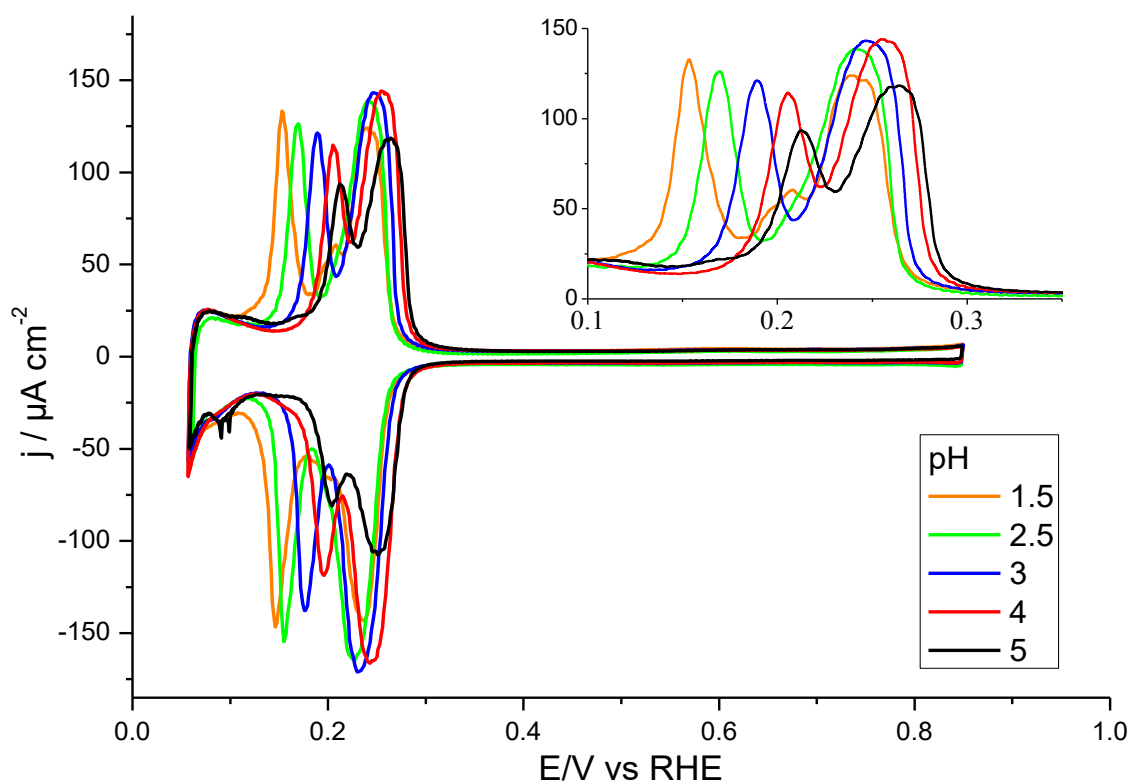

Figure 92: Cyclic voltammograms of CO – cooled Pt{110} electrodes as a function of pH

However, an interesting and ongoing controversy relating to the nature of the adsorbing species in the H_{upd} region of Pt single crystal electrode surfaces may also be highlighted when the pH dependence of the peaks in Figure 92 are scrutinised. For an RHE or Pd/H reference electrode, if the H_{upd} peaks corresponded to just proton electrosorption, there should be no pH dependence since the potential response should be strictly Nernstian. Figure 92 shows this is clearly not the case, an alternative interpretation of non-Nernstian effects needs to be formulated. One attempt to do this has been to assign non-Nernstian potential shifts in H_{upd} peaks as a function of pH to complex, non-stoichiometric combinations of H/OH/O adsorbing at for example step sites[44]. The problem with this interpretation is the inevitable co-existence (presumably at close proximity at the step) of H and OH on a platinum surface at room temperature which should spontaneously react to produce water according to previous ultra-high vacuum studies[51]. In [44], the authors did indeed note that on Pt{110} and Pt{100}, there is a small potential window in which H and OH co-exist on the surface, in what is traditionally called the "hydrogen region". An explanation for this was discussed whereby the stronger bond of OH to these surfaces as compared to Pt{111}, in combination with the stabilization of OH provided by water, prevented the recombination of H and OH into water. It is true that H_2O stabilises OH, but spontaneous formation of 2OH leads to facile and autocatalytic surface reactions with any H present to form water[52]. Hence, even in the presence of co-adsorbed water, the coexistence of H and OH on Pt at room temperature remains difficult to rationalise. There is however some evidence here, that co-adsorption of at least two species is responsible for the non-Nernstian shift in peak potential.

In the present study, differing degrees of specific adsorption of sodium ions and perchlorate anions in addition to hydrogen electrosorption may be used to interpret the data in Figure 92. This model is in agreement with very recent work by McCrum and Janik who used density functional theory to predict that the alkali metal cation potassium should specifically adsorb on Pt, especially for increasing pH [53]. In fact, such co-adsorption might be involved in the non-Nernstian shifts in Pt step peak potential. Much work has been undertaken by the Frumkin School in relation to the pH dependence of anion and cation adsorption[54]. From these studies, it was determined that the specific adsorption of anions and cations is pH dependent. An increase in pH leads to a weakening in the interaction of anions with an electrode surface and a strengthening in the interaction of cations and vice versa. This corresponds in a shift to more negative potentials in the PZC as anion adsorption strength increases and a shift of PZC to more positive potentials as cation interaction strength increases.

In Figure 92, the peak at 0.145 V is observed to shift positively at a rate of 18 mV per pH unit and the 0.25 V peak at a rate of 6 mV per pH unit. The first peak shift of 18 mV per pH unit would be consistent with stronger interaction of the electrode with sodium cations requiring a more positive potential to cause desorption (PZC shifts to more positive potentials with increasing pH). The weakening in the interaction of fluoride anions (shift of PZC to more positive potentials) with the electrode surface as a function of increasing pH would then account for the 6 mV per pH unit positive shift observed for Pt{110}. The magnitudes of the potential shifts probably reflect a complex interaction between H/Na$^+$ and "OH"/F$^-$ competitively adsorbing at locally charged sites. In Figure 93, the influence of both anions and cations is combined for Pt{110} in 0.01 M aqueous perchloric acid and a pH = 2 sodium fluoride buffer. It is evident that since the pH is common to both electrolytes, the presence of Na$^+$(aq) ions causes a slight shift in the 0.145 V peak to slightly more positive potentials and the F$^-$(aq) ions of the buffer engender a shift to more negative potentials in the potential of the 0.25 V peak (they compete more successfully than "OH" for the anion sites) as expected based on the model outlined above.
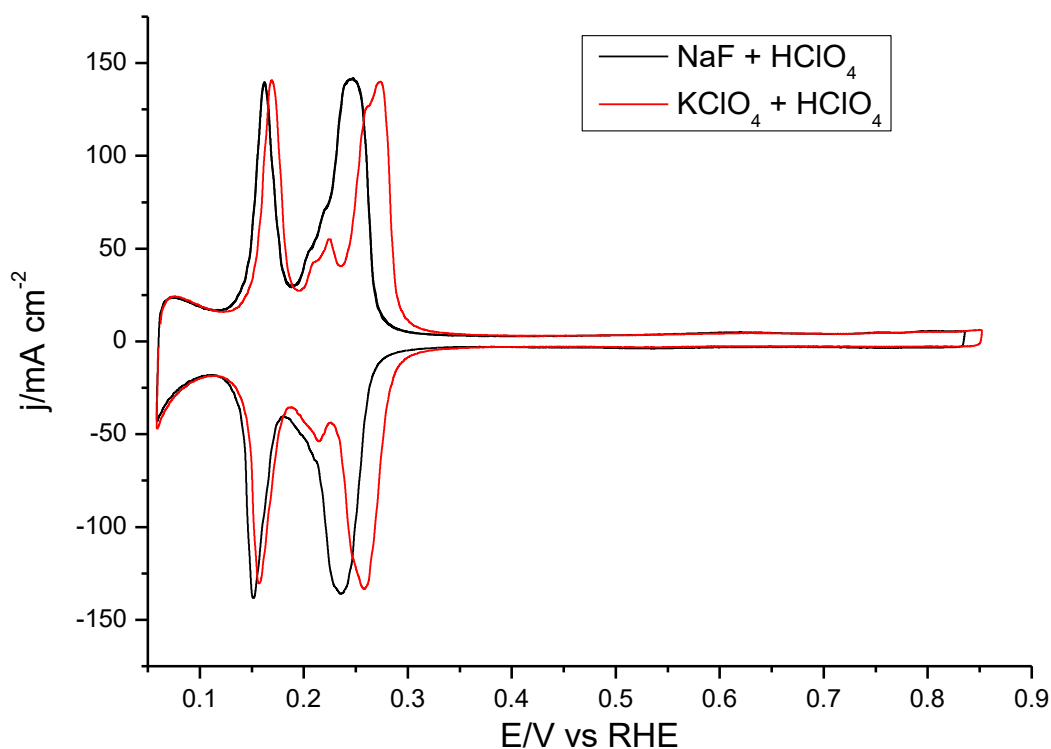

Figure 93: Cyclic voltammetry of CO cooled Pt{110} electrodes at pH=2 using a NaF buffer (black) and unbuffered 0.01 M aqueous perchloric acid (red). Sweep rate = 50 mV/s

4.2.4 CO charge displacement measurements of the potential of zero total charge (PZTC)

In Figure 94, CO charge displacement measurements of the potential of zero total charge (PZTC) are summarised as a function of step density for all surfaces. The total charge is the charge that would flow if all free charges (monopoles, dipoles and electrosorbed species (for example Pt-H)) were stripped from the electrode surface. CO is an excellent chemisorbate for achieving this transformation (for potentials negative of its electrooxidation) and subject to a small correction, may provide a value of potential at which the 'anionic' and 'cationic' charge which flows upon exposure of Pt electrodes to CO are in perfect balance and thus, the PZTC is determined. Unfortunately, in most cases, the CO charge displacement method cannot separate the specific cationic and anionic charge flow contributions from individual local adsorption sites (steps, terraces and kinks). Rather, it may provide a 'global average' of all of these contributions although in the case of Pt{111}, because H_{upd} and anion electrosorption states are well separated, it is indeed possible to deduce the 'definitive' value of PZTC, i.e. for Pt{111}, the global value of PZTC is the same as the local value of PZTC[42, 43]. This is important when surfaces such as Pt{110} in perchloric acid are considered because their voltammetry is manifested as a series of well-defined electrosorption states that span the entire H_{upd} potential range and if it is assumed that each electrosorption state reflects a varying surface charge as a function of potential, then the global PZTC determined using CO charge displacement may not reflect these locally charged states. However, it is logical to assume that at potentials well removed from the PZTC, the direction of transient current flow should reflect the majority charge species (cationic or anionic). Close inspection of Figure 94 indicates that not only is the PZTC both structure and anion sensitive but that certain electrosorption peaks must be dominated by one type of charge. For example, for Pt{110} in perchloric acid, the PZTC coincides with the top of the more negative peak of the 0.25 V doublet. Using the labelling of CO cooled Hupd region from [5] (and shown in Figure 95), where P1 signifies the most negative H_{upd} peak and P6 signifying the most positive, this would broadly indicate that P6 may be ascribed to the electrosorption of anions and those negative of this potential to desorption of cations. This would be in accordance with measurements recorded as a function of pH and varying the sequence anion/cation highlighted previously. However, if all peaks P1 to P6 do correspond to differentially charged states, it should also be possible to calculate the PZTC without having to undertake CO charge displacement.
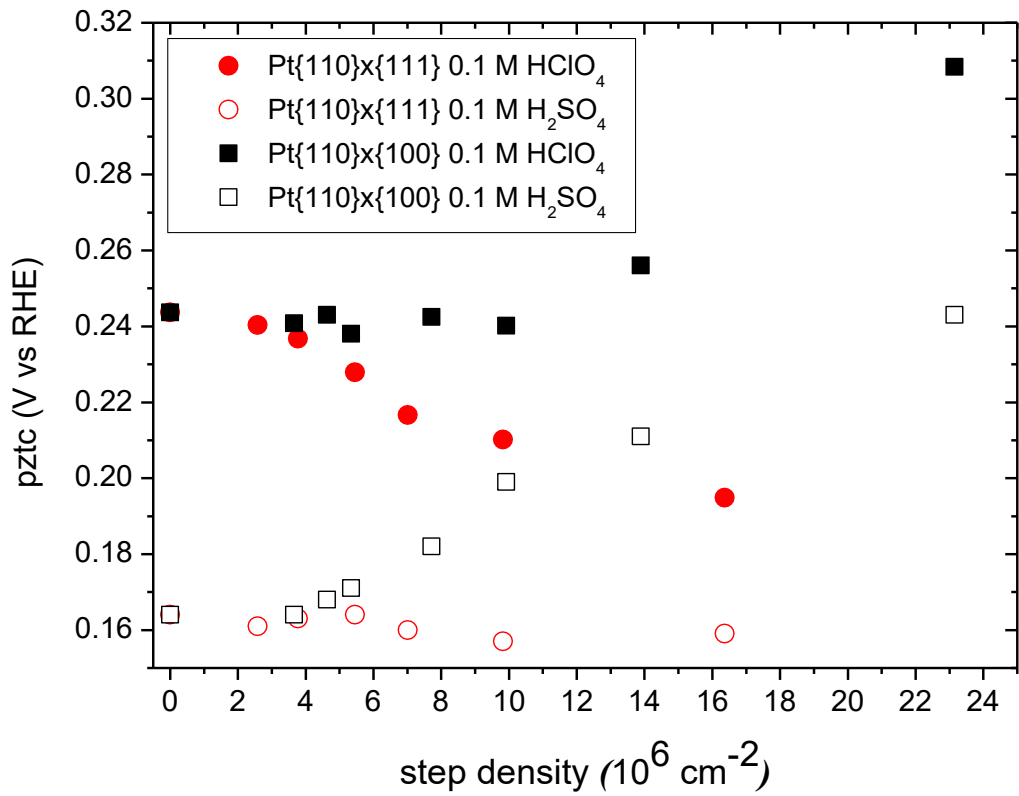
Figure 94: Potential of zero total charge (PZTC) as a function of step density for Pt n{110}x{111} and Pt n{110}x{100} electrodes.
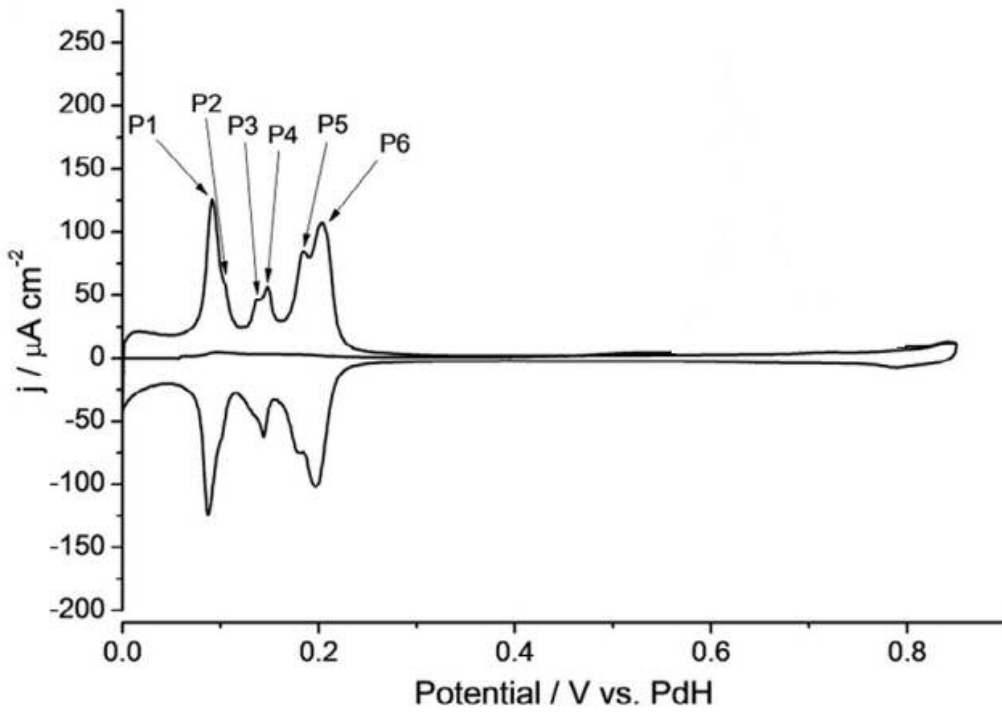

Figure 95: CO cooled Pt{110} electrode in 0.1 M HClO4. Reprinted from [5]

4.2.5 PZTC evaluation without charge displacement?

Figure 96 shows a typical CO cooled Pt{110} CV in 0.1 M perchloric acid with appropriate curve fitting using six Lorentzian peaks. The table below then shows the values of deconvoluted charge per each peak contribution. Also, highlighted in the figure are three local values of PZC centred at each doublet (see earlier). According to this scheme, peaks P1, P3 and P5 would then correspond to cationic charge states and peaks P2, P4 and P6 to anionic charge contributions. At the "global" PZTC (evaluated using CO charge displacement), it is evident that P1 and P3 would correspond to "empty states" since the global PZC is positive of both local PZC for these sites (cations in these sites see a locally positively charged surface so are repelled). However, the corresponding P2 and P4 peaks for analogous reasons should be "filled" with anions (as stated previously, sites exhibit an excess positive charge attracting the anions). The PZTC being at the potential of peak P5 means that only 50% of this cation charge site will be occupied together with 6% of the anionic peak P6. Therefore, if this breakdown of charge contributions is correct, it is evident that in terms of charge at the PZTC:

$$P2 + P4 + 0.06 \times P6 = 0.5 \times P5$$

Putting in the values of these "local" charges (in $\mu C\ cm^{-2}$) from Table 1:

$$P2 + P4 + 0.06 \times P6 = 4.6688 + 14.4192 + 0.06 \times 52.7804 = 22.2548\ \mu C\ cm^{-2}$$

And :$$\qquad 0.5 \times P5 = 0.5 \times 45.838 = 22.919\ \mu C\ cm^{-2}$$

This remarkable agreement between the predicted condition of global PZTC and the actual value of PZTC determined experimentally lends further support to our peak assignments. Additionally, in future work it should be possible to reconstruct each CO charge transient as a function of potential using such analyses whereby electrosorption peaks may be assigned to positive and negative charge contributions, deconvoluted to determine their magnitudes and then combined as a function of potential (filling and emptying of each state). This analysis should be undertaken for other platinum single crystal electrode surfaces in order to generate PZTC values *a priori*. In the present study, all measurements seem to point towards a consistent model involving adsorption/desorption of varying amounts of cations and anions depending on pH, anion/cation adsorption strength and surface structure.
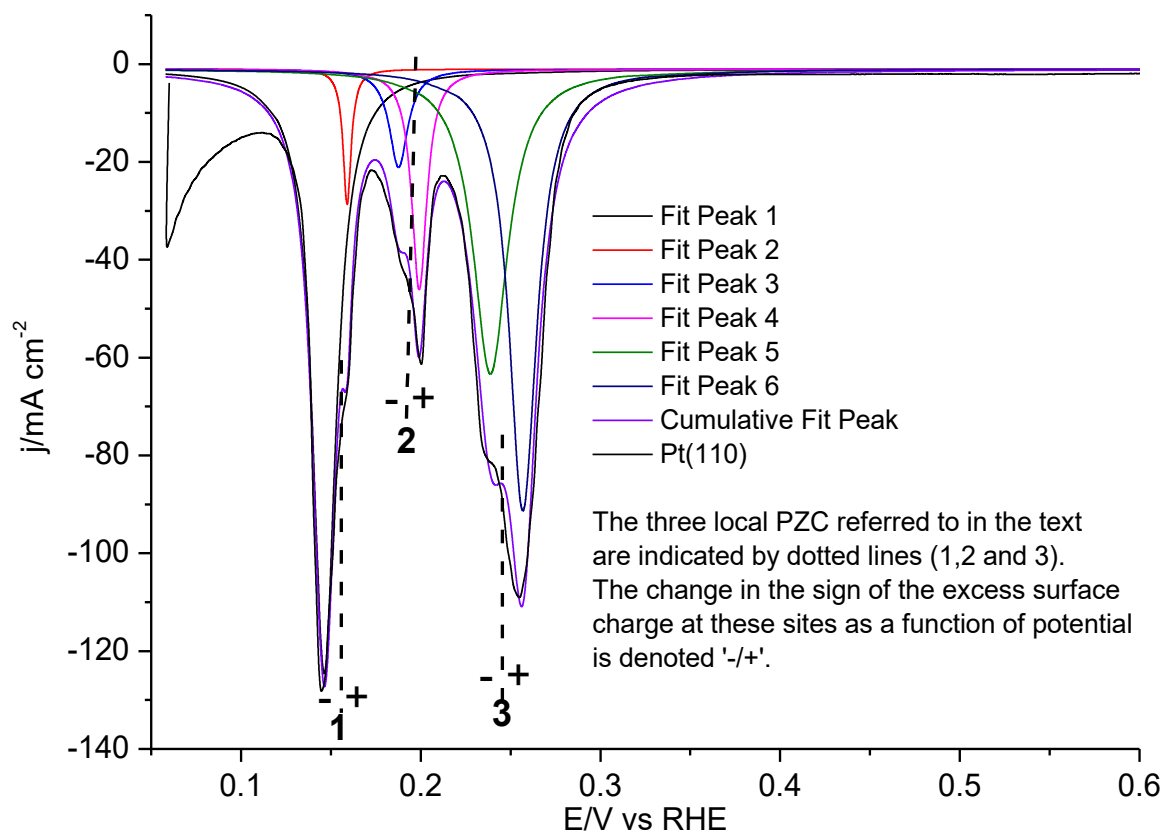
Figure 96: Curve fitting to the 0.85 V to 0.05 V potential sweep of a Pt{110} – (1x1) electrode in 0.1 M aqueous perchloric acid. Sweet rate = 50 mV/s.

Deconvoluted charge for Pt{110} in 0.1 M HClO$_4$.

Peak	Charge (μC cm^{-2})
1	-61.6136
2	-4.6688
3	-7.837
4	-14.4192
5	-45.836
6	-52.7804

4.2.6 Trends in PZTC of stepped Pt{110} electrodes

Returning to Figure 94, the most striking feature of this PZTC data is the disparity in the trends depending on the nature of the step site. For example, in perchloric acid, increasing surface density of {111}x{111} steps results in a steady shift to more negative potentials in the value of PZTC. In contrast, for {110}x{100} stepped surfaces, after an initial steady plateau region, for narrow terraces,

the PZTC shifts to more positive values. Within the model outlined above concerning locally charged sites, the shift to more negative potentials in PZTC as n decreases for Pt n{110}x{111} may be ascribed to a decrease in the intensity of the 0.25 V doublet terrace peak corresponding to P5 and the large P6 anion peak. Since P6 > P5, this means that per the definitions outlined above, the global PZTC value must shift to more negative values.

For the more complicated and reconstructed Pt n{110}x{100} stepped surfaces, it is not straightforward to separate the various charge contributions, especially for Pct. However, the gradual decrease in the intensity of this peak that is observed as the average terrace width decreases might have also resulted in a steady shift in the PZTC to more negative potentials. However, from Figure 85 it is noted that new H_{upd} electrosorption states begin to appear between 0.2 and 0.4 V for n < 4. It is speculated that it is the anion desorption charge in these states that pushes the PZTC to more positive values. This trend of increasing global PZTC is even more pronounced using sulphuric acid electrolyte since the Pt{110} H_{upd} states are confined to a narrower, more negative potential region due to specific adsorption of sulphate and the new H_{upd} states appearing at more positive potential due to {100} steps are much less affected by specifically adsorbing anions. This means that the almost static PZTC observed for lower step densities in perchloric acid is not realised in sulphuric acid electrolyte and instead, a gradual shift to more positive values in the PZTC is seen at all step densities. For Pt n{110}x{111} stepped surfaces in sulphuric acid, the almost negligible change in the value of PZTC reflects the narrow confinement of all H_{upd} peaks within a narrow potential range and therefore, relative changes in step/terrace contributions make very little difference to the overall PZTC.

Compared to previous reports for hydrogen – cooled stepped samples[25, 26], the trends reported in Figure 96 are remarkably similar. The only major difference is a slight off-set in the PZTCs of the CO – cooled samples by approximately 10–15 mV to more positive potentials. This probably reflects the slightly greater degree of disorder present in the hydrogen – cooled samples.

4.3 Conclusions

A comprehensive electrochemical study of CO – cooled single crystal electrodes vicinal to the Pt{110} basal plane has been undertaken. Based on detailed analysis of electrosorption charges/voltammetry, pH, anion and cation effects and PZTC it is concluded that Pt n{110}x{111}

electrodes are unreconstructed and afford systematic variations in H_{upd} and electrosorbed oxide CV peaks as a function of step density. In contrast, similar analyses using Pt n{110}x{100} electrodes indicate a strong tendency towards surface reconstruction, not necessarily just confined to relatively unstable {110}x{100} steps but also possibly residual terrace sites adjacent to the steps. A new model of the Pt{110} H_{upd} region is expounded in which local charged states that vary as a function of potential, pH and ionic adsorption are thought responsible for the variety of CV response recorded. The model allows for interpretation of non-Nernstian shifts in peak potential as a function of pH and the nature of the ions in contact with the electrode surface and points to weak specific adsorption of sodium ions and fluoride anions on Pt{110}together with "OH" and the more usual hydrogen electrosorption. Moreover, it is asserted that by assigning "cationic" and "anionic" contributions to the overall H_{upd} region, one may evaluate the global value of the PZTC without the need of measuring CO charge displacement. The possibility that this model may apply generally to other well-defined Pt electrodes will be the subject of future investigations.

4.5 References

1. Engel, T., H. Niehus, and E. Bauer, *Adsorption of oxygen on w(110). 1.P(2x1) structure.* Surface Science, 1975. **52**(2): p. 237-262.
2. Wagner, F.T. and P.N. Ross, *Long range structural effects in the anomalous voltammetry on ultahigh vacuumLprepared Pt(111).* Journal of Electroanalytical Chemistry, 1988. **250**(2): p. 301-320.
3. Attard, G.A. and R. Price, *Electrochemical investigation of a structure sensitive growth mode - palladium deposition on Pt(100)-Hex-R0.7-Degrees and Pt(100)-(1x1).* Surface Science, 1995. **335**(1-3): p. 63-74.
4. Marković, N.M., et al., *Surface electrochemistry of CO on Pt(110)-(1 × 2) and Pt(110)-(1 × 1) surfaces.* Surface Science, 1997. **384**(1): p. L805-L814.
5. Attard, G.A. and A. Brew, *Cyclic voltammetry and oxygen reduction activity of the Pt{110}-(1 x 1) surface.* Journal of Electroanalytical Chemistry, 2015. **747**: p. 123-129.
6. Hubbard, A.T., R.M. Ishikawa, and J. Katekaru, *Study of platinum-electrodes by means of electrochemistry and low-energy-electron-diffraction. 2.comparison of electrochemical activity of Pt(100) and Pt(111) surfaces.* Journal of Electroanalytical Chemistry, 1978. **86**(2): p. 271-288.
7. Armand, D. and J. Clavilier, *Electrochemical behaviour of the (110) orientation of a platinum surface in acid medium: the role of anions.* Journal of Electroanalytical Chemistry and Interfacial Electrochemistry, 1989. **263**(1): p. 109-126.
8. Markovic, N.M., N.S. Marinkovic, and R.R. Adzic, *Electrosorption of hydrogen and sulfuric acid anions on single crystal platinum stepped surfaces. 2.The 110 zone.* Journal of Electroanalytical Chemistry, 1991. **314**(1-2): p. 289-306.
9. Clavilier, J., et al., *Study of the charge displacement at the constant potential during CO adsorption on Pt(110) and Pt(111) electrodes in contact with a perchloric acid solution.* Journal of Electroanalytical Chemistry, 1992. **330**(1-2): p. 489-497.
10. Swamy, K., E. Bertel, and I. Vilfan, *Step interaction and relaxation at steps: Pt(110).* Surface Science, 1999. **425**(1): p. L369-L375.
11. Attard, G.A. and A. Brew, *Cyclic voltammetry and oxygen reduction activity of the Pt{1 1 0}-(1 × 1) surface.* Journal of Electroanalytical Chemistry, 2015. **747**: p. 123-129.
12. Kibler, L.A., et al., *In-situ STM characterisation of the surface morphology of platinum single crystal electrodes as a function of their preparation.* Journal of Electroanalytical Chemistry, 2000. **484**(1): p. 73-82.
13. Perez, J., H.M. Villullas, and E.R. Gonzalez, *Structure sensitivity of oxygen reduction on platinum single crystal electrodes in acid solutions.* Journal of Electroanalytical Chemistry, 1997. **435**(1): p. 179-187.
14. Marković, N.M., et al., *Structural effects in electrocatalysis: oxygen reduction on platinum low index single-crystal surfaces in perchloric acid solutions.* Journal of Electroanalytical Chemistry, 1994. **377**(1): p. 249-259.
15. Maciá, M.D., et al., *On the kinetics of oxygen reduction on platinum stepped surfaces in acidic media.* Journal of Electroanalytical Chemistry, 2004. **564**: p. 141-150.
16. Kuzume, A., E. Herrero, and J.M. Feliu, *Oxygen reduction on stepped platinum surfaces in acidic media.* Journal of Electroanalytical Chemistry, 2007. **599**(2): p. 333-343.
17. Tanaka, H., et al., *The Influence of Pt Oxide Film on the Activity for the Oxygen Reduction Reaction on Pt Single Crystal Electrodes.* Electrocatalysis, 2014. **5**(4): p. 354-360.
18. Colmati, F., et al., *Surface structure effects on the electrochemical oxidation of ethanol on platinum single crystal electrodes.* Faraday Discussions, 2009. **140**(0): p. 379-397.
19. Taguchi, S. and J.M. Feliu, *Kinetic study of nitrate reduction on Pt(1 1 0) electrode in perchloric acid solution.* Electrochimica Acta, 2008. **53**(10): p. 3626-3634.

20.   Housmans, T.H.M., A.H. Wonders, and M.T.M. Koper, *Structure Sensitivity of Methanol Electrooxidation Pathways on Platinum: An On-Line Electrochemical Mass Spectrometry Study.* The Journal of Physical Chemistry B, 2006. **110**(20): p. 10021-10031.

21.   Vidal-Iglesias, F.J., et al., *Selective electrocatalysis of ammonia oxidation on Pt(1 0 0) sites in alkaline medium.* Electrochemistry Communications, 2003. **5**(1): p. 22-26.

22.   Müller, U. and H. Baltruschat, *Displacement of Ethene and Cyclohexene from Polycrystalline Pt and Pt(110) Electrodes.* The Journal of Physical Chemistry B, 2000. **104**(24): p. 5762-5767.

23.   Sun, S.-G., et al., *An International Journal Devoted to all Aspects of Electrode Kinetics, Interfacial Structure, Properties of Electrolytes, Colloid and Biological ElectrochemistryElectrocatalytic properties of Pt(111), Pt(332), Pt(331) and Pt(110) single crystal electrodes towards ethylene glycol oxidation in sulphuric acid solutions.* Journal of Electroanalytical Chemistry, 1992. **340**(1): p. 213-226.

24.   Cases, F., et al., *Dissociative adsorption of ethanol on Pt (h, k, l) basal surfaces.* Journal of Electroanalytical Chemistry and Interfacial Electrochemistry, 1990. **278**(1): p. 433-440.

25.   Souza-Garcia, J., et al., *Electrochemical features of Pt(S)[n(110) × (100)] surfaces in acidic media.* Electrochemistry Communications, 2013. **34**: p. 291-294.

26.   Souza-Garcia, J., V. Climent, and J.M. Feliu, *Voltammetric characterization of stepped platinum single crystal surfaces vicinal to the (1 1 0) pole.* Electrochemistry Communications, 2009. **11**(7): p. 1515-1518.

27.   Clavilier, J., et al., *An International Journal Devoted to all Aspects of Electrode Kinetics, Interfacial Structure, Properties of Electrolytes, Colloid and Biological ElectrochemistryStudy of the charge displacement at constant potential during CO adsorption on Pt(110) and Pt(111) electrodes in contact with a perchloric acid solution.* Journal of Electroanalytical Chemistry, 1992. **330**(1): p. 489-497.

28.   Orts, J.M., et al., *Electrochemical oxidation of ethylene glycol on Pt single crystal electrodes with basal orientations in acidic medium.* Journal of Electroanalytical Chemistry and Interfacial Electrochemistry, 1990. **290**(1): p. 119-133.

29.   Taguchi, S. and J.M. Feliu, *Electrochemical reduction of nitrate on Pt(S)[n(1 1 1) × (1 1 1)] electrodes in perchloric acid solution.* Electrochimica Acta, 2007. **52**(19): p. 6023-6033.

30.   Hoshi, N., et al., *Surface X-ray Scattering of Stepped Surfaces of Platinum in an Electrochemical Environment: Pt(331) = 3(111)-(111) and Pt(511) = 3(100)-(111).* Langmuir, 2011. **27**(7): p. 4236-4242.

31.   Garcia-Araez, N., *Enthalpic and Entropic Effects on Hydrogen and OH Adsorption on Pt(111), Pt(100), and Pt(110) Electrodes As Evaluated by Gibbs Thermodynamics.* The Journal of Physical Chemistry C, 2011. **115**(2): p. 501-510.

32.   García-Aráez, N., et al., *On the electrochemical behavior of the Pt(1 0 0) vicinal surfaces in bromide solutions.* Surface Science, 2004. **560**(1–3): p. 269-284.

33.   Kolics, A. and A. Wieckowski, *Adsorption of bisulfate and sulfate anions on a Pt(111) electrode.* Journal of Physical Chemistry B, 2001. **105**(13): p. 2588-2595.

34.   Su, Z., et al., *Quantitative SNIFTIRS studies of (bi)sulfate adsorption at the Pt(111) electrode surface.* Physical Chemistry Chemical Physics, 2010. **12**(46): p. 15231-15239.

35.   Garcia-Araez, N., et al., *Elucidation of the Chemical Nature of Adsorbed Species for Pt(111) in H2SO4 Solutions by Thermodynamic Analysis.* Langmuir, 2010. **26**(14): p. 12408-12417.

36.   Garcia-Araez, N., et al., *Thermodynamic evidence for K+-SO42- ion pair formation on Pt(111). New insight into cation specific adsorption.* Physical Chemistry Chemical Physics, 2010. **12**(38): p. 12146-12152.

37.   Rodes, A., et al., *Electrochemical Probing of Step and Terrace Sites on Pt [n(111)×(111)] and Pt[n(111)×(100)]*, in *Fundamental Aspects of Heterogeneous Catalysis Studied by Particle Beams*, H.H. Brongersma and R.A. van Santen, Editors. 1991, Springer US: Boston, MA. p. 75-82.

38. Clavilier, J., *The role of anion on the electrochemical behaviour of a {111} platinum surface; an unusual splitting of the voltammogram in the hydrogen region.* Journal of Electroanalytical Chemistry and Interfacial Electrochemistry, 1979. **107**(1): p. 211-216.

39. Arán-Ais, R.M., et al., *On the behavior of the Pt(1 0 0) and vicinal surfaces in alkaline media.* Electrochimica Acta, 2011. **58**: p. 184-192.

40. Gómez-Marín, A.M. and J.M. Feliu, *Thermodynamic properties of hydrogen–water adsorption at terraces and steps of Pt(111) vicinal surface electrodes.* Surface Science, 2016. **646**: p. 269-281.

41. Schwarz, K., et al., *Partial oxidation of step-bound water leads to anomalous pH effects on metal electrode step-edges.* Physical Chemistry Chemical Physics, 2016. **18**(24): p. 16216-16223.

42. Attard, G.A., et al., *On the global and local values of the potential of zero total charge at well-defined platinum surfaces: stepped and adatom modified surfaces.* Journal of Electroanalytical Chemistry, 2004. **568**: p. 329-342.

43. Climent, V., G.A. Attard, and J.M. Feliu, *Potential of zero charge of platinum stepped surfaces: a combined approach of CO charge displacement and N2O reduction.* Journal of Electroanalytical Chemistry, 2002. **532**(1–2): p. 67-74.

44. van der Niet, M.J.T.C., et al., *Water dissociation on well-defined platinum surfaces: The electrochemical perspective.* Catalysis Today, 2013. **202**: p. 105-113.

45. Vidal-Iglesias, F.J., et al., *CO monolayer oxidation on stepped Pt(S) [(n − 1)(1 0 0) × (1 1 0)] surfaces.* Electrochimica Acta, 2009. **54**(19): p. 4459-4466.

46. Sandoval, A.P., et al., *Interaction of water with methanesulfonic acid on Pt single crystal electrodes.* Electrochemistry Communications, 2015. **50**: p. 47-50.

47. Berná, A., et al., *Voltammetric characterization of Pt single crystal electrodes with basal orientations in trifluoromethanesulphonic acid.* Electrochemistry Communications, 2008. **10**(11): p. 1695-1698.

48. Martínez-Hincapié, R., et al., *Exploring the interfacial neutral pH region of Pt(111) electrodes.* Electrochemistry Communications, 2015. **58**: p. 62-64.

49. Attard, G.A., et al., *Specific adsorption of perchlorate anions on Pt{hkl} single crystal electrodes.* Physical Chemistry Chemical Physics, 2014. **16**(27): p. 13689-13698.

50. Berná, A., V. Climent, and J.M. Feliu, *New understanding of the nature of OH adsorption on Pt(1 1 1) electrodes.* Electrochemistry Communications, 2007. **9**(12): p. 2789-2794.

51. Verheij, L.K., *Kinetic modelling of the hydrogen-oxygen reaction on Pt(111) at low temperature (< 170 K).* Surface Science, 1997. **371**(1): p. 100-110.

52. Michaelides, A. and P. Hu, *Catalytic Water Formation on Platinum: A First-Principles Study.* Journal of the American Chemical Society, 2001. **123**(18): p. 4235-4242.

53. McCrum, I.T. and M.J. Janik, *pH and Alkali Cation Effects on the Pt Cyclic Voltammogram Explained Using Density Functional Theory.* The Journal of Physical Chemistry C, 2016. **120**(1): p. 457-471.

54. Peter Horsman, B.E.C., E. Yeager, ed. *Comprehensive Treatise of Electrochemistry: The Double Layer*. 1980, Springer US. XIX, 453.

Characterisation of stepped Pt single crystals in the [001] zone
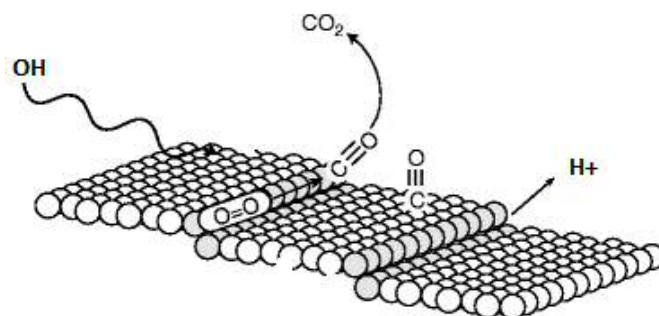
5.1 Introduction

Platinum is one of the most investigated materials in electrochemistry due to its high activity in numerous electrocatalytic reactions[1]. The use of single crystals to investigate electrocatalytic phenomena plays a key role in identifying the surface structure of the active sites specifically responsible for a material's activity and selectivity. Introduction of the flame annealing method by Clavilier[2] facilitated a great advance in the understanding of many structure-sensitive reactions at the atomic scale[1]. Information gained from single crystal studies enables systematic and logical progress to be made in the development of real catalysts (for example in shape-selective nanoparticle synthesis [3, 4]). Many studies have already reported on the surface structure dependence of electrochemical reactions at heterogeneous interfaces, including the oxygen reduction reaction[5-8].

Such studies have been carried out on platinum single crystal electrodes with orientations vicinal to both the Pt(111) and Pt(100) planes which afford activity trends associated with the surface density of linear steps[9-16]. Pt(110) and its vicinal, stepped surfaces have been comparatively less well explored. In this work, platinum surfaces in the [001] zone of the stereographic triangle will be investigated. This chapter in particular employs CV to explore the reactivity, activity and role of specific step/terraced sites in relation to the oxygen reduction and hydrogen peroxide disproportionation reactions. The impact of the polymer exchange membrane Nafion (used in most oxygen based fuel cells) in altering the surface behaviour of stepped platinum single crystal electrode surfaces is also explored. Two series of stepped surfaces are investigated and trends in electrochemical properties as a function of average terrace width and the nature of the linear step will be reported. This chapter will provide an introduction to the reactivity of stepped Pt{hkl}

electrodes and a basis for considering changes engendered by changing the cooling environment of the flame-annealed, stepped Pt{110} electrodes in particular.

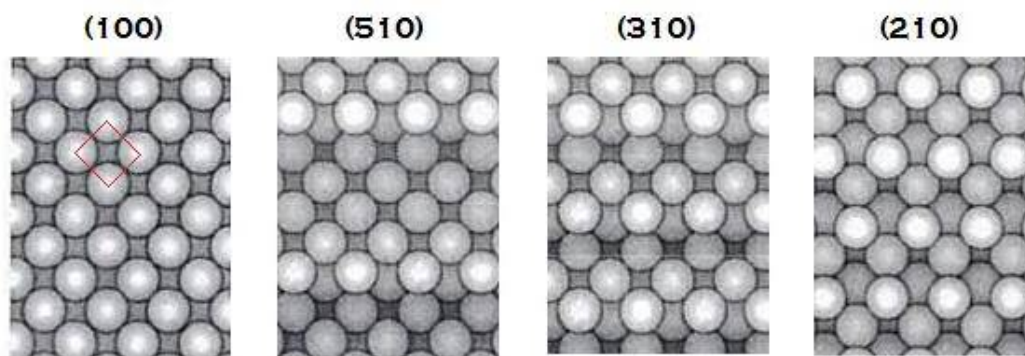## 5.2 Results of Pt(S)[n(100)x(110)] single crystal electrode studies

Figure 97: Hard sphere models of Pt(S)[n(100)x(110)] single crystal surfaces

5.2.1 Cyclic Voltammetry – Perchloric Acid Electrolyte

The voltammetric profiles of several stepped surfaces vicinal to the (100) pole of the stereographic triangle in acidic media are shown in Figure 98. These surfaces contain n-atom wide (100) terraces (2 < n < 20) separated by linear (110) steps. Figure 97 illustrates hard sphere models of some of these surfaces. Voltammograms were measured in 0.1 M $HClO_4$ and 0.1 M H_2SO_4 for comparison to previous electrochemical studies involving single crystal electrodes and to differentiate between electrochemical responses in the presence and absence of specific anion adsorption. There is good agreement with some surfaces that have been reported in the literature[12, 15, 17-20]. However, no publication has previously shown the corresponding voltammograms at potentials positive of 0.8 V. These adsorption states are considered crucial for understanding reactivity trends and are included here for the first time. For results performed in 0.1 M $HClO_4$, a qualitative interpretation of the various voltammetric features is proposed.

Figure 98 and Figure 99 report the voltammetric profiles of the different stepped electrodes in 0.1 M $HClO_4$. The voltammetric profiles indicate reversible behaviour in the potential window negative of the oxide electrosorption region (between 0 and 0.8 V), showing the surfaces to be stable under these conditions. The voltammogram of Pt(100) is characterised by adsorption states centred at approximately 0.3, 0.4 and 0.5 V, corresponding to H_{upd} (0.3 and 0.4 V) and OH_{ad} (0.5 V) formation[21, 22]. Overlap of H and OH adsorption states for all platinum single crystal surfaces (with the notable exception of Pt(111)) in aqueous perchloric acid is widely acknowledged[23]. In

order to understand trends in electrosorption behaviour, we shall adopt this interpretation of the various 'hydrogen underpotential peaks (H UPD)' here. However, in chapter four, it was previously demonstrated that this simple interpretation of the electrosorption at platinum may require some revision.

The gradual introduction of linear (110) steps into the Pt(100) terrace, gives rise to a steady change in the classical Pt(100)-(1x1) voltammetric profile[23]. The new electrosorption states appearing at 0.23 V and below 0.2 V which increase in intensity as step density increases may be ascribed to the presence of steps formed at the junction of the (110) step and (100) terrace sites. Previous work by [24-26] has indicated that this step site is actually highly unstable and susceptible to reconstruction. Here, once again we shall assume that the step site remains stable given its reversibility to potential cycling in the 0 to 0.85 V range. However, it may be that immediately after flame-annealing and cooling in hydrogen, some reconstruction at the step may already have occurred.

The step feature itself at 0.23 V is found to shift to slightly more negative potentials (20 mV) with highly stepped surfaces Pt(210) and Pt(310). This effect has previously been reported for Pt(100)x(111) surfaces[27, 28] and we ascribe the phenomenon to step-step interactions (the negative shift in potential is most marked at highest step densities). Contributions to the voltammogram below 0.2 V also increase with step density, but these features are rather broad and featureless. We have seen already in Chapter three that a similar phenomenon of two electrosorption peaks corresponding to a single type of adsorption site may be interpreted (based on measurements of potential of zero charge, pH and differing cation and anion types) as cations adsorbing at the more negative potentials (in this case protons) and anions (in this case 'OH') at the more positive potential. If this is the case here, one should expect both the growth in the 0.23 V electrosorption peak and the states below 0.2 V to correspond to electrosorption of (mostly) anions and (mostly) cations at the step sites respectively. The corresponding attenuation in all Pt(100)-(1x1) terrace features at potentials positive of 0.3 V is also a notable feature of the influence of steps and the systematic decay in terrace peak intensity suggests strongly that the (1x1) surface is formed after flame-annealing and hydrogen cooling. This would be consistent with previous work by Attard *et al.* who used low energy electron diffraction (LEED) to confirm that stepped Pt(100) electrodes containing (111)x(100) linear steps all gave rise to (1x1) terminations after such treatment[29].
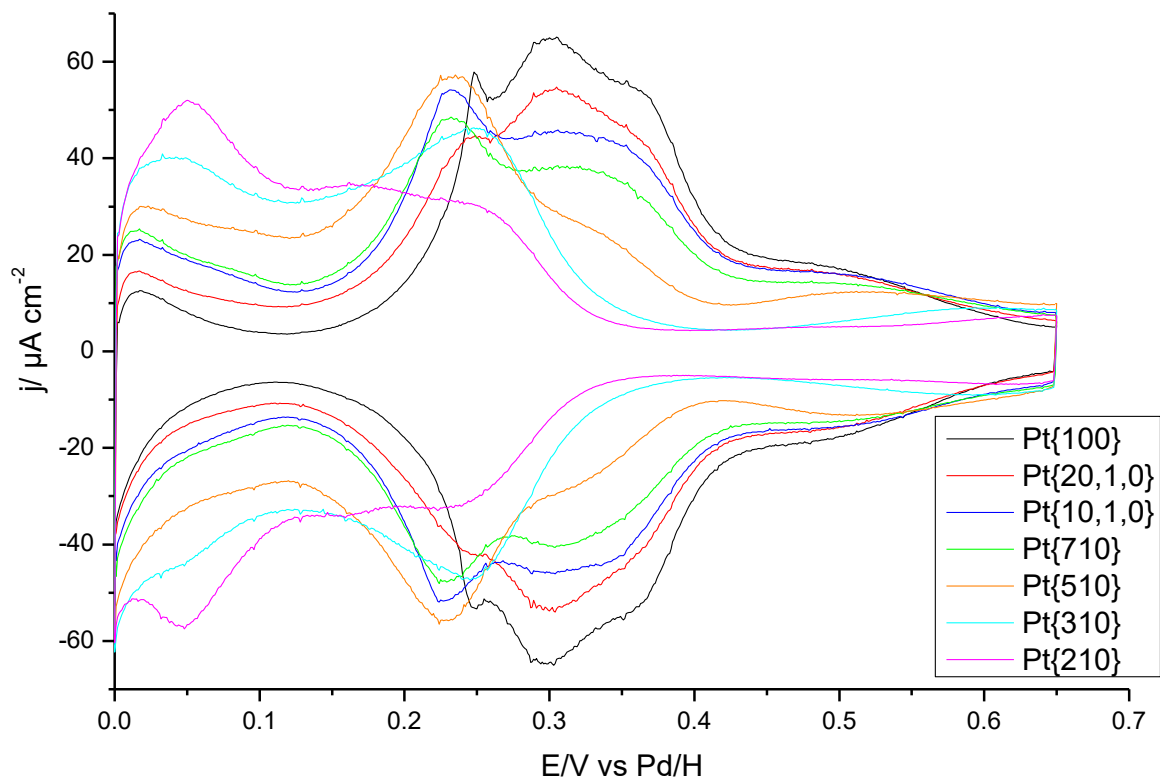
Figure 98: Cyclic Voltammograms of Pt(S)[n(100)x(110)] in 0.1 M HClO₄

Figure 99 shows the potential range corresponding to electrochemical oxide formation. Only the positive-going scans are shown. This is because the subsequent reverse scan indicates marked reconstruction of the electrode surface upon stripping of the oxide adlayer. This phenomenon is well known [30] and corresponds to place-exchange of Pt with oxygen and OH species [24]. Pt(100) exhibits an intense peak in the oxide region at around 0.98 V. This is ascribed to electrosorbed oxide on (100) terraces[27] and is typical of defect free platinum group electrodes including gold[31] and palladium[32]. As seen in earlier chapters, it is also true of Pt(111) and CO-cooled Pt(110). Between the potentials 0.65 – 0.98 V the current density is minimal and starts gradually increasing as the potential is swept positive. Upon close inspection there is a small but sharp feature at ~0.92 V. This is characteristic of a well-defined Pt(100) surface with minimal or no defects combined with a perfect flame anneal[23, 33]. It is often used to identify a high quality Pt(100) single crystal much like the (absence) of the feature at 0.25 V. At potentials positive of the intense oxide electrosorption peak, the current density does not return to a low value. Rather, it steadily increases until the oxygen evolution potential is reached at ~1.6 V (not shown). Although no obvious adsorption features can be elucidated between Pt(100) oxide states and oxygen evolution, current density observed in this region has been ascribed to stronger oxide bonding and sub-surface oxide formation[34]. The potential limit can alter the coverage of oxides and therefore the amount of roughening that occurs.

151

This phenomenon has also been documented previously[35]. A good flame anneal will usually return the original CV features of a well-defined single crystal surface. However, continual excursions to potentials that roughen the surface can irreversibly damage the quality of the single crystals, especially going up to potentials as high as oxygen evolution. Hence, this should generally be avoided.
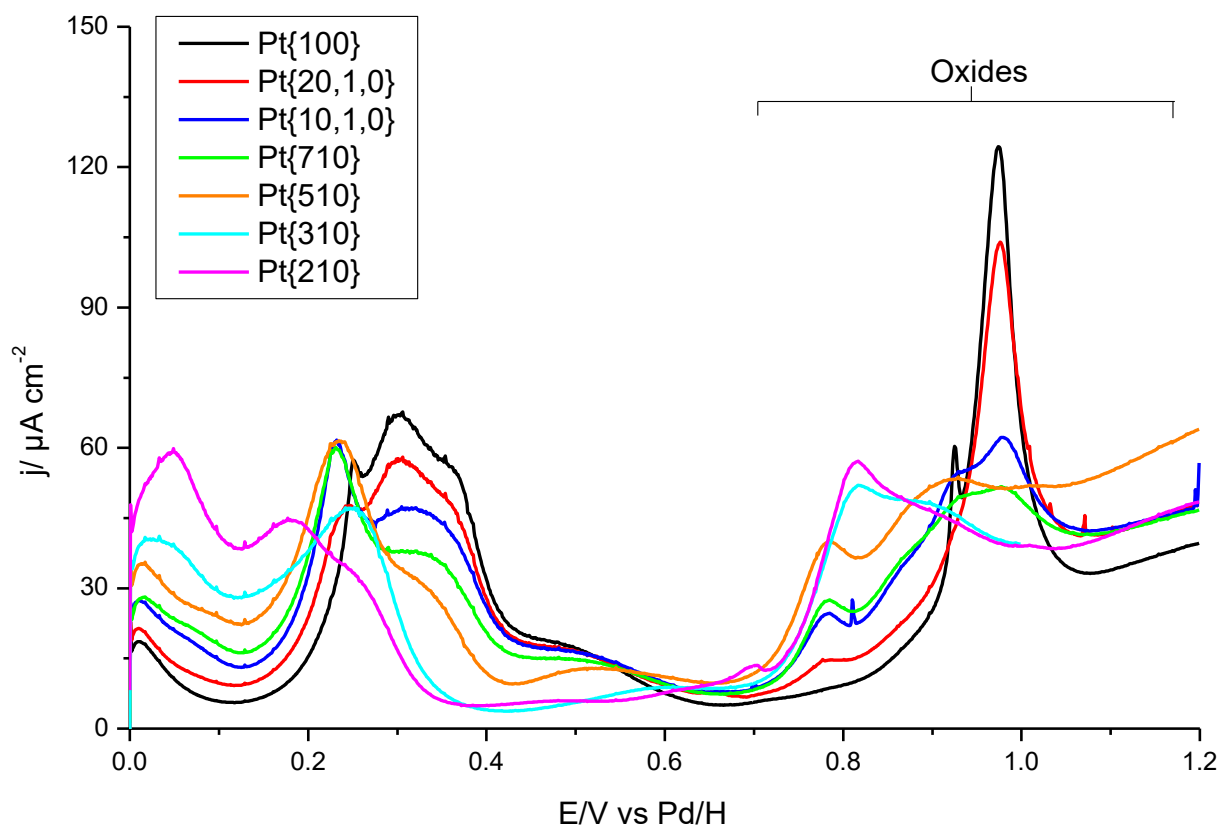

Figure 99: CVs of Pt(S)[n(100)x(110)] surfaces up to 1.2 V, in 0.1 M HClO₄

For all stepped surfaces the oxide adsorption regions are very broad compared to the Pt(100) and CO-cooled Pt n(110)x(111) electrodes (see chapter four), with large contributions of current density in the potential range 0.8- 0.9 V. With the addition of (110) steps, the terrace feature at 0.98 V diminishes in intensity and therefore, one may confirm that this feature should be attributed to oxide formation on Pt(100) terraces. Sharp peaks are representative of long range order. It is clear that addition of (110) steps breaks up the (100) long range order here as closer inspection of the voltammogram profiles in the oxide region reveals small overlapping adsorption features between 0.85-0.92 V which are ascribed to the presence of (110) steps. All stepped surfaces show a main adsorption state at ~0.8 V. The contribution of this feature in the CV profile increases with increasing step density. The Pt(210) electrode exhibits the most intense oxide step peak, a surface which also

corresponds to the largest (110) step contribution of all stepped surfaces studied. However, in comparison with CO-cooled Pt n(110)x(111) stepped surfaces, all of the step oxide features are rather broad (similar to what was found using Pt n(110)x(100) stepped surfaces (chapter four). In chapter four, surface reconstruction at both the step and terrace sites was deduced, even for CO-cooled substrates. In this case, the reconstruction of the (100) terrace sites appears less likely. Hence, a selective reconstruction of the linear (110) steps is proposed to account for the rather broad electrosorption oxide step feature which seems to consist of a multiplicity of overlapping states. This suggestion would be in accord with the low stability of (100)x(110) sites reported both for Pt(110) stepped electrodes cooled in hydrogen and previous studies [24, 26].

5.2.2 Cyclic Voltammetry - Sulphuric Acid Electrolyte

Figure 100 and Figure 101 show the CV profiles of Pt(S)[n(100)x(110)] surfaces in 0.1 M H_2SO_4 electrolyte. These are in good agreement with those already published[20] and they resemble CVs seen for other stepped surfaces containing (100) terraces[15, 16, 20]. This electrolyte contains strongly specifically adsorbing sulphate anions which inhibit OH_{ad} formation[36]. As a consequence, both H_{upd} and oxide formation are perturbed since (bi-)sulphate competes successfully with OH for adsorption sites. Such modifications are readily assimilated via inspection of Figure 100 and Figure 101.

The observation of the characteristic voltammogram of Pt(100)-(1x1) (Figure 100) shows the electrolyte to be clean and free from contamination, with peaks centred at 0.22, 0.33 and 0.6 V. The adsorption state at 0.22 V is attributed to H_{upd} (anions) at defects and overlaps with the state at 0.33 V, which is large and sharp, corresponding to adsorption of the (bi)sulphate anion on large, well-defined (100) terraces together with desorption of hydrogen[21]. The specific adsorption of sulphate leads to a shift in peak potential compared to observations in perchloric acid media since a more negative potential is required to cause displacement of sulphate anions by the H_{upd} layer due to sulphate being strongly specifically adsorbed compared to OH. The small feature at 0.6 V corresponds to OH adsorption on (100) terraces. It is small relative to analogous states exhibited in aqueous perchloric acid due to the strongly adsorbing bisulphate anion blocking most of the available OH adsorption sites[21].

Stepped surfaces presented (Figure 100) are seen to deviate from the Pt(100) voltammogram, where addition of (110) steps leads to the diminution of adsorption states 0.25-0.33 V (as seen for the corresponding peaks in perchloric acid). The OH_{ad} formed at terraces has been inhibited still further by adsorption of the (bi)sulphate together with a decrease in the available Pt(100)-(1x1) terrace sites and therefore only a small electrosorption charge is observed corresponding to the small bump at 0.6 V, marked more clearly in Figure 101. A similar phenomenon is seen for stepped Pt(111) surfaces whereby the so-called "butterfly peak" associated with OH adsorption at Pt(111) terraces diminishes in intensity as a function of increasing step density [11, 13, 37].

A new feature appears with increasing step density at 0.22 V. This behaviour pattern has been previously observed for Pt(S)[n(100)x(111)] surfaces[27]. Simultaneously, current density at potentials negative of 0.25 V also increases with increasing surface density of (110) linear steps and hence both can be linked to the presence of steps on the surface.
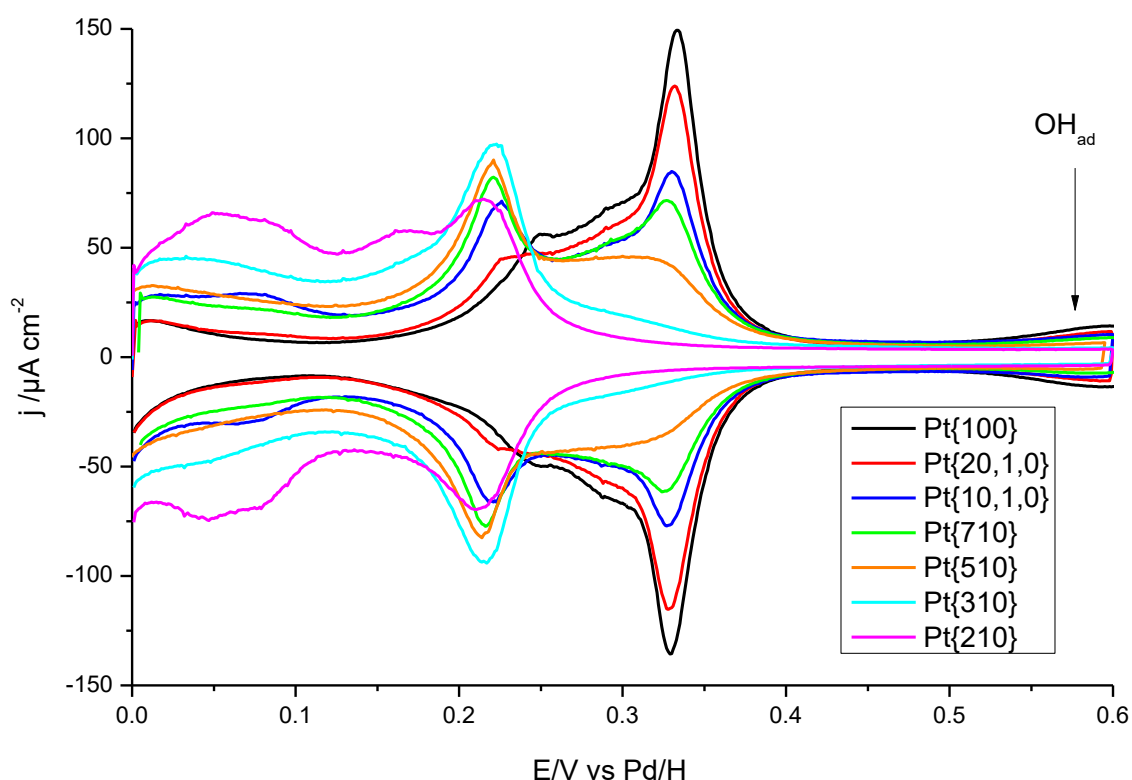

Figure 100: CVs of Pt(S)[n(100)x(110)] in 0.1 M H₂SO₄

Figure 101 shows voltammograms for the Pt(100)x(110) surfaces in 0.1 M H₂SO₄ up to 1.2 V, showing the onset of electrochemical oxide adsorption. Pt(100) shows one main feature at high potentials, a

relatively sharp peak at 0.98 V. This is the same potential as seen in 0.1 M HClO₄ and is attributed to oxide adsorption on (100) terraces[21, 27]. As step density increases, there is a diminution of the peak at 0.98 V and growth of a new adsorption state near 0.8-0.84 V, corresponding to oxide adsorption states on (110) steps. Hence, it is apparent that in this case, the presence of specifically adsorbed anions does not inhibit oxide formation. This is unusual since on polycrystalline electrodes (see also chapter three) and single crystal surfaces such as Pt(111), sulphate anion specific adsorption usually results in a shift to more positive potentials in all oxide peaks. It is speculated here therefore that, in the case of Pt(100) vicinal surfaces, in terms of competition for sites, OH/O species can successfully compete even with sulphate anions. Close inspection of Figure 101 also reveals that at low step density (e.g. Pt(20,1,0)), the step site actually causes the formation of a small, well-defined peak at 0.8 V which broadens at high step density and shifts towards more positive potentials. In chapter four, a similar behaviour for Pt(110) electrodes containing linear (100) step sites was also observed. In that case, step-step interactions and possible step reconstruction were invoked and hence, it is also proposed here to explain step oxide peak broadening for Pt(210). If correct, when (110) linear steps are widely spaced, a well-defined electrosorption peak is generated at 0.8 V (0.84 v on RHE scale) identical in fact to the site at stepped Pt(110) (see chapter four). Of course Pt(210) is the turning point of the zone on moving from Pt(100) to Pt(110) terraces along the stereographic triangle so together with an intrinsic instability and close proximity, some reconstruction is to be expected leading to the broader range of potential for oxide formation relative to well-separated steps.
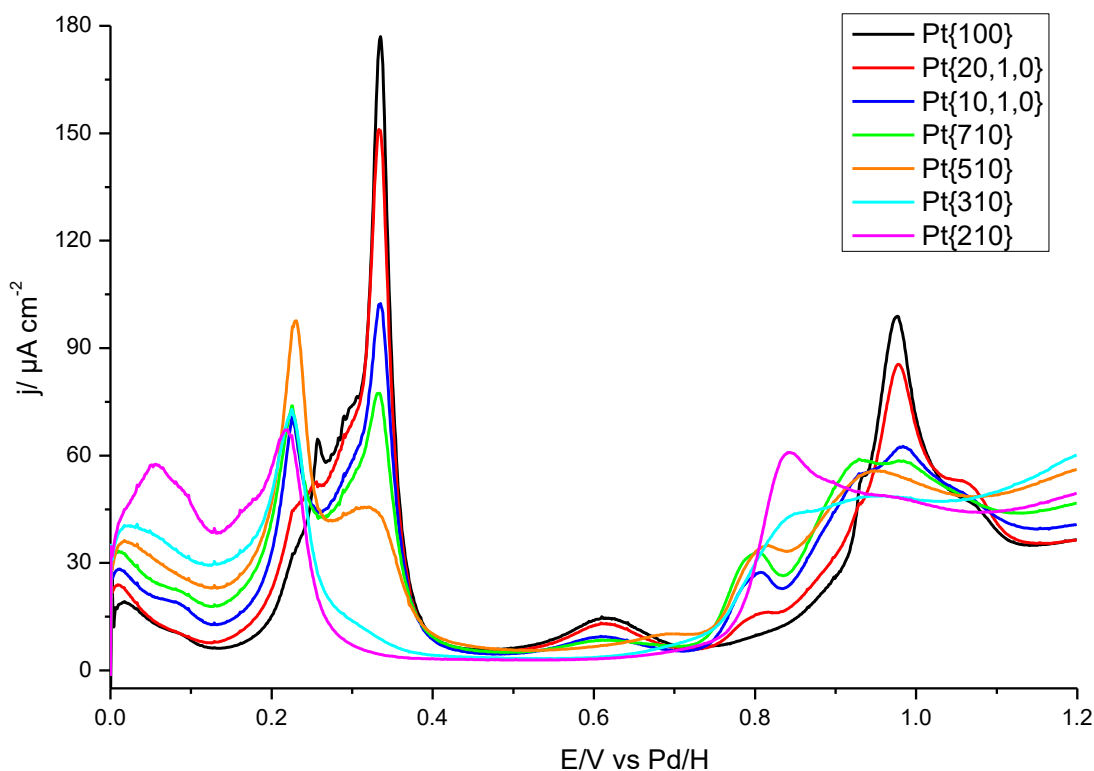
Figure 101: CVs of Pt(S)[n(100)x(110)] up to 1.2 V, in 0.1 M H2SO4

5.2.3 Nafion

The adsorption of Nafion on single crystal platinum electrodes has previously been used as a probe of OH_{ad}, as it has been suggested that the Nafion spike, often seen for thin layers of Nafion on single crystal platinum electrodes, demarcates the region of H_{upd} from OH_{ad} stability[38]. The figures below show for the first time, attempts at adsorbing well-defined Nafion on (110) - stepped Pt(100) single crystal surfaces in 0.1 M $HClO_4$.

Unfortunately, the adsorption of the Nafion films showed evidence of some contamination occurring during film preparation. This is apparent from the blocking of charge in the H_{upd} region, as well as the large contributions of charge density at high potentials seen in most of the figures. This is attributed to the organic solvents that the as-received Nafion is stored in, which can be difficult to fully remove. The "excess" current densities observed at potentials > 0.9 V would then correspond to oxidation of carbonaceous material. Great skill (and luck!) is needed to obtain a truly clean Nafion covered electrode. Better-quality Nafion films on platinum basal planes have been achieved in other chapters of this thesis and are reported elsewhere[38, 39]. When true cleanliness is achieved, the H_{upd} region usually remains relatively unperturbed in terms of overall H_{upd} charge although of course, OH

adsorption states are modified[38]. Despite this contamination, some trends are still apparent and in particular, extrapolations concerning Nafion sulphonate groups may be deduced.
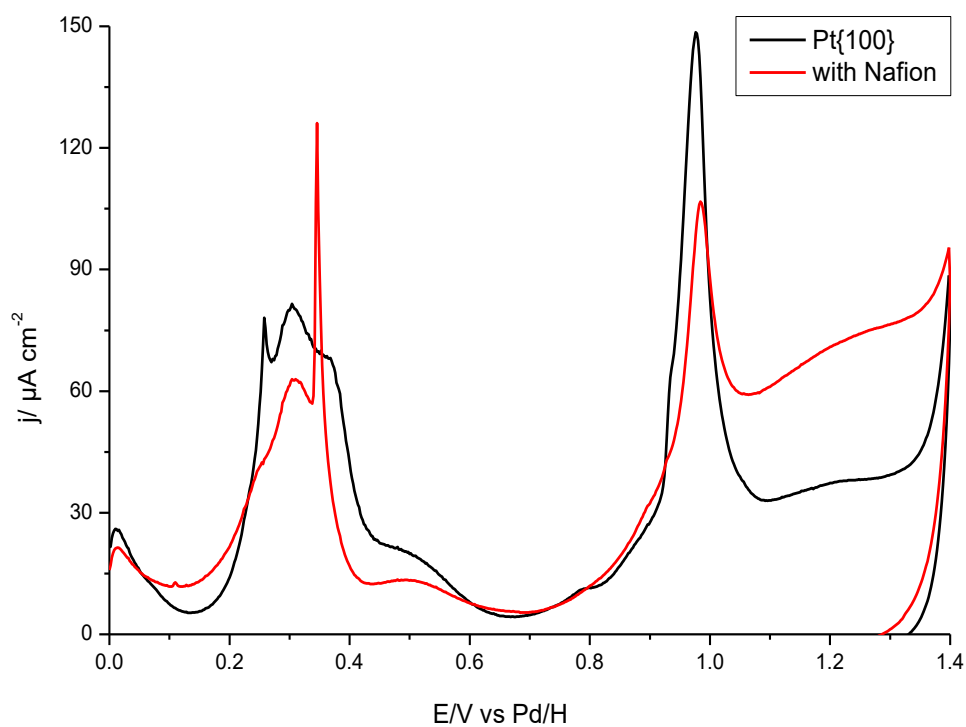

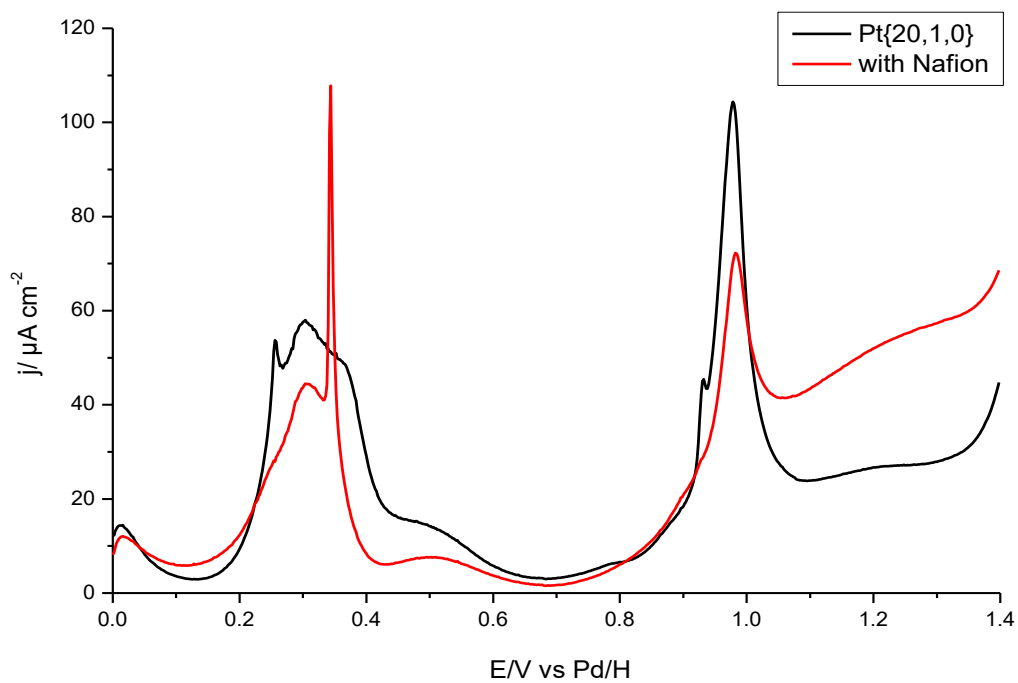*Figure 102: CVs of Nafion on a Pt(100) single crystal in 0.1 M HClO$_4$*

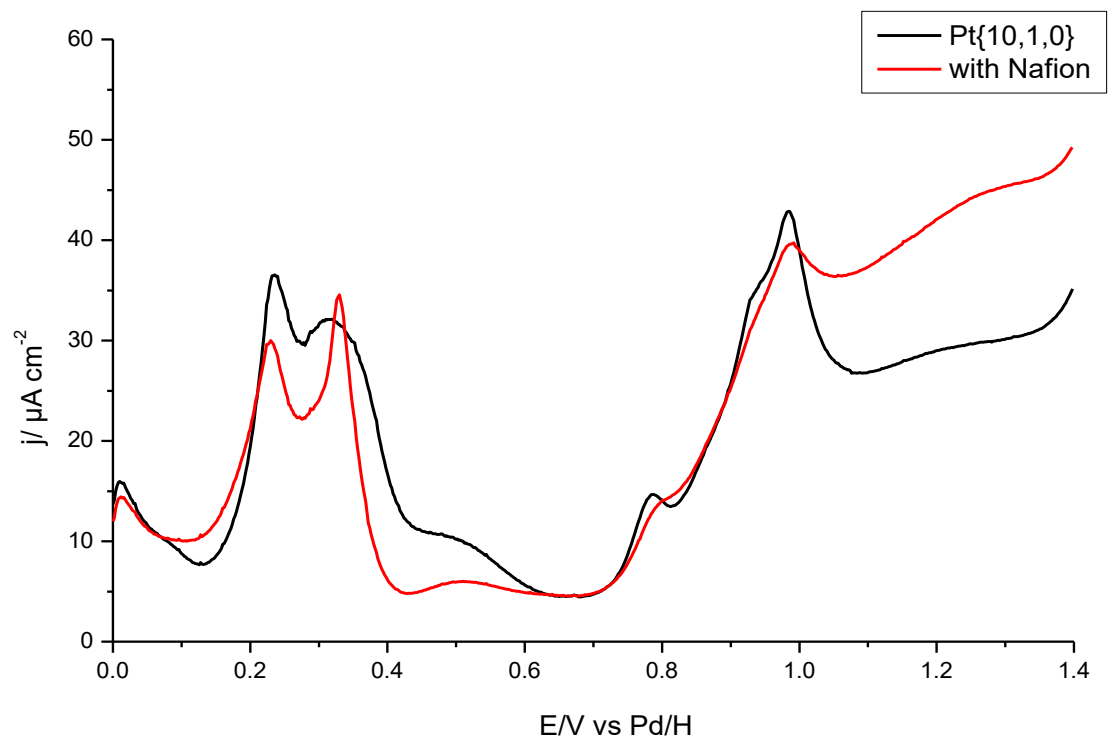*Figure 103: CVs of Nafion on a Pt(20,1,0) single crystal in 0.1 M HClO$_4$*

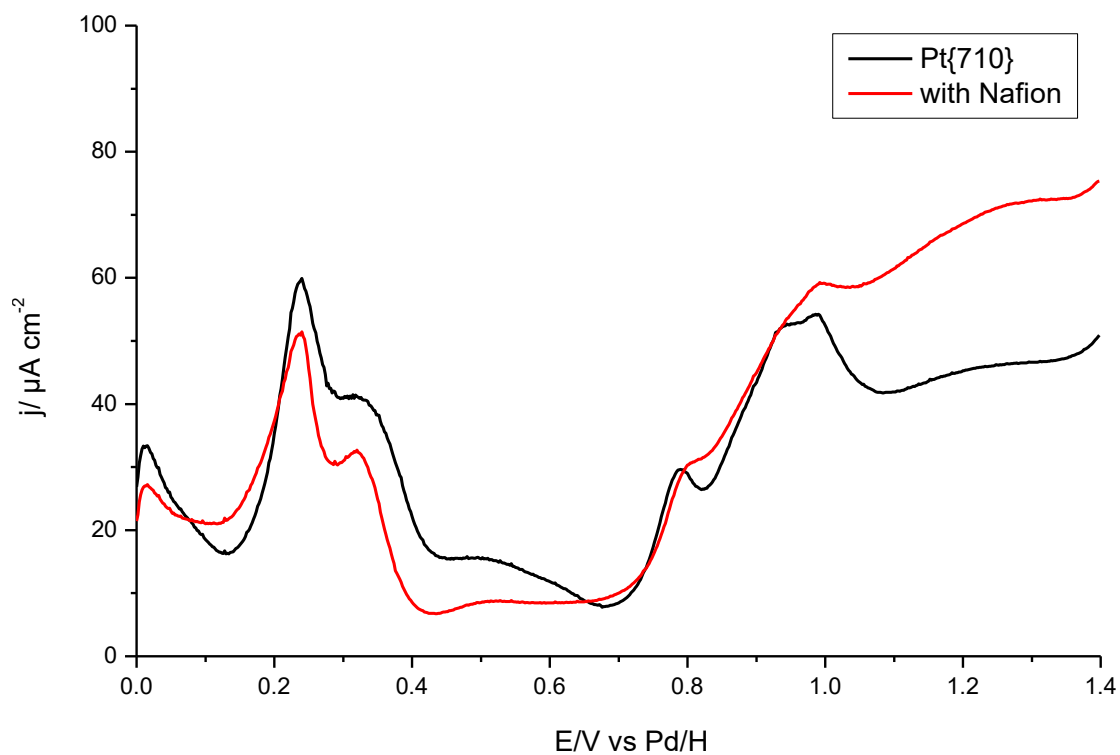*Figure 104: CVs of Nafion on a Pt(10,1,0) single crystal in 0.1 M HClO₄*

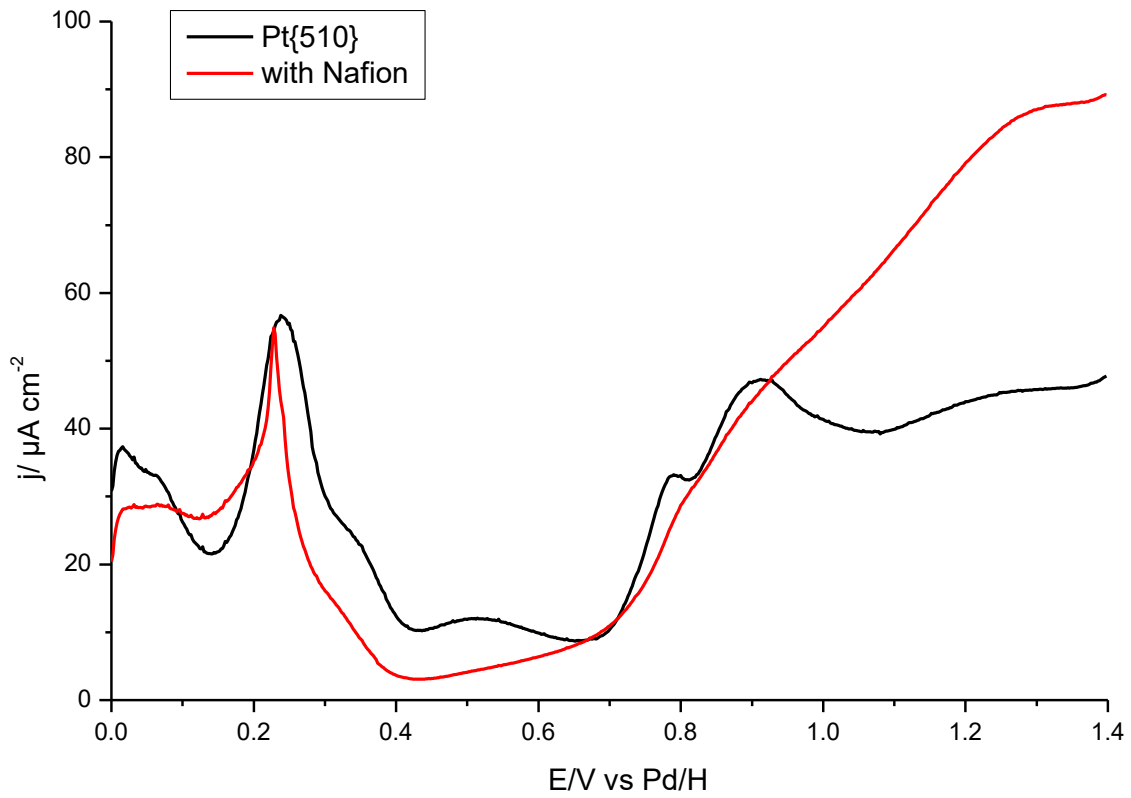*Figure 105: CVs of Nafion on Pt(710) in 0.1 M HClO₄*

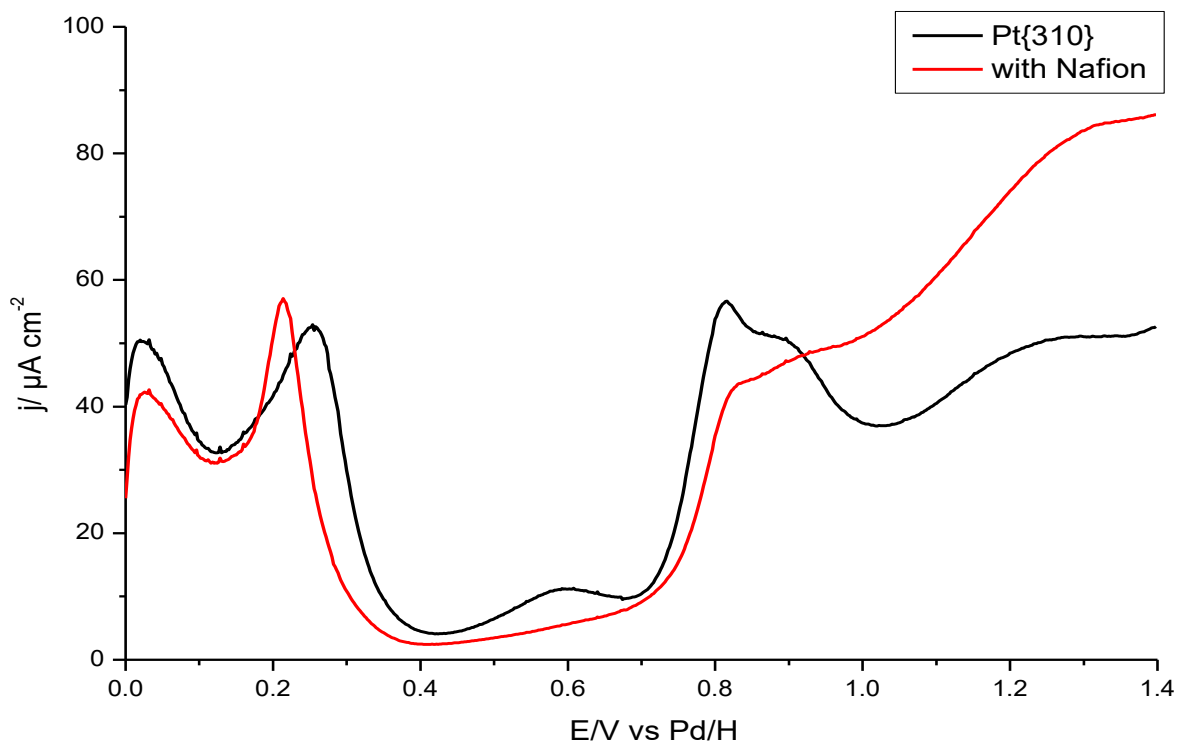*Figure 106: CVs of Nafion on a Pt(510) single crystal in 0.1 M HClO₄*

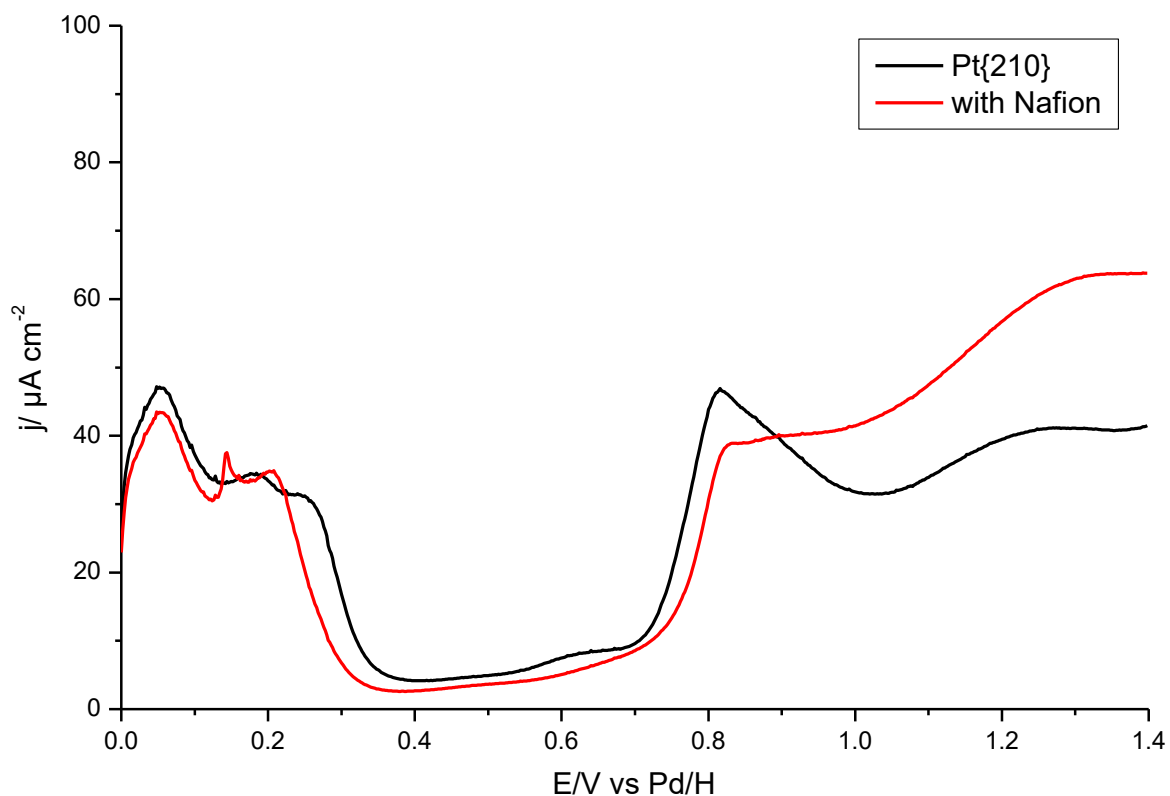*Figure 107: CVs of Nafion on a Pt(310) single crystal in 0.1 M HClO₄*

Figure 108: CV of Nafion on a Pt(210)single crystal in 0.1 M HClO$_4$

General inspection of the CVs in figures reveal several significant changes when compared to Nafion-free surfaces. For Nafion covered Pt(100), a sharp spike is generated in the H$_{upd}$ region. The magnitude of the spike depends on the amount and quality of the Nafion loading[38, 39]. The potential of this sharp peak is close to the PZTC of Pt(100)[40]. This behaviour is indicative of sulphonate adsorption displacing OH species[33]. In particular, it is noted that H$_{upd}$ states negative of the Nafion spike remain unperturbed. Addition of Nafion suppresses charge around 0.3 V onward, which can be labelled as the OH$_{ad}$ region. Some of this charge is displaced into the Nafion spike. Displacement of OH$_{ad}$ by more strongly adsorbing anions is normal behaviour observed with "specifically adsorbing anions", such as sulphate. The terminating groups on the Nafion (sulphonate) display such behaviour here, blocking the OH$_{ad}$ on the surfaces. The hysteresis in the potential of the Nafion spike is much less than observed with Pt(111)[39]. The magnitude and sharpness of the spike together with hysteresis in the forward and reverse potential sweeps corresponds to finite-size effects in the phase transitions occurring in the uniform distribution of variously sized Nafion surface domains[38, 39].

In general, it is seen that the magnitude of the Nafion peak corresponding to Pt(100) terraces diminishes with step density just as was observed for Pt(111)x(111) electrodes in sulphuric and perchloric acid electrolytes [38]. Hence, a decrease in the average terrace width limits the size of the sulphonate domain size leading to attenuation in the spike. This interpretation is in accordance with predictions made in [38] whereby the magnitude of the Nafion spike was strongly correlated with domain size. However, the quenching of the Nafion spike is rather marked with the disappearance of this state for average step separations corresponding to n < 10. For stepped Pt(111) surfaces, the absence of the Nafion spike was observed at around n < 5 [38]. Two reasons for this difference in quenching of the Nafion spike are proposed:

i) it may be that relative to the earlier work [38], the degree of contamination in the Nafion layer in the present study is simply greater leading to attenuation by random distributions of site-blocking agents or,

ii) The extent of OH formation on Pt(100) and Pt(111) sites is different (since the spike has been shown to be a probe of local OH formation [38]). Some evidence for this hypothesis may be gleaned when the magnitudes of the charge in the OH butterfly peak on Pt(111) and the OH peak for Pt(100) are compared. The OH charge for Pt(111) is found to be almost double that of Pt(100)[38, 39] and so it may be that the Pt(100) Nafion voltammetric signature is starting from a lower base than Pt(111) so may 'disappear' at an earlier stage.

Whatever the reason, for both stepped Pt(111) and stepped Pt(100) electrodes, the Nafion terrace peak spike is completely attenuated for sufficiently narrow terraces confirming the highly structure sensitive nature of its adsorption. It is interesting to note that for (111)x(100) linear steps, a sharp Nafion peak is also observed [38]. This means that the Nafion spike is not solely caused by terraces. It is suggested therefore that in the present case of (110)x(100) steps, local disorder due to step reconstruction disfavours an ordered array of sulphonate/Nafion forming thus precluding the observation of a Nafion spike at these local sites.

For the surfaces not showing a clear Nafion spike, other changes in the CV are evident, which are associated with the specific adsorption of sulphonate inhibiting H_{upd} formation and causing for

example H_{upd} states to shift to more negative potentials and become narrower. This is particularly evident for Pt(310) and Pt(210) whereby both step and terrace sites shift to more negative potentials when Nafion is present. The narrowing of H_{upd} peaks has previously been ascribed to attractive lateral interactions within the electrical double layer[41]. Interestingly, a new Nafion "spike" appears for Pt(210) which coincides with the potential of Pt(110) sites [39] and was first observed by Markovic and co-workers using a "polycrystalline" electrode[39]. This indicates that some Pt(110) terraces may be present at the Pt(210) surface as a result of reconstruction of step sites (see earlier).

The presence of Nafion on the platinum surfaces also blocks oxide features and shifts them slightly positive for surfaces containing larger (100) terraces. However, this shift is insignificant compared to what has been documented previously for Nafion on Pt(111)[38, 39]. Considering that an even more strongly specifically adsorbing anion such as sulphate cannot cause a shift to more positive potentials (see earlier), this is not entirely unexpected for the even more weakly specifically adsorbing sulphonate although contamination obscures somewhat the details of the voltammetry in the oxide region. Contamination also makes it difficult to calculate the surface coverage of the Nafion from electrosorption charge measurements of the Nafion spike although in previous work using identical dosing procedures, a nominal film thickness of 3 nm was evaluated when the Nafion spike reached a maximum[38]. It is probable that a similar situation arises here.

5.2.4 ORR and HPORR

Figure 109 shows the RDE voltammetric profiles for oxygen reduction at 1600rpm on stepped Pt(100) platinum crystal surfaces in 0.1 M $HClO_4$. The electrolyte was saturated with oxygen before and during use. The voltammetry was recorded between 0 and 1 V. The curve for the Pt(100) surface shows characteristic behaviour with a well-defined limiting current density value as reported previously[42].

Inspection of the voltammograms reveals that the onset for oxygen reduction is ~0.9 V and for all surfaces a limiting current, j_{lim}, is obtained between 0.2-0.4 V. This signifies a rather large overpotential (deactivation) of the ORR, considering that the equilibrium potential for the ORR occurs at 1.23 V. The voltammograms show two sequential current drops in the potential range below ~0.23 V. The first drop in catalytic activity for the oxygen reduction starts at 0.23 V. This

plateaus at ~0.1-0.15 V before another current decrease until ~0.04 V. This reduction of current at lower potentials has been attributed to adsorbed hydrogen on the surfaces. In this potential region, oxygen (or any other relevant intermediates) need to compete with adsorbed hydrogen for adsorption sites. Previous examination of stationary voltammograms show that in this potential region, H_{upd} has already formed on these surfaces. Therefore, a minimal coverage of hydrogen may first be necessary to block the oxygen adsorption. In this low potential range, hydrogen peroxide formation has previously been detected on other surfaces[43], demonstrating that only two electrons are exchanged. In fact, the results reported here are completely in accordance with models of ORR in which site blocking by anions/hydrogen/contamination lead to a switch from a 4e (water formation) to a 2e transfer (hydrogen peroxide formation) process. A geometrical site blocking effect has been proposed to explain this phenomenon (two contiguous, adjacent metal sites required for the 4e process, 2e transfer when this condition is not met [44]).
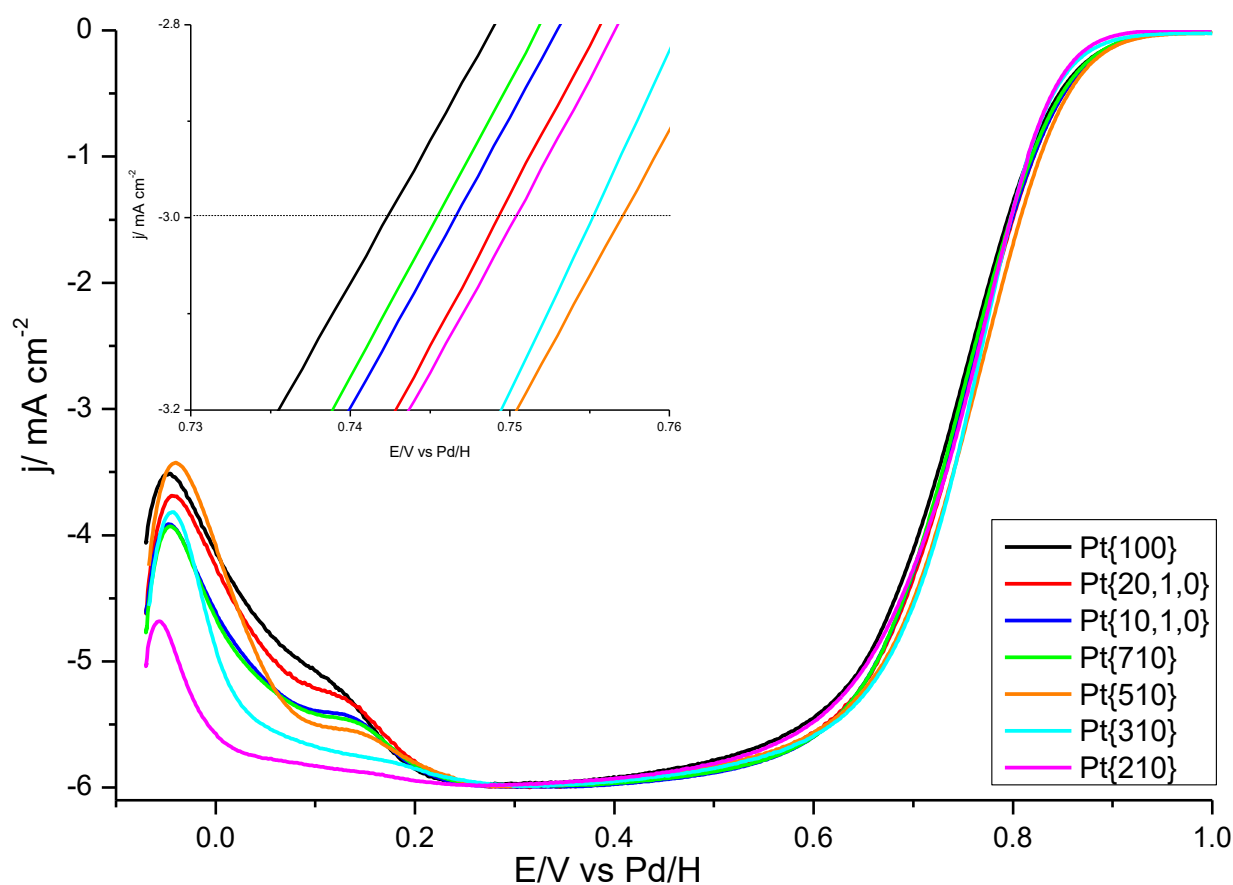

Figure 109: RDE CVs for Pt(S)[n(100)x(110)] up to 1V, at 1600 rpm, in 0.1 M HClO$_4$

The 2e oxygen reduction in the potential range 0.2 to 0 V decreases significantly as a function of increasing step density (ORR current increases). This means that hydrogen peroxide formation is

favoured at hydrogen-covered Pt{100} terrace sites. As a corollary, the hydrogen covered step sites appear not to interfere so much with the usual 4e ORR process.

Kinetic analysis of the oxygen reduction curves has been undertaken in a variety of ways. First, the $E_{1/2}$ (potential at half of the limiting current density, j_{lim}) of all surfaces has been plotted below. For constant surface area, this is a good proxy for ORR activity (the more positive is $E_{1/2}$, the greater the activity of an electrode towards ORR). A "volcano" trend is observed for $E_{1/2}$ values where increase of step density in the (100) terrace initially leads to an increase in activity until a maximum is reached (Pt(510)). After this point, further addition of step sites leads to a decrease in activity. The Pt(100) electrode is documented to exhibit the lowest activity for ORR in aqueous perchloric acid[45]. All of the stepped surfaces display a higher activity than Pt(100). Previous work by Feliu *et. al.*[46], found the best surfaces for ORR possessed an average terrace width of 3 atoms; a little less than found for the surfaces in this study.
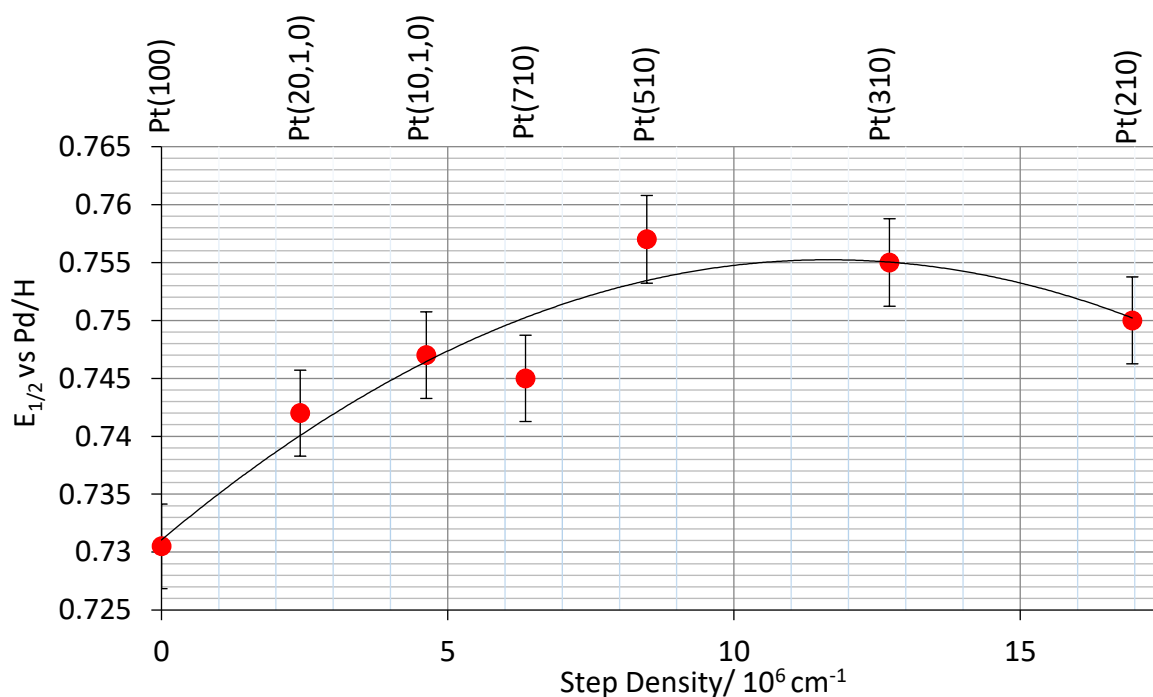

Figure 110: $E_{1/2}$ values for Pt(S)[n(100)x(110)] surfaces

Figure 112 shows the ORR at different rotation rates together with Levich and Tafel plots for Pt(100). Levich analysis, used to determine the total number of electrons involved in the reduction, found that this value was 4 for all surfaces studied. This corresponds to a complete reduction of oxygen to

water in this potential range and is consistent with the known behaviour of platinum towards the ORR[47].
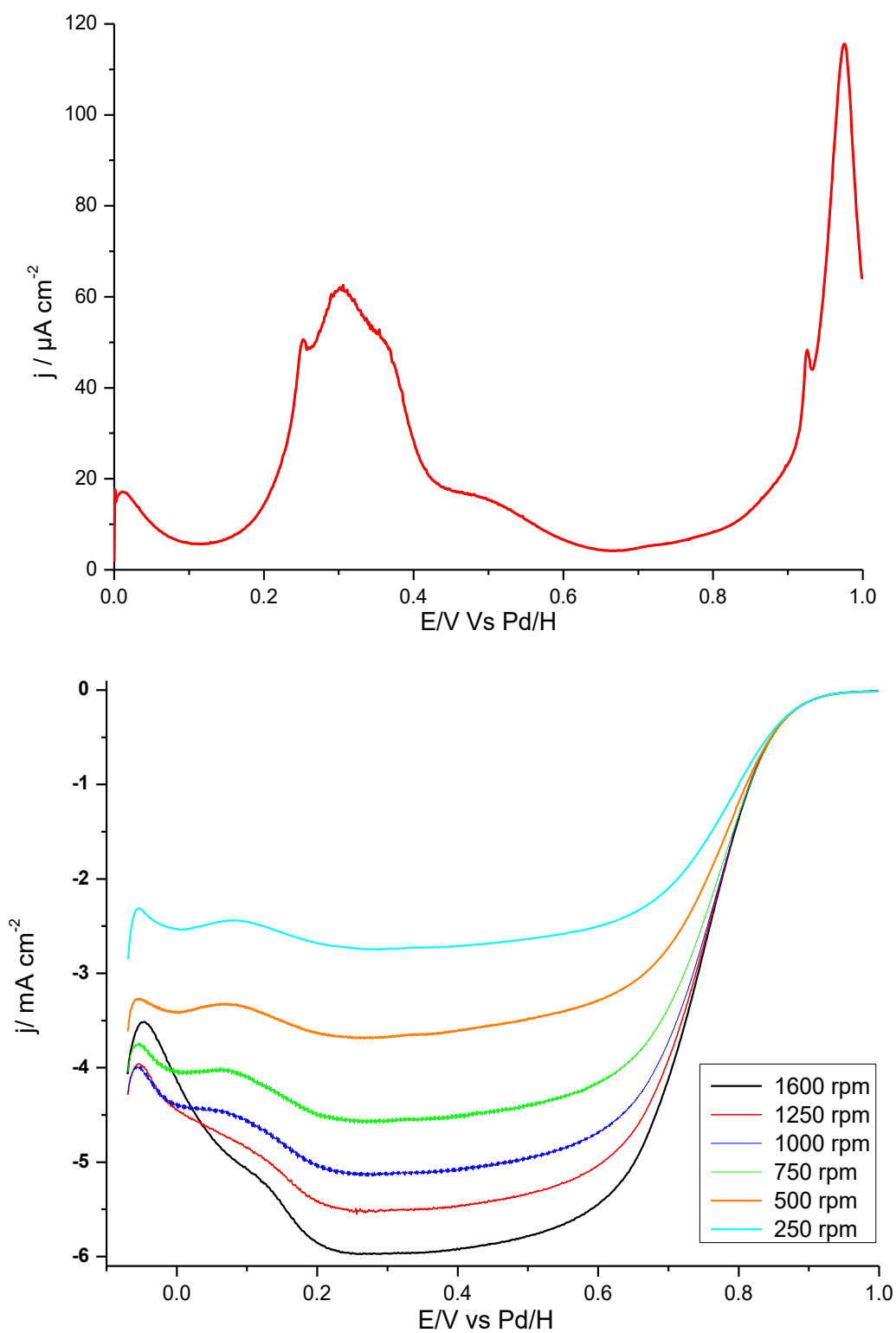

Figure 111: (a) stationary CV of Pt(100), under N_2 and (b Pt(100)) in the RDE at different rotation rates, under O_2. Both in 0.1 M $HClO_4$ electrolyte.
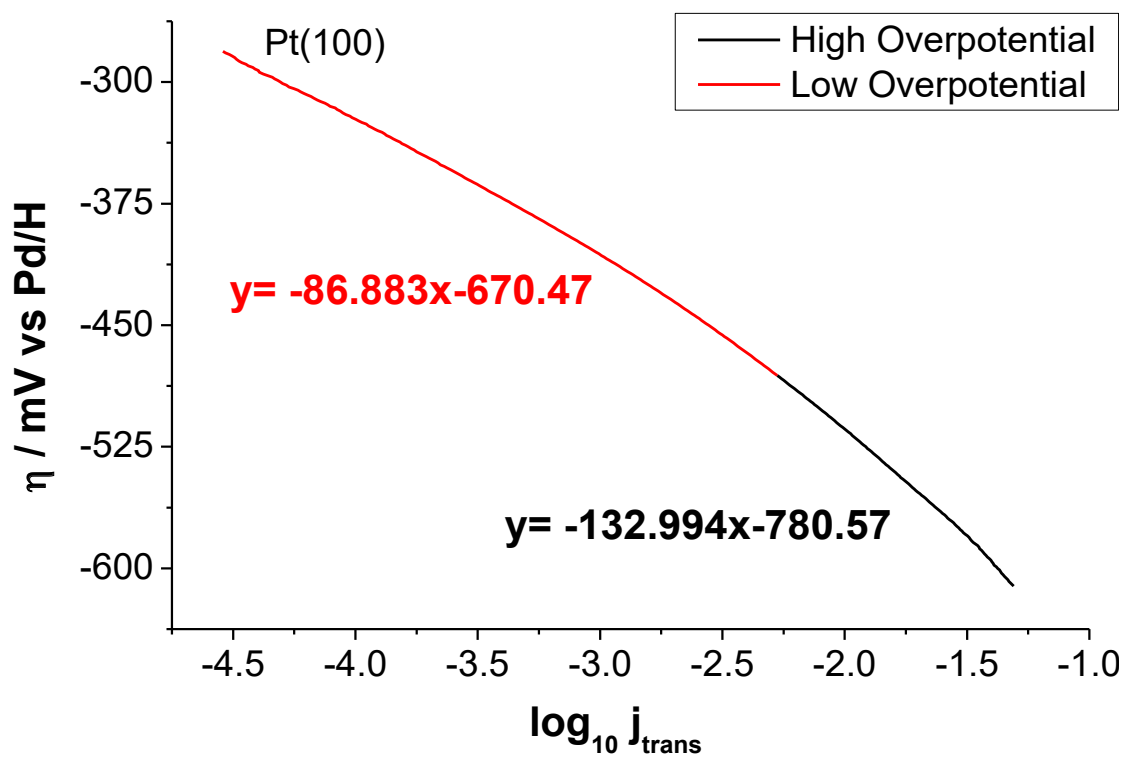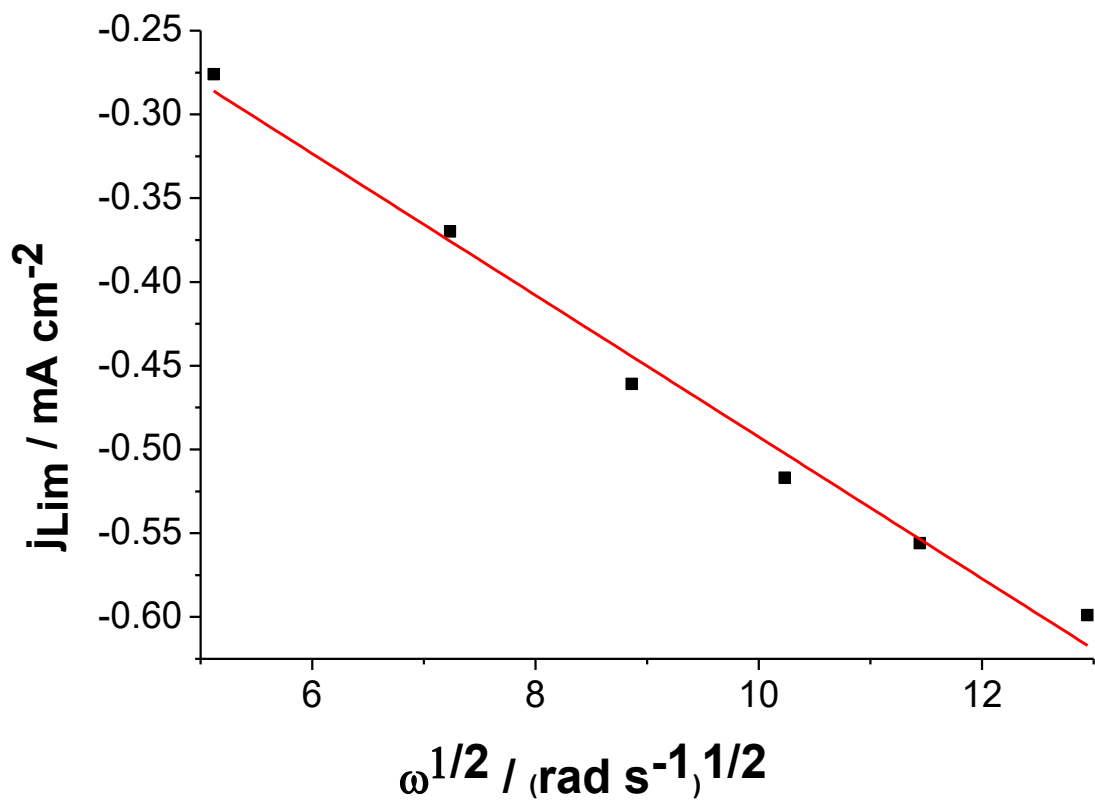
Figure 112: ORR Analysis of Pt(100) from RDE experiments where (a) shows a Levich plot and (b) shows the corresponding Tafel plot.

Tafel plots are presented for all surfaces in Figure 113, where more information regarding the possible mechanism was elucidated. Although straight line sections (Tafel slopes) are difficult to isolate due to their close proximity to one another (and therefore estimates of gradients are subject to errors), the figure shows how the vicinal surfaces exhibit similar kinetic behaviour. The number of electrons up to and including the rate determining step, are calculated from a plot of overpotential vs $\log_{10}$ (j_{trans}), where J_{trans} is the current density in absence of mass transport.
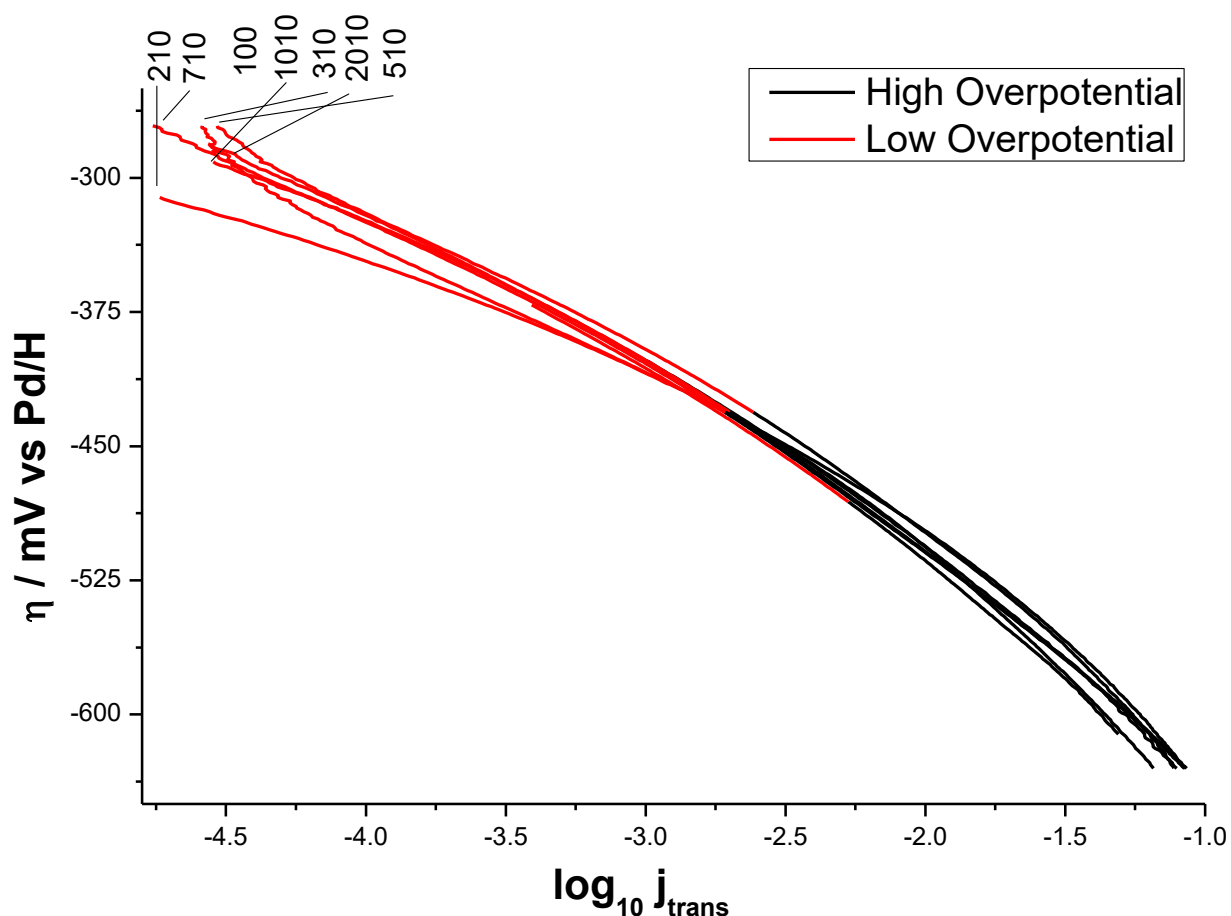

Figure 113: Tafel slopes for Pt(S)[n(100)x(110)] surfaces showing similar gradients

The exchange current density reflects the magnitude of the electrochemical rate constant and can be calculated by extrapolation of the Tafel slope (value of j_{trans} at η=0). Again, because of the subjective choice in deciding the tangent to the curve, the values of intercept are subject to error. However, the values obtained here were of a similar magnitude to other stepped surfaces found previously[45]. For ORR, Tafel plots showed a change in gradient, which is an indication of a mechanism change[48]. Therefore, Tafel plots were obtained for "low" (corresponding to an oxide covered surface) and "high" overpotential ranges (corresponding to a reduced metal surface). The theoretical slope of the former should equal 60 mV/dec for a 2 electron reduction in the "low" overpotential range and 120 mV/dec for a 1 electron transfer in the "high" overpotential range in

the latter[42]. The Tafel slopes have been estimated for all surfaces and are shown in Figure 114 and Figure 115. At "low" overpotentials, the number of electrons up to, and including the rds were evaluated to be between 1.4-1.8. This is a slight deviation from the expected value of 2 and it is speculated that surfaces containing varying amounts of O_{ad} and OH_{ads} with differing abilities in influencing oxygen activity in this potential region may lie at the heart of this effect. For example, for Pt(111) in which a strongly adsorbed OH_{ad} adlayer is fully formed at low ORR overpotentials, it is reported that a Tafel slope of 54 mV dec^{-1} is observed[49]. This is also true of Pt(311) in which all sites bear a strong oxide phase adsorbed at all sites (turning point of zone so consisting entirely of linear steps). Hence, surfaces covered in lower amounts of OH_{ad} or oxide would be predicted to exhibit a somewhat higher Tafel slope. Pt(100) is an example of such a surface since the amount of terrace OH_{ads} is half that of Pt(111) (see earlier) and oxide at terrace sites forms fully at slightly more positive potentials. At "high" overpotentials, the number of electrons up to, and including the rds was ~1 for all surfaces in accordance with previous studies[49]. Hence, the first rate limiting step in the ORR for all stepped surfaces studies not covered in significant amounts of either O_{ad} or OH_{ads} is proposed to be:

$$Pt \ + \ O_2 + H^+ (aq) + e = Pt - OOH \ (ad)$$
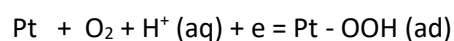
Markovic and co-workers have previously proposed a model of how adsorbed OH (in addition to site blocking) alters the adsorption energy of ORR intermediates, therefore having a deleterious effect on ORR kinetics[50]. This also could explain why the Tafel slope (and ORR mechanism) changes at low overpotentials. The nature of the Pt-OH bond at these potentials is still debated as to whether Pt-OH could be ionic or completely covalent as a function of potential[51]. Whatever the true nature of the "Pt-OH" bond, it has been proposed that this bond changes its binding to Pt as a function of potential (in order to "desorb" an electron localised on the metal side of the interface must transfer over to the OH side thus generating OH$^-$(aq) which immediately is neutralised by protons to form water). The extent to which this transfer happens will determine the overall bond strength and so even after the Pt-OH bond is formed, it should not be assumed that its binding with potential is constant. In addition, it should be noted that if OH forms at more negative potentials (e.g. on Pt(100) compared to on Pt(111)), it should be expected that this OH species will be more polarised at a given potential (say ORR range) and hence, prove more capable of blocking O_2 adsorption. It is proposed that this idea may explain the superior intrinsic activity towards ORR of Pt(111) compared to Pt(100). The introduction of steps (both for Pt(111) and Pt(100)) should lead to the break-up of OH domains formed on these terraced surfaces. Therefore, a decrease in O_2 blocking by OH species is to be

expected and a general increase in ORR activity result. However, too many steps not only limits the number of terrace sites for 4e transfer (by definition) but also introduces a greater amount of site blocking at ORR potentials since step sites become oxidised (OH forms at lowest potentials on steps and so the polarisation of this species at ORR potentials is greatest of all leading to spontaneous oxide formation (ORR requires *metallic* sites to take place [49])). This model of the crucial role of metallic sites being blocked by OH species successfully interprets the volcano curve of activity reported here and also similar relationships found in previous studies[48, 49, 52].

Theoretical calculations predict Pt(111) to be the best Pt surface for ORR under acidic conditions[53]. It is interesting that this theoretical prediction proves correct experimentally only for alkaline electrolytes but not in acid. In fact, it is Pt(331), a surface comprising 3 atom wide (111) terraces with linear (110) steps that has been shown to be the most active pure Pt surface for ORR in $HClO_4$[46].

The assumption that the nature of adsorbed OH changes with potential and hence controls the change in Tafel slope also then explains why only a single Tafel slope is observed for ORR in H_2SO_4 solutions[54], where the sulphate anions block the adsorption of OH (OH changing its binding is not relevant since it is displaced by sulphate).

Low Overpotential		
Surface	**No of electrons in rds**	**j_o / A cm^{-2}**
Pt(100)	1.4	1.92×10^{-8}
Pt(20,1,0)	1.5	6.35×10^{-9}
Pt(10,1,0)	1.7	2.02×10^{-9}
Pt(710)	1.6	3.86×10^{-9}
Pt(510)	1.5	6.98×10^{-9}
Pt(310)	1.6	3.88×10^{-9}
Pt(210)	1.8	7.95×10^{-11}

Figure 114: ORR Tafel analysis for low overpotentials for Pt(S)[n(100)x(110)] surfaces

High Overpotential		
Surface	No of electrons in rds	j_o / A cm^{-2}
Pt(100)	0.9	1.35 x10^{-6}
Pt(20,1,0)	1	5.26 x10^{-7}
Pt(10,1,0)	1	4.52 x10^{-7}
Pt(710)	1	3.03 x10^{-7}
Pt(510)	1	6.51 x10^{-7}
Pt(310)	1	8.11 x10^{-7}
Pt(210)	0.9	1.34 x10^{-6}

Figure 115: ORR Tafel analysis for high overpotentials for Pt(S)[n(100)x(110)] surfaces

5.2.5 Effect of ORR experiments on the Pt surfaces

The effect of the flame annealed Pt surfaces being exposed to gaseous oxygen during the ORR was investigated. CVs were taken before and after the ORR experiments and are shown in Figure 116. From these, an electrode exhibiting higher step density shows to be less perturbed by the ORR experiment, as the CV before and after ORR match closely. This finding has also been found for high Miller index structured nanoparticles[55]. This may simply reflect the fact that the more stepped a surface is, the less order it has to lose. The data shows no new developments in terms of steps, suggesting terraces of n < 4 atoms are more stable towards surface reconstruction under ORR conditions. For surfaces containing low densities of steps, transfer of intensity from the Pt(100)-(1x1) peak at 0.3 – 0.4 V to the potential where defects usually occur (< 0.2 V) indicate that even though the potential was kept below 0.85 V, exposure to ORR conditions resulted in significant reconstruction of all Pt(100)-(1x1) terraces.
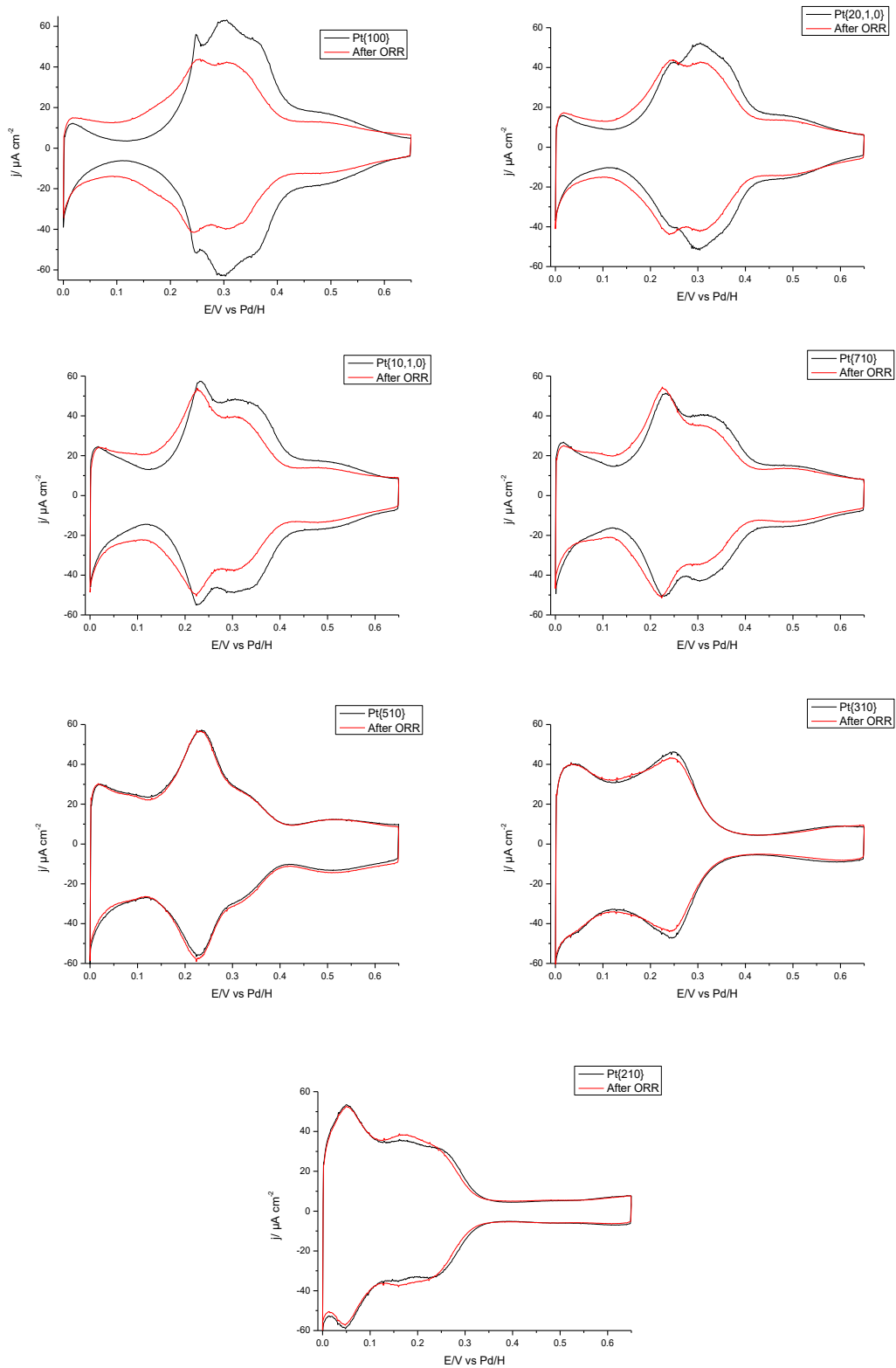
Figure 116: CVs of before and after RDE experiments in 0.1 M HClO₄

5.2.6 HPORR

The results for the activity of Pt(S)[n(100)x(110)] crystal surfaces towards hydrogen peroxide (HP) oxidation and reduction are shown (Figure 1173). Results are shown for Pt surfaces in a 1 mM H_2O_2 + 0.1 M $HClO_4$ solution using an electrode rotation rate of 1600rpm.

The voltammograms follow a similar profile to that seen for the ORR results; however, they are not the same. There are three regions that can be described: the low potential region (E<0.3 V), the limiting current potential range (0.3-0.7 V), and the high potential region (E>0.7 V). In the low potential region of the reduction (0-0.3 V), the changes observed are similar to those seen in the ORR results whereby H_{upd} adlayers appear to inhibit hydrogen peroxide decomposition although in this case, water formation is expected (not hydrogen peroxide!). The current drop below 0.3 V, is more dramatic for large terraced Pt(100) surfaces. For example, the Pt(100) electrode displays greatest reduction in current from 0.25-0.15 V and less so for the more stepped electrodes. Oxygen reduction at a H_{upd} covered surface forms hydrogen peroxide, a 2 electron process as described previously. At low potentials, the H_{upd} seems to act as a site blocking species against the hydrogen peroxide reduction, resulting in the current tending towards zero as H_{upd} coverage increases. This is a very interesting result in itself since at these potentials, the electrode is very negative of the standard reduction potential of hydrogen peroxide and reaction is strongly thermodynamically favoured[44]. The reason why the highly unstable hydrogen peroxide is stable when interacting with a hydrogen covered terrace is unknown. For Pt(111), the same phenomenon is observed[56]. Certainly by introducing steps, the hydrogen peroxide decomposition is indeed strongly catalysed as signified by the tendency to reach the limiting current density for the 2e hydrogen peroxide reduction to form water.

At potentials below 0.7 V, only the 2 electron reduction of HP occurs, confirmed by measurements of the variation of limiting current with rotation rate. Between 0.7-1.0 V, the activity changes from reduction to oxidation of hydrogen peroxide very quickly. The potential at which this occurs changes depending on the geometric nature of the surface, the electrolyte and the rotation rate and this potential has been tabulated below.

Surface	Potential for HPR/HPO crossover (vs. Pd/H)
100	0.930
20,1,0	0.928
10,1,0	0.911
710	0.907
510	0.896
310	0.875
210	0.870

In these studies, the switchover occurs at a lower potential for single crystals with higher step density. This has been observed for other platinum stepped surfaces[49]. The change from oxidation (HPO) to reduction (HPR) or vice versa occurs at a potential at which surface oxide formation commences. These results indicate that surface oxides catalyse the HP oxidation reaction, as stepped surfaces form surface oxides at lower potentials and show a crossover from the HPR to HPO at lower potentials. More explicitly, a correlation of step oxide formation in earlier CVs with the change in the potential of the hydrogen peroxide wave is observed.
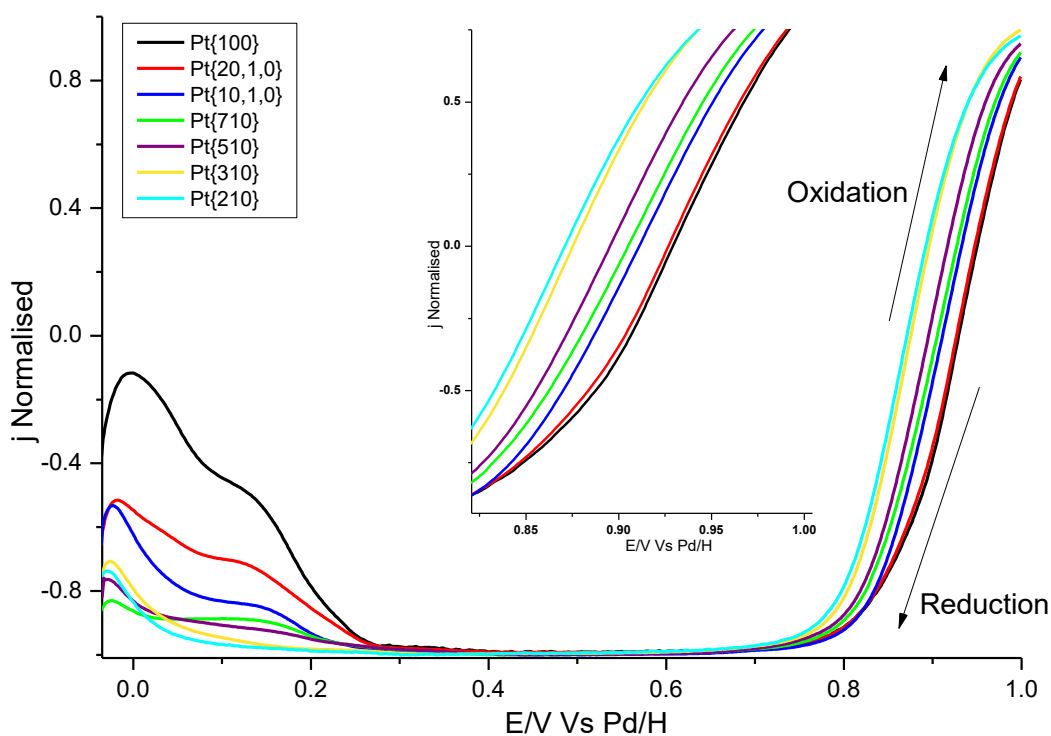

Figure 117: CVs for the HPORR experiments of Pt(S)[n(100)x(110)] surfaces

As mentioned above, previous studies of hydrogen peroxide on polycrystalline platinum attributed the switch from reduction to oxidation as corresponding to a change in the oxidation state of the platinum surface (reduction on metallic sites and oxidation on oxide covered surfaces)[57]. Feliu *et al.* also recently reported the importance Pt oxides play in hydrogen peroxide oxidation in Pt(111)[56]. Here, we have 'tuned' this crossover point by changing step density, thus confirming suggestions made with polycrystalline samples that adsorbed oxide is crucial for HPO.
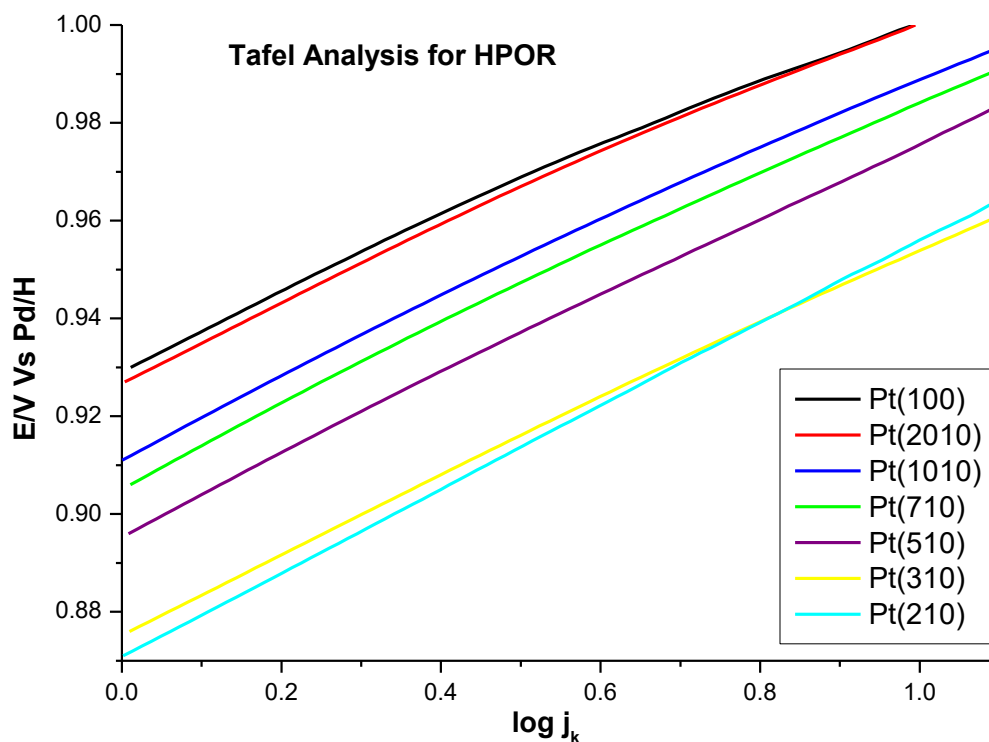

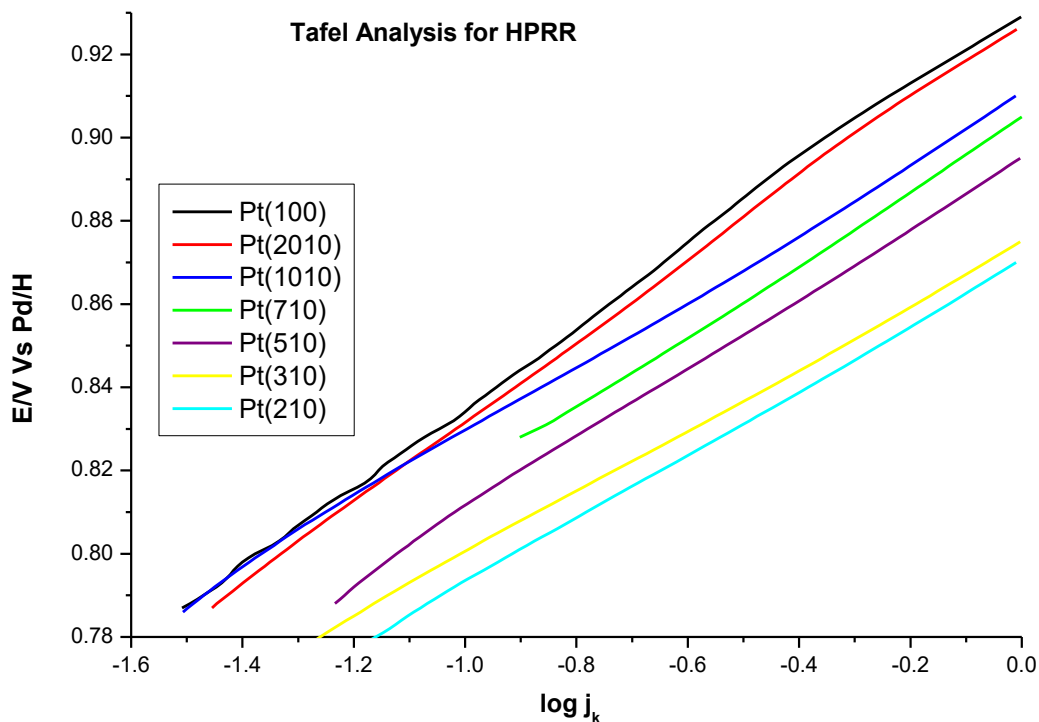*Figure 118: Tafel slopes for HPOR of Pt(S)[n(100)x(110)] surfaces*

Figure 119: Tafel slopes for HPRR of Pt(S)[n(100)x(110)] surfaces

Analysis of the hydrogen peroxide is quite different to the ORR since the hydrogen peroxide wave consists of two overlapping processes, hydrogen peroxide reduction and hydrogen peroxide oxidation. Some parallels can be made between this and the ORR but it is important to understand that the relative positions of the waves shown are not related. For the ORR, the half wave potential was found to shift in a volcano trend with step density, whereas a linear trend discussed above was seen for the hydrogen peroxide studies. One thing is certain, Pt-O species have been found to negatively affect the ORR activity but positively affect the HP oxidation reaction. Tafel analysis has been undertaken and the results shown below. Individually, for each of the oxidation and reduction reaction, there is no change in Tafel slope, indicating no change in mechanism for each individual reaction (they are mass transport limited in both cases). Tafel slopes observed for all [Pt n{100}x{110}] surfaces for hydrogen peroxide reduction varied from 76-97 mV/dec. This is different to experimental data found in reference [49]. As step density increases, the gradient of the Tafel slope decreases. At this potential range the changes which could be attributed to more oxide adsorbed on the surfaces and hence influencing the change. For the hydrogen peroxide oxidation, Tafel slopes vary from 71-85 mV/dec. The gradient of these slopes becomes larger with increasing step density, opposite to that found for [Pt n{111}x{100}] surfaces. The deviation from previous

results[49] has been attributed to the adsorption of more oxide species on these Pt surfaces at this potential range.

5.3 Pt(S)[n(110)x(100)] single crystal electrodes

We now switch from electrodes containing linear (110) steps on (100) terraces to surfaces in which linear (100) steps on (110) terraces form the central structural motif. In chapter four, it was already emphasised that by cooling Pt(S)[n(110)x(100)] surfaces in CO after flame-annealing that some instability arises in the surface due to reconstruction. In this section, hydrogen-cooled Pt n(110)x(100) stepped electrodes (n > 2) will be investigated in order to complete the picture so far as the stability of these more open electrode surfaces are concerned. Figure 120 shows hard sphere models of some Pt n(110)x(100) (n = 2, 3, 5 and ∞) surfaces. Together with the data reported in chapter four, previous work discusses the possibility that these surfaces are highly unstable and facet easily[20].
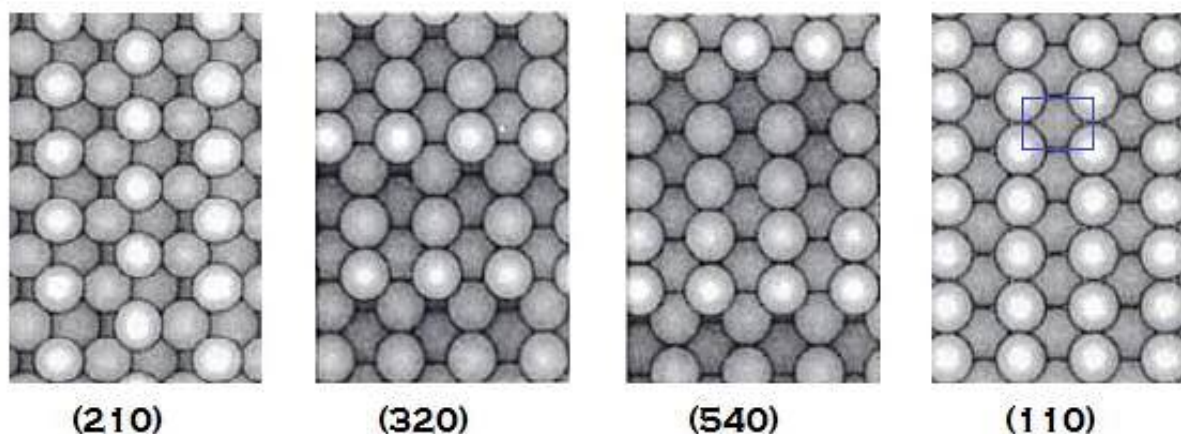

Figure 120: Hard sphere models of Pt(S)[n(110)x(100)] single crystal surfaces

5.3.1 Cyclic Voltammetry - Perchloric Acid Electrolyte

Figure 121 reports the voltammetric profiles of a range of Pt[n(110)x(100)] electrodes in 0.1 M HClO$_4$ in good agreement with earlier reports[20].
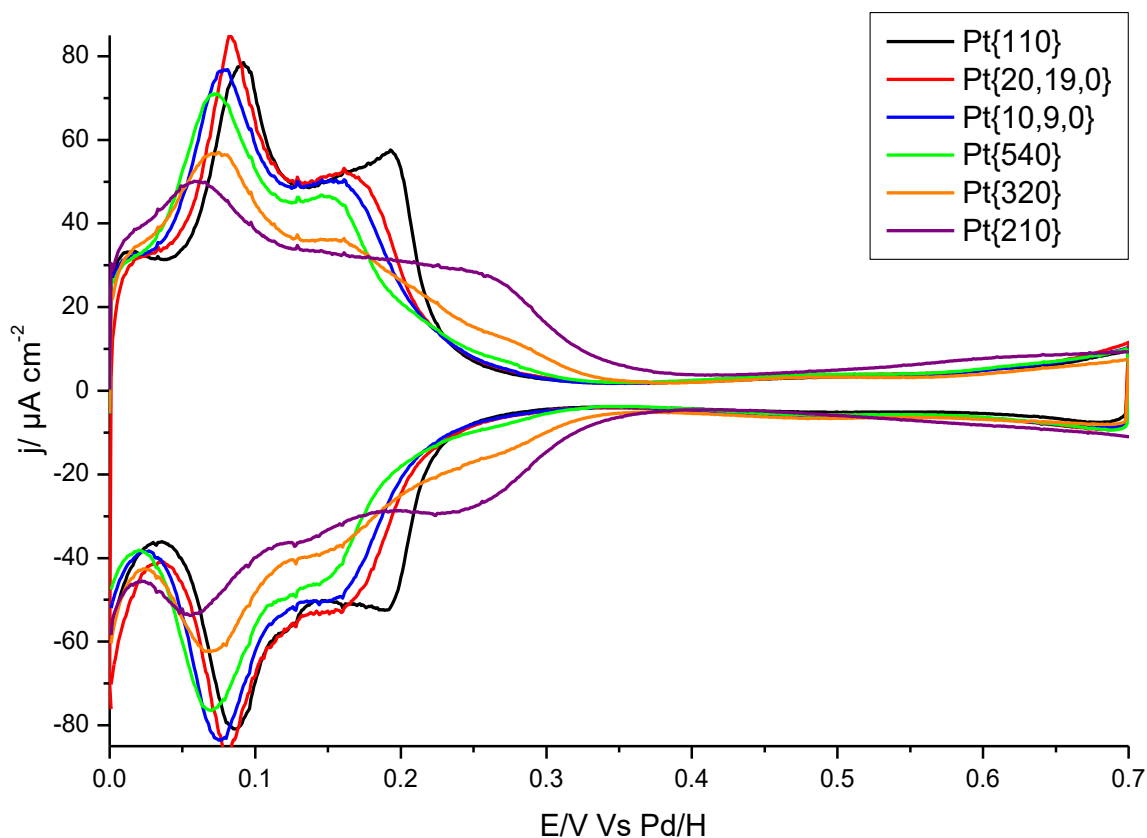
Figure 121: CVs of Pt(S)[n(110)x(100)] surfaces in 0.1 M HClO₄

Figure 121 shows both forward and reverse potential scans between 0-0.7 V in 0.1 M HClO₄. The voltammetric profiles reach stationary distributions of various reversible adsorption-desorption states as long as the upper potential limit is below the oxygen adsorption region at 0.7 V.

When compared with CO-cooled data for these surfaces in chapter four, the lack of good two dimensional long range order in all electrodes is clear as signified by the absence of the three intense doublet features observed at 0.2, 0.15 and 0.09 V (Pd/H) normally seen with CO – cooled electrodes and the strength of intensity of the broad "classical Pt{110} terrace peak" or "Pct" for short at 0.2 V confirms the instability of the surface structure. Since all of these less ordered features formed after flame annealing and hydrogen – cooling have been discussed already in chapter four and are found to agree in terms of voltammetric response with work published in reference [20], it is re-asserted that all hydrogen – cooled Pt n(110)x(100) stepped surfaces contain surface disorder (both terraces and steps). It is noted that the total charge under the adsorption peaks between 0-0.25 V, is larger than 147 μC cm^{-1} (the charge expected for one monolayer of adsorbed hydrogen on (1x1) (110) surface, assuming 1 H atom per site) suggesting other adsorption processes (such as water splitting to form OH$_{ads}$), could be occurring in this potential region. In chapter four, by using

values of PZTC together with changing the nature of the electrosorbing cations and anions, this assumption was confirmed. Unless in the unlikely event of disordered, hydrogen – cooled samples no longer giving rise to H and OH adsorption at different adsorption sites (one dimensional and two dimensional (110) sites and (110)x(100) steps) in the H_{upd} potential region applies, we assign both the broad 0.09 and 0.2 V peaks to "disordered" step and terrace sites respectively. It should be noted that as step density increases, the ability to differentiate between CO - and hydrogen – cooled samples becomes less and less demonstrating that for very open surfaces, even CO- cooling is insufficient to keep the electrode surface in a pristine, unreconstructed state (contrast with Pt n(110)x(111) behaviour).

Figure 122 shows a higher potential range, going up into the oxide region. This has not been previously reported for any stepped Pt n(110) x(100) surfaces in this electrolyte. Again, only the forward scans are shown, as increasing the scanning window results in an unsymmetrical profile as adsorbed oxides change the arrangement of the surface.

The Pt(110) CV shows three distinguishable features in the oxide adsorption region at 0.75, 0.85 and 0.97 V. The feature at 0.75 V is small but reasonably sharp, the feature at 0.85 is smaller and less defined and the sharp feature at 0.97 V is large. The peak at 0.97 V has previously been ascribed to electrosorbed OH/O species on the terrace whereas the peaks at the lower potentials are ascribable to electrosorbed OH/O species at defect sites. Defect sites here include the steps and kinks. The peak at 0.85 V has also been seen in chapter four for the CO – cooled electrodes (0.9 V vs. RHE) so may tentatively be ascribed to adsorption at (110)x(111) linear steps. Of course, as noted in chapter four, this electrosorption site should be absent from Pt n(110) x(100) stepped surfaces. Hence, its presence supports the assertion that the (110)x(100) step sites exhibit marked reconstruction. The peak at 0.75 V has previously been seen using hydrogen and nitrogen-cooled Pt(110) electrodes[58]. There, the feature was deduced to arise from oxide formation on the "rails" of Pt atoms formed as a consequence of residual (1x2) reconstruction. These very low coordinated surface atoms are expected to be the most oxyphilic of all Pt sites and thus exhibit the lowest oxide electrosorption potential.

Pt(110) is a basal plane atomic arrangement, yet its surface begins by being stepped; therefore addition of steps to this surface will likely bring about more than one step feature and hence more than one type of adsorption site.
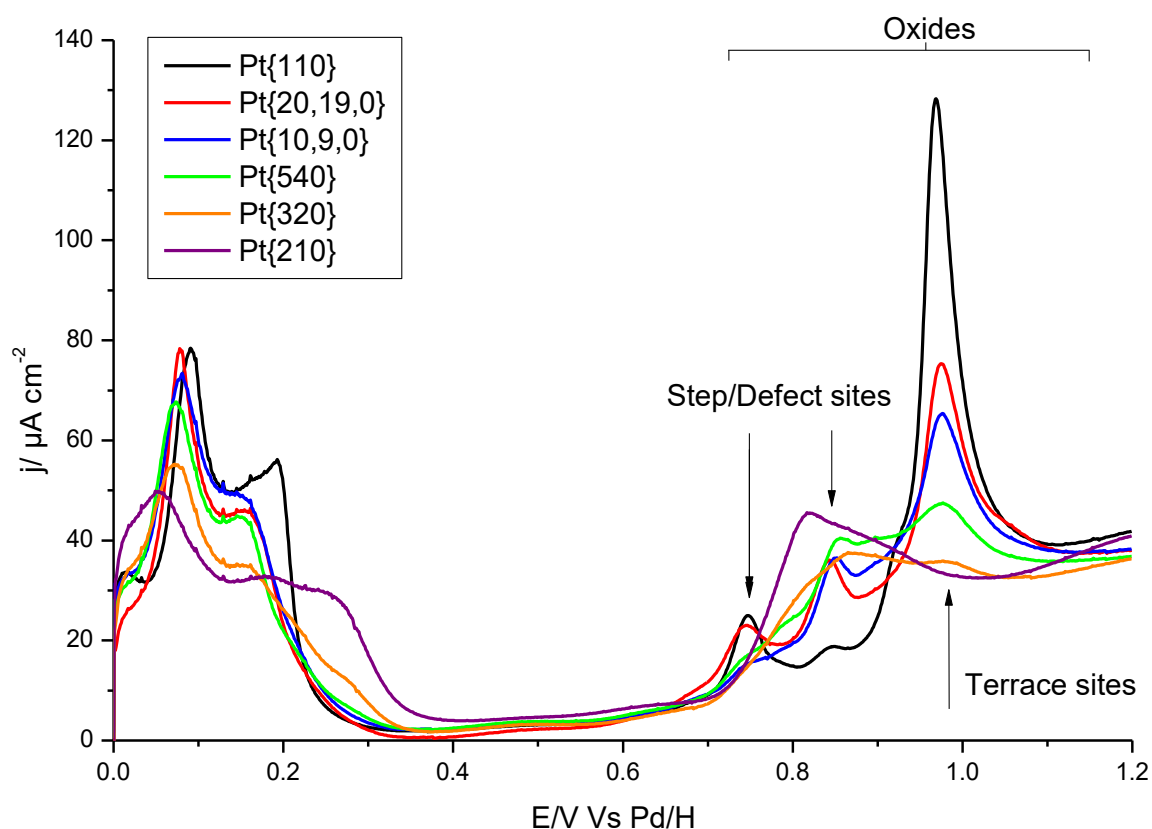

Figure 122: CVs of Pt(S)[n(110)x(100)] surfaces up to 1.2 V, in 0.1 M HClO₄

Overall, addition of (100) steps leads to a broader, less defined oxide adsorption region. In particular, the feature corresponding to oxide adsorption on terrace sites at 0.97 V, diminishes very quickly with the addition of steps. The Pt(20,19,0), (a 20 atom wide (110) terrace), shows the peak at 0.95 V is almost half the size compared to the Pt(110) profile. The adsorption state at 0.85 V is attenuated. The adsorption states at 0.75 and 0.97 V can be ascribed to (110) steps and terraces respectively. The adsorption feature at 0.85 V grows with increasing (100) step density and so may be tentatively ascribed to oxide adsorption on (100) step features. Moreover, it occurs at precisely the potential of the step feature found with low levels of linear step sites.

5.3.2 Cyclic Voltammetry – Sulphuric Acid Electrolyte

Figure 123 shows the voltammograms of Pt(S)[n(110)x(100)] surfaces in 0.1 M H_2SO_4 electrolyte. These are closely matched with those shown by Feliu *et al.* previously[20]. Again, comparison is made with the same data for CO – cooled samples in chapter four.
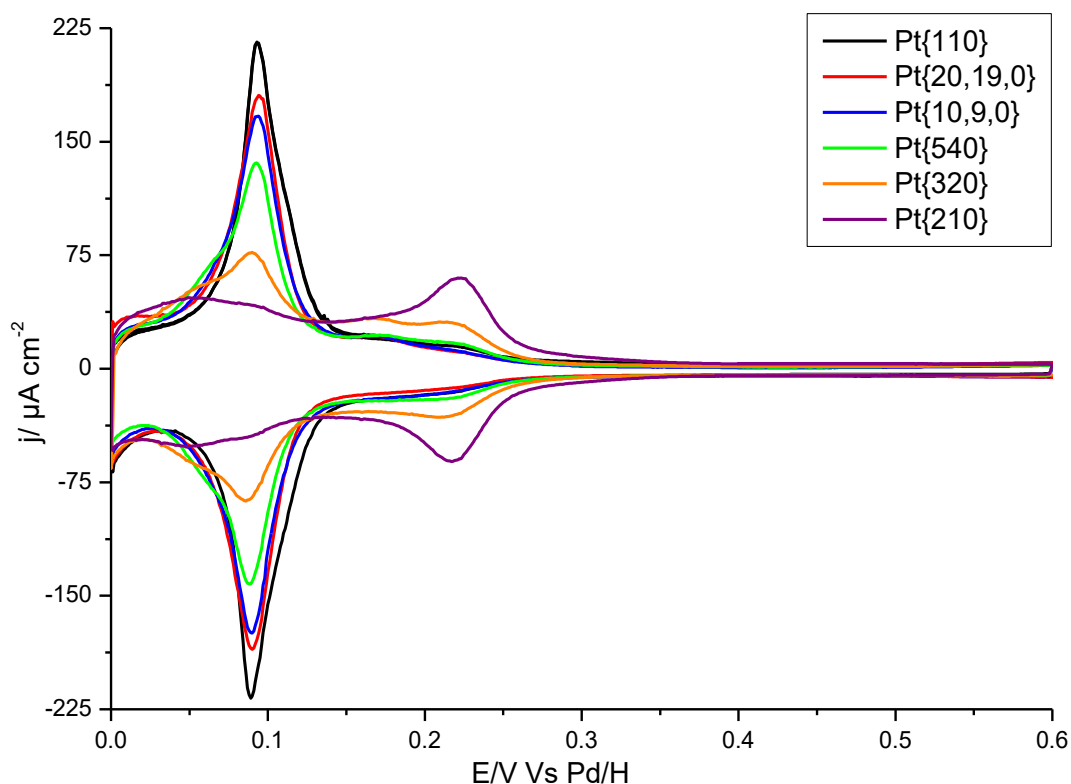

Figure 123: CVs of Pt(S)[n(110)x(100)] surfaces in 0.1 M H_2SO_4

It is seen that in this case, introduction of (100) linear steps show a stepwise deviation from the Pt(110) hydrogen-cooled voltammogram so the influence of the expected (1x1) hard sphere representation of the idealised surface is operative, it is just that all peaks are broadened As step density increases, the characteristic adsorption state near 0.1 V decreases. This can be ascribable to disordered (110) sites at both terraces and steps. For surfaces exhibiting n>5 the broad adsorption state 0.15-0.25 V, grows and becomes more defined as step density increases. The Pt(320) voltammogram shows the appearance of 2 new peaks in this potential region; one at 0.16 V and 0.21 V. The Pt(210) also shows the same features, with the peak at 0.21 V much larger. These new states visible with the addition of (100) steps can be associated with adsorption processes on (100) steps. When these samples were CO cooled in chapter four, a broadly similar trend was also observed, confirming that even CO-cooled samples are strongly reconstructed.

Figure 124 shows the voltammograms of the Pt(110)x(100) surfaces in 0.1 M H_2SO_4, up to 1.2 V. Only the forward scan is shown for reasons described previously. For all surfaces, excursions past potentials of 0.6 V show the onset of electrochemical oxide formation. Some of the oxide adsorption processes here are reversible but get mixed in with the irreversible ones.

The Pt(110) CV shows characteristic oxide adsorption states at 0.82, 0.88 and 1.0 V. The shift to more positive potentials relative to perchloric acid electrolyte reflects the specific adsorption of sulphate anions inhibiting oxide formation (the shift of H_{upd} peaks to more negative potentials relative to perchloric acid is also a manifestation of this phenomenon). Introduction of (100) steps is shown to cause the large oxide adsorption peak at 1.0 V to diminish. This feature can be attributed to oxide adsorption on (110) terraces. For surfaces containing terraces of n>5 atoms, the adsorption state at 0.88 V grows and becomes more defined. These features can therefore be attributed to oxides on (100) steps. The feature at 0.8 V also increases slightly. For the Pt(320) and Pt(210), these features increase, but also broaden and become amalgamated into features that are more difficult to elucidate.
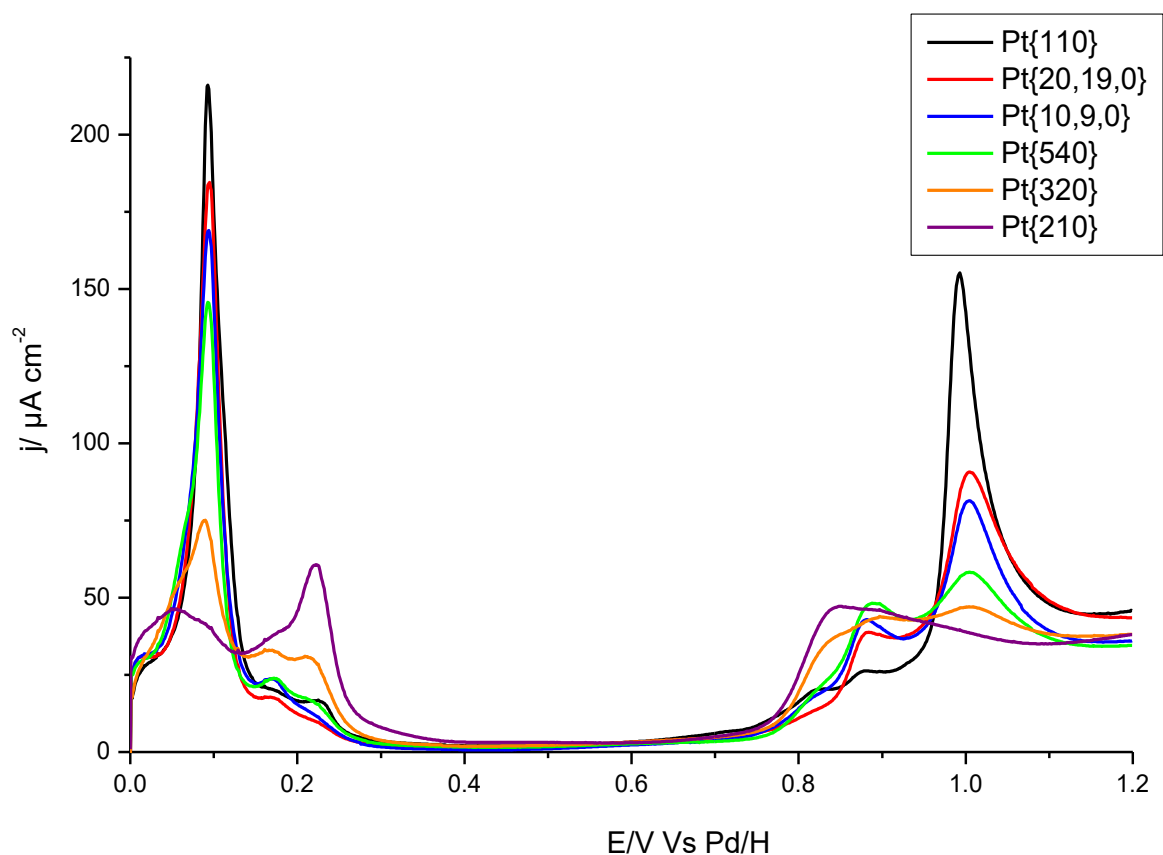

Figure 124: CVs of Pt(S)[n(110)x(100)] surfaces up to 1.2 V, in 0.1 M H_2SO_4

5.3.3 Nafion

The nest six figures show attempts at adsorption of Nafion films on Pt(110)x(100) in 0.1 M HClO$_4$. The adsorption of Nafion films show contamination (especially for Pt(320)) as signified by large electrooxidation currents appearing in the oxide region at potentials positive of 1 V (see earlier). However, for Pt(20, 19, 0) and Pt(10, 9, 0) the amount of contamination is minimal as exemplified by very low electrooxidation currents relative to the clean surface positive of 1 V. It is noted that once again, a correlation is seen between the magnitude of the Nafion induced Pt(110) terrace feature at 0.11 V and the extent of Pt(110) terraces. Pt(320) does not give rise to a Nafion spike but this is clearly due to contamination effects since all of the other surfaces do. It is also interesting that a shift of 40 mV to more positive potentials is seen in the peak for Pt(210) demonstrating that step-step interactions for sulphonate groups may also be occurring. However, the trends seen are very similar to those reported earlier and in previous studies [38, 39] whereby Nafion adsorption leads to weak specific anion adsorption effects causing H$_{upd}$ peaks to both shift negatively and narrow. That the Nafion spike is observed for all surfaces save for Pt(320) also marks out the Pt n(110)x(100) stepped surfaces since for both Pt n(100)x(110) and Pt n(111)x(100) and Pt n(100)x(111), for n < 5, the spike disappears. Reasons for this clear difference are unknown at present but it is speculated that the Pt (110) terrace site affords a particularly stable configuration for sulphonate groups. Unfortunately, Nafion adsorption on Pt n(110)x(111) electrodes was not explored in this study. However, it is predicted that here too, the Nafion spike will be seen at all step densities due to the presence of (110) terrace sites.

The position of the terrace Nafion peak is somewhat negative of the PZTC reported in pure perchloric acid [38, 39] but this again is completely consistent with the stronger specific adsorption of sulphonate groups relative to OH$_{ads}$[41].

The presence of Nafion on the platinum surfaces is shown to fully block the electrochemical adsorption state at the lower potentials (0.75 V), attenuates and shifts the peak at 0.85 V by approximately 10 mV but when clean, hardly affects the oxide terrace peak at 0.98 V at all (see for example Pt(20, 19, 0)). Clearly, the strength of specific adsorption of Nafion with Pt(110) oxides is insufficient to cause potential shifts to more positive potentials, as was found with stepped Pt(100) electrodes earlier in this chapter. The quenching of the 0.75 V "1x2" oxide peak could suggest that

some lifting of this reconstruction may have occurred by Nafion adsorption but similar behaviour exhibited by stepped Pt(110) electrodes in sulphuric acid (see figure 5) tends to suggest that the adsorbed oxide has been displaced by the more strongly specifically adsorbing anion into adsorbing at a more positive potential.

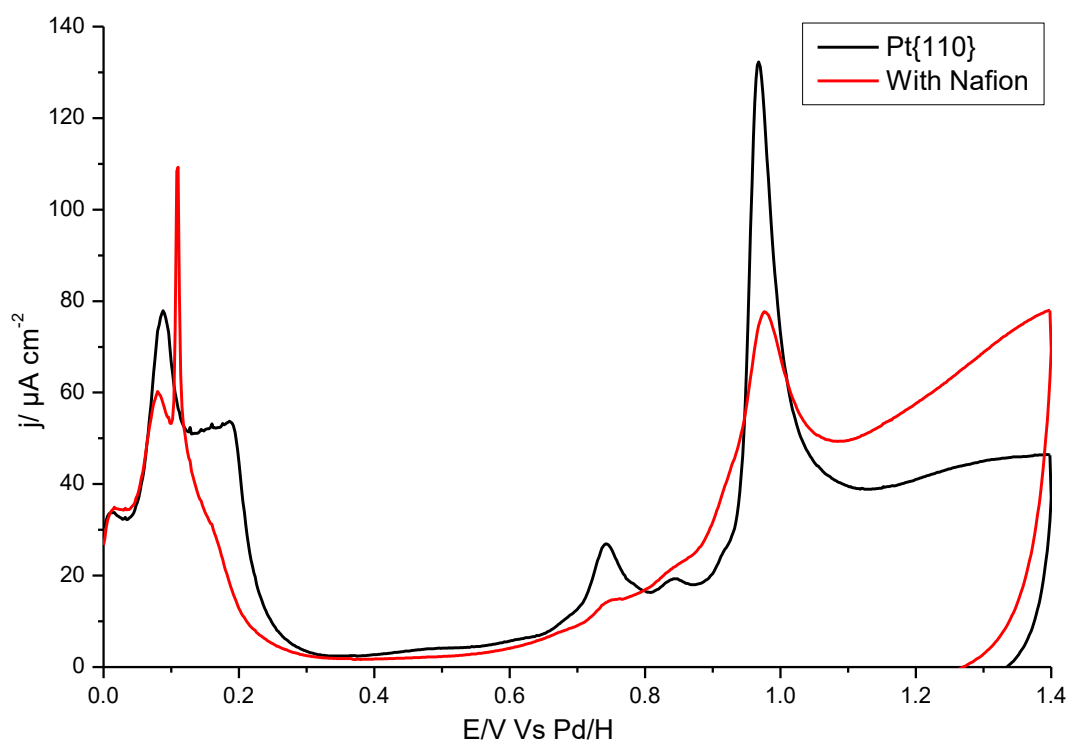*Figure 125: CVs of Nafion on a Pt(110) single crystals in 0.1 M HClO$_4$*

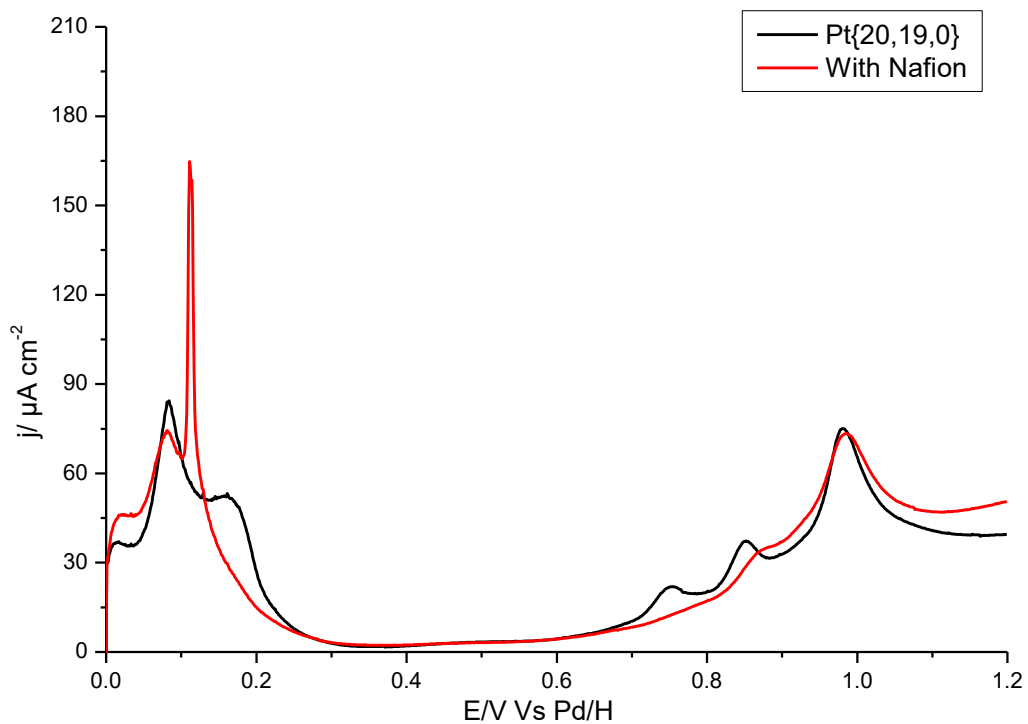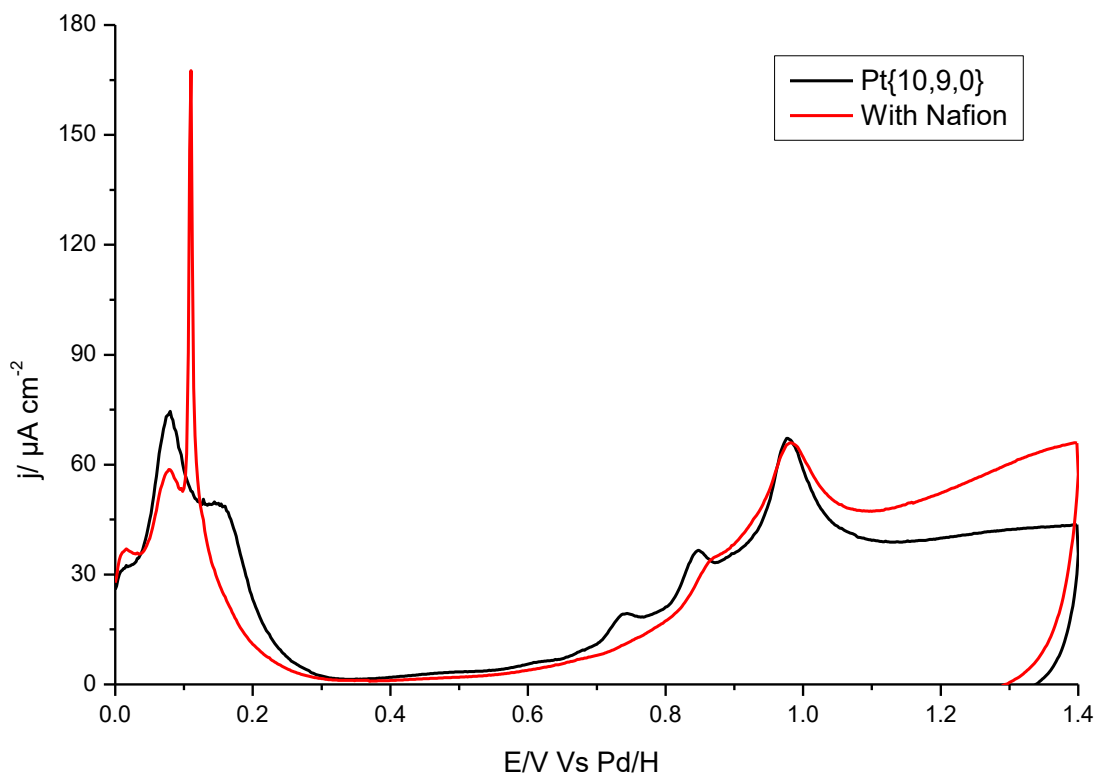*Figure 126: CVs of Nafion on a Pt(20,19,0) single crystals in 0.1 M HClO$_4$*

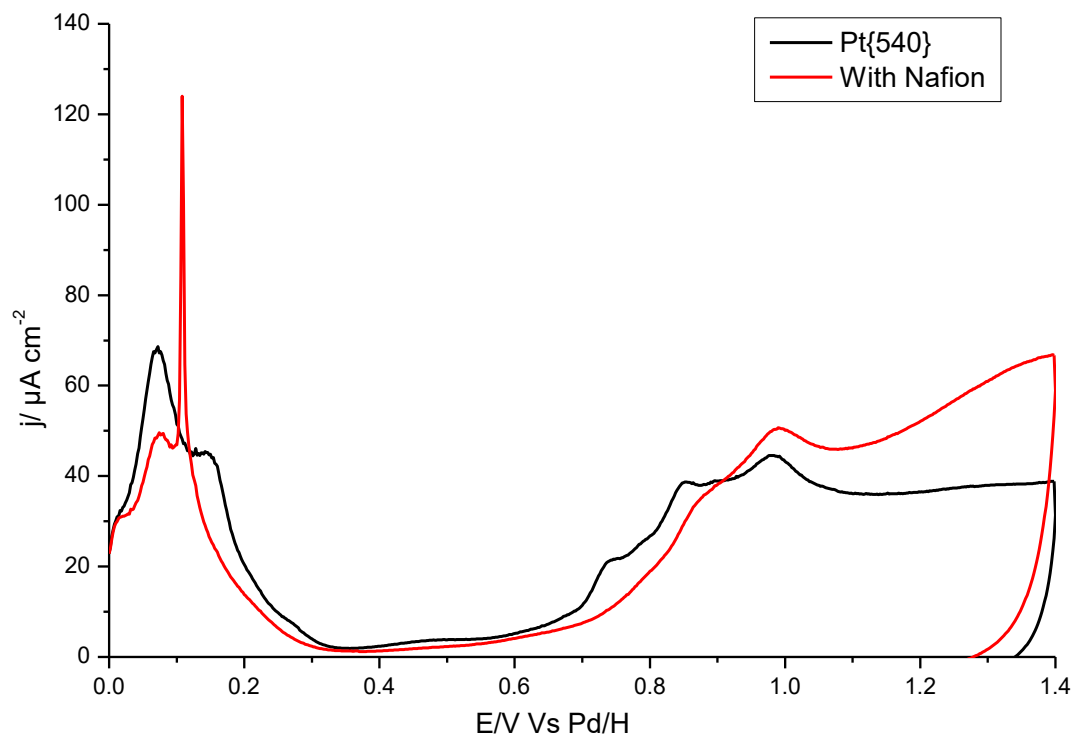*Figure 127: CVs of Nafion on a Pt(10,9,0) single crystals in 0.1 M HClO$_4$*

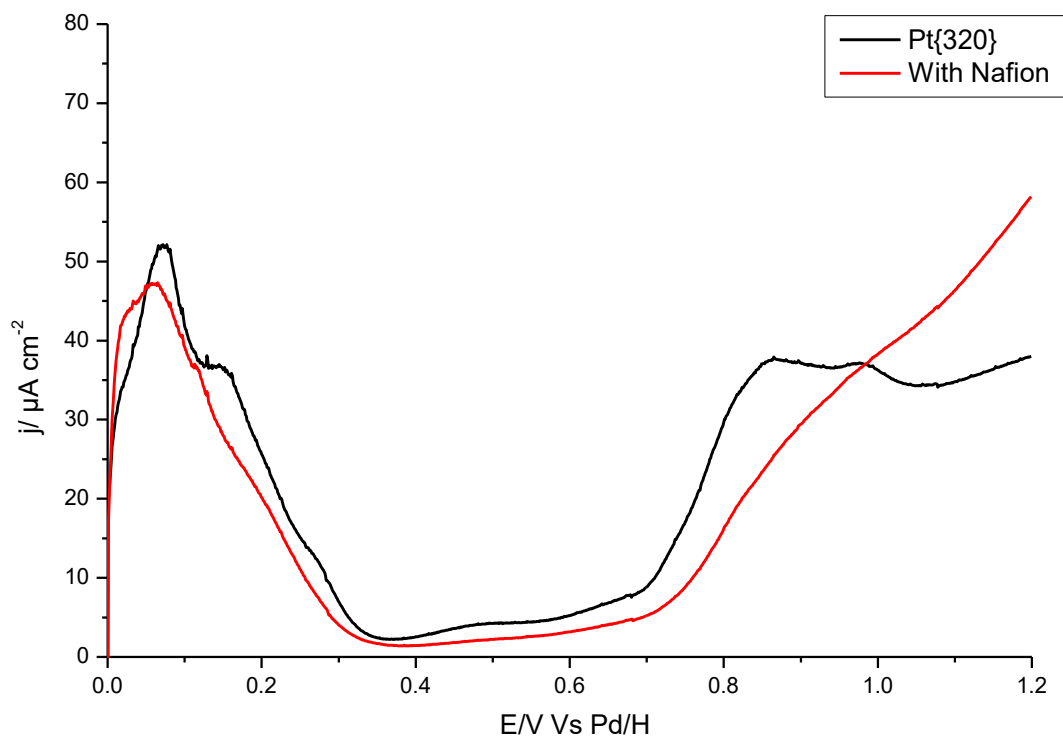*Figure 128: CVs of Nafion on a Pt(540) single crystals in 0.1 M HClO$_4$*

Figure 129: CVs of Nafion on a Pt(320) single crystals in 0.1 M HClO$_4$
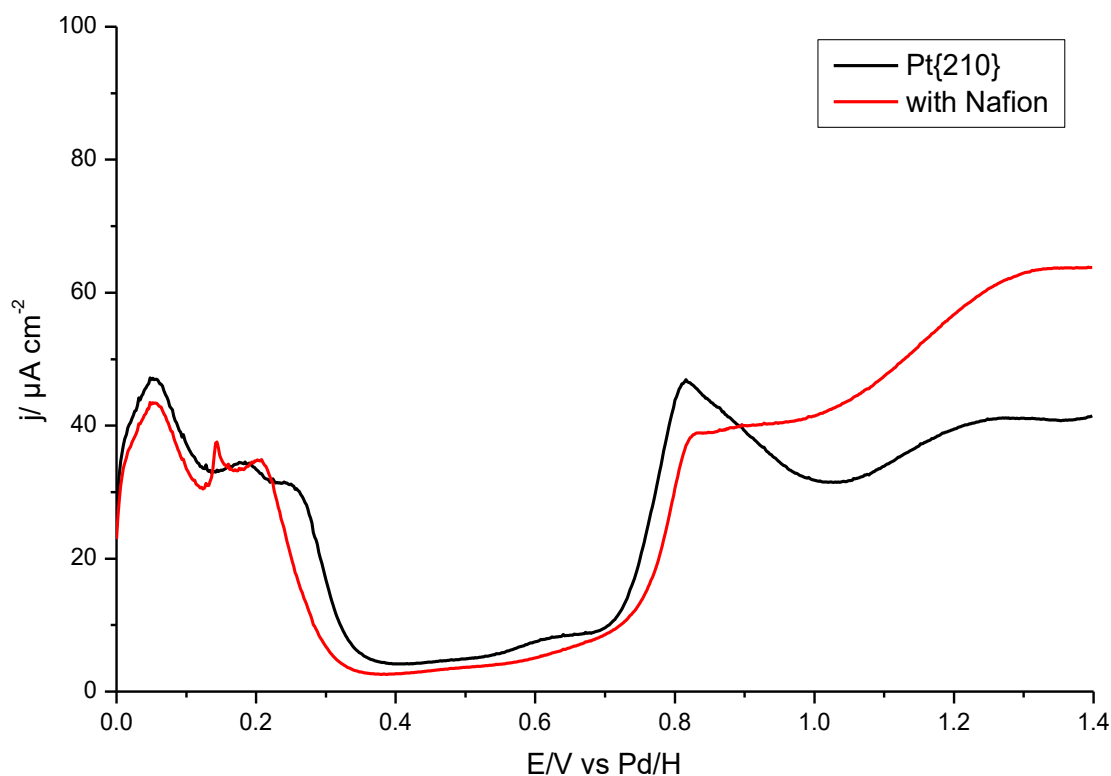
Figure 130: CVs of Nafion on a Pt(210) single crystals in 0.1 M HClO$_4$

5.3.4 ORR and HPORR

Figure 131 shows the voltammetric curves for ORR at 1600rpm for Pt(110) and Pt n(110)x(100) surfaces in 0.1 M HClO$_4$. The electrolyte was saturated in oxygen before and during the experiments. The voltammetry was recorded up to 1 V.

The wave for Pt(110) is in accordance with previous studies showing that a limiting current is reached at around 0.3 V and that the onset of ORR occurs around 0.95 V[42]. The (100) linear stepped surfaces have not been reported previously but show similar behaviour to the Pt(110) electrode. The deactivation of the ORR is again significant considering the equilibrium potential for this reaction is 1.23 V. Each curves follows a stretched "S" shaped curve from around 0.6 V. In the H$_{upd}$ potential region of the voltammogram, the current drops in two sections after reaching limiting current near 0.3 V. There is a small, gradual current decrease between 0.3-0.05 V followed by a sharper, larger current drop between 0.05-0 V. This behaviour at potentials below 0.3 V is usually attributed to H$_{upd}$ adsorption blocking sites and switching the ORR from a 4e to a 2e process with subsequent production of hydrogen peroxide (see earlier).

The area of the ORR results we are most interested in however is in the upper potential region (E>0.6 V). The main difference between the surfaces for the ORR profiles evident in the S shaped curves is the potential at which half the limiting current is observed. The trend in $E_{1/2}$ activity is shown more clearly in Figure 132, where Pt(20,19,0) is shown to exhibit the highest activity. Generally, as step density increases, the $E_{1/2}$ activity decreases. However, the $E_{1/2}$ activity for Pt(110) falls between Pt(320) and Pt(210), so not quite on trend. Although Pt(20,19,0) gives the best activity for these surfaces investigated, this is still 0.38 V below the equilibrium potential for the reaction.
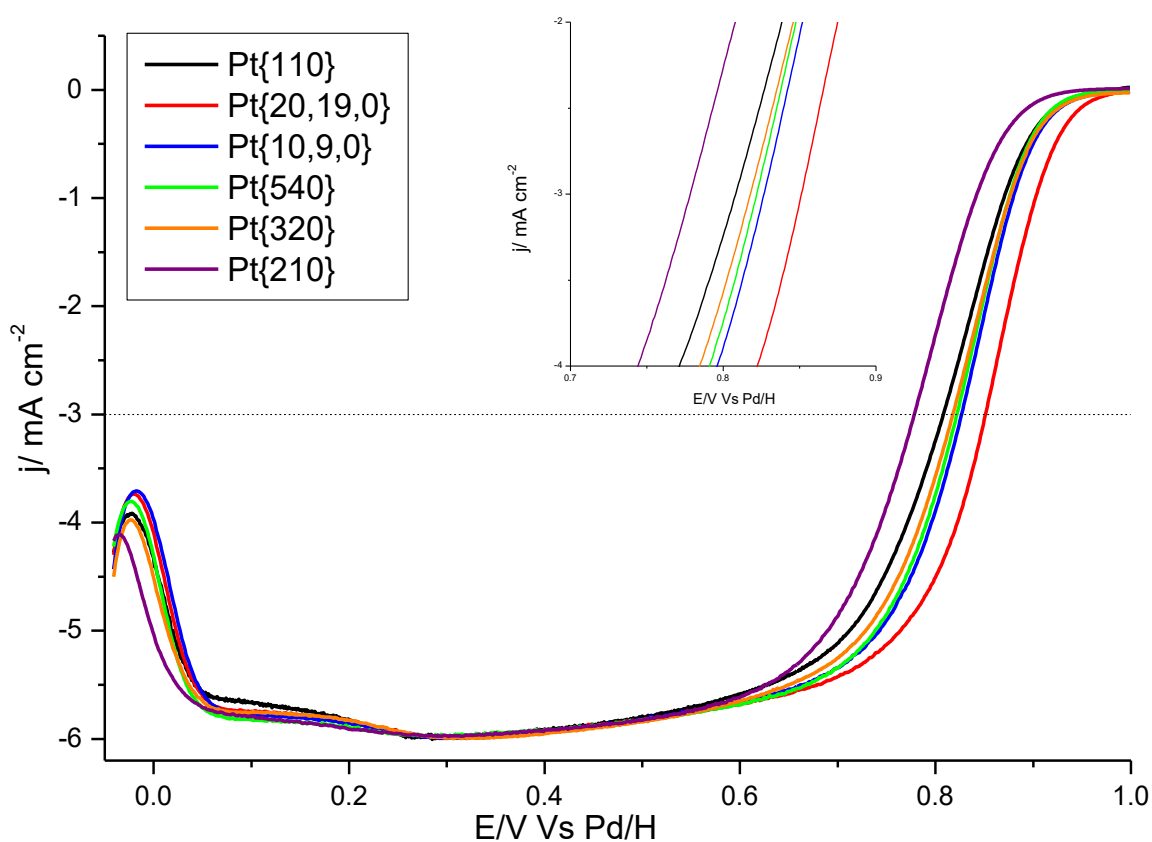

Figure 131: CVs of RDE experiments of Pt(S)[n(110)x(100)] surfaces in 0.1 M HClO₄
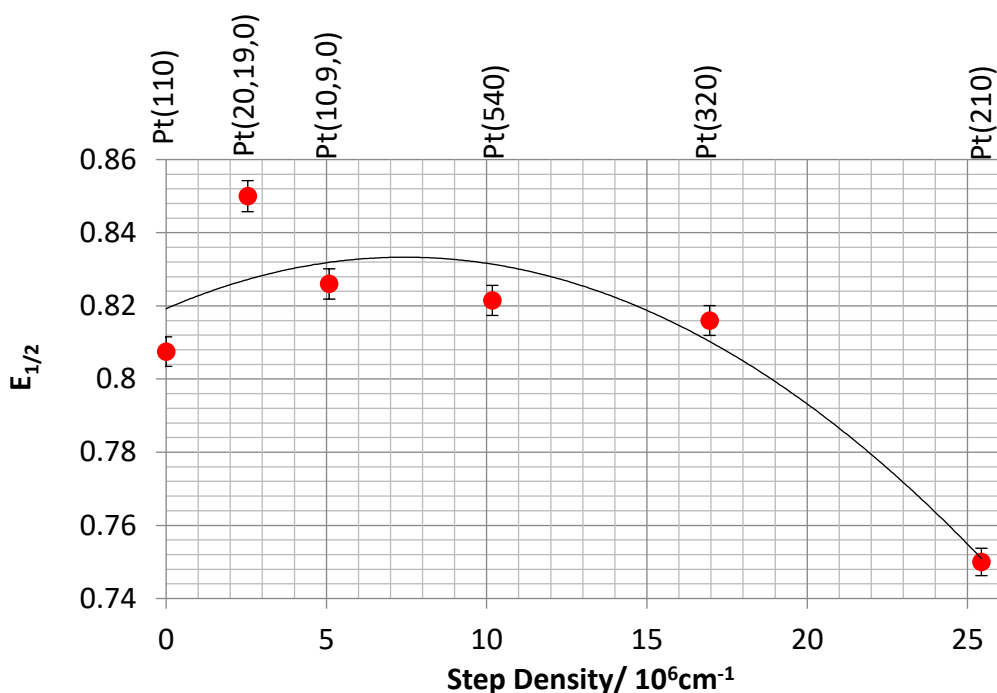
Figure 132: $E_{1/2}$ values for Pt(S)[n(100)x(110)] surfaces

Levich and Tafel analysis has been undertaken and results are shown in Figure 133. A 4-electron reduction was calculated for all surfaces corresponding to complete reduction of oxygen to water in this potential range. This is consistent with the known behaviour of platinum towards the ORR[20].

Tafel analysis has been undertaken to gather more quantitative data on the experiments. The number of electrons up to and including the rate determining step as well as the exchange current density (corresponding to electrochemical rate constant) has been undertaken on both "high" and "low" potential ranges analogous to that approach used previously. All values have been presented clearly in tables, in Figure 134 and Figure 135. The 'theoretical' slope of the lines should be 60 mV/dec for a 2 electron reduction in the "low" overpotential range and 120 mV/dec for a 1 electron transfer in the "high" overpotential range. At "low" overpotentials, the number of electrons up to, and including the rds were between 1.7-1.8. This is a slight deviation to the value of 2 that would be expected. This is attributed to the surfaces containing adsorbed oxide species changing the nature of the surface in this potential region[48] At "high" overpotentials, the number of electrons up to, and including the rds was 0.7-1.0 for all surfaces. Although these surfaces deviate from theoretically proposed values, they are similar for all surfaces, suggesting that the same mechanism occurs on all atomic arrangements of platinum fcc surfaces.

Overall, the Pt(S)[n(110)x(100)] surfaces are shown to be more active for the ORR than Pt(S)[n(100)x(110)]. Specifically, Pt(20,19,0) is reported to be the best platinum surface from the [001] side of the stereographic triangle for ORR activity. There is a caveat to this data that must be remembered (in contrast to all other hydrogen cooled electrodes). In this thesis, it has been proven that hydrogen cooling of stepped Pt(110) surfaces will lead to significant, intrinsic surface disorder. Hence, if the formation of a well-ordered OH adsorbed phase at terrace sites precludes effective ORR electrocatalysis by virtue of its site-blocking capabilities, it therefore follows that breaking up this long range order may give rise to a false interpretation of the best "active site". This has already been demonstrated for hydrogen- and CO- cooled Pt(110) [58] whereby the CO-cooled surface, by virtue of sustaining well-ordered and large (1x1) terrace domains was significantly less active than its hydrogen cooled equivalent. In the context of the stepped surfaces here, future work on ORR trends needs to address CO – cooled stepped electrodes. In spite of this caveat, the weak 'volcano' relationship between step density and ORR activity is not unexpected and the same interpretation of the data as before is postulated. Namely, that steps break up long range terrace order leading to more successful competition for sites by dioxygen molecules relative to adsorbed OH. However, too many steps both limits the number of active terrace sites and affords electro-oxidation (and quenching of ORR) of the surface at more negative potentials.
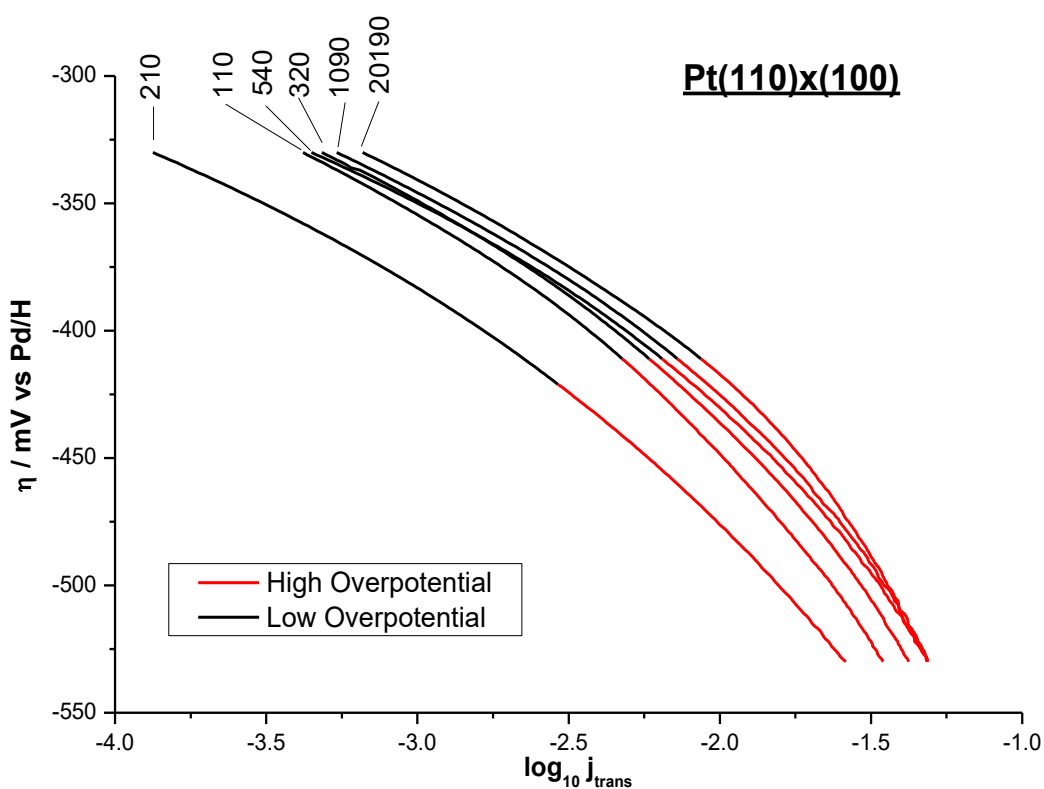

Figure 133: Tafel analysis of Pt(S)[n(110)x(100)] surfaces

Low Overpotential		
Surface	No of electrons up to and rds	j_o / A cm^{-2}
Pt(110)	1.7	1.04 x10^{-8}
Pt(20,19,0)	1.7	1.09 x10^{-8}
Pt(10,9,0)	1.7	9.75 x10^{-9}
Pt(540)	1.8	3.91 x10^{-9}
Pt(320)	1.7	9.62 x10^{-9}
Pt(210)	1.8	1.03 x10^{-9}

Figure 134: Tafel analysis for low overpotentials for Pt(S)[n(100)x(110)] surfaces

High Overpotential		
Surface	No of electrons up to and rds	j_o / A cm^{-2}
Pt(110)	0.9	5.05 x10^{-6}
Pt(20,19,0)	0.7	3.82 x10^{-5}
Pt(10,9,0)	0.8	1.53 x10^{-5}
Pt(540)	1.0	3.11 x10^{-6}
Pt(320)	0.9	6.51 x10^{-6}
Pt(210)	1.0	8.65 x10^{-5}

Figure 135: Tafel analysis for high overpotentials for Pt(S)[n(100)x(110)] surfaces

5.3.5 Effect of the ORR experiments on the Pt surfaces

The effect of the flame annealed Pt surfaces being exposed to gaseous oxygen during the ORR was investigated by comparing CVs in 0.1 M HClO$_4$ before and after the ORR experiment. These are shown in Figure 136. From these, it is seen that these highly stepped surfaces are less perturbed by the ORR experiment, as the CVs of before and after ORR match closely. This was also seen earlier in the chapter for Pt n(100)x(110) stepped electrodes. This may simply reflect the fact that the more stepped a surface is, the less order it has to lose. The data shows no new developments in terms of steps adsorption features. Rather, broadening of all peaks and some transfer of charge from H$_{upd}$ peaks at more positive potentials (terraces) to more negative potentials (steps and defects) is observed.
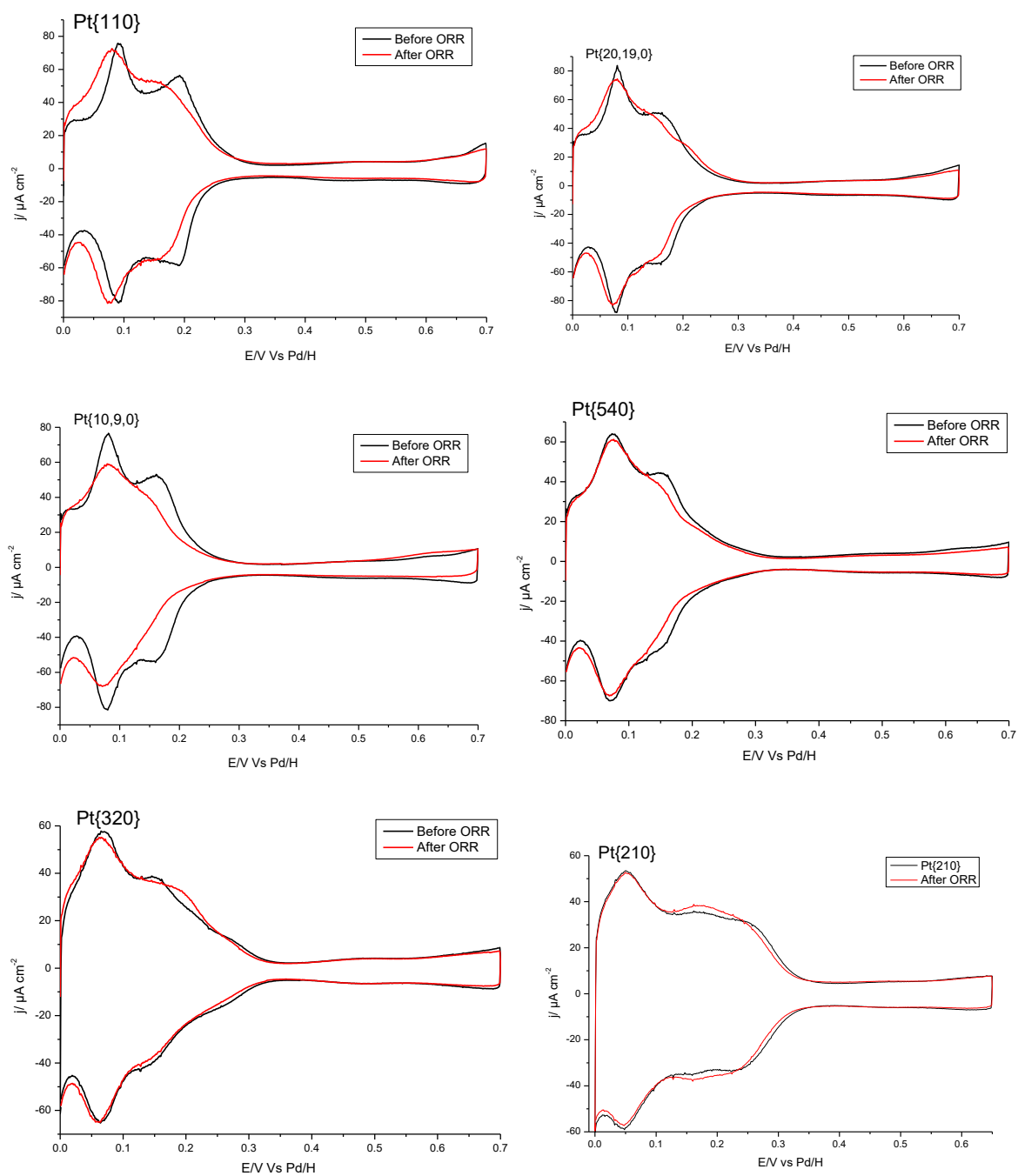
190

Figure 136: CVs of before and after RDE experiments in 0.1 M HClO$_4$

5.3.6 HPORR

The results for the activity of Pt(S)[n(110)x(100)] crystal surfaces towards hydrogen peroxide (1 mM H_2O_2 + 0.1 M $HClO_4$ solution at 1600rpm) oxidation and reduction are shown in Figure 137. The data shows typical hydrogen peroxide voltammogram curves and are similar to those reported earlier. Current densities have been normalised to 1 and -1 (maximum oxidation current and maximum reduction current respectively) to enable easier comparisons.
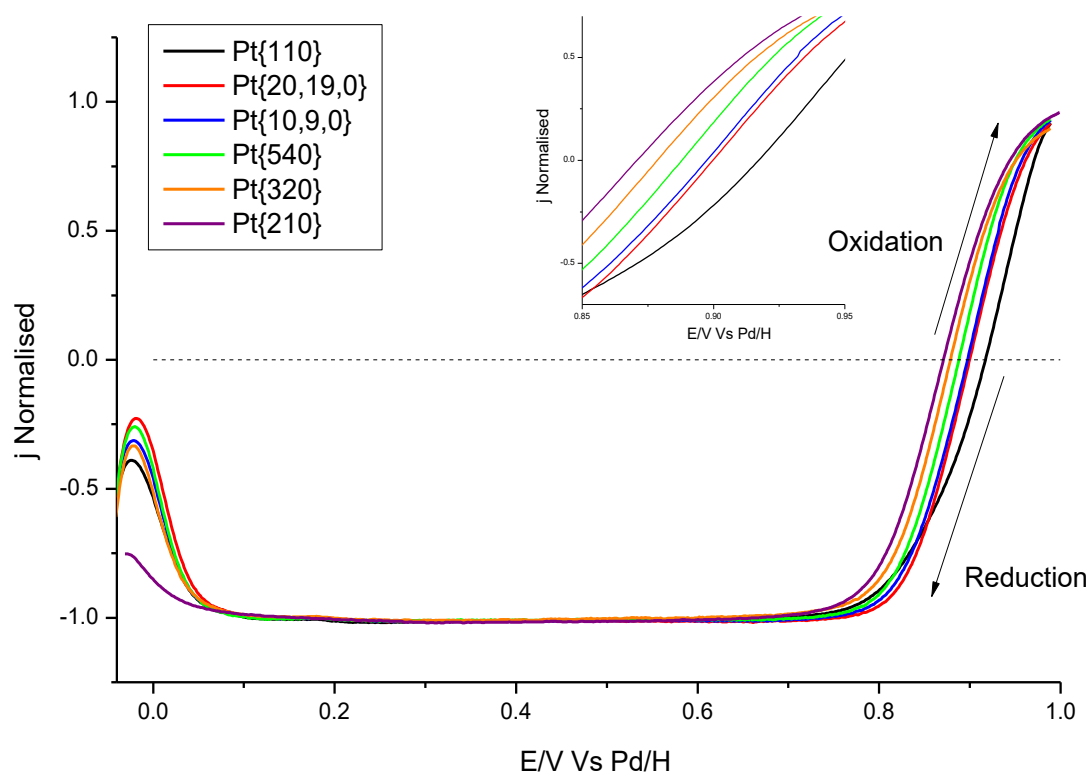
Figure 137: CVs for the HPORR experiments of Pt(S)[n(100)x(110)] surfaces

In general, there are three regions that can be described; low potential region (E<0.1 V), limiting current potential range (0.1-0.7 V), and high potential region (E>0.7 V). In the low potential region, the changes observed are similar to that seen in the ORR results. Here there is only one current drop from the limiting current. All surfaces show a sharp decrease, except Pt(210) which shows a small and more gradual decrease. At low potentials, the H_{upd} has been thought to act as a site blocking species against the hydrogen peroxide reduction, resulting in the current heading towards zero as H_{upd} coverage increases. As this is such a low potential range, it is unlikely that there are any OH_{ad} species present even with these stepped surfaces. This could match the sharp current drop seen in the ORR curve – therefore meaning features below 0.05 are only H_{upd} then above this could be more Hupd with some OH_{ads} or H_{upd} terrace/step being differentiated, as discussed in Chapter 4. At

potentials below 0.7 V, only the 2 electron reduction of HP occurs, validated by the variation of limiting current with rotation rate. Between 0.7-1.0 V, the activity changes from reduction to oxidation of hydrogen peroxide very quickly. The potential at which this occurs changes depending on the geometric nature of the surface, the electrolyte and the rotation rate and has been plotted into a table in Figure 138. In these studies, the switchover occurs at a lower potential for single crystals with higher step density. This trend matches that seen for the ORR activity and has been observed for other platinum stepped surfaces[49]. These results show that the hydrogen peroxide oxidation reaction likely occurs over Pt-O surfaces and hydrogen peroxide reduction occurs over PtOH/PtH/bare Pt metal sites.

Surface	Potential for HPR/HPO crossover (vs. Pd/H)
110	0.916
20,19,0	0.899
10,9,0	0.896
540	0.887
320	0.877
210	0.870

Figure 138: Values showing the potential at which the crossover between HPO and HPR for Pt surfaces

Tafel analysis of the hydrogen peroxide results was undertaken. It is more difficult to quantitatively analyse due to the two competing reactions of oxidation and reduction which are both strongly thermodynamically favoured in the potential range studied. Tafel plots were constructed and slopes shown in the figures below. Tafel slopes observed for all [Pt n{110}x{100}] surfaces for hydrogen peroxide reduction varied from 79-170 mV/dec. This is different to experimental data found in reference [49]. Generally, as step density increases, the gradient of the Tafel slope decreases. For the hydrogen peroxide oxidation, Tafel slopes vary from 70-160 mV/dec. The gradient of these slopes did not show a linear trend with increasing step density. Deviations from the theoretically expected straight line is evident at each end of the high or low potential spectrum. This could be a change in mechanism or more likely a deviation from theoretical behaviour predictions. Overall, introduction of more (100) steps to Pt(110) terrace causes a decrease in both ORR and HPOR activity. The Pt(110) is a bit odd however, as it has the highest potential for the HPORR crossover, but not the highest activity for the ORR.
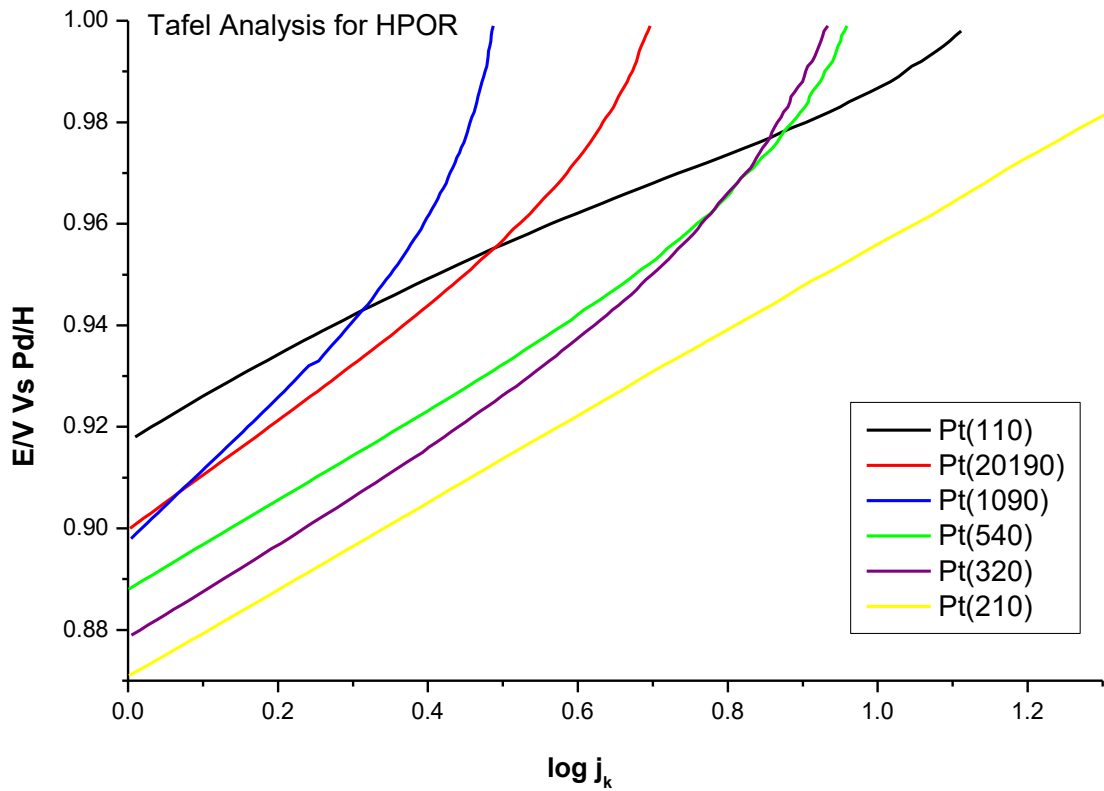
Figure 139: Tafel slopes for HPOR of Pt(S)[n(110)x(100)] surfaces
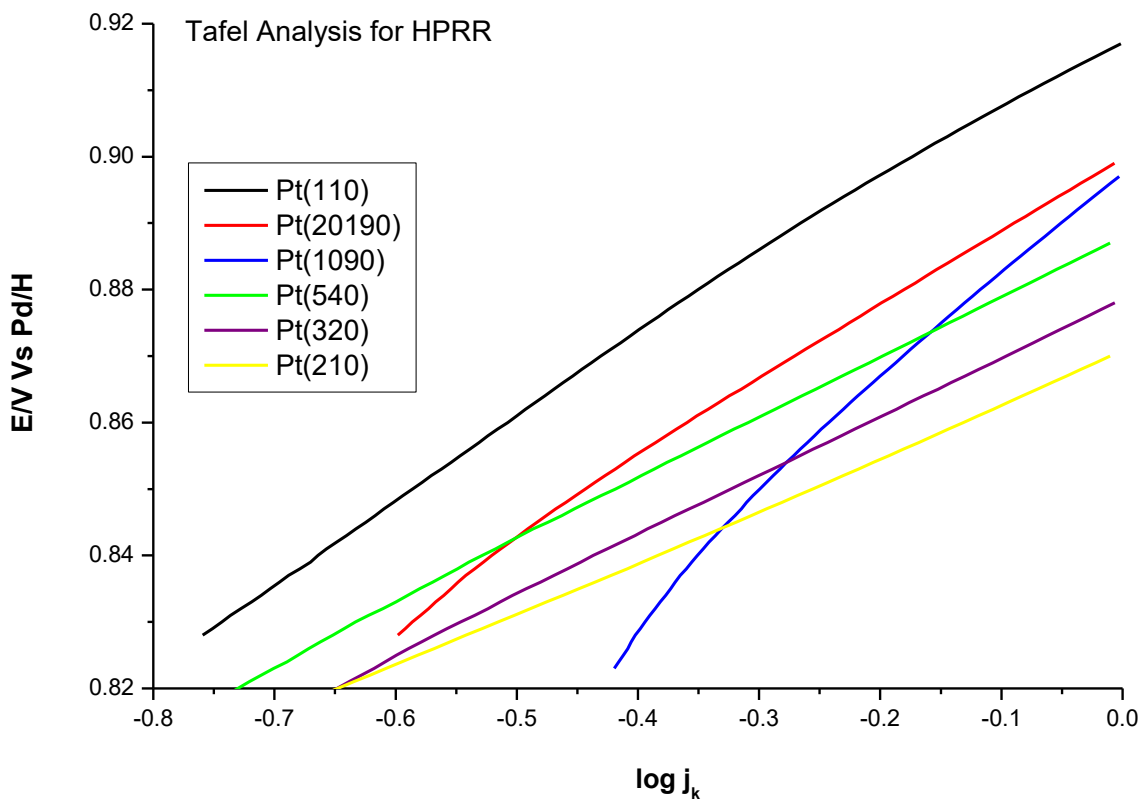

Figure 140: Tafel slopes for HPRR of Pt(S)[n(110)x(100)] surfaces

5.4 Conclusions

A series of stepped Pt electrodes have been prepared (Pt n(100)x(110) and Pt n(110)x(100)). It has been demonstrated that by investigating systematic variations in electrosorption peaks as a function of step density, terrace and step adsorption may be identified. The effect of specific anion adsorption on electrosorption peak potentials may be used to deduce the involvement of adsorbed OH at potentials in the H_{upd} range. The oxide adsorption region on both types of stepped surface were also reported showing distinct adsorption behaviour for step and terrace oxide sites. Nafion adsorption was also investigated and the structure sensitivity of Nafion adsorption was confirmed in that so-called "Nafion spikes", characteristic of terrace adsorption were modulated strongly upon the introduction of steps as indeed where H_{upd} sites negative of the PZTC found in pure perchloric acid media. Interestingly, the Nafion spike persists on Pt(110) terrace-containing surfaces up to the turning point of the zone (Pt(210)) suggesting that Pt(110) terrace sites afford a specific affinity for sulphonate groups contained within the Nafion adlayer. In contrast, for Pt n(100)x(110) surfaces, rapid quenching of the Nafion spike as a function of increasing step density is observed. Reactivity measurements involving oxygen reduction and hydrogen peroxide oxidation/reduction largely revealed the importance of adsorbed oxide/OH in regulating activity.

For ORR, the most active electrode surfaces were found to contain sufficient numbers of linear steps such that long range ordered OH adlayers associated with terraces were disrupted thus allowing unfettered access of oxygen molecules to metallic sites. However, too great a density of defect sites would engender surface oxide formation and attenuation in ORR activity leading to a so-called 'volcano-curve' correlation between ORR activity and step density. For hydrogen peroxide, results are in agreement with previous work showing a switchover from reduction to oxidation when surface oxides formed. Little variation in Tafel slope was observed for hydrogen peroxide reactions confirming the mass transport limited nature of the reaction.

5.5 References

[1] V. Climent, J.M. Feliu, Thirty years of platinum single crystal electrochemistry, Journal of Solid State Electrochemistry 15(7-8) (2011) 1297-1315.

[2] J. Clavilier, R. Faure, G. Guinet, R. Durand, Preparation of mono-crystalline Pt microelectrodes and electrochemical study of the plane surfaces cut in the direction of the (111) and (110) planes, Journal of Electroanalytical Chemistry 107(1) (1980) 205-209.

[3] F. Maillard, P. Sergey, E. Savinova, Size Effects in Electrocatalysis of Fuel Cell Reactions on Supported Metal Nanoparticles, (2008) 507--566.

[4] J.B. Wu, H. Yang, Platinum-Based Oxygen Reduction Electrocatalysts, Accounts of Chemical Research 46(8) (2013) 1848-1857.

[5] K. Wandelt, Properties and influence of surface-defects, Surface Science 251 (1991) 387-395.

[6] M. Bowker, The basis and applications of Hetergenous catalysis, Oxford University Press, Oxford, 1998.

[7] B. Lindstrom, L.J. Pettersson, A brief history of catalysis, Cattech 7(4) (2003) 130-138.

[8] P.P. Lopes, D. Strmcnik, D. Tripkovic, J.G. Connell, V. Stamenkovic, N.M. Markovic, Relationships between Atomic Level Surface Structure and Stability/Activity of Platinum Surface Atoms in Aqueous Environments, ACS Catalysis 6(4) (2016) 2536-2544.

[9] J. Clavilier, D. Armand, S.G. Sun, M. Petit, Electrochemical adsorption behaviour of platinum stepped surfaces in sulfuric-acid solutions, Journal of Electroanalytical Chemistry 205(1-2) (1986) 267-277.

[10] N.M. Markovic, N.S. Marinkovic, R.R. Adzic, Electrosorption of hydrogen and sulfuric acid anions on single crystal platinum stepped surfaces. 1.The 110 zone., Journal of Electroanalytical Chemistry 241(1-2) (1988) 309-328.

[11] P.N. Ross, The role of defects in the specific adsorption of anions on Pt(111), Journal De Chimie Physique Et De Physico-Chimie Biologique 88(7-8) (1991) 1353-1380.

[12] N. Hoshi, S. Kawatani, M. Kudo, Y. Hori, Significant enhancement of the electrochemical reduction of CO2 at the kink sites on Pt(S)-n(110) x (100) and Pt(S)-n(100) x (110), Journal of Electroanalytical Chemistry 467(1-2) (1999) 67-73.

[13] V. Climent, N. Garcia-Araez, E. Herrero, J. Feliu, Potential of zero total charge of platinum single crystals: A local approach to stepped surfaces vicinal to Pt(111), Russian Journal of Electrochemistry 42(11) (2006) 1145-1160.

[14] R. Francke, V. Climent, H. Baltruschat, J.M. Feliu, Electrochemical deposition of copper on stepped platinum surfaces in the 01(1)over-bar zone vicinal to the (100) plane, Journal of Electroanalytical Chemistry 624(1-2) (2008) 228-240.

[15] F.J. Vidal-Iglesias, J. Solla-Gullon, J.M. Campina, E. Herrero, A. Aldaz, J.M. Feliu, CO monolayer oxidation on stepped Pt(S) (n-1)(100) x (110) surfaces, Electrochimica Acta 54(19) (2009) 4459-4466.

[16] R.M. Aran-Ais, M.C. Figueiredo, F.J. Vidal-Iglesias, V. Climent, E. Herrero, J.M. Feliu, On the behavior of the Pt(100) and vicinal surfaces in alkaline media, Electrochimica Acta 58 (2011) 184-192.

[17] K. Mikita, M. Nakamura, N. Hoshi, Situ infrared reflection absorption Spectroscopy of carbon monoxide adsorbed on Pt(S)- n(100)x(110) electrodes, Langmuir 23(17) (2007) 9092-9097.

[18] N. Hoshi, A. Nakahara, M. Nakamura, K. Sumitani, O. Sakata, Surface X-ray scattering of high index plane of platinum containing kink atoms in solid-liquid interface: Pt(310)=3(100)-(110), Electrochimica Acta 53(21) (2008) 6070-6075.

[19] S. Motoo, N. Furuya, Electrochemistry of platinum single crystal surfaces. 2.Structural effect on formic-acid oxidation and poison formation on Pt(111), (100) and (110), Journal of Electroanalytical Chemistry 184(2) (1985) 303-316.

[20] J. Souza-Garcia, C.A. Angelucci, V. Climent, J.M. Feliu, Electrochemical features of Pt(S) n(110) x (100) surfaces in acidic media, Electrochemistry Communications 34 (2013) 291-294.

[21] J. Clavilier, R. Durand, G. Guinet, R. Faure, Electrochemical adsorption behaviour of the Pt(100) in sulfuric-acid solution, Journal of Electroanalytical Chemistry 127(1-3) (1981) 281-287.

[22] A. Rodes, J. Clavilier, J.M. Orts, J.M. Feliu, A. Aldaz, Electrochemical-behaviour of Pt(100) in various acidic media. 2.On the relation between the voltammetric profiles induced by anion specific adsorption studied with a transfer technnique preserving surface cleanliness and structure, Journal of Electroanalytical Chemistry 338(1-2) (1992) 317-338.

[23] A. Rodes, M.A. Zamakhchari, K. Elachi, J. Clavilier, Electrochemical behaviour of Pt(100) in various acidic media. 1.On a new voltammetric profile of Pt(100) in perchloric-acid and effects of surface defects., Journal of Electroanalytical Chemistry 305(1) (1991) 115-129.

[24] N. Garcia-Araez, V. Climent, E. Herrero, J.M. Feliu, On the electrochemical behavior of the Pt(100) vicinal surfaces in bromide solutions, Surface Science 560(1-3) (2004) 269-284.

[25] N. Garcia-Araez, V. Climent, E. Herrero, J. Feliu, J. Lipkowski, Thermodynamic studies of chloride adsorption at the Pt(111) electrode surface from 0.1 M HClO4 Solution, Journal of Electroanalytical Chemistry 576(1) (2005) 33-41.

[26] N. Garcia-Araez, V. Climent, J. Feliu, Potential-Dependent Water Orientation on Pt(111), Pt(100), and Pt(110), As Inferred from Laser-Pulsed Experiments. Electrostatic and Chemical Effects, Journal of Physical Chemistry C 113(21) (2009) 9290-9304.

[27] N. Hoshi, T. Suzuki, Y. Hori, Catalytic activity of CO2 reduction on Pt single-crystal electrodes: Pt(S)- n(111)x(111) , Pt(S)- n(111)x(100) , and Pt(S)- n(100)x(111), Journal of Physical Chemistry B 101(42) (1997) 8520-8524.

[28] A. Ferre-Vilaplana, R. Gisbert, E. Herrero, On the electrochemical properties of platinum stepped surfaces vicinal to the (100) pole. A computational study, Electrochimica Acta 125 (2014) 666-673.

[29] G.A. Attard, R. Price, Electrochemical investigation of a structure sensitive growth mode - palladium deposition on Pt(100)-Hex-R0.7-Degrees and Pt(100)-(1x1), Surface Science 335(1-3) (1995) 63-74.

[30] P.T. Kissinger, W.R. Heineman, Cyclic Voltammetry, Journal of Chemical Education 60(9) (1983) 702-706.

[31] D.M. Kolb, Electrochemical surface science, Angewandte Chemie-International Edition 40(7) (2001) 1162-1181.

[32] J. Inukai, M. Ito, Electrodeposition processes of palladium and rhodium monolayers on Pt(111) and Pt(100) electrodes studied by IR reflection-absorption spectroscopy, Journal of Electroanalytical Chemistry 358(1-2) (1993) 307-315.

[33] F.C. Nart, T. Iwasita, M. Weber, Sulfate adsorption on well-defined Pt(100) electrodes, Electrochimica Acta 39(13) (1994) 2093-2096.

[34] D.V. Heyd, D.A. Harrington, Platinum oxide-growth kinetics for cyclic voltammetry, Journal of Electroanalytical Chemistry 335(1-2) (1992) 19-31.

[35] S.D. James, Multilayer oxide films on anodized platinum, Journal of the Electrochemical Society 116(12) (1969) 1681-&.

[36] D. Armand, J. Clavilier, Influenceof specific adsorption of anions on the electrochemical-behaviour of the Pt(100) surface in acid-medium - comparisons with Pt(111), Journal of Electroanalytical Chemistry 270(1-2) (1989) 331-347.

[37] N.S. Marinkovic, N.M. Markovic, R.R. Adzic, Hydrogen adsorption on single-crystal platinum electrodes in alkaline solutions, Journal of Electroanalytical Chemistry 330(1-2) (1992) 433-452.

[38] M. Ahmed, D. Morgan, G.A. Attard, E. Wright, D. Thompsett, J. Sharman, Unprecedented Structural Sensitivity toward Average Terrace Width: Nafion Adsorption at Pt{hkl} Electrodes, Journal of Physical Chemistry C 115(34) (2011) 17020-17027.

[39] R. Subbaraman, D. Strmcnik, V. Stamenkovic, N.M. Markovic, Three Phase Interfaces at Electrified Metal-Solid Electrolyte Systems 1. Study of the Pt(hkl)-Nafion Interface, Journal of Physical Chemistry C 114(18) (2010) 8414-8422.

[40] K. Domke, E. Herrero, A. Rodes, J.M. Feliu, Determination of the potentials of zero total charge of Pt(100) stepped surfaces in the 01(1)-over-bar zone. Effect of the step density and anion adsorption, Journal of Electroanalytical Chemistry 552 (2003) 115-128.

[41] A.N. Frumkin, O.A. Petrii, B.B. Damaskin, Comprehensive Treatise of Electrochemistry, 1980.

[42] N.M. Markovic, R.R. Adzic, B.D. Cahan, E.B. Yeager, Structural effects in electrocatalysis - oxygen redution on platinum low-index single crystal surfaces in perchloric acid solutions, Journal of Electroanalytical Chemistry 377(1-2) (1994) 249-259.

[43] N.M. Markovic, H.A. Gasteiger, N. Philip, Oxygen reduction on platinum low-index single-crystal surfaces in alkaline solution: Rotating ring disk(Pt(hkl)) studies, Journal of Physical Chemistry 100(16) (1996) 6715-6721.

[44] I. Katsounaros, W.B. Schneider, J.C. Meier, U. Benedikt, P.U. Biedermann, A.A. Auer, K.J.J. Mayrhofer, Hydrogen peroxide electrochemistry on platinum: towards understanding the oxygen reduction reaction mechanism, Physical Chemistry Chemical Physics 14(20) (2012) 7384-7391.

[45] N.M. Markovic, T.J. Schmidt, V. Stamenkovic, P.N. Ross, Oxygen Reduction Reaction on Pt and Pt Bimetallic Surfaces: A Selective Review, Fuel Cells 1(2) (2001) 105-116.

[46] A. Kuzume, E. Herrero, J.M. Feliu, Oxygen reduction on stepped platinum surfaces in acidic media, Journal of Electroanalytical Chemistry 599(2) (2007) 333-343.

[47] S. Treimer, A. Tang, D.C. Johnson, A consideration of the application of Koutecky-Levich plots in the diagnoses of charge-transfer mechanisms at rotated disk electrodes, Electroanalysis 14(3) (2002) 165-171.

[48] R. Subbaraman, D. Strmcnik, A.P. Paulikas, V.R. Stamenkovic, N.M. Markovic, Oxygen Reduction Reaction at Three-Phase Interfaces, Chemphyschem 11(13) (2010) 2825-2833.

[49] A. Brew, *Electrochemical studies of the oxygen reduction reaction: platinum and platinum bimetallic single crystal electrodes.* Electrochemical studies of the oxygen reduction reaction: platinum and platinum bimetallic single crystal electrodes., Chemistry, Cardiff University, 2015.

[50] J.X. Wang, N.M. Markovic, R.R. Adzic, Kinetic analysis of oxygen reduction on Pt(111) in acid solutions: Intrinsic kinetic parameters and anion adsorption effects, Journal of Physical Chemistry B 108(13) (2004) 4127-4133.

[51] A.M. Gomez-Marin, R. Rizo, J.M. Feliu, Some reflections on the understanding of the oxygen reduction reaction at Pt(111), Beilstein Journal of Nanotechnology 4 (2013) 956-967.

[52] R. Rizo, E. Herrero, J.M. Feliu, Oxygen reduction reaction on stepped platinum surfaces in alkaline media, Physical Chemistry Chemical Physics 15(37) (2013) 15416-15425.

[53] J.A. Keith, G. Jerkiewicz, T. Jacob, Theoretical Investigations of the Oxygen Reduction Reaction on Pt(111), Chemphyschem 11(13) (2010) 2779-2794.

[54] A. Bjoerling, E. Herrero, J.M. Feliu, Electrochemical Oxidation of Pt(111) Vicinal Surfaces: Effects of Surface Structure and Specific Anion Adsorption, Journal of Physical Chemistry C 115(31) (2011) 15509-15515.

[55] J. Greeley, J. Rossmeisl, A. Hellman, J.K. Norskov, Theoretical trends in particle size effects for the oxygen reduction reaction, Zeitschrift Fur Physikalische Chemie-International Journal of Research in Physical Chemistry & Chemical Physics 221(9-10) (2007) 1209-1220.

[56] A.M. Gomez-Marin, K.J.P. Schouten, M.T.M. Koper, J.M. Feliu, Interaction of hydrogen peroxide with a Pt(111) electrode, Electrochemistry Communications 22 (2012) 153-156.

[57] A.M. Gomez-Marin, R. Rizo, J.M. Feliu, Oxygen reduction reaction at Pt single crystals: a critical overview, Catalysis Science & Technology 4(6) (2014) 1685-1698.

[58] G.A. Attard, A. Brew, Cyclic voltammetry and oxygen reduction activity of the Pt{110}-(1 x 1) surface, Journal of Electroanalytical Chemistry 747 (2015) 123-129.

Probing the nature of electrochemical oxides on Pt(*hkl*) single crystal surfaces
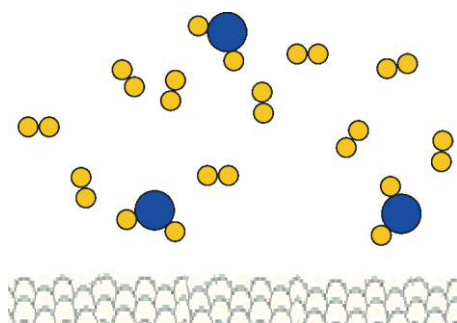
6.1 Introduction

Electrochemical oxides on platinum electrodes cause a sharp decline in activity for the ORR. The exact role of how such species inhibit the ORR is not well understood. If improvements in the ORR are to be made, more information about the nature of electrochemical oxide growth on platinum ('PtO') is needed, and the right approach for the improved design of electrocatalysts for fuel cell cathodes can be made. The mechanism of PtO formation is an important topic of experimental and theoretical research in this, and stimulates much debate in the electrochemical community[1-3]. There is a large amount of literature attempting to elucidate the oxide growth on platinum, some that have since been published after the present study was completed.[4-8] In particular, previous studies have addressed the mechanism of Pt oxide growth. Some have assumed a hydroxide species is firstly deposited with varying configurations/stoichiometry during the stages of oxide growth, matching oxide electrosorption peaks/charges seen in the voltammogram[8, 9]. Contrary to this, other conclusions from electrochemical and spectroscopic studies on a platinum wire electrode in aqueous sulphuric acid gave oxide as the chemisorbed species[10], however this could be due to the strongly adsorbing nature of the bisulphate anion present which is known to block OH adsorption[11, 12].

This chapter attempts to further investigate the nucleation and growth of electrochemical oxides on well-defined Pt single crystal electrodes as model electrocatalytic surfaces. Three investigations have been carried out:

1. Holding of the potential constant at the commencement of oxide formation to understand the growth behaviour and rate of electrochemical oxide formation on platinum.

2. Using chronoamperometry to gain further kinetic information concerning with rates of oxide growth on single crystal surfaces.

3. Investigating how fast potential scanning of platinum single crystal electrodes affects the surface structure and the behaviour of adsorbing/desorbing species.

6.2 Investigating the role of potential and time on Electrochemical Oxide growth

Multiple voltammetric investigations have been undertaken regarding the role of potential and time on electrochemical oxide formation and stripping. These effects have been studied on Pt basal and stepped Pt(s)[n{100}x{110}] single crystal electrodes in perchloric acid, as well as sulphate and chloride-containing electrolytes. In this study, the effect of holding the potential at 1 V for various lengths of time was undertaken and the subsequent voltammograms measured. Previously, surface disordering experiments showed features in platinum single crystal CVs that affect surface composition when scanning above 1.15 V (vs Pd/H) for Pt{111}[13]. As a consequence, a potential of 1 V was chosen for the current potential hold experiments. At this potential, initial stages of oxide formation are relevant but there is limited possibility of sub-surface oxide adsorption. Thermal oxides (from flame annealing) were stripped from the surface by running a negative going potential sweep before the potential holding experiment was undertaken. This allowed the study of electrochemically formed oxides exclusively. A model of how the oxygen reduction reaction (ORR) kinetics are influenced by surface structure and electrochemical oxide formation is presented.

6.2.1. The role of potential and time upon cyclic voltammograms

6.2.1.1. Pt{111}

The effect upon the CV of Pt{111} of holding the potential at 1 V for various lengths of time are shown in Figure 141. The Pt{111} plane represents the most stable facet on Pt nanoparticles, which are widely used as ORR catalyst in polymer electrolyte membrane fuel cells[14, 15]. Initial inspection of the results in Figure 141 for Pt{111}, show that holding the potential at 1 V encourages the adsorption of oxide species onto the surface. This is evident by the increase in the electrosorption stripping charge between 0.5 and 1 V relative to the "clean" Pt{111} curve (black line). There is no direct correlation between the amount of time the potential is held and the amount of oxide adsorbed, suggesting a saturation point of oxides on the surface or change in oxide formation as holding time is varied. Specifically, the hydrogen underpotential deposition (H_{upd}) region is unperturbed as all CV profiles match between 0-0.4 V; including the "clean" Pt{111} electrode (which

has only been scanned in a potential region where no oxide species adsorb, 0-0.85 V). The broad, so-called "butterfly" peak at ~0.72 V, (which is known to correspond to highly ordered adsorption/desorption of OH species on Pt{111} terraces), does not lose its sharpness, but simply modifies what would be the normal "Gaussian" shape obtained from a normal oxide stripping peak. Pt{111} fcc terraces are known to be stable up to 1.15 V in HClO$_4$ electrolytes and therefore the main conclusion here is that electrosorbed oxides adsorbed at potentials of 1 V do not perturb the underlying Pt{111} structure with time. This shows that at this potential, sub-surface oxides are not present. A positive sweep from 0-0.85 V, after each experiment showed that the Pt{111} terrace was not reconstructed. In fact, this result agrees with surface studies of oxygen adsorption on Pt{111}, which show that so long as the coverage of oxygen adatoms remains less than 0.25 monolayers, no surface restructuring will occur[16, 17]. Oxygen coverages exceeding a critical value such as 0.25 on Pt{111} lead to restructuring[18]. Hence, in the present electrochemical studies, it may be useful to bear this fact in mind since if applicable, it explains why even electrochemical oxide, so long as it is only a 'small' amount, should not lead to surface modifications. This may be confirmed by inspection of the many CVs in the present study which adsorb oxide up to 0.85 V reversibly. However, if more positive potentials are accessed then irreversibility in the oxide stripping peak begins to occur together with changes in the H$_{upd}$ voltammetric response.

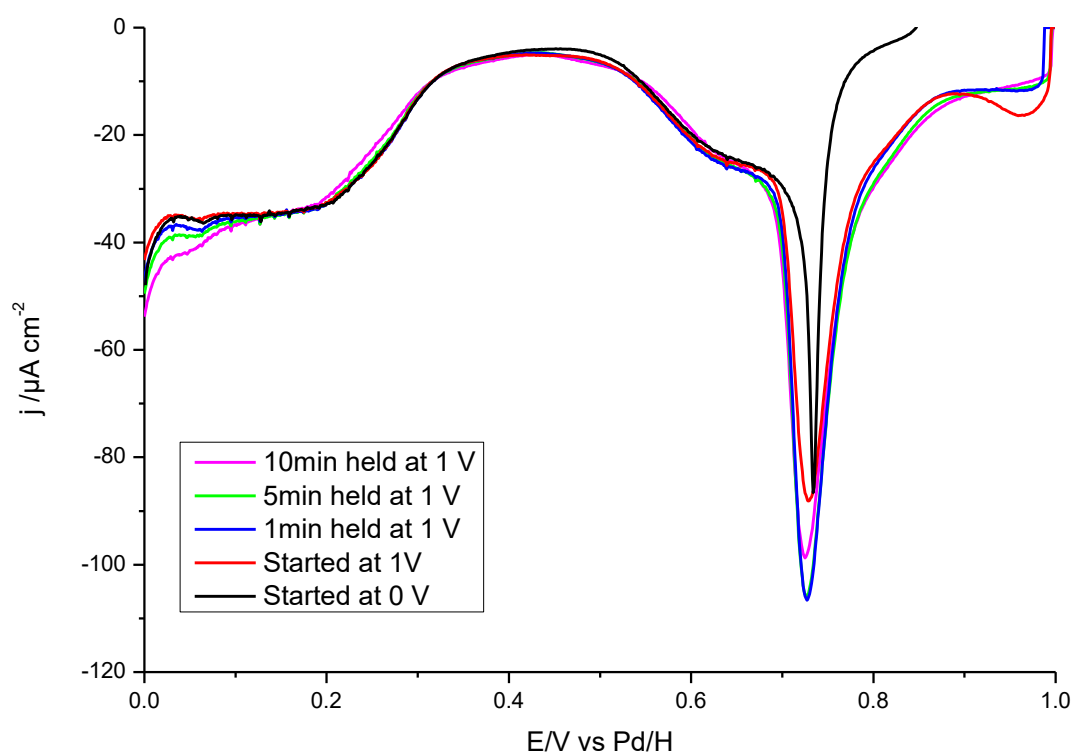Figure 141: CVs of Pt{111} (1st negative going sweep from 1 V) where potential was held at 1V (pre-scans) for differing times in 0.1M HClO$_4$, scan rate 50mV/s

6.2.1.2. Pt{100}

The results for the Pt{100} electrode of holding the potential at 1 V are shown in Figure 142. The {100} surface is a "more open", less densely packed arrangement of platinum atoms than Pt{111} and therefore is more prone to reconstruction (roughening) by oxide formation. Unlike for Pt{111}, which only electrosorbs oxide (reversibly) up to 0.85 V (for Pt{111} a potential up to 1 – 1.2 V is possible).

Unsurprisingly, initial observation shows larger amounts of oxide being desorbed in the potential region 0.75-0.95V, compared to Pt{111}. Again, time does not affect the amount of oxide adsorbed, but its stripping peak (~0.7-0.9 V) does shift to a more negative potential and broadens slightly. This can be ascribed to the slow reconstruction of the Pt{100} terrace, as the oxide layer is held for longer and longer periods of time. Hence, the peak at most positive potentials (0.87 V) corresponds to oxide on Pt{100}-(1x1), but slowly, place-exchange occurs, generating more and more step sites and therefore a drift to more negative potentials for the oxide stripping peak (oxide held more strongly at steps than terraces – see later).

Two sharp 'mystery peaks' appear in the H_{upd} region of Pt{100} at ~0.18 V and ~0.26 V) following the stripping of the oxide. The peak at ~ 0.26 V decreases in intensity as the potential is held for longer, whereas the peak at ~ 0.18 V increases in magnitude. One reason could be reconstruction of the clean surface by the adsorbed (then desorbed) oxide, followed by lifting of the reconstruction by adsorbed hydrogen. Hypothetically, sub-surface oxides could already be forming at 1 V for this surface. A positive sweep from 0 to 0.85 V reveals that Pt{100}-(1x1) terraces are reconstructed, unlike what was observed for the Pt{111} results as signified by the appearance of new H_{upd} states around 0.21 V corresponding to step sites[19-21]. Another reason for these mystery peaks could be the stripping of a strongly adsorbed anion impurity picked up during holding of the potential; although if this were true, one would expect the positive going CV from 0 V to return to its original profile, which it didn't. Finally, the breakdown of perchlorate to chloride anions could also generate a similar effect. These possible reasons for the appearances of the stripping peaks at potentials < 0.25 V will be explored in more detail later.
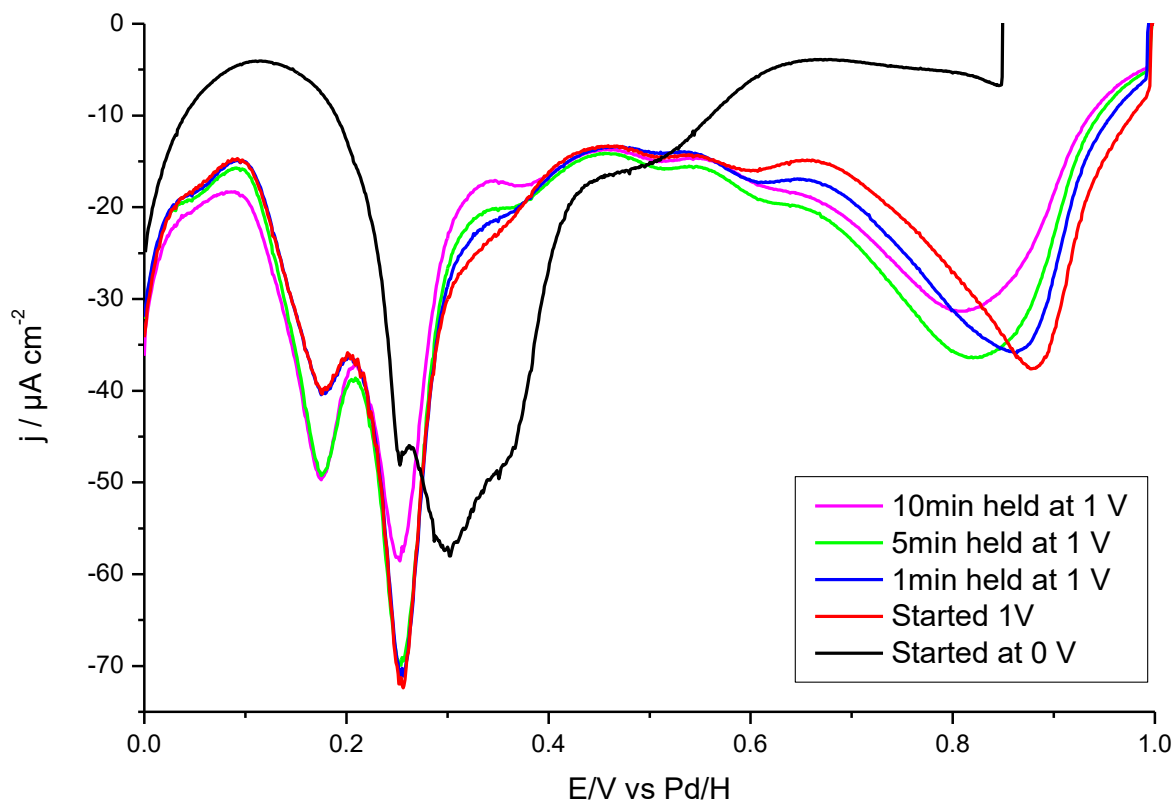
Figure 142: CVs of Pt{100} (1st negative going sweep from 1 V) where potential was held at 1V (pre-scans) for differing times in 0.1M HClO₄, scan rate 50mV/s

6.2.1.2.1. Investigating the nature of the "mystery" peaks

Previously, platinum surfaces containing {100} terraces showed two "mystery" peaks in the H_{upd} region following oxide adsorption and desorption. To try to understand the true nature of the "mystery" peaks, a stock solution of KCl was sequentially added in an electrochemical cell containing 0.1 M HClO₄. CVs were recorded after each amount was added. By adding chloride anions into solution it could be determined if peaks observed are from the breakdown of perchlorate.
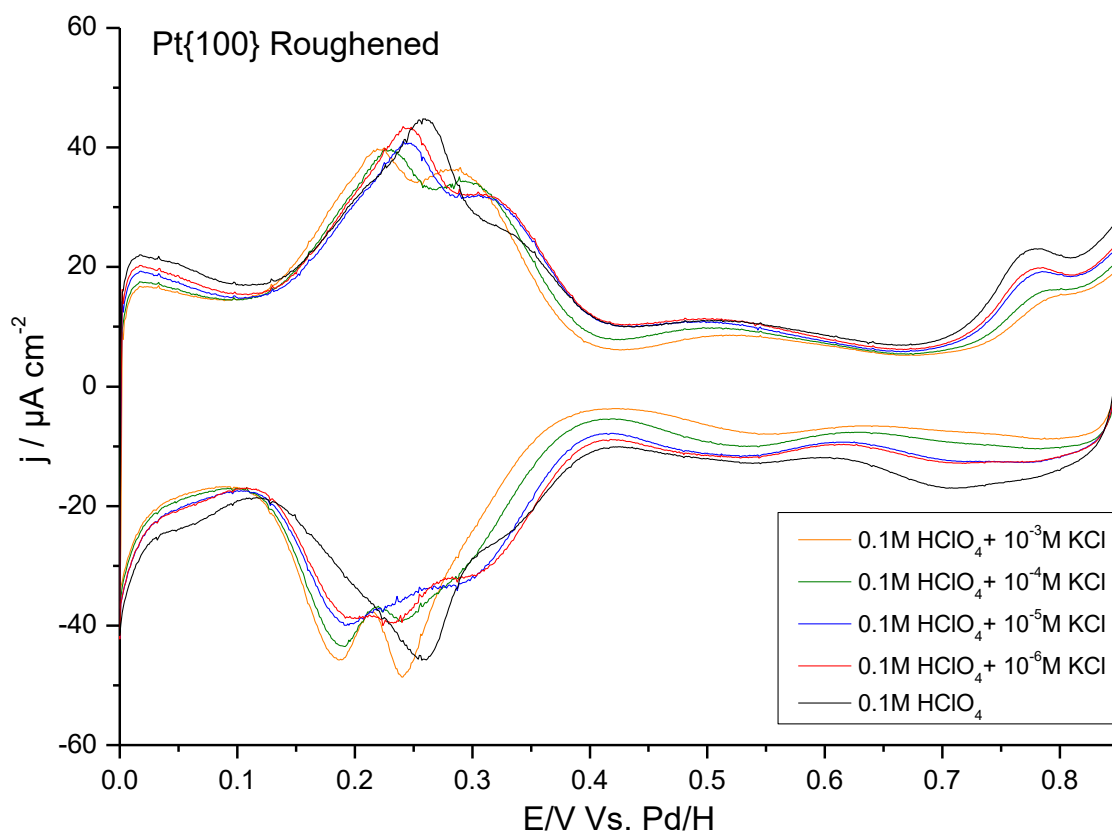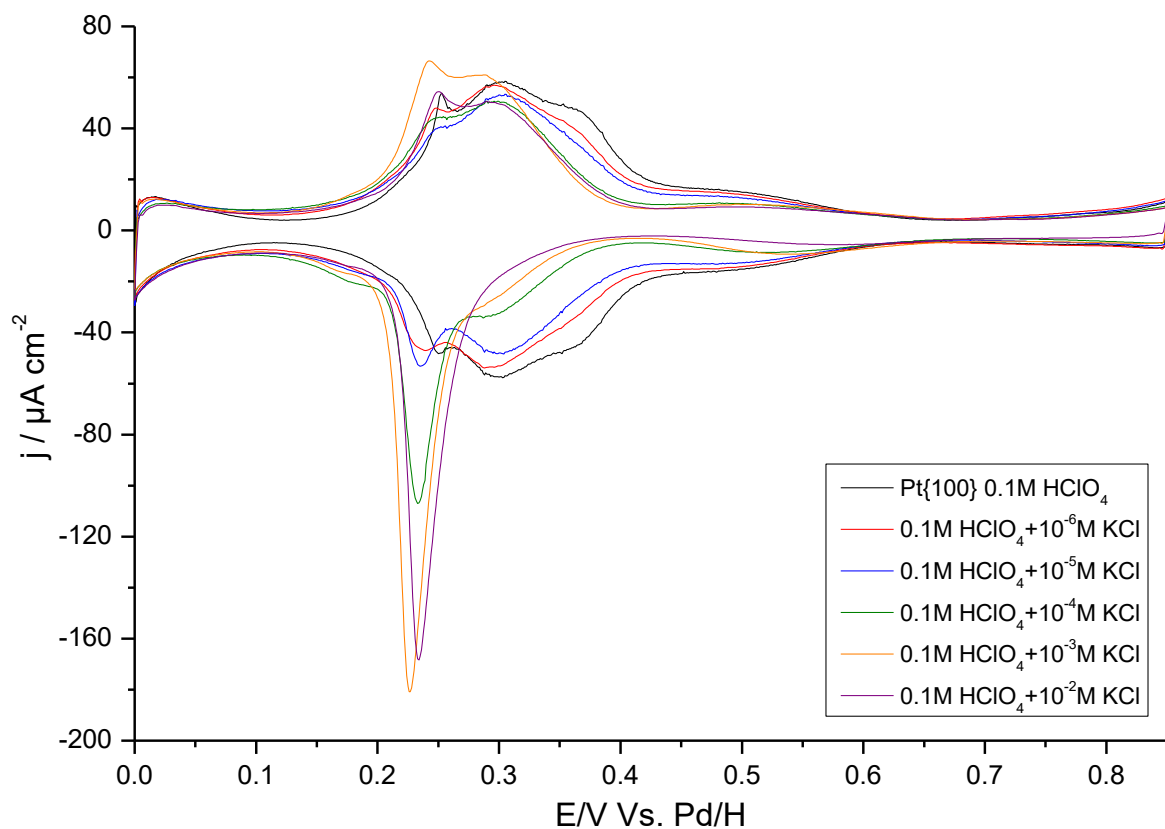
Figure 143: CVs showing the result of addition of KCl for smooth and electrochemically roughened Pt{100}, 0.1M HClO₄ solution, scan rate 50mV/s

The addition of chloride to the perchloric acid electrolyte shows the diminution of features related

to ordered Pt{100} terrace in perchloric acid between 0.25 and 0.6 V, along with the development of

a desorption peak at ~0.23 V. This is expected as Cl⁻ is a strongly adsorbing anion and blocks all OH and H_{upd} features unless a more negative potential is reached. The potential at which the chloride anion desorbs is comparable to one of the mystery peaks seen in earlier experiments. This experiment was conducted on both flat and electrochemically roughened Pt{100} to see if the Cl⁻ anion adsorbed at different potentials depending on the presence of terraces or steps. The roughened surface did indeed show the peak at 0.23 V but also an additional desorption peak at 0.18 V, comparable to results seen previously. Although appearing at the same potentials as the mystery peaks, there are small differences. Close inspection shows the magnitude of the "mystery peaks" could not be generated using addition of chloride. As well as this, the solution was tested for its cleanliness, where a flame annealed Pt CV showed no presence of chloride anions. Superficially, the mystery peaks in earlier investigations behave as if a strongly adsorbing anion is present, but that anion cannot be chloride. As a final note, increasing the concentration of KCl led to the peak at 0.17 V being diminished and the peak at ~0.23 V being increased in size on the roughened Pt{100}.

In order to completely eliminate the possibility of perchlorate degradation and chloride formation as a possible explanation of the "mystery" peaks, sulphate solution was added sequentially to the 0.1 M $HClO_4$ electrolyte and changes observed. Once a suitable concentration was added the potential was held at 1V for 0, 1 and 5 minutes followed by oxide stripping. A CV was collected between each experiment to check to cleanliness of the electrolyte after sulphate addition.
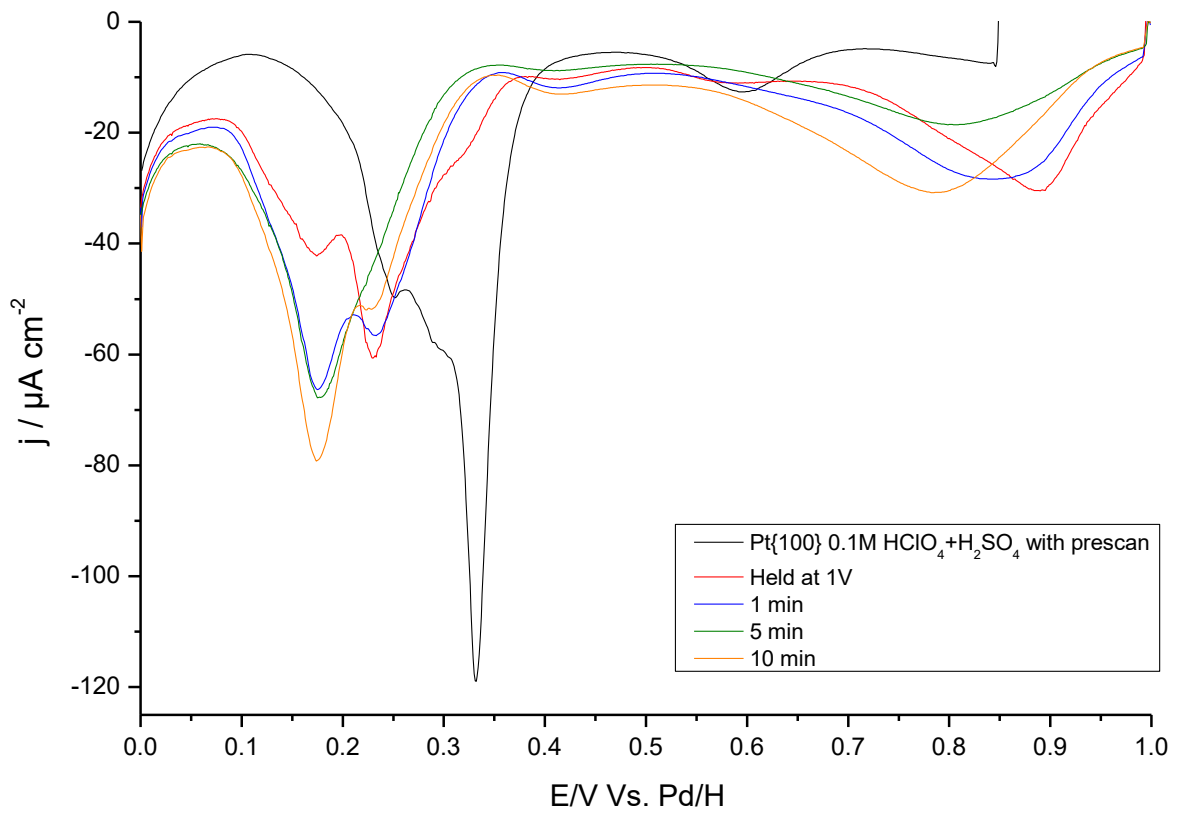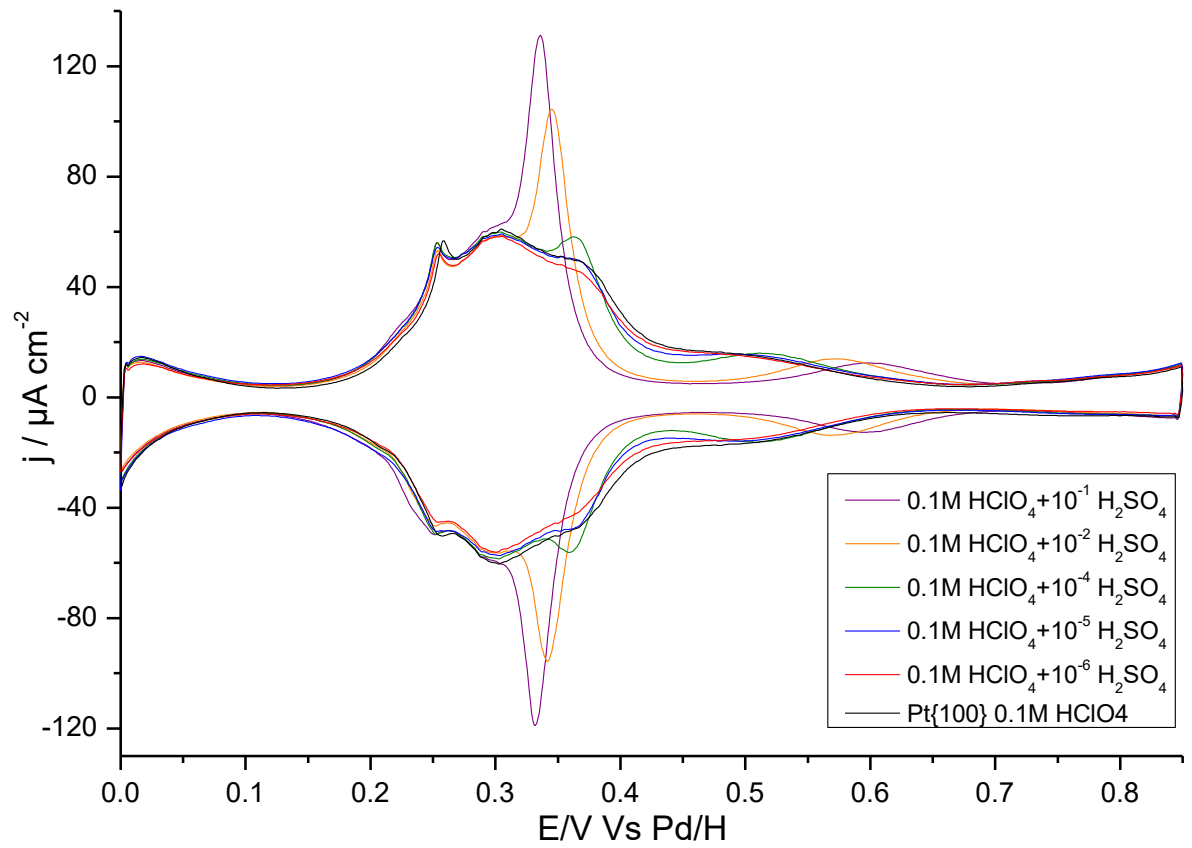
Figure 144: CVs showing the result of addition of H_2SO_4 for Pt{100}, 0.1M $HClO_4$ solution, scan rate 50mV/s

Upon increasing the concentration of sulphate in the solution, the well-defined features for a flame annealed Pt{100} electrode are blocked and there is some growth of peaks attributable to Pt{100} terraces with specifically adsorbed bisulphate (peak at 0.33 V). The sulphate is a much stronger adsorbing anion than perchlorate, which is the reason this change is observed (shift of OH at 0.45 V to peak at 0.55 V and H_{upd} at 0.37 V shifting to 0.33 V).

Holding the potential at 1 V in the sulphate spiked solution, results in similar features to those seen in the initial studies. As there is still perchlorate in the cell one could argue that it could be still be decomposing into Cl^- anions but this is unlikely as sulphate is a much more strongly adsorbing anion at these concentrations and would compete successfully with the adsorption of perchlorate. The oxide stripping peak at ~ 0.7-0.9 V shifts negatively with holding time, as expected, since the Pt{100} terraces are simultaneously reconstructing (surface roughening, not forming the clean surface "hex" phase[22]). This is evident by the absence of the peak at 0.33 V associated with sulphate on Pt{100}-(1x1) terraces. We deduce that the 0.23 V peak and the 0.18 V peaks are due to either subsurface oxide or reconstruction of terrace and step sites respectively which relax back to a more normal (terrace and step) configuration after hydrogen is adsorbed.

6.2.1.3. Pt{110}

When subjected to the same conditions, the Pt{110} electrode (Figure 145) shows some similarities to Pt{100} whereby the oxide stripping peak appears in the potential region ~0.7-0.9 V and shifts to more negative potentials as the time of holding the potential at 1 V is increased. There is also a broad peak ~0.3-0.5 V related to desorption of oxide. The H_{upd} peaks associated with the clean Pt{110} surface (0.04 V and 0.18 V) are still visible but seem to be positioned over a feature which increases their overall intensity relative to a surface with no oxide adsorbed. This could be due to similar reasons outlined for Pt{100} such as surface reconstruction from adsorbed oxide species, perchlorate degradation, or even a badly wetting meniscus (the oxide covered surface at this low potential may exhibit a marked change in its surface energy relative to the oxide-free surface) so the meniscus may start to creep along the sides of the crystal resulting in an apparently larger current).
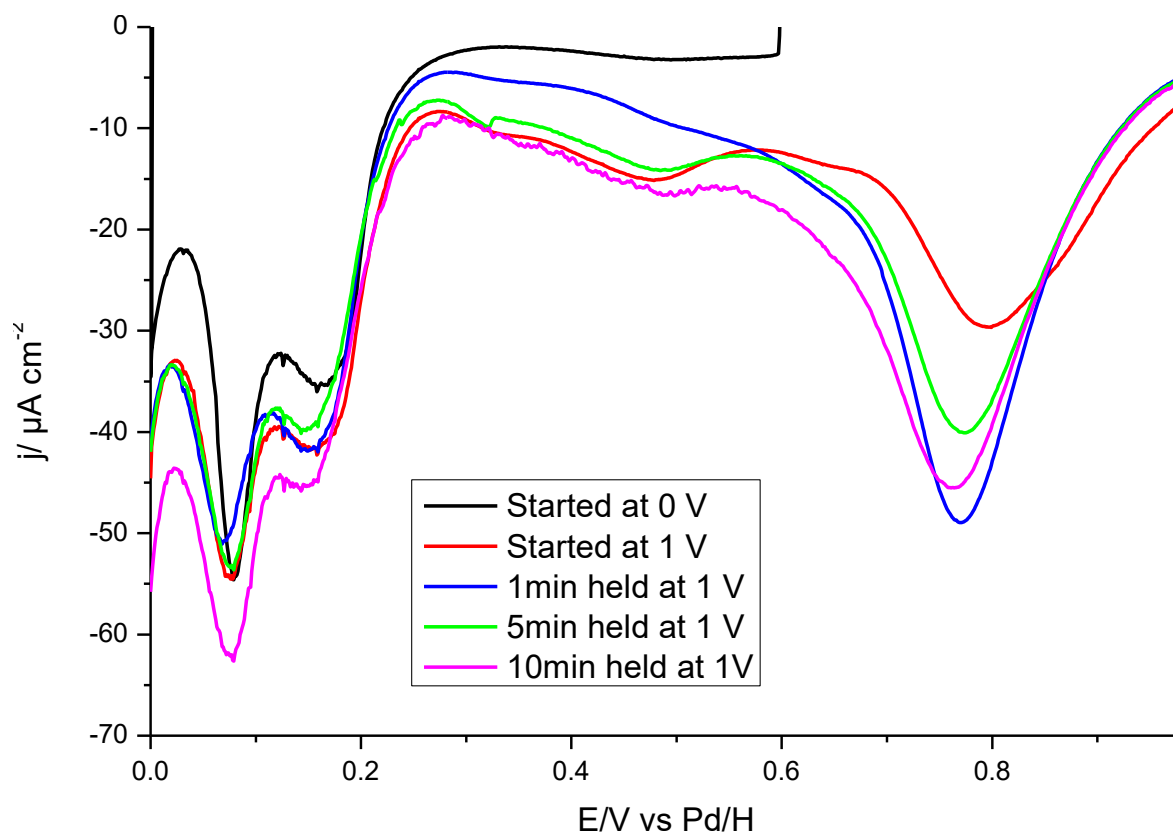
Figure 145: CVs of Pt{110} (1st negative potential sweep from 1 V) where potential was held at 1V for differing times in 0.1M HClO₄, scan rate 50mV/s

6.2.1.4. Stepped Pt Surfaces

The same 'potential-hold' experiments were undertaken on single crystal Pt(s)[n{100}x{110}] surfaces. Analysis of the voltammetric profiles in Figure 146 indicate that single crystal electrodes show a broad oxide stripping peak in the potential region 0.6-0.9 V. This is also seen in Figure 147. As seen for the Pt{100} results, the oxide stripping peak shifts negatively as the time the potential is held increases. The oxide stripping peak sharpens as the single crystal surface becomes more stepped (i.e from Pt{20,1,0}→Pt{210}). The peak also becomes sharper and smoother as a function of time. Two mystery peaks in the H$_{upd}$ region ~ 0.18 V and 0.26 V appear for all surfaces except Pt{210}. The Pt{210} shows an unperturbed H$_{upd}$ region after oxide stripping for the most part. For the other stepped surfaces, the ratio of the mystery peaks changes as the potential holding time increases, where a higher step density favours the peak at the lower potential. The Pt{510} and Pt{310} show two peaks, although they are somewhat slightly merged. Hence, all changes reported above are associated with residual Pt{100} terrace sites being affected by having oxide adsorbed upon them. All stepped electrodes show a monotonically increasing oxide peak intensity as a function of holding time and a decrease in the potential shift seen with Pt{100}. Based on the fact

that close inspection reveals two oxide stripping peaks at 0.9 and 0.75 V with the 0.9 V peak decreasing in intensity as step density increases leaving behind the single 0.75 V peak, we deduce that the former is due to stripping from terrace sites and the latter (0.75 V) peak stripping of oxide from defect sites. Thus the so-called 'potential shift' observed on Pt{100} may be confirmed as greater and greater generation of defects. Hence, the red curve in the voltammograms signifies the least defective surface since the 0.9 V stripping peak is the largest of all surfaces studied.
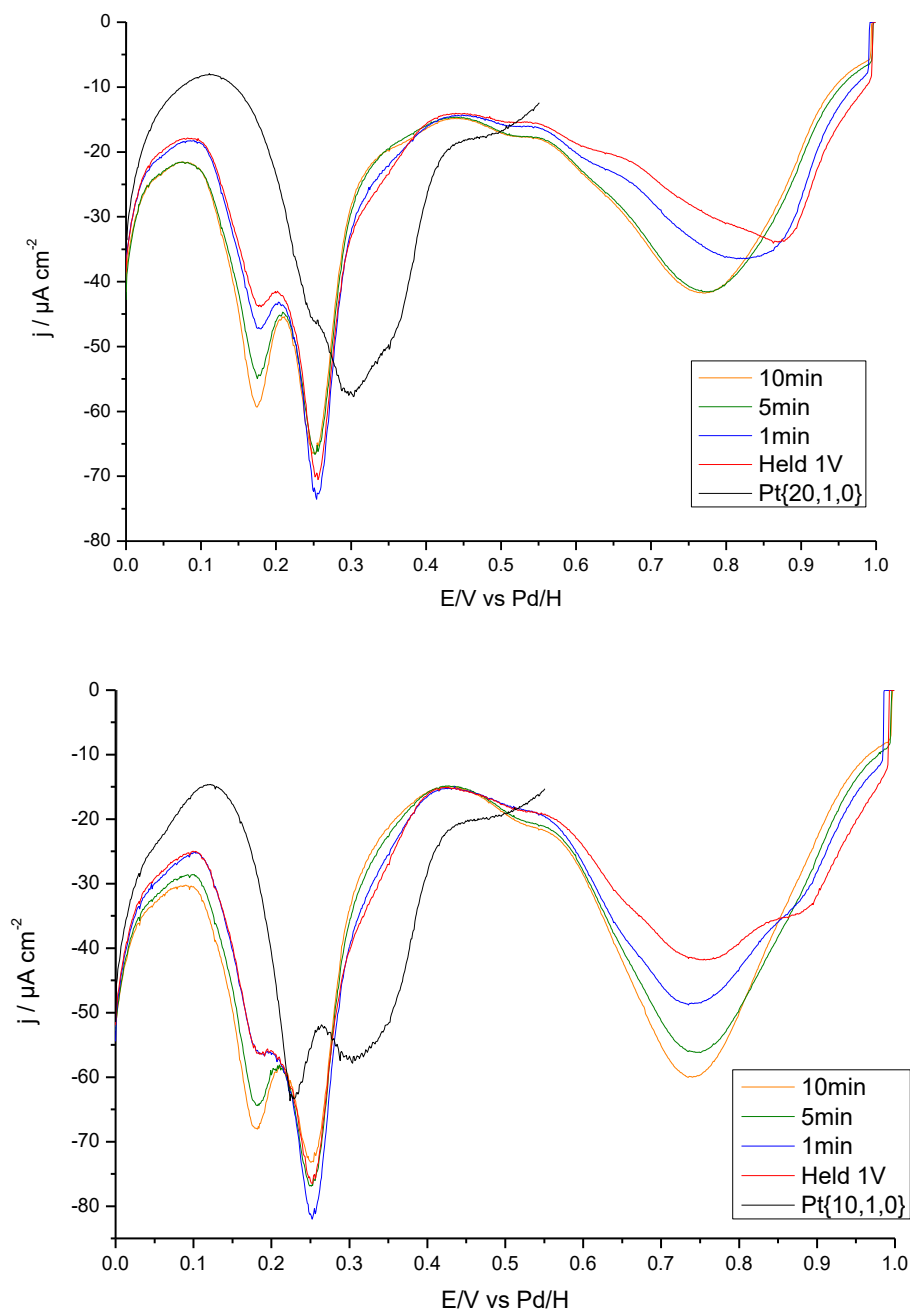

Figure 146: CVs of Pt{20,1,0} and Pt{10,1,0} (1st negative going sweep from 1 V) where potential was held at 1V (pre-scans) for differing times in 0.1M HClO4, scan rate 50mV/s
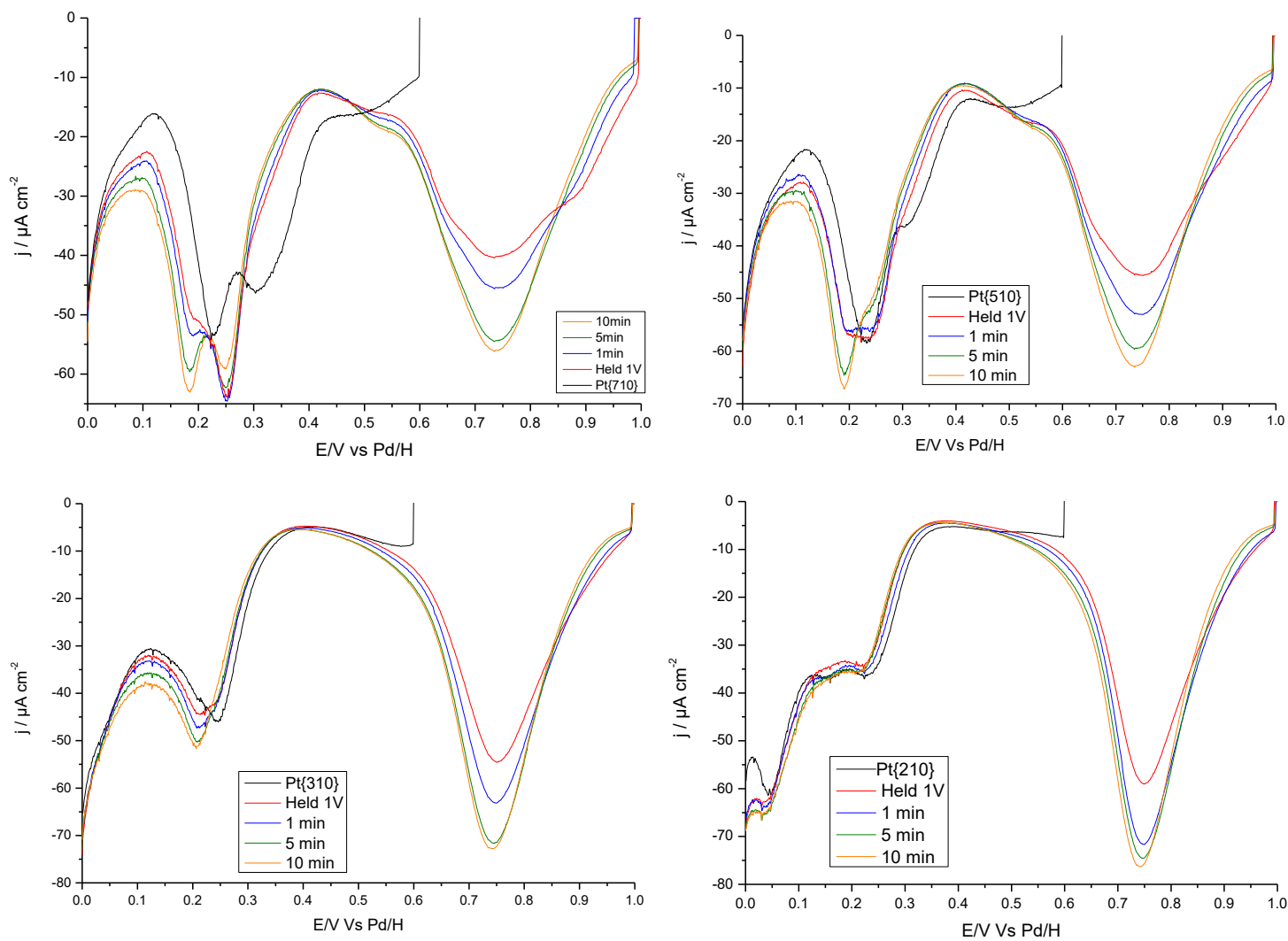
Figure 147: CVs of Pt{710}, Pt{510}, Pt{310} and Pt{210} (1st negative going sweep from 1 V) where potential was held at 1V for differing times in 0.1M HClO$_4$, scan rate 50mV/s

6.2.2. Investigations into how the role of potential and time on oxide deposition affects the ORR activity

Adsorbed oxides and surface reconstruction is known to affect the activity for the very important Oxygen Reduction Reaction (ORR). ORR experiments were undertaken in the rotating disc electrode (RDE) cell in a hanging meniscus configuration following potential hold experiments in the stationary voltammetry cell in order to elucidate relationships between the potential hold experiments and the ORR.

Figure 148: ORR curves for Pt{111} holding the potential in the RDE cell. 0.1 M HClO₄, scan rate 30mV/s. Expanded region used to determine $E_{1/2}$ is shown as inset.

The effect upon the activity of Pt{111} towards the ORR after holding the potential at 1V is shown in Figure 148. Broadly speaking, as time is increased (and consequently the amount of electrosorbed oxide) the ORR reaction is increasingly inhibited. Since ORR only occurs on metallic sites, if electrosorbed oxide is present, this must be removed before ORR can take place and hence, a reduction in ORR activity is generally seen with increasing amounts of electrosorbed oxide. However, the ORR activity of Pt{111} has not been affected significantly by holding the potential at 1 V in accordance with the known structural stability of this plane. This correlates with the effect seen in

the stationary cyclic voltammograms, where only a slight deviation from the normal CV was observed. The exact trend of decreasing activity is (where time potential held at 1V): 0min>5 min>1 min>10 min. Hence, because the amount of electrosorbed oxide after loading is below the critical amount necessary to cause reconstruction, once it is stripped off in the negative going ORR potential cycle, the electrode surface returns to its original state.
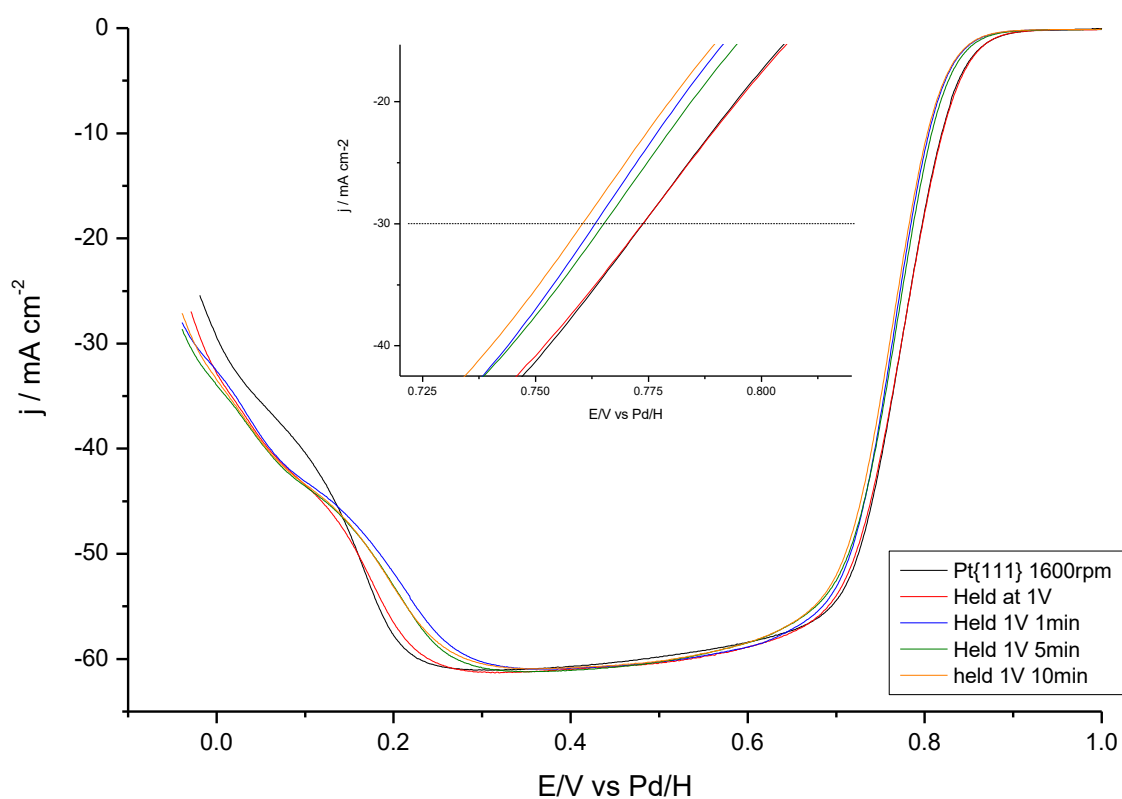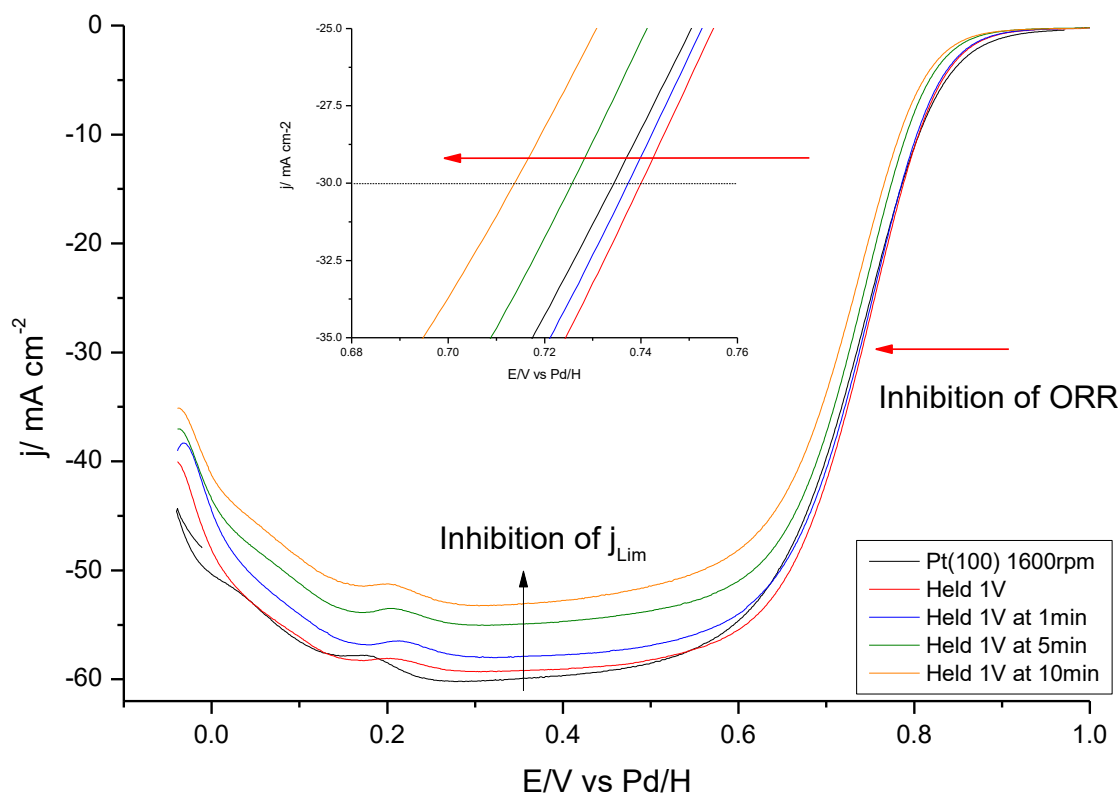

Figure 149: ORR curves for Pt{100} holding the potential in the RDE cell. 0.1M HClO₄, scan rate 30mV/s. Expanded region used to determine E$_{1/2}$ is shown as inset.

The effect of holding the potential at 1 V on the ORR for Pt{100} is shown in Figure 149. Generally, as the time held at 1 V is increased the ORR activity is inhibited as shown by the red arrow. A closer view of the ORR curves around E$_{1/2}$ is also shown inset. Remarkably, there is a strong inhibition of the limiting current, (shown by the black arrow), unlike the results for Pt{111}. This could be due to some hydrogen peroxide being present, resulting in a 2e⁻ reduction (and hence, on average the number of electrons transferred decreases from a value of 4 leading to a decrease in the magnitude of the limiting current density. Previous work has shown that blocking of Pt sites by strongly adsorbed species favours the pathway for the 2 electron reduction of oxygen[16]. Interestingly, when the potential is started at 1 V and held for 1 min, the ORR activity is slightly increased compared to the ORR for a clean Pt{100} (potential not being held , black CV). Pt{100} has been shown to reconstruct at this potential, as seen by the stationary voltammetric results and so the

reconstructed surface appears at first to improve the ORR activity. It is suggested that a slight disordering of the adsorbed OH layer on Pt{100} terraces discussed in chapter five allows metal sites to be more available to oxygen in competition with OH formation.

6.2.3. Conclusions

Dynamics of oxide formation were studied using CV in absence of strongly specific anion adsorption. The results for the Pt{111} surface showed little perturbation of the classic voltammetric profile in 0.1 M perchloric acid, under typical scanning conditions. As time held at 1 V was increased oxide desorption grew until a saturation point. RDE curves although not significantly affected, were inhibited as the time that the potential was held was increased.

The results for Pt{100} and its vicinal stepped surfaces indicated that surface reconstruction (roughening) occurred when the potential was held at 1V. The amount of oxide adsorbed (measured from the magnitude of the oxide desorption peaks) also did not show a linear relationship with the amount of time the potential was held. For example, the time of 5 min showed larger desorption peaks compared to 10 min. The formation of two "mystery peaks" in the lower H_{upd} potential region were speculated to be related to the adsorption of sub-surface oxides causing slow reconstruction of the {100} (1x1) terrace. The influence of fortuitous anion impurities or perchlorate decomposition to form chloride could be excluded. The ORR results of Pt{100} showed that initial surface reconstruction marginally improved the activity for the ORR before inhibiting it but prolonged oxide formation resulted in a switch from a 4e to 2e ORR mechanism. This would be consistent with hydrogen peroxide formation during ORR being promoted by adatoms or molecules adsorbing on platinum. Stepped Pt{100} surfaces revealed that stripping from {100} terrace and defect sites could be distinguished via the potential of the oxide stripping peak with defects giving rise to a stripping peak at more negative potentials. This means that during the initial stages of ORR (negative potential sweep), a Pt{100} terrace is first to 'shed' its electrochemical oxide layer followed by defects. Since ORR can only occur at metallic sites and Pt defects remain oxide covered, it is deduced that the improvement in ORR kinetics is due solely to break up of long range order in the {100} terraces, not the electrocatalytic activity of defect sites themselves.

The Pt{110} electrode exhibited an oxide stripping peak in the potential region 0.7-0.9 V, similar to that of Pt{100} but it was not shown to reconstruct in the H_{upd} region like Pt{100}. However, we note

here that in chapter four, it was established that hydrogen-cooled Pt{110} electrodes already contain a significant degree of surface disorder compared to CO-cooled electrodes. Hence, a small amount of surface disordering would be far less marked on an already defective surface compared with a pristine, defect free terraced surface. Hence, the partial deviation seen in the H_{upd} profile relative to the normal CV was probably due to some reconstruction, although much less than evident for Pt{100}.

6.3. Chronoamperometric studies of electrochemical oxide formation

Chronoamperometry studies were undertaken on Pt{hkl} single crystals in in 0.1 M perchloric acid and 0.1 M sulphuric acid electrolytes in an attempt to elucidate kinetic information concerning adsorbed electrochemical adsorbed oxides. This type of study has previously been undertaken using microelectrodes[23, 24] and so the application to macroscopic single crystal studies affords a new departure.

Current decay transients were monitored as potential was stepped positive from 0.4 V, in increasing steps up to 1.1 V. Attempts to interpret data qualitatively and quantitatively to further understand the role of potential and time on electrochemical oxide formation are shown. Interpretation of current-time transient data has been undertaken by plotting the natural logarithm of the current density versus time, based on references[23, 25, 26], where surface charging and chemistry are ostensibly assumed to be first order kinetic processes with no dependence on bulk diffusion.

All basal platinum single crystal electrodes were firstly investigated to obtain a fundamental understanding of trends and then work was expanded to include stepped Pt(s)[n{100}x{110}] (where ∞ > n ≥ 2 denotes terrace width). The potential was always stepped from 0.4 V as this is close to the potential of zero total charge (pztc) for both Pt{111} and Pt{100}, and the H_{upd} process was not of interest. The potential was stepped to 0.5/0.6/0.7/0.8/0.9/1.0/1.1 V independently for each surface together with flame annealing between potentials to ensure ordered surfaces were present before each potential step. Each step was repeated to ensure reproducibility of the technique. This study produced a large amount of data (data collect multiple times on over 15 electrode surfaces) and therefore only the main findings and key figures are presented.

6.3.1. Kinetic analysis of the chronoamperometric studies on Pt basal planes

Quantitative analysis of the results has been undertaken. Current-time transient plots were transformed into natural logarithm of current density versus time. This method was based on a paper in which chronoamperometry was used to distinguish kinetic parameters of binary monolayers[23]. For an ideal electrochemical reaction involving a surface-bound species, the oxidation state of the monolayer exhibits a single exponential decay in time according to the following relation:

$$i = kQ \, \exp(-kt)$$

where i represents current response, t is time, k is the apparent rate constant for a given overpotential, and Q is the total charge passed in the redox transformation. This relationship can be transformed into linear relationship by taking the natural logarithm of the equation:

$$ln \, i = LnkQ - kt$$

The linearity of a semi-log plot indicates the predominance of a single rate constant for heterogeneous electron transfer[23].

We have used this approach to interpret our results, however this is related only to oxidation state of the monolayer on a microelectrode. Therefore, it is expected that results may deviated from expected behaviour.

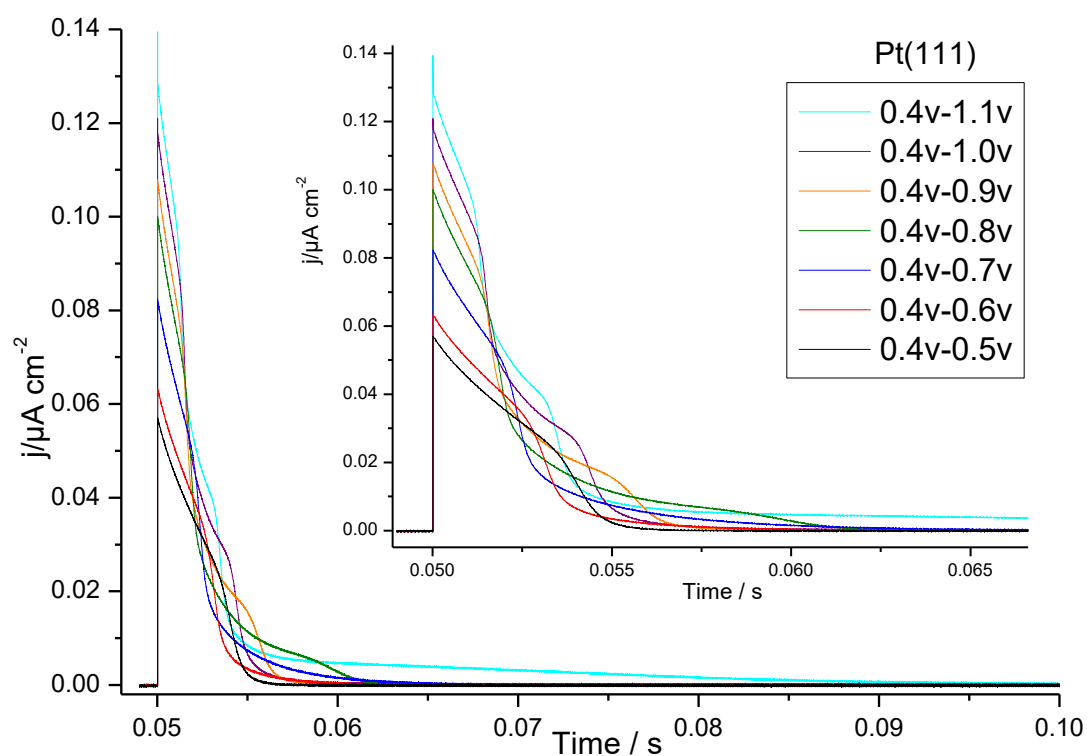## 6.3.1.1. Chronoamperometric results in perchloric acid electrolyte

Figure 150: Chronoamperometry profiles of Pt{111} in 0.1 M HClO4

Figure 150 shows the j-t curves obtained from chronoamperometry studies of Pt{111} in 0.1 M HClO$_4$. Initial observations show the results are not simple exponentials as expected and previously reported for microelectrodes[23, 25]. This indicates the possibility of several overlapping processes occurring. Comparison with stationary cyclic voltammograms allows connections with adsorption processes to be made, including charging of the double layer and adsorption of OH and oxides. As the size of the potential step increases (i.e. 0.4 - 0.5 V cf. to 0.4 – 1.1 V) so does the complexity of the current decay. This was true of all single crystal surfaces investigated and is evident by inspection of stationary CVs. First a qualitive assessment of the results is undertaken, with rationalisation behind the assignment of features seen.

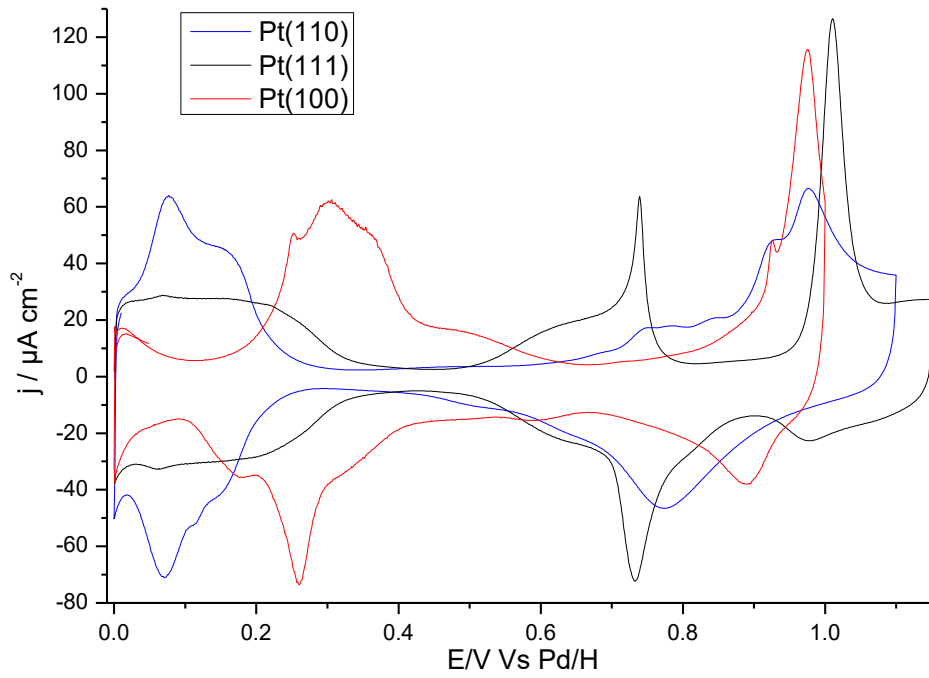*Figure 151: CVs of Pt{111} (black, Pt{100} (red) and Pt{110} (blue) in 0.1 M HClO$_4$.*

Ln j vs. time plots

All transient j-t curves were transposed into Ln j vs. time plots. A linear response supports a first order process. As can be seen from the following Ln graphs this is not completely what was found.
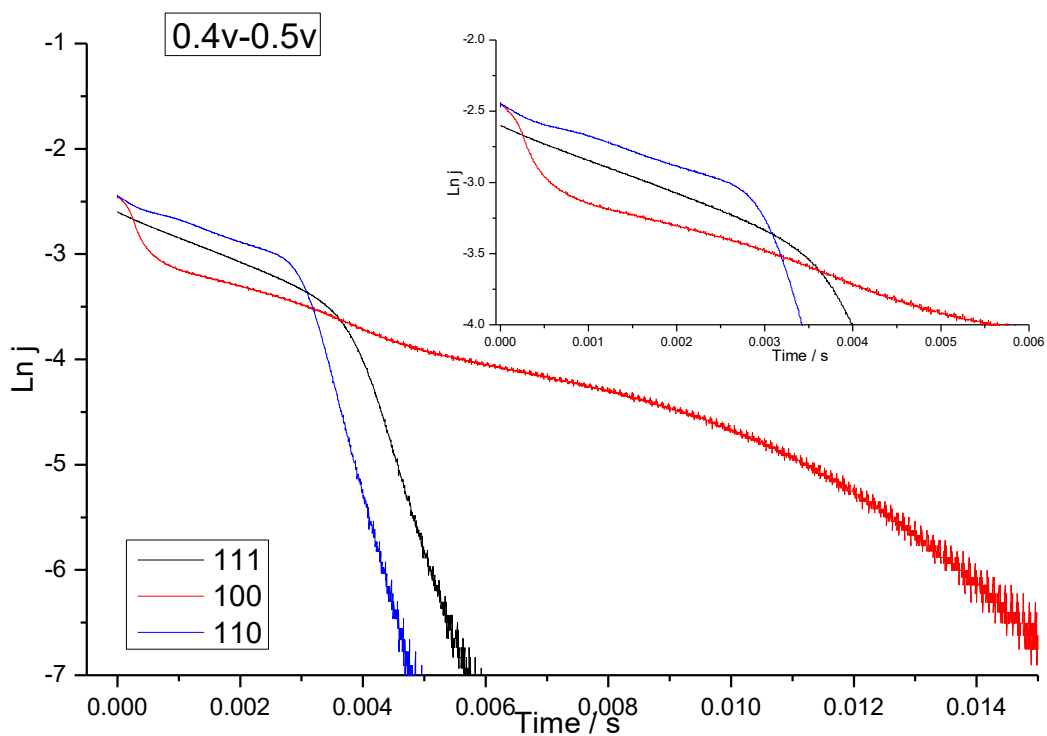

Figure 152: Ln vs j plot of potential step 0.4-0.5 V, for Pt(hkl) in 0.1 M HClO$_4$

The results of the Ln j v Time plots (Figure 152) for the Pt{111} and Pt{110} initially show a steady linear decrease which then leads to a sharp linear decrease. Rapidly decreasing currents indicate the end of the first order process. Comparison of cyclic voltammograms in this electrolyte show this can be partially linked to double layer charge for these surfaces. More so for the Pt{111} as this is the dominant process occurring in this potential window (as seen in CV, Figure 150). The Pt{100} deviates further from the expected linear response and is more complicated because the starting step potential of 0.4 V, already shows some H desorption/OH adsorption in the CV. Interestingly, the Pt{100} transient time scale is much longer (over double) compared to Pt{110} and Pt{111}.
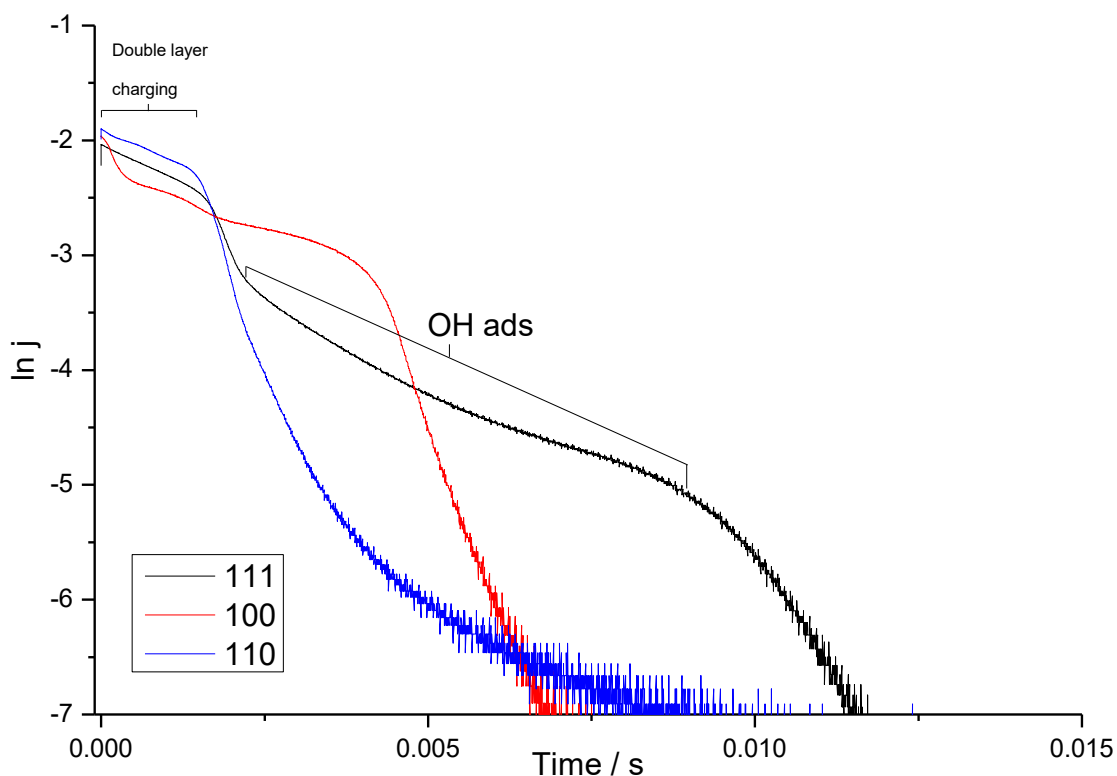
Figure 153: Ln vs j plot of potential step *0.4-0.8 V, for Pt(hkl) in 0.1 M HClO₄*

First observations for the potential step from 0.4-0.8 V in Figure 153, show that more complicated Ln plots are produced for the larger potential step. This correlates with more adsorption/desorption process occurring, as seen in the CV. Potential steps from 0.4-0.5 V to 0.4-0.8 V showed consistent progression of the Ln plot changing as the linear response for the next first order process. This potential was chosen due to 0.8 V being the potential just after the Pt{111} OH_{ad} "butterfly peak"[27].

For the 0.4-0.8 V potential step, the results for Pt{111} shows two gradually decreasing linear sections joined by a sharp decreasing slope; one around 0-20 ms and the other 30-70 ms.

Consideration of the charging must be included now to make sure the transients are being analysed as accurately as possible. When the electrode comes into contact with the electrolyte, a double layer is formed at the interface; behaving in many respects, like an electrolytic capacitor. When the applied potential is changed, current flows to charge the double layer capacitance. This charging process complicates the electrochemical measurement as the potential at the interface does not reach the applied potential values until the charging process is complete. The current required to charge the double layer must flow through a resistance corresponding to the total cell resistance.

The time required to charge the electrode surface is related to RC time constant in accordance with Bard *et al.[28]* The product of RC represents the cell time constant. It is reported that only 5-10 times longer than this produces useful analytical information[29].

$$t=(RC)*10$$

In an electrochemical cell the resistance is dependent upon the specific conductance of the electrolyte, k, and the electrode radius, r_s, in the following equation:[29]

$$R= 1/ (4\pi \, k \, r_s)$$

For a solution of 0.1 M $HClO_4$, ($k=1.04 \times 10^{-2}$ $Ohms^{-1}$ cm^{-1}[30] r_s= 0.10-0.15 cm, and 20 μF cm^{-2} for C), the time constant was calculated as 50-70 μs. Ten times this value = 5×10^{-4} to 7×10^{-4} s. The time constant was also calculated using impedance and equivalent circuit software. For Pt{111}, the cell resistance R was obtained from impedance measurements (R = ~138 Ohms, higher than expected). Capacitance was estimated from the double layer charging in CV (current density in double layer region, mA cm^{-2} /sweep rate, mV s^{-1} gave capacitance in μF cm^{-2}) and shown to be around 10.63 μF cm^{-2} (lower than expected). Hence, the time constant of the cell RC was evaluated as (approx.) 1.4 ms using this approach. Both approaches give a fast time for the charging. Therefore, the sharp decline seen in the beginning of the chronoamperometry results is most likely to be corresponding to double layer charging and features following showing the more gradual linear sections to electrosorption processes. This could be true for all surfaces as the charging time for each surface was calculated to be in less than milliseconds, far less than the overall transients.

Going back to the individual electrodes, for Pt{111}, the 0.4-0.8 V window shows double layer charging and OH adsorption in the CV. However, the transient shows two sections of electrosorption process. Could the two sections of OH adsorption could be attributed to different adsorption behaviours on the surface? Feliu has previously discussed how the shape of the butterfly region

219

could be attributed to two types of water/OH adsorption[31] which could explain the behaviour seen here. The time we are attributing to double layer charging is much smaller compared to the section we are attributing to OH adsorption. It is interesting that the sharp gradient which is being attributed to the charging process at the beginning, also shows to occur before and after the more gradual electrosorption processes (seen more clearly as larger potential steps are undertaken), but also, the time constants for these sections change depending on the potential step. This is discussed later.

The Pt{100} results in a similar plot-profile as seen for its 0.4-0.5 V potential step. Interestingly, the timescale towards zero current is shorter. The gradient is comparable, indicating the rate for the adsorption/charging are still the same.
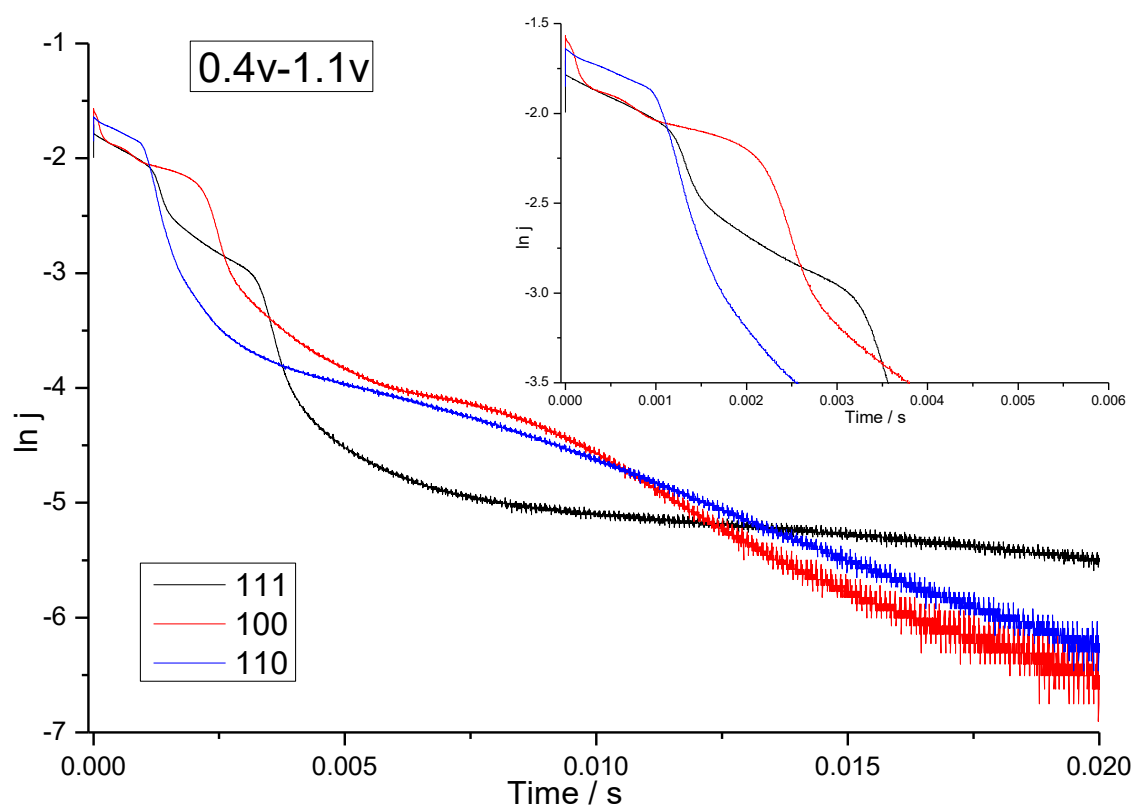
Figure 154: Ln vs j plots of *0.4-1.1 V*, for Pt(hkl) in 0.1 M HClO4

The Ln plots for the potential step 0.4-1.1 V is shown in Figure 154. At this potential, CVs for all three basal planes show H_{upd}, OH_{ads} and Oxide adsorption. This is representative in the Ln plots shown. Inspection of the Pt{111} result exhibits three gradual "sections" joined by two steep sections. The gradual sections are again, likely to be related to electrosorption processes occurring; OH adsorption and oxide formation on the Pt{111} surface, as seen in the CV. The Pt{100} result exhibits two

distinct gradual "sections"; 0-3 ms and 3-20 ms. The first section has been attributed to combined H$_{upd}$ and OH adsorption, as these processes overlap for this surface in the corresponding CV. The second "section" has been attributed to the oxide present on the Pt{100} surface clearly, shown by a peak ~1 V in the CV. The steeper sections are now attributed to charging of the double layer. The Pt{110} also shows two gradual "sections". The first linear response may be attributed to reversible oxide adsorption from the residual current response seen in the CV. The second gradual response (3-7 ms), is ascribed to adsorbed oxides on the surface. Both Pt{100} and Pt{110} in the oxide formation process tend to give rise to a broad charging peak rather than a straight line suggesting a more complicated nucleation and growth process is occurring on these terraces. It is speculated that surface reconstruction as well as oxide formation may be responsible for this phenomenon.

Figure 155 reports the Ln j vs Time plots for the potential step 0.4-1.1 V of Pt(s)[n{100}x{110}] stepped surfaces. At this potential step, the surfaces show to have a significant amount of electrochemical oxide adsorbed.
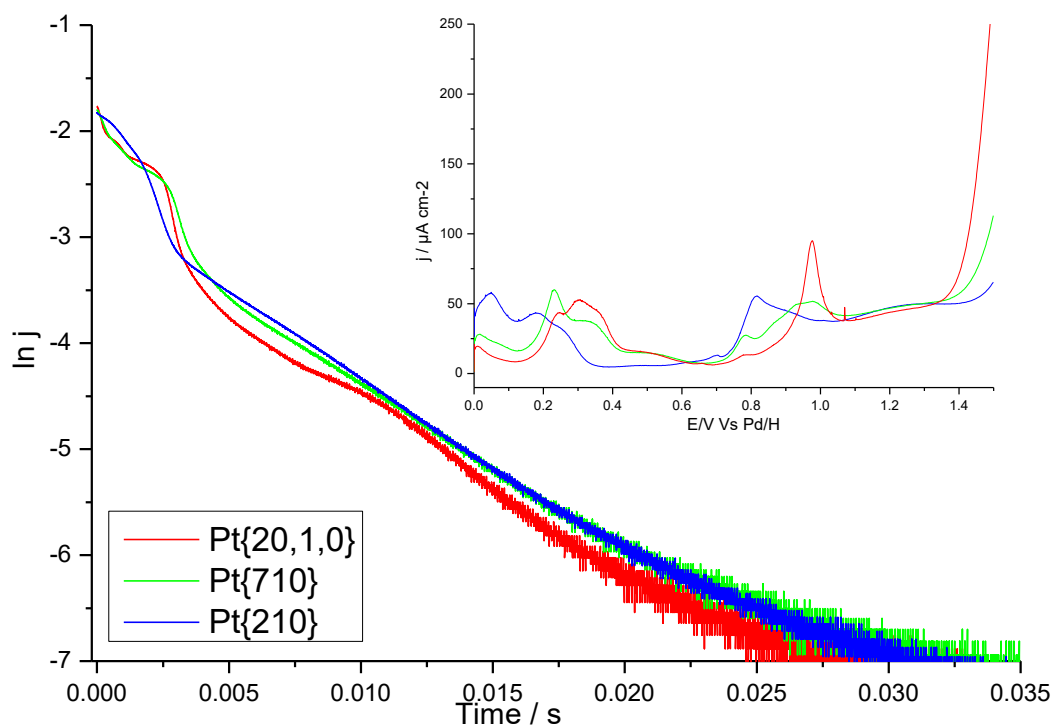
Figure 155: Ln vs j plots for potential step 0.4-1.1 V, of Select Pt[n(100x110)] surfaces

The ln plot for Pt{20,1,0} exhibits a similar result to that seen for the Pt{100} surface. This is expected, as this surface contains large {100} ordered terraces. In fact the final oxide formation stage is seen to generate a peak rather than a straight line for Pt{20,1,0} which diminishes as more and more steps are introduced, potentially meaning that the process on steps is first order but a

221

second process, in addition to oxide formation is present at the Pt{100} terraces. Two linear sections can be delineated from the plot in Figure 155 (0-3 ms and 5-10 ms), attributed to overlapping H_{upd} and OH_{ads}, and oxide adsorption respectively. The ln plots for the Pt{710} surface is shown to decrease much faster than Pt{20,1,0} making it more difficult to see the linear sections, if in fact there are any. The ln plot for the Pt{210} has the highest step density. As can be seen by comparing it against the Pt{20,10} and Pt{710}, it differs markedly and is better compared against the ln plot for Pt{110} in Figure 154. The Pt{210} ln plot exhibits a linear section at 0-2 ms, which due to the gradient, easily merges in with a sharp decrease of current, linking the next linear section at 3 ms. Comparison with the CV shows that at 0.4 V, no adsorption processes are occurring, but by 1.1 V a large amount of electrosorbed oxide is present on the surface.

Rate Values for Pt(hkl) in HClO$_4$ electrolyte

Quantitative rate constant data has been roughly calculated for some of the surfaces and is shown in Figure 156. It is important to note that this analysis, along with the qualitative analysis above, has been based on the idea of the electrosorption processes seen in the CV occurring in the same order. Rates have been calculated by taking linear "sections" and applying the equation from [23]. From the rates calculated (based on the assumption all processes are following a similar behaviour as microelectrodes quoted in [23]), several trends may be observed. The first is that all rates seem much slower than expected. Secondly, Pt{111} exhibits the slowest rate of oxide formation than any of the Pt(hkl) surfaces studies (39 versus 150 s^{-1} for Pt{110} for example). For Pt{100}, because of the peaked nature of the transient, it proved very difficult to justify the extraction of a first order rate constant. Pt(110) also gives rise to a much less peaked oxide response than Pt{100} so it was possible to fit a line to the data without too much error. Hence, it is speculated that the rate of surface reconstruction via oxide formation is much slower than on Pt{100}, justifying this procedure so that some comparison could be made with relative oxide formation rates. For the 1.1 V transient, data for Pt{110} showed a slight acceleration for oxide formation in sulphuric acid (not shown) relative to in perchloric acid (150 vs. 127 s^{-1}).

Analysis is more difficult on the discussion of the OH or OH/H ads attributed "sections". Although rate constants can be compared, it is unlikely that it will be like for like when considering the processes occurring in the CV. For example, the potential jump 0.4-0.8 V should only shows OH_{ads} for Pt{111}, but for Pt{100} you are starting in a potential region where adsorption process are already occurring to a potential which other processes end/begin. For the Pt{110} this is also a complicated

case as the CV is much different again. Results have shown that it's very difficult to interpret what the chronoamperometry curves are showing and what information one can extract that would be useful. So, although rate values have been calculated for said OH/H regions this cannot be compared directly.

Potential step from 0.4v-:	Pt{111}		Pt{100}			Pt{110}	
	OH ads k/s^{-1}	Oxide ads k/s^{-1}	OH/H ads k/s^{-1}		Oxide ads k/s^{-1}	OH/H ads k/s^{-1}	Oxide ads k/s^{-1}
0.5v	-	-	183.11	130.11	-	206.28	-
0.6v	-	-	188.95	133.56	-	263.55	-
0.7v	-	-	162.00	128.81	-	214.67	-
0.8v	268.42	-	182.64	142.87	-	255.26	-
0.9v	294.90	-	169.24	130.24	-	234.08	-
1v	283.28	-	191.50	145.56	N/A	255.54	107.74*
1.1v	286.10	38.92	181.46	133.25	N/A	235.64	126.71*

*Figure 156: Rate values obtained by taking gradient of linear response from previous Ln plots.*

6.3.2. Conclusions

Chronoamperometry studies were undertaken on Pt(*hkl*) single crystal surfaces to elucidate kinetic information about adsorption processes, with emphasis on electrochemical oxide adsorption behaviour.

In summary, a linear response is only seen to be exhibited in the Ln plots when the potential step is higher than that of a process seen in the CV. For example, ln plots for a potential step from 0.4-0.8 V exhibits a linear trend in the case of the Pt{111} and its CV corresponds to before and after the butterfly OH$_{ads}$ peak. As the potential step window increases, the time constant of each linear response appears to decrease, but the gradient generally stays the same. This is apparent in both Ln plots and *i*-t curves for each crystal surface. This is not directly associated with rate, but jumping up to a higher potential generates more adsorption processes occurring on the surface, and therefore it may be possible that adsorption processes occurring at lower potential finish quicker. The discussion of desorption processes such as H desorption has not been discussed as an influence in the transient data but was considered to affect the results seen for the Pt{100}.

A big question has arisen from this work – why is there evidence of a fast charging process after a slower electrosorption process? A simplified answer could be that this is the charging process

throughout (due to the gradients of said sections being comparable) and the charging process is still happening throughout most of the experiment, even though the calculated charging time is only around 1 ms. When the potential step is applied, the actual potential at the interface will not truly reach the desired potential until the current has stopped flowing (due to ohmic drop).The figure below sketches the idea that although typically a fast process, it could take much longer for the charging phase to be completed over the large macro electrode. This raises an important question; can the charging be deconvoluted from electrosorption processes as we have attempted to do in this chapter?
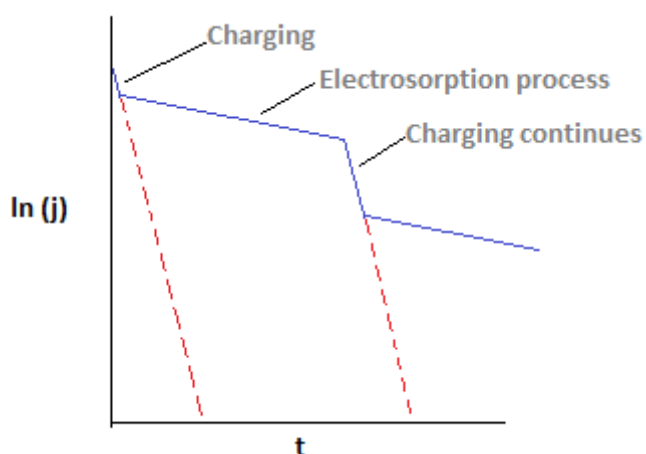
We suggest no, as our analysis has shown some unusual kinetic results.

Overall, we have attempted to qualitatively assign electrosorption processes sequentially to the chronoamperometry results as they are observed in the CV. Although rate constants showed unusal result, it is still likely that OH adsorption and oxide formation are sequential processes where oxide does not form before OH is adsorbed. All surfaces containing large {100} terraces have been found to exhibit kinetics that are probably not straight forward first order processes, but also include a nucleation and growth of place exchanged oxide (surface roughening). This reaction is thought to be comparable in rate to oxide formation, and so giving rise to a non-linear peaked response. For oxide formation, it is indicated that the rate of oxide formation is qualitatively in the order Pt{100} > Pt{110} > Pt{111}. For stepped Pt{100} electrodes, the oxide formation process becomes much faster than surface roughening as step density increases.

6.4. Investigating the effect of continuous high potential cycling on structure controlled surfaces to mimic fuel cell systems

The performance of platinum as a catalyst for PEMFCs has been extensively studied using both polycrystalline and well-defined surfaces, and shape controlled nanoparticles[14, 32]. Electrochemical conditions, such as scan rate and potential excursion limits, have strong influence on the electrochemical behaviour towards adsorption/desorption of ions including the effect on ORR activity. Whilst many studies have used ideal conditions (closed circuit) to try to understand the true nature of the ORR mechanism, realistically, the conditions in fuel cell operations are not so idyllic[33, 34]. For a metal to be suitable as a fuel cell catalyst, it must be able to withstand the harsh chemical environment in the cell[32, 33] This includes the presence of strong oxidants, reactive radicals, low pH, high temperatures and rapid potential fluctuations. During operation, the cathode potential oscillates between 0.9 and 0.6 V (idle-to-peak power operation transients) but can reach potentials as high as 1.5 V during start-up/shutdown cycles[35]. Catalysts that are stable get covered in oxide film that inhibit dissolution but also the ORR. Short term stability (kinetic activity) as well as long term stability are both extremely important in overall system durability. Considering the conditions inside a real fuel cell system is important to apply to fundamental studies, if improvements are to be made.

Therefore, the effect of high potential fast cycling on Pt single crystals was investigated. After a flame anneal and collection of a normal CV scan to ensure the standard, pristine surface was formed, high potential fast cycling conditions were applied. Three high potential excursion limits were chosen (1.0, 1.2 and 1.4 V), with a scan rate of 0.5 V/s. These conditions were applied until the voltammogram stopped changing, usually this point was established after 100-200 cycles. The effect of these non-ideal conditions towards the ORR and application of a Nafion film upon the surface was also explored. Nafion is commonly used as the PEM in PEMFCs and therefore it is important to understand how large potential perturbations affect its behaviour with platinum and its activity towards the ORR. Electrochemical procedures are widely known to cause changes in the surface structure of single crystal electrodes, but it is important to understand how these conditions affect the interactions at the electrocatalyst surface on a fundamental level[36-38].

6.4.1. The effect of high potential fast scanning conditions upon the Pt{111} surface

Pt{111} is the most closely packed and ordered basal plane surface. The effect of fast cycling up to 1.0, 1.2, and 1.4 V upon the {111} surface structure are shown in the voltammogram in Figure 157. Initial observations show distinct changes in the CV profile between normal and 1 V fast scans, and 1.2 & 1.4 V fast scans. The resulting CV after 1 V fast scans shows a minor perturbation of the butterfly peak at 0.74 V and oxide peak at 1.2 V, demonstrating that there is no surface reconstruction for this potential limit. Minute changes seen for fast cycling up to 1 V can be attributed to picking up small amounts of contamination in the solution. The resulting CVs after fast cycling to 1.2 and 1.4 V show marked changes in the H_{upd} and OH/Oxide regions. The usual H_{upd} profile, (0-0.25 V), has transformed and exhibits a large peak below 0.05 V followed by a smaller peak around 0.15 V. This is comparable to the H_{upd} region of Pt{110} (Figure 165), suggesting surface reconstruction from the original large {111} terraces. Due to the size of the peak near 0.05 V, the surface still exhibits some order, perhaps small domains of {111} and {110} features. There is also a diminution of the OH and oxide adsorption peaks, and in their place, a broader adsorption feature between 0.6-1.0 V. There are two distinguishable peaks in this broad region at 0.72 V and 0.85 V, relating to OH adsorption on {111} sites and oxide adsorption on steps sites respectively.

The effect of the different high potential cycles upon the ORR are shown in Figure 158. Higher potential perturbations are initially shown to reduce the overpotential for the ORR, by around 30 mV. Fast cycling up to 1.2 V results in the highest activity towards the ORR, (measured using potential at $E_{1/2}$). This is closely followed by fast cycling conditions up to 1.4 V, then normal scan conditions and lastly, fast cycling up to 1.0 V. The ORR curves below 0.2 V, show two different responses for the two pairs of scanning conditions (normal & 1.0 V and 1.2 & 1.4 V). Clearly Pt{111} terraces favour 2e⁻ reduction of oxygen to form hydrogen peroxide in the H_{upd} region (see chapter five), whereas the introduction of steps breaks up the long range order and a significant increase in reduction current is observed in the H_{upd} region corresponding to a switch back to a 4e⁻ reduction pathway.
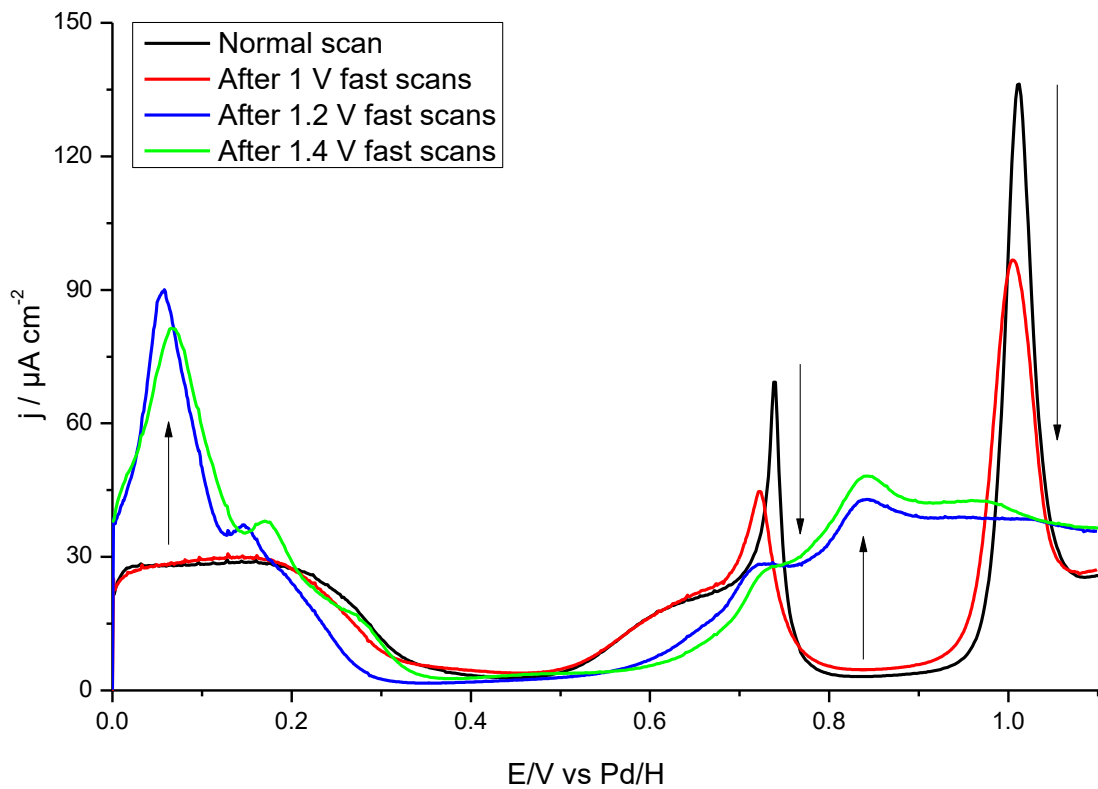
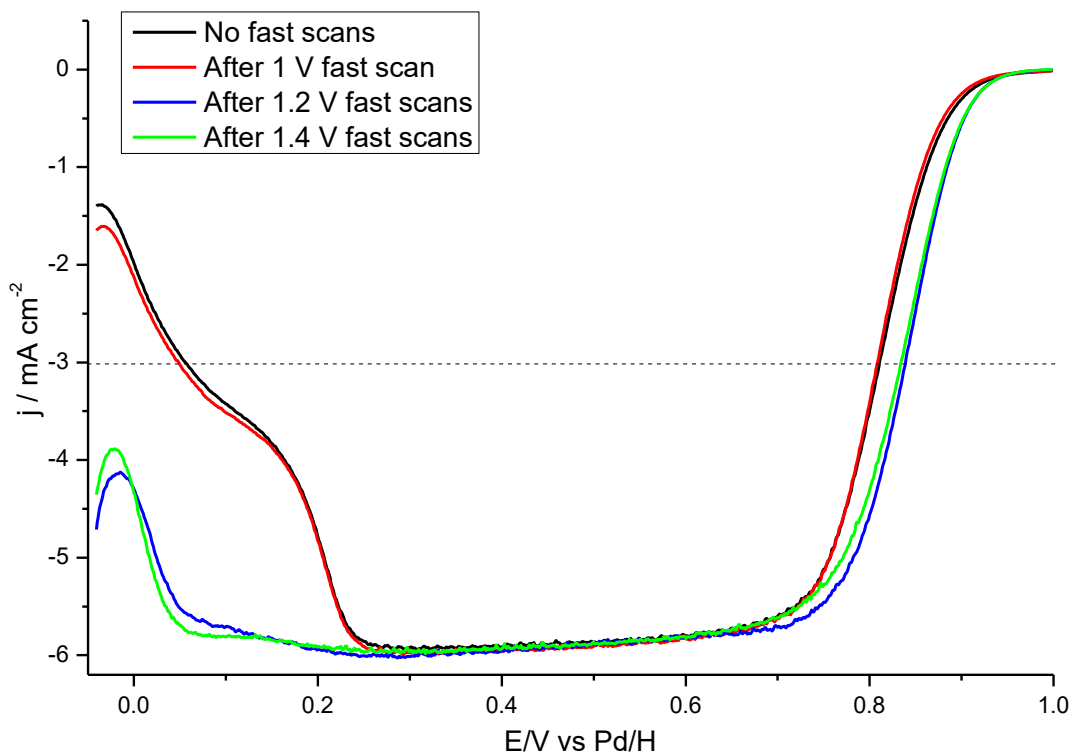*Figure 157: CVs of Pt(111) in 0.1 M HClO₄, after fast scans*

Figure 158: RDE curves of Pt(111) in 0.1 M HClO₄, saturated with O₂, after fast scans

This result is in accordance with expectations based on adsorbed OH acting as a site-blocker for ORR on Pt{111} and disruption of this OH network will cause promotion of ORR. Hence, it may be that in real fuel cells incorporating Pt nanoparticles based on {111} morphology, activity may actually improve with use (excluding sintering, corrosion and other effects).

When Nafion was added to the Pt{111} electrode, a benefit from the high potential excursion would be that the surface contamination arising from Nafion could be removed. Hence, although cycling to 1.4 V disrupts surface order, it leaves behind a Pt/Nafion interface free of contamination.

The effect of fast high potential scanning of Nafion on Pt{111} was therefore investigated and the resulting voltammograms are shown in Figure 159. The CV is indicative of a good quality Nafion surface as demonstrated by little perturbation of the H_{upd} region (0-0.3 V), a sharp peak at 0.45 V (corresponding to specific adsorption of the sulphonate group from Nafion), OH perturbation where the original butterfly peak at 0.74 V is inhibited and shifted positive to around 0.82 V, and a positive shift of the oxide peak to 1.08 V[39]. The thickness and coverage of the Nafion layer adsorbed determines the nature of the Nafion spike and level of perturbation of the OH and oxide features[39].

Applying fast scans up to 1.0 V upon the Nafion/Pt{111} creates small defects on the surface as seen by new features appearing in the CV at 0.05 V, attributed to {110} defects[36, 40]. The OH that was originally perturbed to 0.82 V is shifted to 0.8 V, and the oxide adsorption peak is diminished and shifted negative. Evidently, the underlying Pt{111} structure is being reconstructed, and affecting how the Nafion overlayer interacts. The OH and oxide adsorption features appear to be slightly more affected by fast scanning cycling when Nafion is present on the Pt surface. For the 1 V fast cycling, the Nafion adsorption spike at 0.45 V is attenuated and shifted -30 mV. The effect of applying fast cycling conditions up to 1.2 and 1.4 V changes the Pt{111} surface considerably together with the response of the Nafion layer.

For fast scans to 1.2 V, the usually well-defined oxide adsorption region changes into a broad, featureless combination of adsorption states for potentials > 0.6 V. The H_{upd} region also significantly changes, resulting in new peaks at 0.05 and 0.15 V. That the Nafion is still present (in spite of all

spikes and oxide changes being absent) may be confirmed by comparison with Figure 157. If the new H_{upd} states after surface roughening are compared, the peaks in Figure 159 are narrower, as would be expected from the presence of specifically adsorbed sulphonates. Recent work by Ahmed *et al.* [39] also suggested there are no features present in the CV for Nafion on a platinum surface for high stepped {111} surfaces. However, as established in chapter five, Pt{110} terraces do give rise to Nafion spikes irrespective of the step density as do indeed {100}x{111} steps[39].

The effect of fast scans on the Pt{111}/Nafion surfaces and the resulting ORR activity are shown in Figure 160. Nafion on the platinum surface inhibits the ORR activity which is evident by comparing $E_{1/2}$ values for Nafion-covered and Nafion-free Pt{111} data. Interestingly, as with the Nafion-free Pt ORR results in Figure 158, fast cycling conditions to higher potentials are found to improve the activity of the surface towards the ORR. Fast cycling up to 1.2 V and 1.4 V give the highest activity for the ORR with exactly the same value of $E_{1/2}$ for both Nafion-covered and Nafion-free surfaces. This means that oxygen can compete successfully with weakly specifically adsorbed sulphonate anions for metallic sites whilst at the same time, adsorbed and presumably ordered OH overlayers no longer inhibit oxygen adsorption. This result may provide some support for earlier results in chapter five whereby Nafion was found not to affect the potential of oxide formation on both Pt{100} and Pt{110} terraces. Hence, a very rough Pt{111} surface not only precludes formation of a network of OH species (the so-called butterfly peak), but also, the formation of **a network of Nafion sulphonate species** at the {111} terrace. This network would be responsible for the shift to more positive potentials of the Pt{111} terrace oxide peak when Nafion is adsorbed.
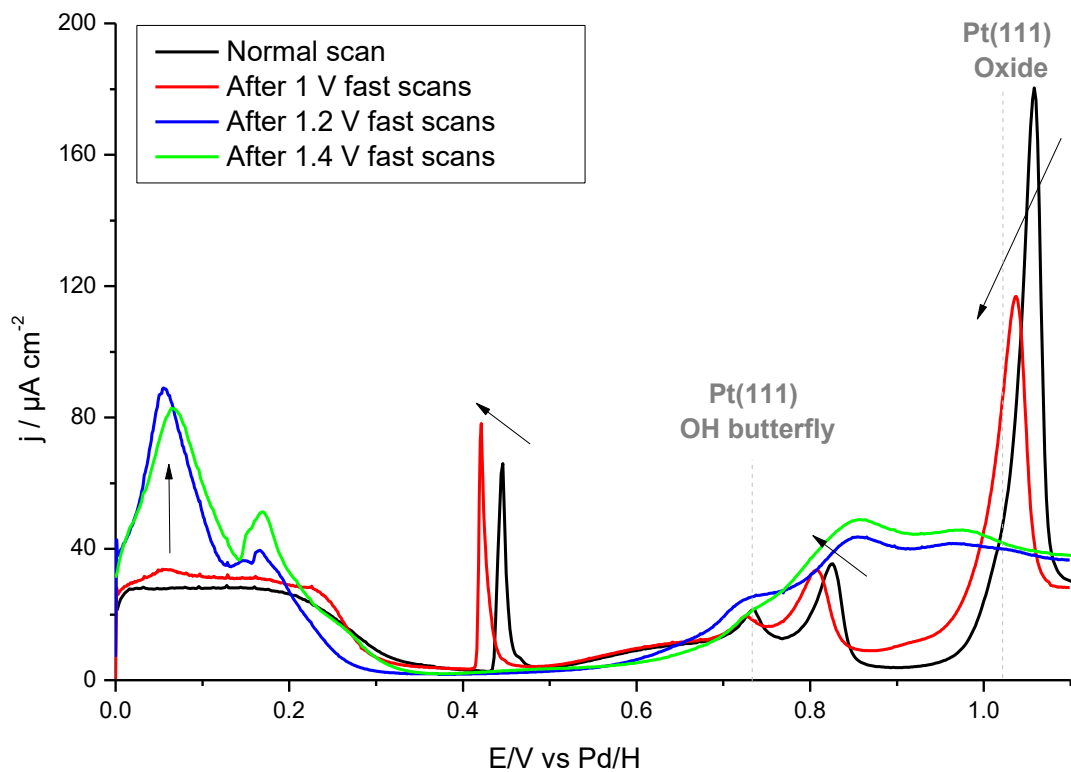
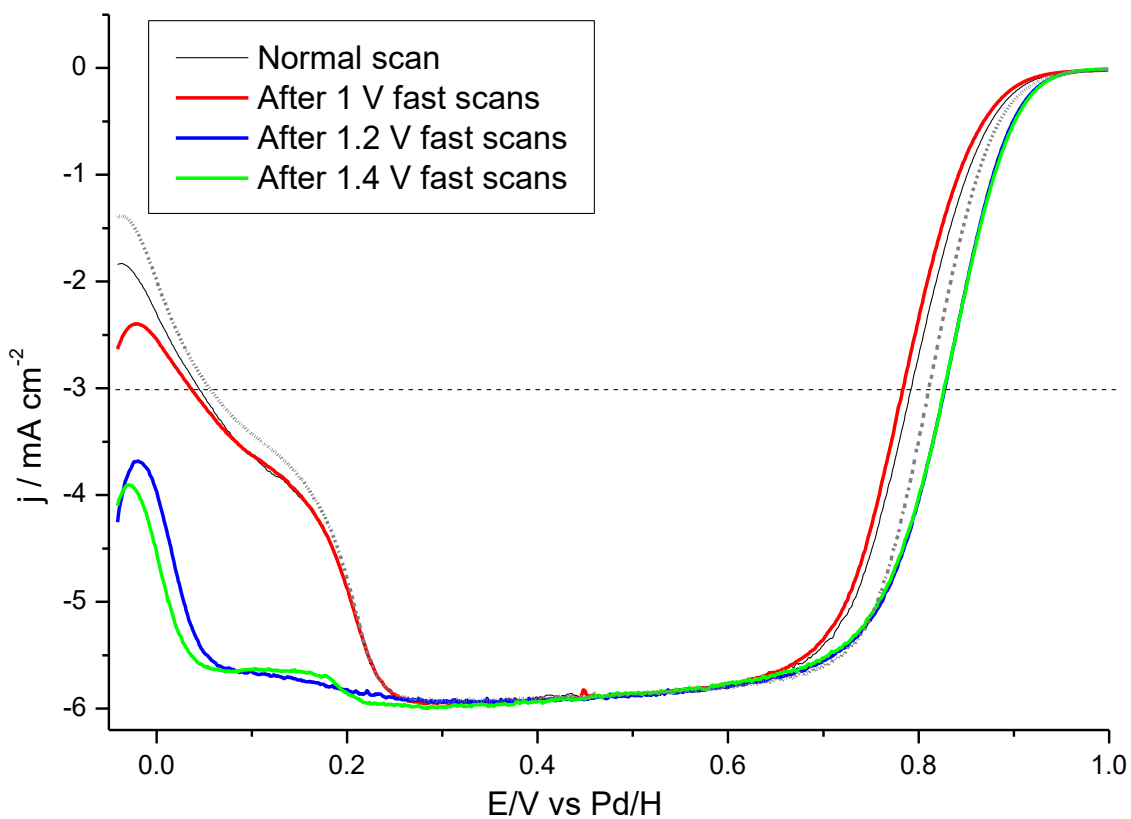*Figure 159: CVs of Nafion on Pt(111) in 0.1 M HClO₄, after fast scans*

Figure 160: RDE curves of Nafion on Pt{111} in 0.1 M HClO₄, saturated with O₂, after fast scans. Nafion free Pt{111} shown as dashed line for comparison.

6.4.2. The effect of high potential fast scanning conditions upon the Pt{100} surface

The effect upon the Pt{100} voltammogram of fast scans is shown in Figure 161. The arrows indicate the trends observed in the CV reflected by increasing the upper potential limit. All CVs show a large deviation from the original well-ordered/known Pt{100} surface regardless of the upper potential limit. Fast scanning conditions are shown to inhibit the H_{upd} and OH adsorption states 0.3-0.5 V as well as the sharp oxide terrace peak near 1.0 V. Diminution of the oxide peak results in redistribution of charge from 0.7 V onwards, resulting in a broad oxide adsorption region. This is typical of marked surface reconstruction. There is an increase of current in the most negative regions of the voltammogram (0-0.2 V), indicating adsorption processes on stepped sites. New peaks are also evident at 0.22 and 0.28 V, which can be attributed to H_{upd} and OH on step features respectively (see Nafion results later). This feature attenuates when higher potential limits applied. A new oxide adsorption feature at 0.8 V grows with increasing scan potential limit.

The effect of fast cycling on the ORR is shown in Figure 162. The disordering of the surface increases as the potential limit increases, which in turn causes an increase in the ORR activity. The 1 V potential scan engenders the largest improvement of the $E_{½}$ for the ORR whereby a positive shift of ~30 mV was seen. Again, it is asserted that OH species forming on terraces are disrupted as a consequence of destroying the long range order of the {100} terraces leading to less competition for oxygen to adsorb thus improving the ORR kinetics.
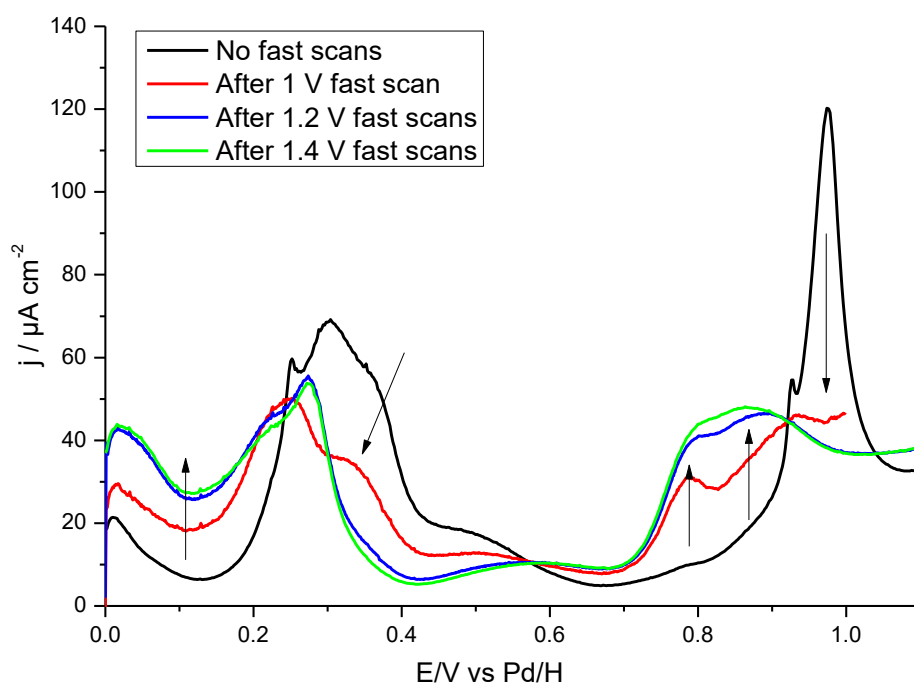

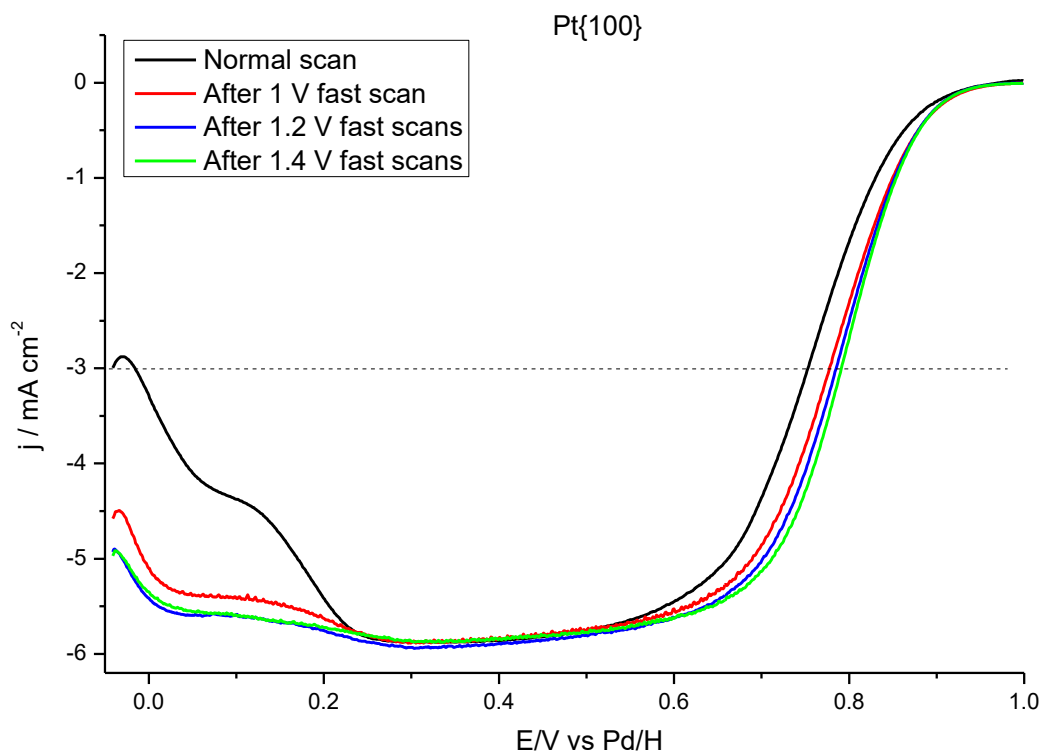*Figure 161: CVs of Pt{100} in 0.1 M HClO₄, after fast scans*

Figure 162: RDE curves of Pt{100} in 0.1 M HClO₄,, saturated with O₂, after fast scans

Again, at potentials between 0 and 0.25 V, the introduction of defects is found to disfavour hydrogen peroxide formation as signified by the increase in ORR reduction current.

High potential fast cycling conditioning was also undertaken on Nafion coated Pt{100} and the results are shown in Figure 163. Arrows indicate the change in the voltammogram as the upper potential limit is increased. The presence of Nafion on Pt{100} produces a large spike ~0.36 V and quenches the OH related features normally found positive of this potential (see Figure 161). Interestingly, the OH and oxide adsorption features are only diminished for the Pt{100} surface and are not shifted in potential, (cf. Pt{111}, where OH and oxide features were inhibited and shifted positive). Upon applying high potential fast cycling conditions, the potential at which the Nafion spike is observed shifts to lower potentials. Intriguingly, the Nafion spike can still be seen even after fast cycling to 1.2 V. In addition, the redistribution of current is very similar to the results seen for the Nafion free Pt{100} surface. The presence of Nafion on the surface inhibits the new feature seen at 0.28 V for the 1.2 and 1.4 V potential limits, indicating a likely OH adsorption process. In fact this Nafion spike has been positively identified previously as arising from Nafion adsorbed on Pt{100}x{111} step sites[39]. It should be noted that the Pt{100} OH peak between 0.4 and 0.6 V is only partially quenched by the Nafion.

The corresponding ORR curves are shown in Figure 164. The same trend (as expected from the CV results) is seen as found with clean Pt{100} whereby an increasing to a high potential limit results in higher activity for ORR. Again, a perturbation of OH adsorbed on Pt{100} terraces is suggested as causing this increase in activity. However, if sulphonate from Nafion does displace OH at 0.25 V, why should the improvement in activity arise? It could be that the sulphonate layer itself (ordered on Pt{100} terraces) is responsible and an ordered adlayer is broken up by the introduction of surface defects. In actual fact, the 0.4-0.6 V OH peak still survives Nafion adsorption and so it is this OH state that is probably responsible for a change in ORR activity as a result of surface roughening.
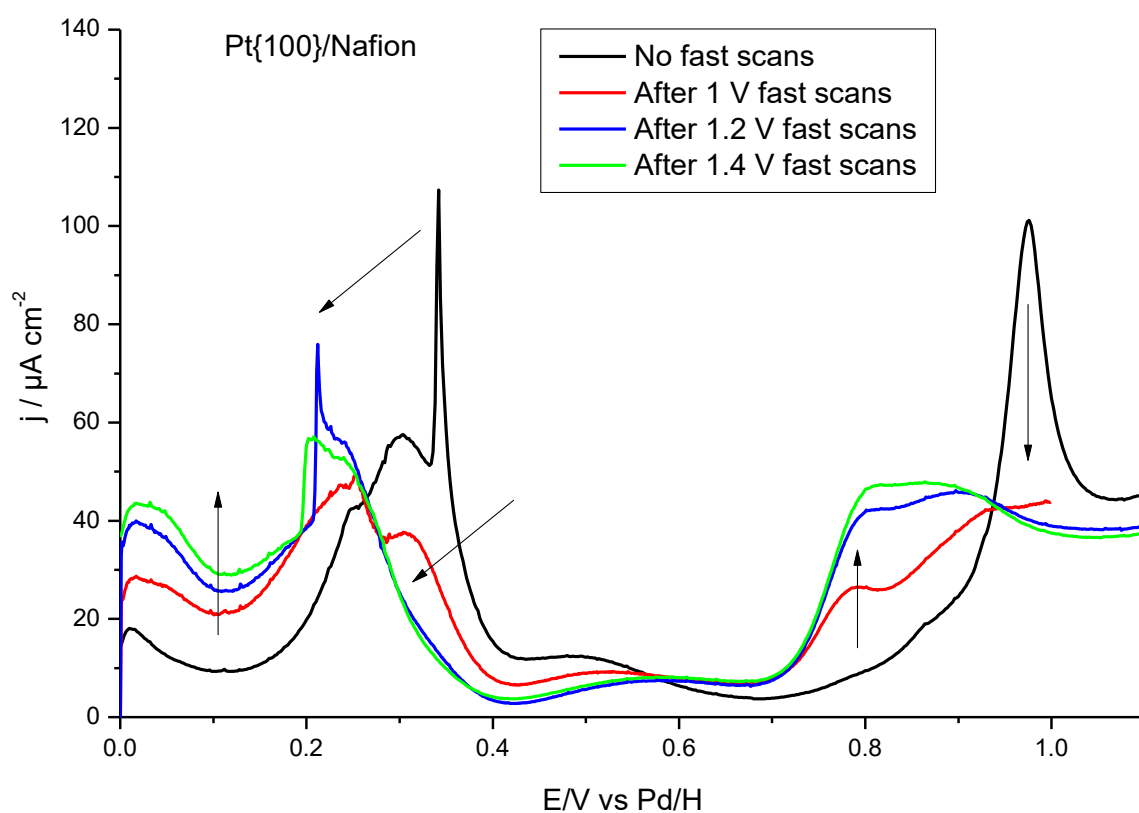

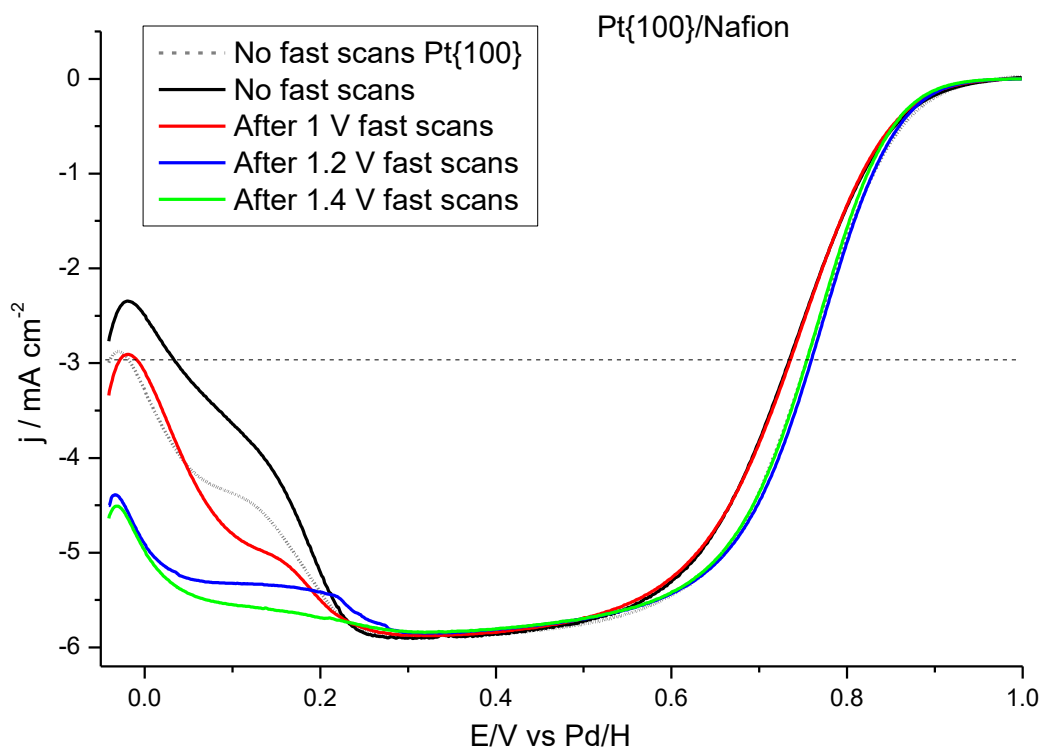*Figure 163: CVs of Nafion on Pt{100} in 0.1 M HClO₄, after fast scans*

Figure 164: RDE curves of Nafion on Pt{100} in 0.1 M HClO₄, saturated with O₂, after fast scans

6.4.3. The effect of high potential fast scanning conditions upon the Pt{110} surface

When cooled under hydrogen, the Pt{110} exhibits the highest activity for the ORR out of the three basal planes[16]. Recently however, this assertion has been questioned[41] since when prepared in a well-ordered Pt{110}-(1x1) state, Pt{110} exhibits a lower activity than Pt{111}. Nonetheless, for hydrogen- cooled Pt{110} samples in which significant surface disorder is present this assertion is true. Hence, although this surface is considered "flat", it actually contains large domains of stepped terraces. The results of the high potential fast cycling conditions on Pt{110} are shown in Figure 165. Arrows show the changes in the CV as the upper potential limit is increased. Initial comparisons with the "normal" scan (no fast cycling) show minimal changes in the H_{upd}/OH features and considerable change in the oxide adsorption region. Upon applying high potential fast cycling conditions, the initial state visible at 0.09 V decreases and shifts negative. The adsorption state at 0.18 V also diminishes as the potential limit is increased. In the oxide region, the three adsorption peaks at 0.75, 0.85 and 0.98 V decrease and are replaced with a broad oxide region that starts near 0.65 V and increases to its maximum at around 0.9 V. The corresponding ORR curves are shown in Figure 166. The effect upon the surface of high potential fast cycling conditions improves the ORR by ~30 mV, although there is little difference once the upper potential limit passes 1 V.
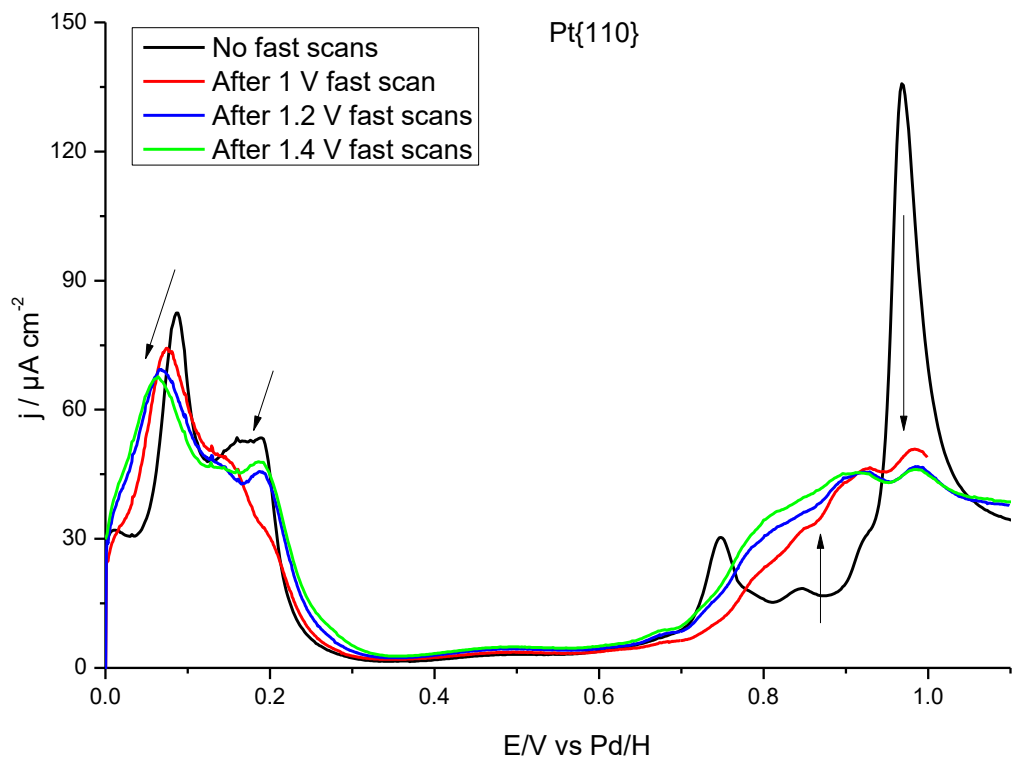
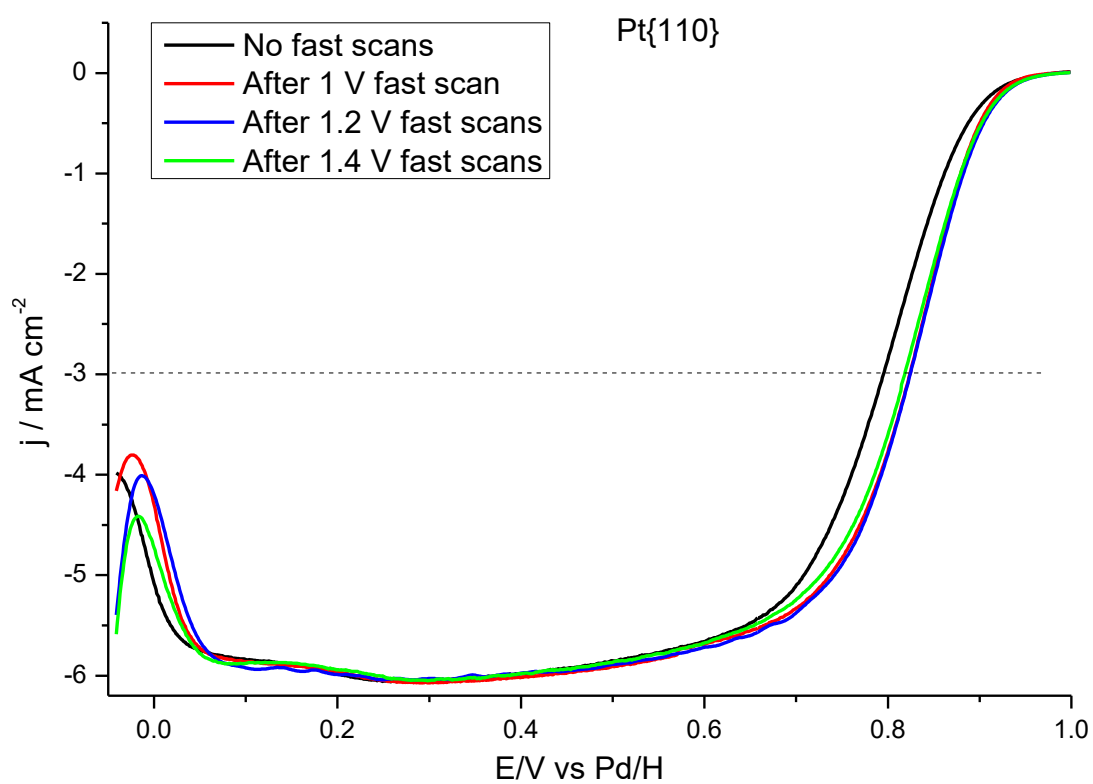*Figure 165: CVs of Pt{110} in 0.1 M HClO₄, after fast scans*

Figure 166: RDE curves of Pt{110} in 0.1 M HClO₄, saturated with O₂, after fast scans

The effect of high potential fast cycling conditions on a Nafion covered Pt{110} surface was investigated and the results are shown in Figure 167. Under normal scan conditions, addition of Nafion to the Pt{110} surface creates a new sharp feature corresponding to Nafion sulphonate adsorption at 0.12 V together with inhibition of the small feature at 0.18 V and blocking of all oxide adsorption features between 0.6-1.0 V. It does not change the adsorption feature at 0.05 V, therefore confirming it to be mostly H_{upd} (see chapter five). Upon applying fast cycling conditions, the Nafion adsorption spike is attenuated along with the feature at 0.98 V in the oxide region. A small feature at 0.8 V decreases upon increasing the potential limit. High potential, fast scanning conditions reconstruct the surface of the {110} and the presence of Nafion does not affect how the surface rearranges. The corresponding ORR curves are shown in Figure 168. As previously seen, reconstructing the Pt{110} surface is shown to increase the activity towards the ORR. Interestingly, increasing the upper potential limit does not result in an increase in ORR activity. The upper potential limit of 1 V actually gives the highest ORR activity (increase by 80 mV), followed by 1.2 V, then 1.4 V and finally no fast cycling scans.
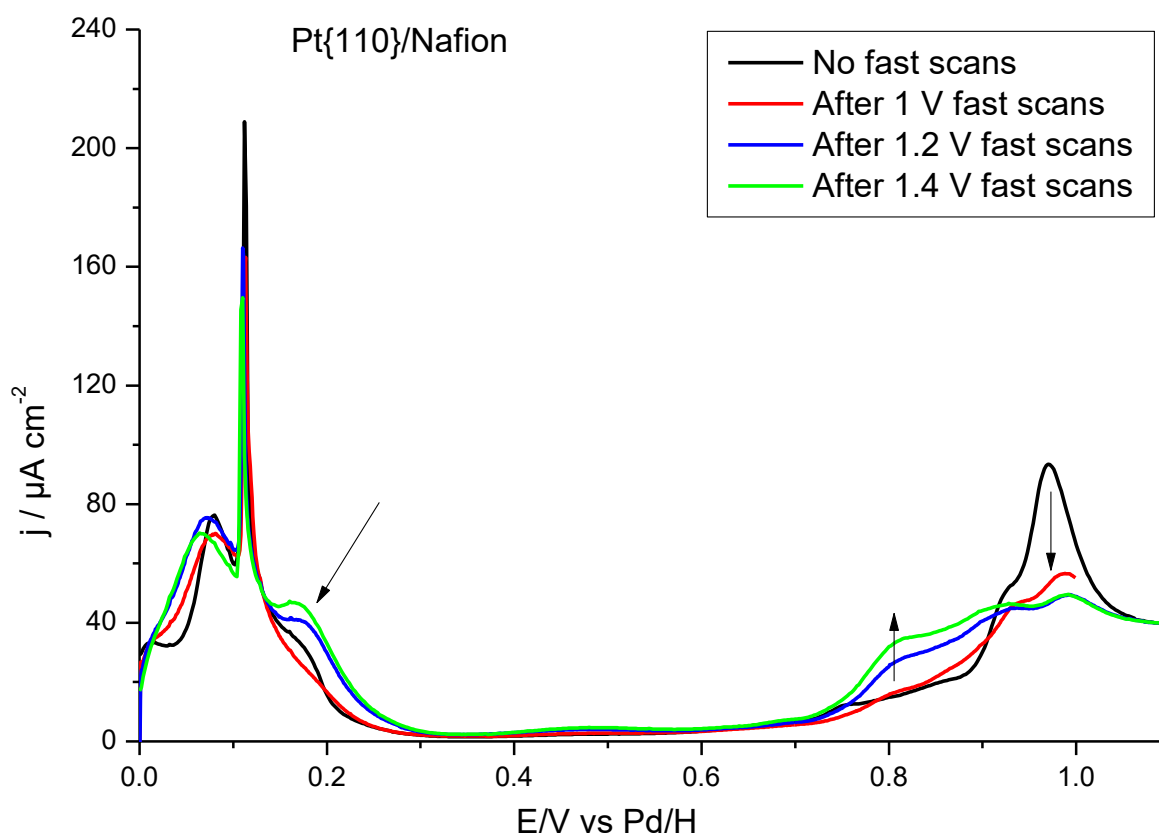

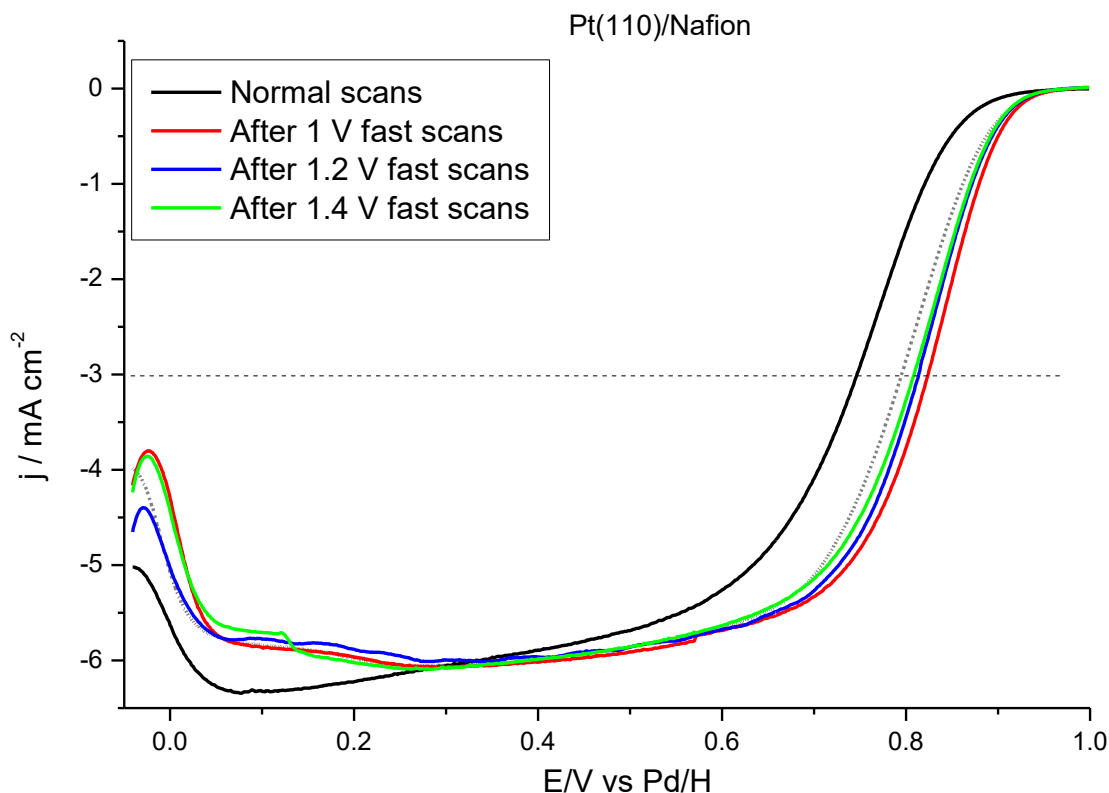*Figure 167: CVs of Nafion Pt{110} in 0.1 M HClO₄, after fast scans*

Figure 168: RDE curves of Nafion on Pt{110} in 0.1 M HClO₄, saturated with O₂, after fast scans. Comparison with Nafion free Pt{110}, (dashed - - -), also shown.

The strong attenuation in the ORR activity on Pt{110} following Nafion deposition confirms the relatively strong interaction of sulphonate anions with this surface (see earlier). The extent of increase in ORR activity following potential cycling is ascribed to break up of residual terrace OH adsorption as usual. It should also be noted that the generation of hydrogen peroxide in the H_{upd} region is negligible when Nafion is present. This is a new finding that probably requires further investigation since potential cycling decreases reduction current in this potential range.

6.4.4. Conclusions

This section has tried to link 'real' electrocatalytic conditions encountered in fuel cells with fundamental studies of Nafion adsorbed on single crystal surfaces and their relative stability under high potential cycling. It is found in all cases that terrace sites are deleterious for ORR due to the formation of adsorbed OH adlayers that compete successfully with oxygen for metallic sites. Nafion, containing as it does weakly specifically adsorbing sulphonate anions, always leads to a decrease in ORR activity relative to measurements in pure perchloric acid. Potential cycling introduces defects into the electrode surfaces under investigation and as a consequence breaks up any ordered

adlayers formed by OH or sulphonate leading to promotion of ORR. However, in general both Nafion-covered and Nafion-free electrochemically roughened surfaces tend towards identical ORR activity, i.e. Nafion does not seem to affect the ORR activity of roughened surfaces very much although Pt{110} sites were discovered to be particularly susceptible to interference from Nafion. From these high potential fast scan conditions, Pt{111} was found to be the most stable surface, as its CV displayed the smallest changes after potential cycling to 1V. Across the selection of surfaces tested and all upper potential limits applied, Pt{111} gave the highest activity towards the ORR when the upper potential limit was 1.2 V. This was also true for this potential limit when Nafion was on the surface. Clearly, the residual {111} terraces are highly active for ORR at low pH as predicted by theoretical calculations [42, 43].

The atomic surface arrangement that was most affected by high potential fast scanning conditions was Pt{100}, where large changes were seen at most negative potentials. Increasing the upper potential limit was shown to increase the activity for the ORR.

6.5. Conclusions of chapter

The study of the initial stages of electrochemical oxide adsorption together with their rates of formation and their impact on surface structure over a range of well-defined Pt(hkl) electrodes has been investigated. Furthermore, attempts have been made to bridge the gap between fundamental and applied studies of electrocatalytic interfaces relevant to the ORR. The role of potential and time in generating oxide was first examined and deductions of adsorption followed by surface reconstruction were made in the case of Pt{100}. This behaviour was less marked for Pt{110} and absent (up to 1V) for Pt{111}. Subsequent determinations of the rate constants for the oxide adsorption confirmed that the oxide formation was not a simple first order process on Pt{100} (and to a lesser extent Pt{110}) and involved a second reaction associated with surface roughening. It was clear from these studies that initial oxide formation on Pt{111} led to little perturbation of either surface structure or ORR activity. In contrast, Pt{100} displays the greatest instability and susceptibility towards structure-activity enhancements.

Chronoamperometry studies were undertaken on Pt{hkl} single crystals in in 0.1 M perchloric acid electrolyte in an attempt to elucidate kinetic information concerning adsorbed electrochemical adsorbed oxides. Results showed unexpected deviations from linear responses but some sequential qualitative analysis was undertaken to assign electrosorption process to features seen in chronoamperometry results and compared to CV. Some quantitative kinetic data was also derived

which showed that Pt{111} had the slowest formation of oxide on its surface. On the whole, using chronoamperometry to study macroelectrodes provided much food for thought and the analysis and understanding was incomplete.

Fast potential cycling of the electrode surfaces in the absence/presence of Nafion also confirmed the likelihood of structural changes occurring in real fuel cells under ORR conditions and the inhibiting effect of Nafion if the catalyst particles contain terrace sites. Roughened catalyst particles should exhibit an enhanced ORR activity, even in the presence of Nafion.

6.6. References

[1] D. Gilroy, B.E. Conway, Surface oxidation and reduction of platinum electrodes - coverage kinetic and hysteresis studies, Canadian Journal of Chemistry 46(6) (1968) 875-&.

[2] S.D. James, Multilayer oxide films on anodized platinum, Journal of the Electrochemical Society 116(12) (1969) 1681-&.

[3] B.E. Conway, G. Jerkiewicz, Surface orientation dependence of oxide film growth at platinum single-crystals, Journal of Electroanalytical Chemistry 339(1-2) (1992) 123-146.

[4] E.L. Redmond, B.P. Setzler, F.M. Alamgir, T.F. Fuller, Elucidating the oxide growth mechanism on platinum at the cathode in PEM fuel cells, Physical Chemistry Chemical Physics 16(11) (2014) 5301-5311.

[5] S.G. Rinaldo, W. Lee, J. Stumper, M. Eikerling, Mechanistic Principles of Platinum Oxide Formation and Reduction, Electrocatalysis 5(3) (2014) 262-272.

[6] B.E. Conway, Electrochemical oxide film formation at noble-metals as a surface-chemical process, Progress in Surface Science 49(4) (1995) 331-452.

[7] A.J. Appleby, Theory of Successive Electron-Transfer Steps in Cyclic Voltammetry - Application to Oxygen Pseudocapacitance on Platinum, Journal of the Electrochemical Society 120(9) (1973) 1205-1214.

[8] Angerste.H, B.E. Conway, W.B.A. Sharp, Real Condition of Electrochemically Oxidized Platinum Surfaces. 1.Resolution of Components Processes, Journal of Electroanalytical Chemistry 43(1) (1973) 9-36.

[9] Stonehar.P, Kozlowsk.Ha, B.E. Conway, Potentiodynamic examination of electrode kinetics for electroactive adsorbed species - applications to reduction of noble metal surfaces, Proceedings of the Royal Society of London Series a-Mathematical and Physical Sciences 310(1503) (1969) 541-&.

[10] G. Jerkiewicz, G. Vatankhah, J. Lessard, M.P. Soriaga, Y.S. Park, Surface-oxide growth at platinum electrodes in aqueous H2SO4 Reexamination of its mechanism through combined cyclic-voltammetry, electrochemical quartz-crystal nanobalance, and Auger electron spectroscopy measurements, Electrochimica Acta 49(9-10) (2004) 1451-1459.

[11] A. Rodes, J. Clavilier, J.M. Orts, J.M. Feliu, A. Aldaz, Electrochemical-behaviour of Pt(100) in various acidic media. 2.On the relation between the voltammetric profiles induced by anion specific adsorption studied with a transfer technnique preserving surface cleanliness and structure, Journal of Electroanalytical Chemistry 338(1-2) (1992) 317-338.

[12] J. Bao, D.D. Macdonald, Growth Kinetics of the Anodic Oxide Film on Platinum under Potentiodynamic Polarization Conditions, Zeitschrift Fur Physikalische Chemie-International Journal of Research in Physical Chemistry & Chemical Physics 227(5) (2013) 541-559.

[13] A.M. Gomez-Marin, R. Rizo, J.M. Feliu, Some reflections on the understanding of the oxygen reduction reaction at Pt(111), Beilstein Journal of Nanotechnology 4 (2013) 956-967.

[14] J. Zhang, PEM Fuel Cell Electrocatalysts and Catalyst Layers: Fundamentals and Applications, Springer London2008.

[15] J.K. Norskov, J. Rossmeisl, A. Logadottir, L. Lindqvist, J.R. Kitchin, T. Bligaard, H. Jonsson, Origin of the overpotential for oxygen reduction at a fuel-cell cathode, Journal of Physical Chemistry B 108(46) (2004) 17886-17892.

[16] A.M. Gomez-Marin, R. Rizo, J.M. Feliu, Oxygen reduction reaction at Pt single crystals: a critical overview, Catalysis Science & Technology 4(6) (2014) 1685-1698.

[17] J.X. Wang, N.M. Markovic, R.R. Adzic, Kinetic analysis of oxygen reduction on Pt(111) in acid solutions: Intrinsic kinetic parameters and anion adsorption effects, Journal of Physical Chemistry B 108(13) (2004) 4127-4133.

[18] A. Bjoerling, E. Ahlberg, J.M. Feliu, Kinetics of surface modification induced by submonolayer electrochemical oxygen adsorption on Pt(111), Electrochemistry Communications 12(3) (2010) 359-361.

[19] M.D. Macia, J.M. Campina, E. Herrero, J.M. Feliu, On the kinetics of oxygen reduction on platinum stepped surfaces in acidic media, Journal of Electroanalytical Chemistry 564(1-2) (2004) 141-150.

[20] A. Kuzume, E. Herrero, J.M. Feliu, Oxygen reduction on stepped platinum surfaces in acidic media, Journal of Electroanalytical Chemistry 599(2) (2007) 333-343.

[21] F.J. Vidal-Iglesias, J. Solla-Gullon, J.M. Campina, E. Herrero, A. Aldaz, J.M. Feliu, CO monolayer oxidation on stepped Pt(S) (n-1)(100) x (110) surfaces, Electrochimica Acta 54(19) (2009) 4459-4466.

[22] G.A. Attard, R. Price, Electrochemical investigation of a structure sensitive growth mode - palladium deposition on Pt(100)-Hex-R0.7-Degrees and Pt(100)-(1x1), Surface Science 335(1-3) (1995) 63-74.

[23] C. Zuliani, D.A. Walsh, T.E. Keyes, R.J. Forster, Formation and Growth of Oxide Layers at Platinum and Gold Nano- and Microelectrodes, Analytical Chemistry 82(17) (2010) 7135-7140.

[24] J. Clavilier, R. Faure, G. Guinet, R. Durand, Preparation of mono-crystalline Pt microelectrodes and electrochemical study of the plane surfaces cut in the direction of the (111) and (110) planes, Journal of Electroanalytical Chemistry 107(1) (1980) 205-209.

[25] R.J. Forster, L.R. Faulkner, Kinetic separation of faradaic currents - binary monolayers as model systems, Analytical Chemistry 67(7) (1995) 1232-1239.

[26] H.O. Finklea, D.D. Hanshew, Electron-transfer kinetics in organized thiol monolayers with attached pentaammine(pyridine)ruthenium redox centres, Journal of the American Chemical Society 114(9) (1992) 3173-3181.

[27] V. Climent, J.M. Feliu, Thirty years of platinum single crystal electrochemistry, Journal of Solid State Electrochemistry 15(7-8) (2011) 1297-1315.

[28] A.J. Bard, L.R. Faulkner, Electrochemical methods: fundamentals and applications, Wiley1980.

[29] R.J. Forster, MICROELECTRODES - NEW DIMENSIONS IN ELECTROCHEMISTRY, Chemical Society Reviews 23(4) (1994) 289-297.

[30] J. Barr, J. Gillespie, E.A. Robinson, The Sulphuric Acid Solvent System Part II. Conductivity measurements on solutions of come acids, 1961, pp. 1266-1273.

[31] A. Berna, V. Climent, J.M. Feliu, New understanding of the nature of OH adsorption on Pt(111) electrodes, Electrochemistry Communications 9(12) (2007) 2789-2794.

[32] J. Zhang, Electrocatalysts for PEM fuel cell oxygen reduction reaction: Challenges and perspectives, Abstracts of Papers of the American Chemical Society 239 (2010).

[33] O.T. Holton, J.W. Stevenson, The Role of Platinum in Proton Exchange Membrane Fuel Cells Evaluation of platinum's unique properties for use in both the anode and cathode of a proton exchange membrane fuel cell, Platinum Metals Review 57(4) (2013) 259-271.

[34] C.A. Rice, P. Urchaga, A.O. Pistono, B.W. McFerrin, B.T. McComb, J.W. Hu, Platinum Dissolution in Fuel Cell Electrodes: Enhanced Degradation from Surface Area Assessment in Automotive Accelerated Stress Tests, Journal of the Electrochemical Society 162(10) (2015) F1175-F1180.

[35] K.E. Martin, J.P. Kopasz, K.W. McMurphy, Status of Fuel Cells and the Challenges Facing Fuel Cell Technology Today, Fuel Cell Chemistry and Operation 1040 (2010) 1-13.

[36] J.C. Canullo, W.E. Triaca, A.J. Arvia, Changes in the electrochemical rsponse of polycrystalline platinum-electrodes promoted by the fast repetitive square-wave potential signals, Journal of Electroanalytical Chemistry 175(1-2) (1984) 337-340.

[37] J.C. Canullo, W.E. Triaca, A.J. Arvia, Electrochemical faceting of single-crystal platinum-electrodes, Journal of Electroanalytical Chemistry 200(1-2) (1986) 397-400.

[38] R.M. Cervino, W.E. Triaca, A.J. Arvia, A novel effect - changes in the electrochemical response of polycrystalline platinum prooted by very fast potential perturbations, Journal of the Electrochemical Society 132(1) (1985) 266-267.

[39] M. Ahmed, D. Morgan, G.A. Attard, E. Wright, D. Thompsett, J. Sharman, Unprecedented Structural Sensitivity toward Average Terrace Width: Nafion Adsorption at Pt{hkl} Electrodes, Journal of Physical Chemistry C 115(34) (2011) 17020-17027.

[40] P.N. Ross, The role of defects in the specific adsorption of anions on Pt(111), Journal De Chimie Physique Et De Physico-Chimie Biologique 88(7-8) (1991) 1353-1380.

[41] G.A. Attard, A. Brew, Cyclic voltammetry and oxygen reduction activity of the Pt{110}-(1 x 1) surface, Journal of Electroanalytical Chemistry 747 (2015) 123-129.

[42] E.a.S.W. Santos, Electrochemical Electron Transfer: From Marcus Theory to Electrocatalysis, (2008) 31--55.

[43] M.J. Eslamibidgoli, M.H. Eikerling, Electrochemical Formation of Reactive Oxygen Species at Pt (111)-A Density Functional Theory Study, ACS Catalysis 5(10) (2015) 6090-6098.

Conclusions
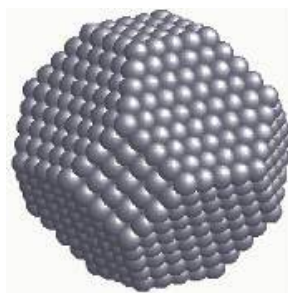
7.1 Introduction

The objective of this research was to gain further understanding of electrochemical oxides and related surface species on platinum and their impact upon important catalytic processes such as the oxygen reduction reaction. Platinum electrocatalysts used in the fuel cells endure significant changes due to harsh conditions and so, the identity of these species as a function of applied potential, (particularly at potentials relevant to loss of ORR activity) is important. There is a fundamental need for such studies due to a current absence of adequate methods that may elucidate the structure of the electrode-electrolyte interface in situ. An understanding of these effects at single crystal surfaces will in turn inform the design of improved electrocatalysts for fuel cells.

The information gained in this work has increased our understanding of the properties of the Pt fcc surfaces in the [001] zone in particular.

7.2 Conclusions

The voltammetry of Pt{111}, Pt{100}, Pt{110} and Pt{311} single crystal electrodes as a function of perchloric acid concentration (0.05 – 2.00 M) was studied in order to test the assertion made in recent reports by Watanabe *et al.*[1, 2] that perchlorate anions specifically adsorb on polycrystalline platinum. For Pt{111}, it was found that OH_{ads} and electrochemical oxide states are both perturbed significantly as perchloric acid concentration is increased. This is suggested to be due to specific adsorption of perchlorate anions competing with OH_{ads} for adsorption sites. The hydrogen underpotential deposition (H_{upd}) region of Pt{111} however remains unchanged, although evidence for perchlorate anion decomposition to chloride on Pt{111} is found. For Pt{100}, perchlorate anions were found to be non-specifically adsorbed on this plane, but changes in all H_{upd} states were observed as perchloric acid concentration increased. This manifested itself as a redistribution of

charge from the H_{upd} state situated at more positive potential to the one at more negative potential. For Pt{110} and Pt{311}, marginal changes in the onset of electrochemical oxide formation are recorded, associated with specific adsorption of perchlorate. Specific adsorption of perchlorate anions on Pt{111} is deleterious to electrocatalytic activity in relation to the oxygen reduction reaction (ORR) as measured using a rotating disc electrode (RDE) in a hanging meniscus configuration. This study supports previous work suggesting that a large component of the ORR activity on platinum is governed by simple site blocking from specifically adsorbed anions and/or electrosorbed oxide[2, 3, 4].

When anion adsorption is probed as a function of pH at constant perchlorate anion concentration, it is found that, in agreement with findings from the Frumkin School[203], decreasing pH leads to an increase in perchlorate-surface interactions. However, at constant pH and varying perchlorate anion concentration, a more complicated set of interactions are observed whereby both cation and anion adsorption may be observed. This is exemplified for oxide formation on Pt{100} in which cations are found to inhibit oxide formation. Other examples are outlined and in the case of Nafion-modified P({111} surfaces, a specific cation interaction with the OH/water peak is noted leading to a shift to more negative potentials. The possibility of non-covalent interactions of cations with electrosorbed water and specific cation adsorption influencing non-Nernstian peak potential shifts is in accordance with recent experimental and theoretical investigations[5, 6, 7].

A comprehensive electrochemical study of CO – cooled single crystal electrodes vicinal to the Pt{110} basal plane was also undertaken. Detailed analysis of electrosorption charges/voltammetry, pH, anion and cation effects and PZTC concluded that Pt n{110}x{111} electrodes are unreconstructed and afford systematic variations in H_{upd} and electrosorbed oxide CV peaks as a function of step density. In contrast, Pt n{110}x{100} electrodes indicated a strong tendency towards surface reconstruction. A new model of the Pt{110} H_{upd} region was developed in which local charged states that vary as a function of potential, pH and ionic adsorption are responsible for the variety of CV responses recorded. The model allows for interpretation of non-Nernstian shifts in peak potential as a function of pH and the nature of the ions in contact with the electrode surface. Weak specific adsorption of sodium ions and fluoride anions on Pt{110} together with "OH" and the more usual hydrogen electrosorption was found. By assigning "cationic" and "anionic" contributions to the overall H_{upd} region, one may evaluate the global value of the PZTC without the need of measuring CO charge displacement. The possibility that this model may apply generally to other well-defined Pt electrodes will be the subject of future investigations.

Characterization of stepped (Pt n{100}x{110} and Pt n{110}x{100}) electrodes were undertaken using a variety of different electrochemical methods, in various electrolytic solutions. Limited work had previously been undertaken on these surfaces[8, 9]. By investigating systematic variations in electrosorption peaks as a function of step density, terrace and step adsorption could be identified. The effect of specific anion adsorption on electrosorption peak potentials was used to deduce the involvement of adsorbed OH at potentials in the H_{upd} range. The oxide adsorption region on both types of stepped surface were also reported showing distinct adsorption behaviour for step and terrace oxide sites. Nafion adsorption was also investigated and the structure sensitivity of Nafion adsorption was confirmed in that so-called "Nafion spikes", characteristic of terrace adsorption were modulated strongly upon the introduction of steps. This is also conducive of where H_{upd} sites negative of the PZTC found in pure perchloric acid media. Interestingly, the Nafion spike persists on Pt{110} terrace-containing surfaces up to the turning point of the zone (Pt{210}) suggesting that Pt{110} terrace sites afford a specific affinity for sulphonate groups contained within the Nafion adlayer. Pt n{100}x{110} surfaces showed rapid quenching of the Nafion spike as a function of increasing step density. Reactivity measurements involving oxygen reduction and hydrogen peroxide oxidation/reduction largely revealed the importance of adsorbed oxide/OH in regulating activity.

For ORR, the most active electrode surfaces were found to contain sufficient numbers of linear steps such that long range ordered OH adlayers associated with terraces were disrupted thus allowing unfettered access of oxygen molecules to metallic sites. However, too great a density of defect sites would stimulate surface oxide formation and attenuation in ORR activity leading to a so-called 'volcano-curve' correlation between ORR activity and step density. For hydrogen peroxide, results are in agreement with previous work showing a switchover from reduction to oxidation when surface oxides formed. Little variation in Tafel slope was observed for hydrogen peroxide reactions confirming the mass transport limited nature of the reaction.

The study of the initial stages of electrochemical oxide adsorption together with their rates of formation and their impact on surface structure over a range of well-defined Pt{hkl} electrodes was investigated. The role of potential and time in generating oxide was first examined and deductions of adsorption followed by surface reconstruction were made in the case of Pt{100}. This behaviour was less marked for Pt{110} and absent (up to 1 V) for Pt{111}. Subsequent determinations of the rate constants for the oxide adsorption confirmed that the oxide formation was not a simple first order process on Pt{100} (and to a lesser extent Pt{110}) and involved a second reaction associated with

surface roughening. It was clear from these studies that initial oxide formation on Pt{111} led to little perturbation of either surface structure or ORR activity. In contrast, Pt{100} displays the greatest instability and susceptibility towards structure-activity enhancements. Fast potential cycling of the electrode surfaces in the absence/presence of Nafion also confirmed the likelihood of structural changes occurring in real fuel cells under ORR conditions and the inhibiting effect of Nafion if the catalyst particles contain terrace sites. Roughened catalyst particles should actually exhibit an enhanced ORR activity, even in the presence of Nafion.

7.3 Further Work

The work in this thesis has led to a greater understanding of electrosorbed species on platinum single crystals but there are still more questions that have been raised. Hence, future work should be directed towards the following in order to address some of these aspects:

- Since alkali metals have been found to be specifically adsorbed on Pt{hkl}, studies under alkaline conditions (where cation-platinum interactions are maximized) should prove highly interesting. The corresponding influence on ORR may then be used to understand interactions within the emerging area of alkaline polymeric electrolytes.

- The stability and potential induced structural transitions under fuel cell-like conditions with bimetallic systems. Corrosion of less noble metal components may readily be revealed using different Pt-M (M = Ni, Co, Fe) single crystals and it may be that some sites (steps?) may be less resilient than others (terraces).

- Utilisation of other surface sensitive techniques such as XPS, EC-STM and SHINERS to further study adsorbed Nafion and oxide growth on Pt{hkl} surfaces both in situ and ex situ.

- Nafion adsorption on CO-cooled stepped Pt{110} surfaces – would the prediction of Nafion spikes occurring on all Pt{110} stepped surfaces turn out to be correct?

- Re-examine Pt{hkl} surfaces other than stepped Pt{110} in relation to the studies in chapter four to understand if the proposed model of localized states may apply generally.

7.4 References

[1] J. Omura, H. Yano, M. Watanabe, H. Uchida, Electrochemical Quartz Crystal Microbalance Analysis of the Oxygen Reduction Reaction on Pt-Based Electrodes. Part 1: Effect of Adsorbed Anions on the Oxygen Reduction Activities of Pt in HF, HClO4, and H2SO4 Solutions, Langmuir 27(10) (2011) 6464-6470.

[2] J. Omura, H. Yano, D.A. Tryk, M. Watanabe, H. Uchida, Electrochemical Quartz Crystal Microbalance Analysis of the Oxygen Reduction Reaction on Pt-Based Electrodes. Part 2: Adsorption of Oxygen Species and ClO4- Anions on Pt and Pt-Co Alloy in HClO4 Solutions, Langmuir 30(1) (2014) 432-439.

[3] A.M. Gomez-Marin, R. Rizo, J.M. Feliu, Oxygen reduction reaction at Pt single crystals: a critical overview, Catalysis Science & Technology 4(6) (2014) 1685-1698.

[4] A.M. Gomez-Marin, J.M. Feliu, Role of oxygen-containing species at Pt(111) on the oxygen reduction reaction in acid media, Journal of Solid State Electrochemistry 19(9) (2015) 2831-2841

[5] D. Strmcnik, D.F. van der Vliet, K.C. Chang, V. Komanicky, K. Kodama, H. You, V.R. Stamenkovic, N.M. Markovic, Effects of Li+, K+, and Ba2+ Cations on the ORR at Model and High Surface Area Pt and Au Surfaces in Alkaline Solutions, Journal of Physical Chemistry Letters 2(21) (2011) 2733-2736.

[6] K. Kodama, Y. Morimoto, D.S. Strmcnik, N.M. Markovic, The role of non-covalent interactions on CO bulk oxidation on Pt single crystal electrodes in alkaline electrolytes, Electrochimica Acta 152 (2015) 38-43.

[7] P.P. Lopes, D. Strmcnik, D. Tripkovic, J.G. Connell, V. Stamenkovic, N.M. Markovic, Relationships between Atomic Level Surface Structure and Stability/Activity of Platinum Surface Atoms in Aqueous Environments, ACS Catalysis 6(4) (2016) 2536-2544.

[8] F.J. Vidal-Iglesias, J. Solla-Gullon, J.M. Campina, E. Herrero, A. Aldaz, J.M. Feliu, CO monolayer oxidation on stepped Pt(S) (n-1)(100) x (110) surfaces, Electrochimica Acta 54(19) (2009) 4459-4466.

[9] J. Souza-Garcia, C.A. Angelucci, V. Climent, J.M. Feliu, Electrochemical features of Pt(S) n(110) x (100) surfaces in acidic media, Electrochemistry Communications 34 (2013) 291-294.